NOTICE

AVIS

The quality of this microform is heavily dependent upon the quality of the original thesis submitted for microfilming. Every effort has been made to ensure the highest quality of reproduction possible.

If pages are missing, contact the university which granted the degree.

Some pages may have indistinct print especially if the original pages were typed with a poor typewriter ribbon or if the university sent us an inferior photocopy.

Reproduction in full or in part of this microform is governed by the Canadian Copyright Act, R.S.C. 1970, c. C-30, and subsequent amendments.

La qualité de cette microforme dépend grandement de la qualité de la thèse soumise au microfilmage. Nous avons tout fait pour assurer une qualité supérieure de reproduction.

S'il manque des pages, veuillez communiquer avec l'université qui a conféré le grade.

La qualité d'impression de certaines pages peut laisser à désirer, surtout si les pages originales ont été dactylographiées à l'aide d'un ruban usé ou si l'université nous a fait parvenir une photocopie de qualité inférieure.

La reproduction, même partielle, de cette microforme est soumise à la Loi canadienne sur le droit d'auteur, SRC 1970, c. C-30, et ses amendements subséquents.

Canada

UNIVERSITY OF ALBERTA

AN EIGENVECTOR-BASED STRATEGY
FOR ANALYSIS OF INELASTIC STRUCTURES

by

JOSÉ NAPOLEÃO FILHO

A THESIS
SUBMITTED TO THE FACULTY OF GRADUATE STUDIES AND RESEARCH
IN PARTIAL FULFILMENT OF THE REQUIREMENTS FOR THE DEGREE OF
DOCTOR OF PHILOSOPHY

DEPARTMENT OF CIVIL ENGINEERING

EDMONTON, ALBERTA

SPRING, 1990

NOTICE

AVIS

The quality of this microform is heavily dependent upon the quality of the original thesis submitted for microfilming. Every effort has been made to ensure the highest quality of reproduction possible.

If pages are missing, contact the university which granted the degree.

Some pages may have indistinct print especially if the original pages were typed with a poor typewriter ribbon or if the university sent us an inferior photocopy.

Reproduction in full or in part of this microform is governed by the Canadian Copyright Act, R.S.C. 1970. c. C-30, and subsequent amendments.

La qualité de cette microforme dépend grandement de la qualité de la thèse soumise au microfilmage. Nous avons tout fait pour assurer une qualité supérieure de reproduction.

S'il manque des pages, veuillez communiquer avec l'université qui a conféré le grade.

La qualité d'impression de certaines pages peut laisser à désirer, surtout si les pages originales ont été dactylographiées à l'aide d'un ruban usé ou si l'université nous a fait parvenir une photocopie de qualité inférieure.

La reproduction, même partielle, de cette microforme est soumise à la Loi canadienne sur le droit d'auteur, SRC 1970, c. C-30, et ses amendements subséquents.

ISBN 0-315-60210-4

Canada

micro.

FROM: Jose
TO : Dr. MacGregor
DATE : February 16, 1990

Dear Prof. MacGregor

In order to submit my thesis to a preliminary

check by the Faculty of Graduate Studies, I need

a written permission to use the attached photograph

,

copy of the Beam B 1.5/71 taken from the

F. Morrisson Test Archives.

Thanks you for your cooperation.

Jose Yepolo Rifl

I hereby give you permission
... this photograph ...
...

UNIVERSITY OF ALBERTA

RELEASE FORM

NAME OF AUTHOR: JOSÉ NAPOLEÃO FILHO

TITLE OF THESIS: AN EIGENVECTOR-BASED STRATEGY FOR ANALYSIS OF INELASTIC STRUCTURES

DEGREE: DOCTOR OF PHILOSOPHY

YEAR THIS DEGREE GRANTED: SPRING 1990

Permission is hereby granted to the University of Alberta Library to reproduce single copies of this thesis and to lend or sell such copies for private, scholarly or scientific research purposes only.

The author reserves other publication rights, and neither the thesis nor extensive extracts from it may be printed or otherwise reproduced without the author's written permission.

(signed) *José Napoleão Filho*

PERMANENT ADDRESS:

Departamento de Engenharia Civil

Pontifícia Universidade Católica (PUC-RJ)
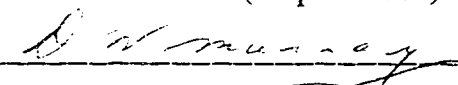
R. Mq. S. Vicente, 225

Rio de Janeiro, 22453, Brasil

Date : March 9th, 1990.

UNIVERSITY OF ALBERTA
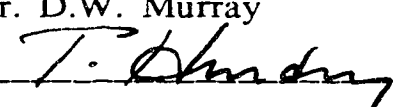
FACULTY OF GRADUATE STUDIES AND RESEARCH

The undersigned certify that they have read, and recommend to the Faculty of Graduate Studies and Research, a thesis entitled AN EIGENVECTOR-BASED STRATEGY FOR ANALYSIS OF INELASTIC STRUCTURES submitted by JOSE NAPOLEAO FILHO in partial fulfilment of the requirements for the degree of DOCTOR OF PHILOSOPHY.
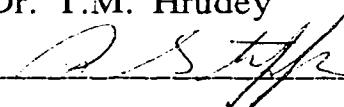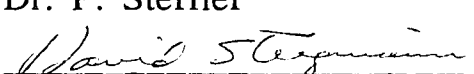
_____
Dr. A.E. Elwi (Supervisor)

_____
Dr. D.W. Murray

_____
Dr. T.M. Hrudey

_____
Dr. P. Steffler

_____
Dr. D. Steigmann

_____
Dr. G.S. Dhatt (External Examiner)

Date: ____MARCH 9TH , 1990_____

To my family:

Lúcia

Natércia

and

Bruno

ABSTRACT

In the realm of materially nonlinear structures, an assessment of current solution strategies has suggested the need for more efficient methods of analysis. A simpler iterative phase, a fast convergence rate and a low cost are the specific demands. The strategy should also be able to trace complex load-deflection histories, composed of ascending branches, prolonged flat segments, limit points and unstable descending paths. Furthermore, the correct failure mode should be captured.

To satisfy these requirements, an eigenvector-based strategy has been proposed. Its formulation is based on a transformation of the equilibrium equations, from the basis of the global degrees of freedom to the basis of the eigenvectors of the tangent stiffness matrix. In addition, progressive damage in inelastic materials causes domination of the eigenvectors associated with the lowest eigenvalues upon the incremental displacement response of inelastic structures. This allows for the reduction of the involved degrees of freedom.

The formulation of the strategy is organized in two phases. In the pre-iterative phase, the finite arc-length of the load-deflection curve is adopted as an independent parameter. Its size varies with the current value of the stiffness parameter which is a measure of the level of nonlinearity. A criterion for unloading, based on the

presence of negative pivots in the factorized stiffness matrix, is also included within this phase. Following the check for participation of preselected eigenvectors, the transformation and reduction of the incremental equilibrium equations take place.

In the iterative phase, the generalized displacement increments and the generalized forces comprise the incremental-iterative equilibrium equations. These variables are constrained to an iteration path which is orthogonal to the arc-length. The modified Newton-Raphson method is the iterative scheme followed in this phase.

Four materially nonlinear structures serve as applications for the proposed strategy. Comparison with other existing methods is also provided. A fast rate of convergence and savings in CPU time, as much as 45%, are achieved.

ACKNOWLEDGEMENTS

TABLE OF CONTENTS

Chapter 7 : Summary, Conclusions and Recommendations

LIST OF TABLES

LIST OF FIGURES

LIST OF SYMBOLS

General:

{ }	Column vector.
< >	Row vector.
[ ]	Matrix.
[ ]^T	Transposed matrix.
[ ]$^{-1}$	Inversed matrix.
TOL	Tolerance.
DOF	Degree of freedom.
det	Determinant.
SNRM	Standard Newton Raphson Method.
CALM	Constant Arc-Length Method.
ESS	Eigenvector-based Solution Strategy.
#ITE	Number of iterations.
h	Halfbandwidth.
p	Number of preselected eigenvectors.
N	Number of global degrees of freedom.
M	Number of dominant eigenvector components.
Π	Product.
Σ	Summation.

Scalars:

$\Delta\rho^i$	Load factor increment at the $(i)^{th}$ iteration.
$\Delta\rho^1$	Load factor increment at the first iteration.
ρ^{i-1}	Load factor at the $(i-1)^{th}$ iteration.

p^b Prescribed load factor.

g_* A real and scalar function.

Δr_p Prescribed displacement increment.

$\left(\Delta r_p^1\right)_I$ First component of the prescribed displacement increment at the first iteration.

$\left(\Delta r_p^1\right)_{II}$ Second component of the prescribed displacement increment at the first iteration.

ΔL^i Finite arc-length at the $(i)^{th}$ iteration.

C_L Factor to control the global arc-length size.

C_r Factor to control the displacement component of the arc-length size.

C_p Factor to control the load component of the arc-length size.

Δu_i Component of the displacement increment vector.

R_i Component of the reference force vector.

δ_{ij} Kronecker delta.

λ_i The ith eigenvalue.

$\Delta\alpha_i$ The ith generalized displacement increment.

$\Delta\gamma_i$ The ith generalized unbalanced force.

β_i Relative size parameter related to the ith relative size parameter.

$\| \Delta\alpha_i \{\phi\}_i \|$ Euclidean norm of the ith eigenvector component.

$\| \{\Delta r\} \|$ Euclidean norm of the displacement increment vector.

θ_i Angle parameter related to the ith eigenvector component.

$|\Delta\alpha_i|$ Absolute norm of the ith generalized displacement.

P_i Participation parameter related to the ith eigenvector component.

$\Delta\alpha_a$	Generalized displacement increment related to the approximate displacement increment vector.
β_a	Relative size parameter related to the approximate displacement increment vector.
θ_a	Angle parameter related to the approximate displacement increment vector.
P_a	Participation parameter related to the approximate displacement increment vector.
$|\Delta\alpha_a|$	Absolute norm of the generalized displacement increment related to the approximate displacement increment vector.
μ	Shift.
ω_i	The ith eigenvalue of the shifted stiffness matrix.
$\Delta\alpha_i^c$	The ith generalized displacement increment related to the first displacement increment vector.
$\|\{\Delta r\}^c\|$	Euclidean norm of the first displacement increment vector.
k^c	Overall stiffness at the beginning of a solution step.
$\Delta\rho^c$	The first load factor increment in a solution step.
k_1^c	Overall stiffness at the beginning of the first solution step.
S_p	Stiffness parameter.
$\|\{\Delta r\}_1^c\|$	Euclidean norm of the first displacement increment vector at the first solution step.
$\Delta\rho_1^c$	First load factor increment at the first solution step.
$\Delta\rho^b$	Net load factor increment at the end of a solution step.
$\Delta\rho_1^b$	Net load factor increment at the end of the first solution step.

$\left\| \sum_{i=1}^{\#ITE} \{\Delta\alpha\}^i \right\|$ Euclidean norm of the accumulated generalized displacement incre   vector in a typical solution step.

$\left\| \sum_{i=1}^{\#ITE} \{\Delta\alpha\}^i_1 \right\|$ Euclidean norm of the accumulated generalized displacement increment vector in the first solution step.

ΔL^c Finite arc-length at the beginning of a solution step.

ΔL^c_1 Finite arc-length at the beginning of the first solution step.

ΔL^1 Finite arc-length after adjustment.

f Factor of adjustment of the arc-length size.

$\Delta\rho^1$ Adjusted first load factor increment.

ρ^1 Total load factor after the first iteration of a solution step.

ΔW^c Incremental work at the beginning of a solution step.

d_{ii} The ith pivot of the stiffness matrix.

ΔW_i The ith incremental generalized work.

ρ^i Total load factor at the ith iteration.

$\left\| \{\Delta\alpha\}^i \right\|$ Euclidean norm of the generalized displacement increment vector at the ith iteration.

$\left\| \{\Delta\gamma\}^i \right\|$ Euclidean norm of the generalized unbalanced force vector at the ith iteration.

δ Radius of the convergence domain.

E Modulus of elasticity.

ν Poisson's ratio.

G Shear modulus.

H' Hardening or softening modulus.

F Yield function.

F_y	Yield stress.
E_i	Secant elasticity modulus of the reinforcement.
$E_{1,2,3}$	Moduli of elasticity in the orthotropy axes.
G_{12}	Shear modulus in the orthotropy axes 1 and 2.
v_{ij}	Poisson's ratio in the orthotropy axes i and j.
f_{cu}	Uniaxial compressive strength of concrete.
f_{cb}	Biaxial compressive strength of concrete.
f_{tu}	Uniaxial tensile strength of concrete.
ε_{cu}	Uniaxial compressive peak strain of concrete.
ε_{cb}	Biaxial compressive peak strain of concrete.
ε_{tu}	Uniaxial tensile strain of concrete.
G_f	Fracture energy density.
d_{gp}	Minimum distance between Gaussian points.
α_{DBR}	Slope of the tensile descending branch.
ε_p	Component of plastic strain.

Vectors :

$\{\Delta r\}^i$	Displacement increment vector at the $(i)^{th}$ iteration.
$\{\Delta Q\}^{i-1}$	Unbalanced load vector at the $(i-1)^{th}$ iteration.
$\{R\}$	Reference force vector.
$\{F\}^{i-1}$	Equivalent internal nodal force vector at the $(i-1)^{th}$ iteration.
$\{\Delta r\}^i_I$	First component of the displacement increment vector.
$\{\Delta r\}^i_{II}$	Second component of the displacement increment vector.

$\{\Sigma \Delta r\}^i$	Accumulated displacement increment vector up to the $(i)^{th}$ iteration.
$\{\Delta \varphi\}^i$	Typical generalized displacement increment vector at the $(i)^{th}$ iteration.
$\{\tilde{R}\}$	Transformed reference force vector.
$\{\widetilde{\Delta Q}\}^{i-1}$	Transformed unbalanced force vector at the $(i-1)^{th}$ iteration.
$\{\Sigma \Delta \varphi\}^i$	Accumulated generalized displacement increment vector at the $(i)^{th}$ iteration.
$\{e\}_i$	The $(i)^{th}$ natural basis vector.
$\{\Delta R\}$	External force increment vector.
$\{\Delta u\}$	Set of components of the displacement increment vector
$\{\Delta u\}_v$	Displacement increment vector at the basis [V].
$\{\Delta Q\}_v$	Unbalanced force vector at the basis [V].
$\{\phi\}_i$	The ith eigenvector.
$\{\Delta \alpha\}$	Generalized displacement increment vector.
$\{\Delta \gamma\}$	Generalized unbalanced force vector.
$\{\Delta r\}_u$	Unit displacement increment vector.
$\{\Delta r\}_a$	Approximate displacement increment vector.
$\{\Delta r\}^c$	First displacement increment vector of a solution step.
$\{\psi\}_i$	The ith eigenvector of the shifted stiffness matrix.
$\{\Delta r\}_u^c$	First unit displacement increment vector.
$\{\Delta \alpha\}^c$	First generalized displacement increment vector.
$\{\gamma\}^c$	First generalized unbalanced force vector in a solution step.

$[\Lambda]_t^a$	Main diagonal matrix of the eigenvalues at the beginning of a solution step.
$\{\Delta\alpha\}^1$	Adjusted first generalized displacement increment vector.
$\{\alpha\}^1$	Total generalized displacement vector after the first iteration of a solution step.
$\{T\}_a$	Arc-length vector at the beginning of a solution step.
$\{\Delta\alpha\}^i$	Generalized displacement increment vector at the ith iteration.
$\{\Delta w\}^i$	Iteration path vector at the ith iteration.
$\{\Delta\gamma\}^{i-1}$	Generalized unbalanced force vector at the $(i-1)^{th}$ iteration.
$\{\Delta\alpha\}_I^i$	First component of the generalized displacement increment vector at the ith iteration.
$\{\Delta\alpha\}_{II}^i$	Second component of the generalized displacement increment displacement increment vector at the ith iteration.
$\{\alpha\}^i$	Total generalized displacement vector at the ith iteration.
$\{r\}^i$	Total displacement vector at the ith iteration.
$\{\Delta\tau\}$	Position vector of the iteration point.
$\{p\}_u$	Unit load factor vector.
$\{\sigma\}$	Vector of total stresses.
$\{\varepsilon\}$	Vector of total strains.
$\{\Delta\sigma\}$	Vector of increment of stresses.
$\{\Delta\varepsilon\}$	Vector of increment of strains.

Matrices:

$[K_t]^{i-1}$ — Tangent stiffness matrix at the $(i-1)^{th}$ iteration.

$[K_t]^{i-1}_G$ — Geometrical tangent stiffness matrix at the $(i-1)^{th}$ iteration.

$[K]_l$ — Linear stiffness matrix.

$[V]$ — A set of general basis vectors.

$[\widetilde{K}]_l$ — Transformed linear stiffness matrix.

$[\widetilde{K}]^{i-1}_G$ — Transformed geometrical stiffness matrix at the $(i)^{th}$ iteration.

$[E]$ — Set of natural basis vectors.

$[K]_{tv}$ — Tangent stiffness matrix at the basis $[V]$.

$[\Phi]$ — Set on N eigenvectors.

$[\Lambda]$ — Main diagonal matrix of the eigenvalues.

$[\Lambda]^a_t$ — Main diagonal tangent matrix of the eigenvalues at the beginning of a solution step.

$[I]$ — Identity matrix.

$[K]^a_t$ — Tangent stiffness matrix at the beginning of a solution step.

$[\hat{K}]^a_t$ — Shifted tangent stiffness matrix at the beginning of a solution step.

$[\Psi]$ — Set of eigenvectors of the shifted stiffness matrix.

$[\Omega]$ — Main diagonal matrix of the eigenvalues of the shifted stiffness matrix.

$[L]$ — Lower-unit triangular matrix.

$[D]$ — Main diagonal matrix of the pivots of the stiffness matrix.

$[C]_e$ — Elastic constitutive matrix.

$[C]_{ep}$ — Elastic-plastic constitutive matrix.

$[C]_{hp}$ — Hypoelastic constitutive matrix.

CHAPTER 1

INTRODUCTION

1.1 Problem Statement

It has been known from the beginning of this century that engineering materials, such as steel and concrete, behave highly nonlinearly (Timoshenko 1983, De Coursy 1987). More recently, the improvement of experimental techniques and test apparatus have enhanced the knowledge of the post-ultimate behavior of these materials to the point where complete stress-strain curves can be traced.

The impact of the progress of the experimental studies of materials on the numerical analysis of structures can be felt through two specific requirements. First, a material model capable of reproducing the complex nonlinearities, inherent to the material, is needed. Second, an efficient solution strategy is of paramount importance in order to ..ace the complete load-deflection curve of the structure and to capture the correct failure mode.

Robust material models for steel and concrete have already been developed during the last two decades and are available in the technical literature (Chen and Ting 1980, Elwi and Murray 1979, Balakrishnan and Murray 1988, Owen and Hinton 1980).

The development of novel solution strategies, however, has been mostly restricted to the field of geometrically nonlinear structures made of linearly elastic materials (Noor and Peters 1983, Riks 1984). For materially nonlinear structures, the emphasis has

been put on solution strategies that are able to describe load-deflection curves in the range prior to ultimate load. In this case, the classical Newton-Raphson methods often suffice (Balakrishnan and Murray 1989). Recently, however, a limited number of innovative solution strategies for materially nonlinear structures has emerged. These strategies have been applied to the investigation of the post-ultimate response of plain and reinforced concrete structures (Crisfield 1986, De Borst 1987). The common points in these methods are the implementation of an arc-length constraint on the iterative path such that the load level becomes a dependent parameter, and an iterative technique that involves the total number of the global degrees of freedom.

Nevertheless, some deficiencies have become apparent in the performance of these strategies. For instance, the overcoming of limit points has been difficult due to the adoption of an arbitrary arc-length. On the other hand, if the arc-length is too small, the solution provides an excessive number of solution steps. In addition, the iterative phase of these strategies requires a great amount of computational effort leading to a high cost. This is caused by the commonly used procedure of updating the stiffness matrix for each iteration and by the involvement of load and displacement vectors for which the dimension is the total number of degrees of freedom.

Therefore, it seems that there is a need for a solution strategy that would present a simpler iterative phase, where a low number of iterations and a reduced number of degrees of freedom could be achieved. In addition, a control scheme for the size of the solution

step is strongly necessary. Finally, the solution strategy should be able to overcome limit points and to trace unstable post-ultimate behavior with due account for the capture of the failure mode.

1.2 Objectives

The objectives of this study are:

1. To develop a self-controlled solution strategy that is able to trace the <u>complete</u> load-deflection curves of materially nonlinear structures with a reduced number of degrees of freedom.

2. To apply the developed solution strategy to the analysis of large scale structures.

3. To evaluate and compare the developed solution strategy with existing methods.

4. To recommend areas of future research.

1.3 Scope

Considering inelastic structures, the formulation of equilibrium adopted in this study is incremental and iterative within the framework of the finite element method. This formulation is further restricted to deal with time-independent and static equilibrium problems. Only limit point problems, as defined by Thompson (1963), are of interest. Bifurcation problems are not considered.

Displacements and strains are assumed to be small. As a result, the current equilibrium configuration of the structure refers to the undeformed state as the initial configuration.

The applied loads are treated as conservative and

proportional to a preselected reference force. Nevertheless, an additional constant load vector can be accomodated within the equilibrium formulation (Ramm 1981).

The materially nonlinear structures considered in this study are modeled as two-dimensional members. In the discretization of these structures, the two-dimensional isoparametric element, with eight nodes and 3x3 as integration rule, is utilized to model the concrete and the steel members. The simple truss element is adopted to discretize the reinforcement. Thus, shallow and deep beams made of steel and reinforced concrete are of special interest.

1.4 Outline

Following this introduction, a brief review of some current solution strategies, which are suitable to deal with inelastic structures, forms the contents of Chapter 2.

In Chapter 3, the eigenvectors of the tangent stiffness matrix are selected as a basis upon which the equilibrium problem is formulated. The conventional incremental equilibrium equations are transformed to the eigenvector basis. The resulting equilibrium equations are diagonal and therefore totally uncoupled.

Chapter 4 presents an investigation of the dominance of some eigenvectors upon the incremental displacement response of materially nonlinear structures. Analytical parameters are developed as tools to carry out such an investigation. Five case studies are considered. The prominent result is that the previous diagonal system of equations is drasticaly reduced to a system whose dimension is the small number of the dominant degrees of

freedom.

Considering Chapters 3 and 4 as background material, Chapter 5 proceeds with the formulation of an eigenvector-based solution strategy, which has been organized in two phases: pre-iterative and iterative. Details, such as flowcharts and estimates of the computational work required in each phase, are also included.

In Chapter 6, four materially nonlinear structures are chosen as challenging applications of the proposed solution strategy. Evaluation of the eigenvector-based solution strategy and comparison with other methods complement this Chapter.

Finally, Chapter 7 contains a summary of the developed work, as well as conclusions and recommendations for future research. An Appendix describing the utilized material models ends this study.

CHAPTER 2

LITERATURE REVIEW

2.1 Introduction

In the context of the finite element method, the formulation of the static equilibrium of materially and/or geometrically nonlinear structures results in a set of nonlinear algebraic equations. The solution of these equations requires the application of a strategy, which is incremental and iterative in nature.

The development of solution strategies has followed a number of basic concepts. First, the control of a single load parameter has led to the formulation of the so-called load control methods, among which the Newton-Raphson strategies are well known. Second, the control of a single or a set of specific global degrees of freedom has led to the displacement control strategies. A third concept unifies the previous ideas, whereby load and displacements are concomitantly controlled. The arc-length strategies are based on this concept. Accounting for these concepts as background, many variants of the existing methods have emerged during the past three decades. Comprehensive reviews on the basic methods and their variants are available in the literature (Tillerson et al. 1973, Bergan et al. 1978, Ramm 1981, Noor 1981, Riks 1987, Bellini and Chulya 1987 and Felippa 1988).

The objective of this chapter is to present a selective review of some solution strategies which are currently in use. A general incremetal-iterative formulation, in which the load factor and the

6

displacement increment vector are the interdependent variables, is first intoduced. As special cases of this general formulation, the classical Newton-Raphson methods, the displacement control strategy and the arc-length methods are reviewed. Then, the novel class of the reduction methods are addressed. Next, a layout of the organization of the solution strategies in the program NISA (Stegmüller et al. 1983) is presented. A discussion on the limitations of the current solution strategies ends this Chapter.

2.2 General Formulation

Considering a typical iteration within a solution step, illustrated in Fig. 2.1, the displacement increment vector is computed through the solution of the following set of equilibrium equations

$$[K]_t^{i-1} \{\Delta r\}^i = \Delta\rho^i \{R\} + \{\Delta Q\}^{i-1}, \qquad [2.1]$$

where $[K]_t^{i-1}$ is the tangent stiffness matrix updated at the end of the previous iteration; $\{\Delta r\}^i$ and $\Delta\rho^i$ are respectively the unknown increments of displacements and load factor. In addition, the vector of unbalanced forces is given as

$$\{\Delta Q\}^{i-1} = \rho^{i-1} \{R\} - \{F\}^{i-1}, \qquad [2.2]$$

where ρ^{i-1}, $\{R\}$ and $\{F\}^{i-1}$ are respectively the total load factor at the end of the previous iteration, the vector of the reference forces and the vector of the internal equivalent nodal loads.

Since the number of unknowns in [2.1], (N+1), is greater than the number of equations (N), an auxiliary equation is needed so that a solution can be found. Usually, this additional equation represents a constraint for the unknown variables $\{\Delta r\}^i$ and $\Delta \rho^i$. A general constraint equation can then be expressed as

$$g(\{\Delta r\}^i, \ \Delta \rho^i) = 0,$$

[2.3]

where g is a scalar and real function. The system formed by the equations [2.1] and [2.3] can now be solved iteratively for the unknown variables $\{\Delta r\}^i$ and $\Delta \rho^i$ with the aid of a specific solution strategy.

2.3 The Newton-Raphson Methods

The classical Newton-Raphson methods are the most representative of the load control concept. For these methods, expressions [2.1] and [2.3] specialize to yield respectively

$$[K]^{i-1} \{\Delta r\}^i = \rho^{i-1} \{R\} - \{F\}^{i-1}$$

[2.4]

and

$$\Delta \rho^i = 0, \text{ that is, } \rho^{i-1} = \rho^i = \rho^b,$$

[2.5]

where ρ^b is a known load factor prescribed by the analyst. Geometrically, expression [2.5] represents a plane orthogonal to the axis of the load factor and also represents the iteration path for these methods. The trace of this plane is shown in Fig. 2.2.

The names Initial Stiffness, Modified Newton-Raphson and Standard Newton-Raphson have been coined to identify the scheme through which the stiffness matrix is updated in the expression [2.4]. Thus, the stiffness matrix is updated only at the beginning of the first solution step in the case of the Initial Stiffness Method. In the Modified Newton-Raphson Method, the stiffness matrix is updated only at the beginning of the solution step. On the other hand, the stiffness matrix is updated for every iteration in the Standard Newton-Raphson Method. These schemes are illustrated in Fig. 2.2.

Kao (1974) has compared the efficiency of these methods. In short, a considerable number of iterations is required to provide an accurate solution in the highly nonlinear range. Crisfield (1979) has improved the efficiency of the Newton-Raphson methods by implementing an acceleration factor. Zienkiewicz et al. (1969) applied these methods in the analysis of elasto-plastic structures subjected to loads up to the ultimate level.

2.4 The Displacement Control Method

In the displacement control method, analogous to load control, the value of a preselected global degree of freedom is prescribed at the beginning of a solution step. This yields

$$\Delta r_p^1 = \Delta r_p^*,$$ [2.6]

where the subscript p denotes the order of the prescribed degree of freedom, whereas $*$ designates the prescribed value.

Based on the linearized form of the set of equations [2.1], the displacement increment vector can be decomposed in two parts. This gives

$$\{\Delta r\}^i = \{\Delta r\}^i_I + \Delta\rho^i \{\Delta r\}^i_{II} ,$$

[2.7]

where the displacement components $\{\Delta r\}^i_I$ and $\{\Delta r\}^i_{II}$ can be computed respectively through the solution of

$$[K]^{i-1} \{\Delta r\}^i_I = \{\Delta Q\}^{i-1}$$

[2.8]

and

$$[K]^{i-1} \{\Delta r\}^i_{II} = \{R\}.$$

[2.9]

In addition to the expressions [2.8] and [2.9], the constraint equation [2.3] is specialized to yield

$$\left(\Delta r_p^1\right)_I + \Delta\rho^1 \left(\Delta r_p^1\right)_{II} = \Delta r_p^* ,$$

[2.10]

which is defined within the pre-iterative phase, as shown in Fig. 2.3. Thus, the first load factor increment is computed from [2.10] as

$$\Delta\rho^1 = \frac{\Delta r_p^* - \left(\Delta r_p^1\right)_I}{\left(\Delta r_p^1\right)_{II}} .$$

[2.11]

Throughout the iterative phase, $\Delta r_p^i = 0$ and [2.11] is simply

$$\Delta \rho^i = -\frac{\left(\Delta r_p^i\right)_1}{\left(\Delta r_p^i\right)_{II}} \quad , \qquad i=2, \ldots, b \ .$$

[2.12]

The set of equations [2.7], [2.8], [2.9], [2.11] and [2.12] comprises the framework of the displacement control method. The pre-iterative and iterative phases of this method are illustrated in Fig. 2.3. The original version of this method, due to Pian and Tong (1970), has come out with the drawbacks of lack of symmetry and bandness of the stiffness matrix. Batoz and Dhatt (1979) have circumvented these problems by postulating the displacement decomposition stated in [2.7] and the partial solutions of [2.8] and [2.9]. Although the method can overcome limit points, failures in the description of snap-back behavior have been reported by Riks (1979).

2.5 The Arc-Length Methods

The arc-length methods unify the concepts of load and displacement control. In this class of methods, the load factor increment and the displacement increment vector are the unknown variables. The equilibrium formulation makes use of the same equations [2.7], [2.8] and [2.9] as for the displacement control method.

The novel concept in the arc-length methodology is the definition of a finite arc-length as a constraint equation. This feature makes the method very robust, since a unique relation between the

continuous arc-length and the load factor or the norm of displacements is now available. Figure 2.4 illustrates the continuous and the finite arc-lengths and also the character of uniqueness mentioned above.

The arc-length has been defined in various forms by different researchers. An account of some available definitions has been given by Bellini and Chulya 1987. A general expression for the arc-length can be stated as

$$\left(\Delta L^{i}\right)^{2} = C_{L}\left[C_{\rho}\left(\left(\rho^{i-1}-\rho^{a}\right)+\Delta\rho^{i}\right)^{2} + C_{r}\left(\langle\Sigma\Delta r\rangle^{i}\{\Sigma\Delta r\}^{i}\right)\right], \qquad [2.13]$$

where ΔL^{i} is the finite arc-length that corresponds to the ith iteration and C_{ρ}, C_{r} and C_{L} are prescribed constants that regulate the magnitude of the load component, of the displacement component and of the overall size of the arc-length, respectively. The other ingredients of [2.13] are illustrated in Fig.2.5.

Some of the proposed definitions of the arc-length are outlined by specialization of the general expression [2.13]. Table 2.1 summarizes the results of this process and refers to the original sources in the technical literature. It is noted that some methods have adopted a constraint equation in addition to the arc-length definition. The reason behind this rests on the fact that a linearization of the iteration path is sometimes preferable and leads to a much simpler formulation (Wempner 1971, Riks 1972 and Ramm 1981). Figure 2.5 shows some of the iteration paths described in Table 2.1. In addition to these contributions, Fried (1984) has

suggested an orthogonal iteration path, also indicated in Fig. 2.5. Another point of attention is the attempt of controlling only the component of the arc-length that relates to the load level (Park 1982, Crisfield 1981 and De Borst 1986). A control of the global size of the arc-length has not been envisaged to date.

2.6 The Reduction Methods

So far, the development and application of the reduction methods have been restricted to the area of geometrically nonlinear structures. The basic idea behind this class of solution strategies is to reduce the total number of global degrees of freedom of the discretized structure. To accomplish this goal, a set of basis vectors is needed in order to transform the equilibrium and constraint equations from the basis of the global degrees of freedom to the basis given by the selected vectors. Usually, a Rayleigh-Ritz technique (Bathe and Wilson 1976) is employed in this basis transformation.

Considering linearly elastic material and geometrically nonlinear behavior, the incremental-iterative equilibrium equations are expressed as

$$\left[[K]_L + [K]_{tG}^{i-1} \right] \left\{ \Delta r \right\}^i = \Delta \rho^i \left\{ R \right\} + \left\{ \Delta Q \right\}^{i-1},$$

[2.14]

where $[K]_L$ and $[K]_t^{i-1}{}_G$ are respectively the linear stiffness matrix and the tangent nonlinear geometrical stiffness matrix. The other terms

in [2.14] are the same as for [2.1]. The displacement increment vector in [2.14] can also be decomposed according to expression [2.7].

Assuming a general set of basis vectors such as

$$[V] = \left[\{v\}_1, \ldots, \{v\}_j, \ldots, \{v\}_m \right], \quad M < N \qquad [2.15]$$

where $\{v\}_j$ is the jth basis vector, the displacement increment vector is given as a linear combination of the M basis vectors. This yields

$$\{\Delta r\}^i = [V] \{\Delta\varphi\}^i, \qquad [2.16]$$

where $\{\Delta\varphi\}^i$ is the generalized displacement increment vector. After the substitution of [2.16] into [2.14] and the consecutive premultiplication by $[V]^T$, the following expression results

$$[V]^T \left[[K]_L + [K]_t^{i-1}{}_G \right] [V] \{\Delta\varphi\}^i = \Delta\rho^i [V]^T \{R\} + [V]^T \{\Delta Q\}^{i-1}, \qquad [2.17]$$

which can be further simplified as

$$\left[[\tilde{K}]_L + [\tilde{K}]_t^{i-1}{}_G \right] \{\Delta\varphi\}^i = \Delta\rho^i \{\tilde{R}\} + \{\widetilde{\Delta Q}\}^{i-1}. \qquad [2.18]$$

The symbol ~ in [2.18] denotes the transformed matrix or vector. Furthermore, the set of M equations in [2.18] represents the statement of equilibrium in the basis of the selected basis vectors.

Similarly to [2.17], the original arc-length constraint equation [2.13] can be transformed to the new basis. This yields

$$\langle\Sigma\Delta\varphi\rangle^i [V]^T [V] \{\Sigma\Delta\varphi\}^i + \left(\left(\rho^{i-1} - \rho^a\right) + \Delta\rho^i\right)^2 = \left(\Delta L^i\right)^2, \qquad [2.19]$$

where all the constants in [2.13] are made equal to the unity for the sake of simplicity. The set of equations [2.18] and [2.19] forms the framework of the reduction methods. In addition, it is noted that the dimension of the original system of equations has been reduced from N+1 to M+1.

The crucial point within the reduction methods is the selection of the basis vectors in [2.16]. Nagy (1977) and Almroth et al. (1978) have proposed a linear global di placement solution in addition to some buckling modes to constitute the set of the basis vectors. On the other hand, Noor and Peters (1980) have adopted path derivative vectors. These vectors are obtained by differentiating the equilibrium equations with respect to the arc-length.

2.7 Solution Strategies in the Program NISA

The work to be presented in Chapters 3 through 6 has made extensive use of and has been implemented in the NISA code (Stegmüller et al. 1983).

The classical Newton-Raphson Methods, the Displacement Control Method and the Arc-Length Method are implemented in the current version of the program NISA. Within each method, the stiffness matrix can be updated according to the schemes given by the Initial Stiffness, Modified Newton-Raphson and the Standard Newton-Raphson schemes. The implemented version of the Arc-Length Method adopts a constant arc-length which has been

proposed by Ramm (1981). The Displacement Control Method follows the formulation due to Batoz and Dhatt (1979).

The original code of the program has included a single subroutine to cast all methods. The current version, however, incorporates a master subroutine for each method. This subroutine calls other auxiliary routines that take care of checking the convergence criteria for displacements and unbalanced forces and of computing the stiffness parameter. In addition, a general subroutine that initializes the selected solution strategy has also been implemented. The layout of the organization of the subroutines for the outlined methods is shown in Fig. 2.6.

2.8 Discussion

Despite the progress that the field of solution strategies has undergone, some challenges are still present. This is specially true in the application of the existing solution strategies in the analysis of reinforced concrete structures. For this type of problem, sharp changes in stiffness may occur due to the highly nonlinear material behavior. In severely damaged zones, strain localization may take place. Typical load-deflection curves of reinforced concrete structures usually present ascending branches with drastic changes in stiffness, limit points and unstable and steep descending branches. In addition, the capture of the correct failure mode is also a demanding problem.

The Newton-Raphson Methods are generally able to describe load-deflection histories prior to the level of ultimate load. The arbitrarily prescribed load increments and the possibility of

encountering a nearly singular stiffness matrix often hamper the overcoming of limit points. Even within the ascending branches, a considerable number of iterations is usually required to trace the highly nonlinear ranges of behavior.

The Displacement Control Method can pass limit points. However, the method fails in the description of snap-back behavior, since the selected global degree of freedom can not be prescribed at the snap-back point.

The Arc-Length Methods are capable of overcoming limit points and of tracing problems including snap-back behavior. Nevertheless, the iterative phase of these methods requires a great amount of computational effort due to the large dimensions of the matrices and vectors involved. For some of the arc-length methods, the equation that gives the load factor increment is of a quadratic order (Table 2.1). This is costly and demands a criterion for the selection of the right root. Another difficulty relates to the uncontrolled size of the arc-length. If the arc-length is large, limit points might : be captured and the resulting solution may drift from the correct curve.

The Reduction Methods have been applied only in the realm of geometrically nonlinear structures. Applications in the field of materially nonlinear structures are not known in the technical literature. The major drawback in these methods is the lack of orthonormality among the basis vectors. The resulting equilibrium equations are reduced, but still coupled. In addition, a rational criterion for mode selection has not been proposed in the available methods. Nevertheless, this class of methods is undoubtedly the most

promising direction to be followed in the development of novel solution strategies.

METHOD	C_ρ	C_r	C_L	ARC-LENGTH EQUATION	CONSTRAINT EQUATION	Order i $\Delta\varphi$(4)	ITERATION PATH (1)	REFERENCE
The Updated Normal Path	1	1	1	$(\Delta L^i)^2 = (\rho^{i-1} - \rho^a + \Delta\rho)^2 + \langle\Sigma\Delta r\rangle^i\{\Sigma\Delta r\}^i$	$(\rho^{i-1} - \rho^a)\Delta\rho^i + \langle\Sigma\Delta r\rangle^{i-1}\{\Delta r\}^i = 0$	1st	Sequel of Normal Planes	Wempner 1971 Riks 1972
The Constant Arc-Length	1	1	1	$(\Delta L^i)^2 = (\Delta\rho)^2 + \langle\Delta r\rangle^i\{\Delta r\}^i$	$\Delta\rho^i\Delta\rho^i + \langle\Delta r\rangle^i\{\Delta r\}^i = 0$	1st	A Fixed Normal Plane	Ramm 1981
The Spherical Arc-Length	1	1	1	$(\Delta L^i)^2 = (\rho^{i-1} - \rho^a + \Delta\rho)^2 + \langle\Sigma\Delta r\rangle^i\{\Sigma\Delta r\}^i$	The Arc-Length Equation	2nd	A Sphere	Crisfield 1981 Ramm 1981
The Circular Arc-Length	0	1	1	$(\Delta L^i)^2 = \langle\Sigma\Delta r\rangle^i\{\Sigma\Delta r\}^i$	The Arc-Length Equation	2nd	A Circle	Crisfield 1981
The Ellipsoidal Arc-Length	S_p (3)	1	1	$(\Delta L^i)^2 = S_\rho(\rho^{i-1} - \rho^a + \Delta\rho)^2 + \langle\Sigma\Delta r\rangle^i\{\Sigma\Delta r\}^i$	The Arc-Length Equation	2nd	An Ellipsoid	Park 1982
The Indirect Displacement Control	0	1	1	$(\Delta L^i)^2 = \langle\Sigma\Delta r\rangle^{i-1}\{\Sigma\Delta r\}^i$ (2)	The Arc-Length Equation	1st	Sequel of Normal Planes	De Borst 1986

(1): Classification for the particular case of two degrees of freedom.
(2): A set of preselected degrees of freedom is used in this relation
(3): Sp stands for stiffness parameter (Bergan et al. 1978)
(4): Order of the load factor increment within the constraint equation.

Table 2.1: A summary of the arc-length and constraint equations.
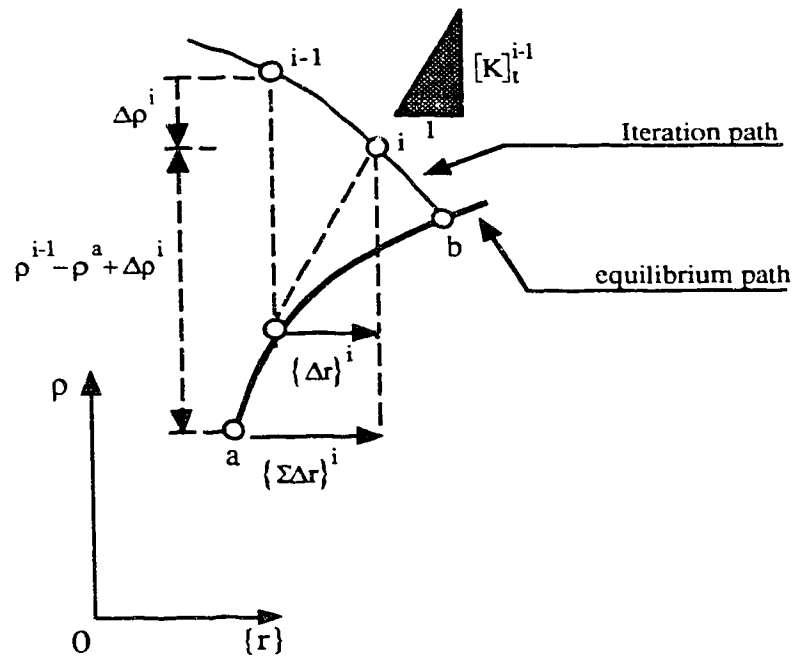
Figure 2.1: A typical iteration within a solution step.
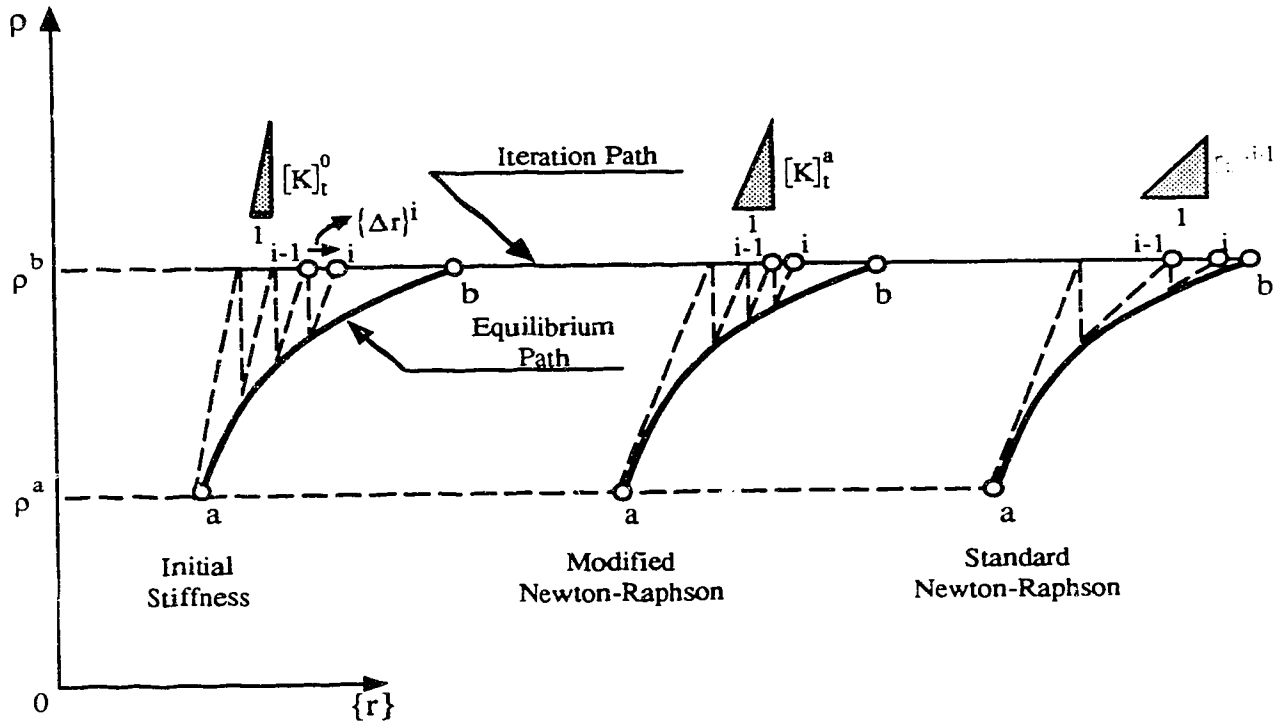
Figure 2.2: Illustration of the Newton-Raphson iterative schemes.
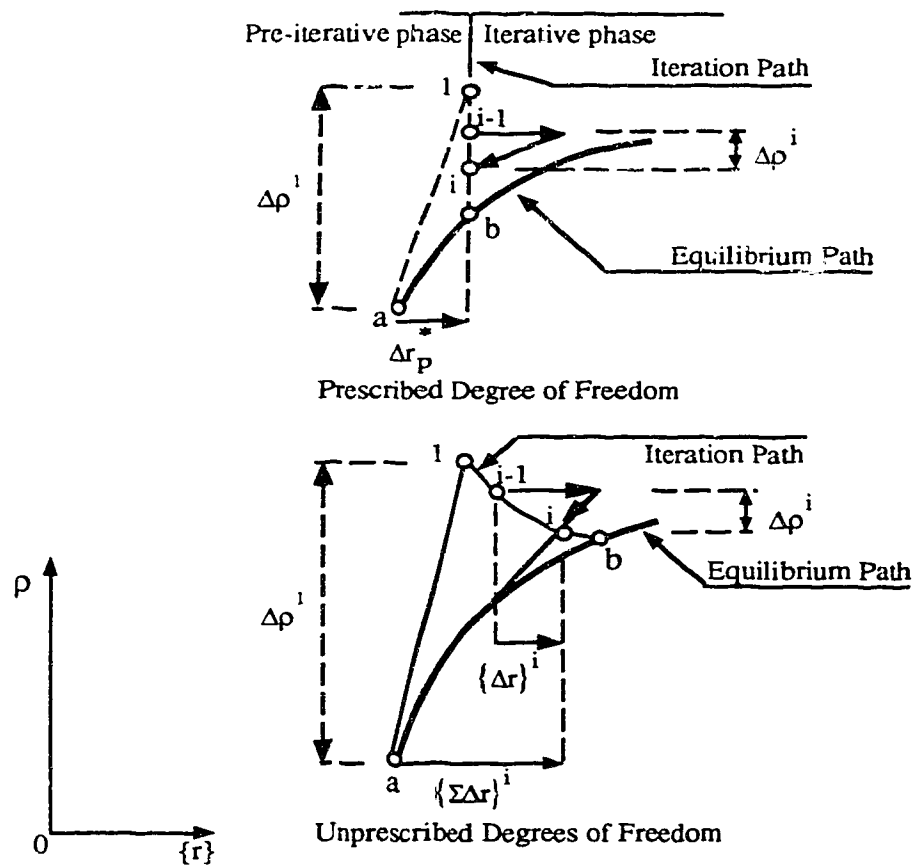
Figure 2.3: Illustration of the displacement control method.
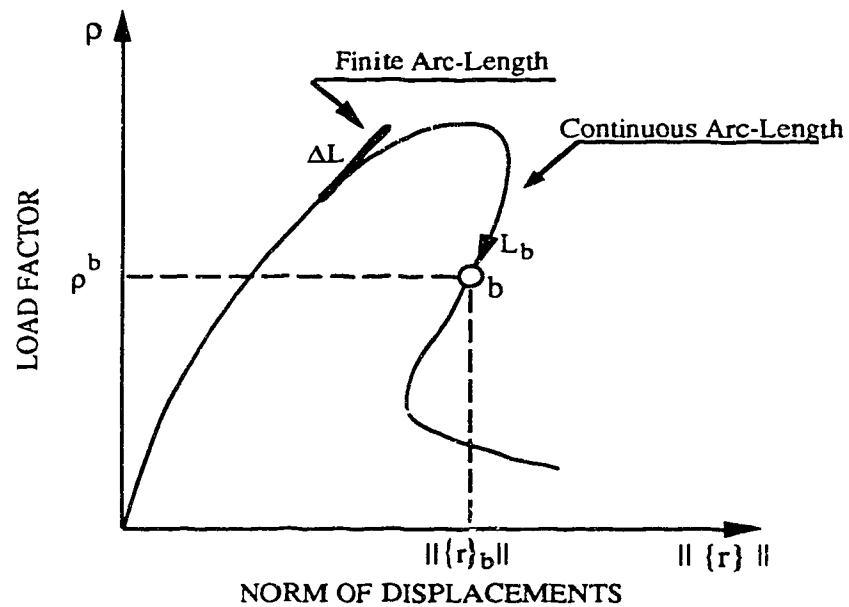
Figure 2.4: Illustration of the continuous and finite arc-lengths.
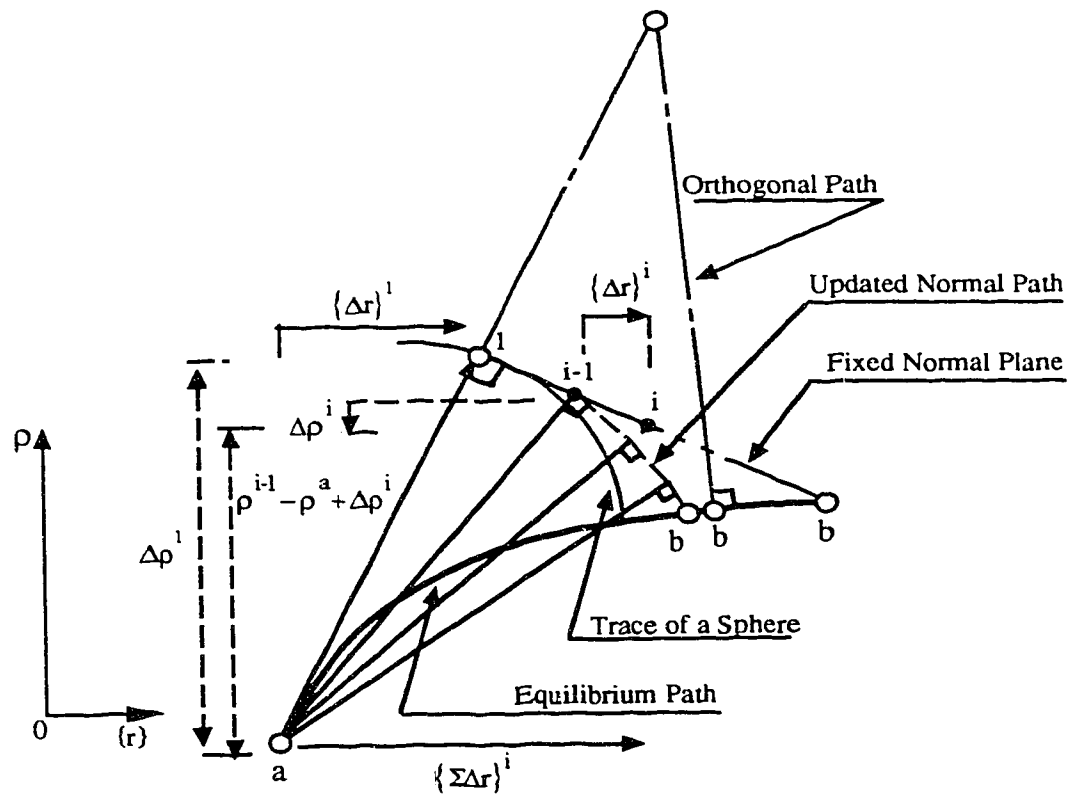
Figure 2.5: Illustration of Some Arc-Length Methods.
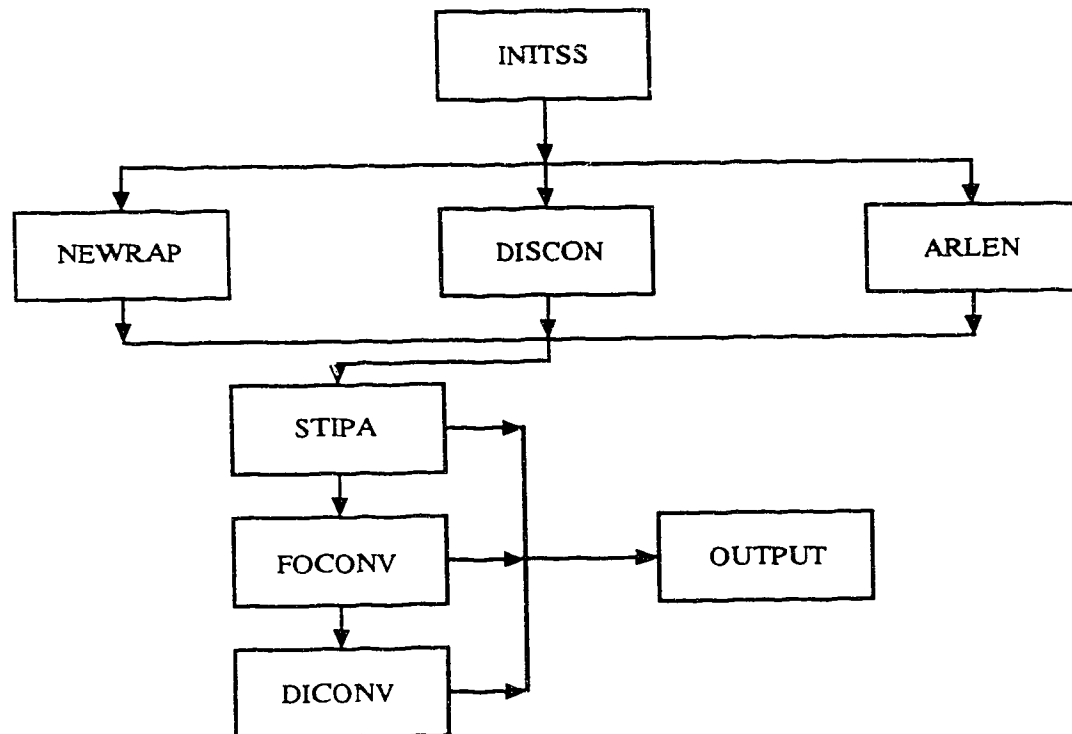
Figure 2.6: Layout of subroutines about solution strategies in NISA.

CHAPTER 3

FORMULATION OF THE INCREMENTAL EQUILIBRIUM EQUATIONS IN THE BASIS OF THE EIGENVECTORS

3.1 Introduction

The formulation of the incremental equilibrium equations for a nonlinear structure, within the framework of the finite element method, has traditionally employed the natural basis for the equilibrium description. The natural basis, as described by Bathe and Wilson (1976), is formed by unit vectors which are associated with the nodal displacements in the direction of the global coordinate axes. Coupled equilibrium equations and symmetrically banded stiffness matrices are direct consequences of this approach. Furthermore, considerable computational effort is required through the steps of factorization, reduction and backsubstitution in the Gauss elimination process adopted for the equation solver as discussed by Wilson (1989).

To simplify the formulation, a change of base vectors may be considered. Change of basis has been common in some disciplines of structural analysis. In structural dynamics (Clough and Penzien ,1975), the mode superposition method adopts the natural modes of vibration as a convenient basis for the description of the dynamic equilibrium of linearly elastic structures. Recently, Wilson and Bayo (1986) have argued that special Ritz vectors would comprise a more effective basis for dynamic analysis, although the generated vectors are load dependent. For geometrically nonlinear structures, Almroth

et al. (1978) and Noor and Peters (1980) introduced a reduced basis technique. Almroth et al. selected linear solution vectors, whereas Noor chose path derivatives to form the reduced basis. Nagy (1977) adopted the buckling modes as base vectors to investigate problems with mild change in geometry. In a broader scope, Argyris (1965) proposed pure straining modes, imposed at element level, to constitute an alternative basis to be used in the element formulation and applied to various nonlinear problems. However, the large majority of the base vectors mentioned above have been applied to linearly elastic materials and have given rise to coupled equilibrium equations. A summary of the properties and implications of some bases reported in the technical literature is given in Table 3.1. Some of the studies report that uncoupled equilibrium equations and simpler solutions for the unknown displacement increments constitute the beneficial consequences of a change from the natural to the eigenvector basis.

The objective of this Chapter is to formulate the incremental equilibrium equations in the basis of the eigenvectors of the tangent stiffness matrix of structures with material nonlinearities. Firstly, the formulation of the incremental equilibrium equations in the natural basis is briefly presented. Then, a change to a general basis is carried out, followed by the formulation of incremental equilibrium in the basis of the eigenvectors. A discussion on the form of the resulting equilibrium equations finalizes the Chapter.

3.2 Incremental Equilibrium Equations in the Natural Basis

The displacement formulation in the finite element method has conventionally applied the natural unit vectors,

$$<e>_i = <0,....,0,e_i=1,0,....,0> \qquad i = 1,2,....,N \qquad [3.1]$$

as a basis to define the N-dimensional vector space of the global degrees of freedom. From all the N vector coordinates in [3.1], only the ith coordinate is nonzero and corresponds to the ith global degree of freedom of the structure. The displacement increment vector is in the same vector space and therefore can be written as a linear combination of the base vectors,

$$\{\Delta r\} = \sum_{i=1}^{N} \Delta u_i \{e\}_i, \qquad [3.2]$$

where Δu_i is the ith scalar displacement increment. Similarly, the reference force vector can be defined in terms of the base vectors as

$$\{R\} = \sum_{i=1}^{N} R_i \{e\}_i, \qquad [3.3]$$

where R_i is the ith scalar reference force.

Under the condition of proportional loading, the applied incremental force vector is denoted by

$$\{\Delta R\} = \Delta p \{R\}, \qquad [3.4]$$

where $\Delta\rho$ is the load factor. Substituting [3.3] into [3.4] gives

$$\{\Delta R\} = \Delta\rho \sum_{i=1}^{N} R_i \{e\}_i. \tag{3.5}$$

Expression [3.5] can easily be extended to incorporate the case of nonproportional loading by allowing for multiple and distinct load factors.

The matrix forms of expressions [3.2] and [3.5] are respectively,

$$\{\Delta r\} = [E] \{\Delta u\} \tag{3.6}$$

and

$$\{\Delta R\} = \Delta\rho [E] \{R\}, \tag{3.7}$$

where the columns of [E] are the natural base vectors expressed in [3.1]. Thus, [E] is a unit diagonal matrix and defines an orthonormal basis since

$$<e>_i \{e\}_j = \delta_{ij}, \tag{3.8}$$

where δ_{ij} is the Kronecker delta as denoted by Hawkins (1963).

Within a typical solution step, the incremental equilibrium equations can be described as

$$[K] \{\Delta r\} = \{\Delta Q\}, \tag{3.9}$$

where $[K]_t$ is the tangent stiffness matrix and $\{\Delta Q\}$ is the unbalanced force increment vector which is defined as a function of the external and internal force vectors, respectively $\{R\}$ and $\{F\}$, as

$$\{\Delta Q\} = (\rho + \Delta\rho)\{R\} - \{F\}. \qquad [3.10]$$

Similarly to $\{\Delta r\}$, the unbalanced force increment vector $\{\Delta Q\}$ is in the same vector space defined by the vectors in [3.1]. The jth column of $[K]_t$ represents the set of nodal forces necessary to mantain equilibrium for the set of displacements given by $\{e\}_j$. Therefore, $[K]_t$ is, as well, formulated in the vector space spanned by the natural base vectors.

If the natural base vectors do not constitute a convenient basis from the practical standpoint, a change of basis may be performed on the displacement increment and unbalanced force increment vectors.

3.3 Change of Basis

Let a new set of base vectors be written as

$$[V] = [\ \{v\}_1, \dots, \{v\}_N\ ]. \qquad [3.11]$$

The displacement and the unbalanced force increment vectors are now written as

$$\{\Delta r\} = [V]\{\Delta u\}_v \qquad [3.12]$$

and

$$\{\Delta Q\} = [V]\{\Delta Q\}_v, \qquad [3.13]$$

where the vectors with subscript v in [3.12] and [3.13] contain respectively the scalar components of the displacement increment and unbalanced force increment vectors in the new coordinates defined by [3.11]. Substituting [3.12] and [3.13] into [3.9] gives

$$[K]_t \, [V] \, \{\Delta u\}_v = [V] \, \{\Delta Q\}_v. \tag{3.14}$$

Premultiplying [3.14] by the inverse of the matrix [V] yields

$$[V]^{-1} \, [K]_t \, [V] \, \{\Delta u\}_v = \{\Delta Q\}_v, \tag{3.15}$$

which is further reduced to

$$[K]_{t_v} \, \{\Delta u\}_v = \{\Delta Q\}_v, \tag{3.16}$$

where $[K]_{t_v}$ represents the tangent stiffness matrix in the new basis.

Considering a general basis, the numerical solution of [3.16] may still require a considerable amount of computational effort since it involves operations such as matrix inversion and multiplication. In the particular case of an orthonormal basis, the property

$$[V]^T = [V]^{-1} \tag{3.17}$$

holds and the inversion is reduced to a transposition operation as demonstrated by Pettofrezo (1966). Despite this simplication, the equations outlined in [3.16] may be coupled if the transformed stiffness is not represented by a main diagonal matrix. Uncoupled equations are achieved if the base vectors satisfy the eigenproblem.

The research work reported herein employs the eigenvectors of the tangent stiffness matrix as base vectors.

3.4 Incremental Equilibrium Equations in the Eigenvector Basis

The eigenproblem, related to materially nonlinear structures, is stated as

$$[K]_t \{\phi\}_i = \lambda_i \{\phi\}_i. \tag{3.18}$$

The solution of [3.18] furnishes N eigenpairs $(\lambda_i, \{\phi\}_i)$, where λ_i is an eigenvalue and $\{\phi\}_i$ is the corresponding eigenvector. It is also of practical significance to note that the expression [3.18] can be thought of as a set of N equilibrium equations. The right hand side is a set of external forces proportional to a set of displacements $\{\phi\}_i$. The proportionality factor is the uncoupled stiffness λ_i. The left hand side denotes a set of equilibrating forces required to mantain the deformed shape represented by the eigenvector $\{\phi\}_i$.

The linearity of the standard eigenproblem in [3.18] is not in conflict with the nonlinear nature of the stiffness matrix. The lack of conflict is realized if the stiffness matrix is linearized within a typically small displacement increment.

The expression [3.18] can be expanded in matrix form to include all eigenpairs

$$[K]_t [\Phi] = [\Phi] [\Lambda], \tag{3.19}$$

where the columns of $[\Phi]$ are the eigenvectors and $[\Lambda]$ is a diagonal matrix formed by the eigenvalues. The eigenvectors of a symmetric

and positive definite matrix are linearly independent and orthogonal (Wilkinson 1965). If the eigenvectors are further normalized with respect to their Euclidean norms, then

$$<\phi>_i \{\phi\}_j = \delta_{ij}. \qquad [3.20]$$

Expanding [3.20] to include all eigenvectors gives

$$[\phi_i]^T [\Phi] = [I], \qquad [3.21]$$

in which [I] is the identity matrix. Therefore, the eigenvectors of the tangent stiffness matrix comprise an orthonormal basis for the N-dimensional vector space of the global degrees of freedom. Thus, the displacement and unbalanced force increment vectors can be expressed as a linear combination of the normalized eigenvectors

$$\{\Delta r\} = \sum_{i=1}^{N} \Delta \alpha_i \{\phi\}_i \qquad [\quad]$$

and

$$\{\Delta Q\} = \sum_{i=1}^{N} \Delta \gamma_i \{\phi\}_i \qquad [3.23]$$

in which $\Delta \alpha_i$ and $\Delta \gamma_i$ are respectively the generalized displacement and the generalized unbalanced force increments corresponding to the ith eigenvector. In matrix format, expressions [3.22] and [3.23] are written as

$$\{\Delta r\} = [\Phi] \{\Delta \alpha\}$$ [3.24]

and

$$\{\Delta Q\} = [\Phi] \{\Delta \gamma\}$$ [3.25]

Substituting [3.24] and [3.25] into the incremental equilibrium equations, expression [3.9], yields

$$[K]_t [\Phi] \{\Delta \alpha\} = [\Phi] \{\Delta \gamma\}$$ [3.26]

Substituting [3.19] into [3.26] gives

$$[\Phi] [\Lambda] \{\Delta \alpha\} = [\Phi] \{\Delta \gamma\}$$ [3.27]

After premultiplying [3.27] by $[\Phi]^T$ and recalling the orthonormality property of the eigenvectors in [3.21], expression [3.27] is further reduced to

$$[\Lambda] \{\Delta \alpha\} = \{\Delta \gamma\}.$$ [3.28]

The above expression represents the set of incremental equilibrium equations formulated in the basis of the eigenvectors of the tangent stiffness matrix. From [3.28], the ith generalized displacement is conveniently computed as

$$\Delta \alpha_i = \Delta \gamma_i / \lambda_i$$ [3.29]

in which $\Delta\gamma_i$ is the ith generalized unbalanced force increment. The eigenvalue λ_i in [3.29] is interpreted as the uncoupled stiffness which is associated with the eigenvector $\{\phi\}_i$.

The generalized unbalanced force increment vector can be expressed in terms of the unbalanced force increment vector given in the natural basis. From expression [3.25],

$$\{\Delta\gamma\} = [\Phi]^T \{\Delta Q\}, \qquad [3.30]$$

where the ith generalized unbalanced force increment is

$$\Delta\gamma_i = <\phi>_i \{\Delta Q\}. \qquad [3.31]$$

Substituting [3.31] into [3.29] yields

$$\Delta\alpha_i = (<\phi>_i \{\Delta Q\}) / \lambda_i. \qquad [3.32]$$

This expression is employed to calculate the generalized displacement increments within the iterative process of the solution strategy covered in Chapter 5. From [3.32], the equilibrium equations

$$\lambda_i \Delta\alpha_i = <\phi>_i \{\Delta Q\}, \qquad i = 1,2, \dots ,N \qquad [3.33]$$

are completely uncoupled as opposed to the standard form established in [3.9].

3.5 Discussion

Some important observations can be drawn from the form of the equations in [3.32]. Firstly, it is noted that the generalized

displacement increment can easily be computed by [3.32] since all participating variables are uncoupled.

Under the assumption of distinct eigenvalues, the eigenvalue λ_i is directly identified as the stiffness coefficient that corresponds to the type of deformation mode represented by the eigenvector $\{\phi\}_i$. An extensional stiffness, for example, is associated with an extension mode and so on.

The direction of the unbalanced force increment vector, relative to the eigenvector, affects the computation of the numerator of [3.32]. For instance, the generalized displacement increment vanishes in the case of orthogonality between $\{\Delta Q\}$ and $\{\phi\}_i$.

The degree of nonlinearity that a structural member exhibits, such as progressive cracking or crushing for concrete and yielding for metals, can reasonably reduce the stiffness coefficient λ_i, which gives rise to a larger generalized displacement $\Delta\alpha_i$ in [3.32]. Theoretically, the eigenvalue λ_i can assume a zero value at limit points of a structural response characterized by progressive damage. However, a zero eigenvalue is not commonly encountered in a computational analysis of a practical problem. Moreover, the orthogonality condition [3.20] does not take place at a limit point as pointed out by De Borst (1986). In addition, the unbalanced force increments in [3.32] are expected to decrease at the vicinity of a limit point. Thus, the generalized displacement increment is usually finite and computable at a limit point.

Lastly, the calculation of the generalized displacement increments requires the solution of the eigenproblem stated in [3.19]. Fortunately, efficient techniques such as the subspace iteration

method, described by Bathe (1971) and improved by Moler and Stewart (1973) and further by Wilson and Farhat (1988), provides economy and accuracy in the solution of the eigenproblem.

Type of Base Vectors	Type of Problem		Orthogonal	Generation of the Base Vectors	Equilibrium Equations	Level of Implementation	References
	Static	Dynamic					
Pure Straining Modes	Materially & Geometrically Nonlinear	Materially & Geometrically Linear	No	Heuristic	Full & Coupled	Element	Argyris (1965)
Natural Modes of Vibration		Materially & Geometrically Linear	Yes	Eigenanalysis	Full & Uncoupled	Structure	Clough & Penzien (1975)
Buckling Modes	Materially Linear & Geometrically Nonlinear		Yes	Eigenanalysis	Reduced & Uncoupled	Structure	Nagy (1977)
Linear Solution Vectors	Materially Linear & Geometrically Nonlinear		No	Displacement Solution of Equilibrium Euations	Reduced & Coupled	Structure	Almroth et al (1978)
Path Derivative Vectors	Materially Linear & Geometrically Nonlinear		No	Differentiation relative to the Arc Length	Reduced & Coupled	Structure	Noor (1980)
Ritz Vectors		Materially & Geometrically Linear	No	Static Solution for Dynamic Forces	Reduced & Coupled	Structure	Wilson and Bayo (1986)

Table 3.1 : Summary of the properties of some sets of base vectors reported in the technical literature.

CHAPTER 4

DOMINATION OF EIGENVECTORS OF MATERIALLY NONLINEAR STRUCTURES

4.1 Introduction

An eigenanalysis of a nonsingular tangent stiffness matrix provides all basic modes of deformation (the eigenvectors) of a materially nonlinear structure. According to expression [3.22] in the previous Chapter, the actual displacement increment vector can be decomposed in terms of the eigenvectors. All modes of deformation must comply with the conditions of kinematic admissibility, which are the prescribed displacement boundary conditions and the internal strain compatibility as discussed by Malvern (1969).

In practice, structures sustain and transfer loads by deflecting through specific modes of deformation. Structural members, such as shallow beams, corbels and rods, for instance, deform through bending, shear distortion and extension modes respectively.

The structural stiffness represents an integrated synthesis of more elemental properties, such as material properties and geometric proportions. Therefore, it seems reasonable to expect that, among all eigenvectors of the stiffness matrix, a very small number of modes would be active in the actual deformation mode exhibited by the structure, when subjected to the particular distribution of the externally applied loads. The participation of the activated eigenvectors in the displacement response would be accentuated in the presence of progressive damage, such as cracking and crushing

for concrete and yielding for metals. Thus, a linear combination of the active eigenvectors would accurately approximate the actual displacement response of the materially nonlinear structure within an incremental solution step. In this context, the most participating eigenvectors would dominate the deformational behavior of the structure and will henceforth be called the dominant eigenvectors.

Domination of eigenvectors is present in the dynamic analysis of linearly elastic structures. According to Hurty et al. (1971), the fundamental mode of vibration, which usually corresponds to the lowest natural frequency, may dominate the dynamic response of standard buildings subjected to common load distributions, such as wind loads. For static equilibrium problems involving materially nonlinear structures, however, domination of eigenvectors has not been investigated to date. Rots et al. (1987) performed an eigenanalysis of the stiffness matrix of tensile plain concrete specimens while studying non-homogeneity of deformation beyond the peak point of the pertinent load-deflection curve. Nevertheless, no reference to the existence of domination has been reported.

The objective of this Chapter is to develop and apply analytical parameters in order to investigate and demonstrate the existence of domination of certain eigenvectors on the displacement response of materially nonlinear structures. The investigation will cover the complete load history of the structure, from the undeformed state to physical structural collapse due to extensive material damage.

Different material constitutive relations are considered, since the level of domination of some eigenvectors may vary according to the type of material behavior.

The structural members chosen as case studies for this investigation are steel and reinforced concrete structures whose strengths and particular deflections have been predicted through the application of limit analysis or observed in experiments.

After this introduction, a brief description of the material models used in this study is presented. This is followed by the formulation of the analytical parameters to measure the domination of specific eigenvectors. After the formulation of the analytical parameters, the concept of an approximate displacement increment vector is developed. Then, the analytical parameters are applied to five case studies dealing with real structures. A discussion about the evidence of domination and further implications ends the Chapter.

4.2 Material Constitutive Relations

An elastoplastic constitutive relation, with bilinear stress-strain description for softening, yielding and hardening, has been used to describe the behavior of steel structures and the reinforcement in reinforced concrete members. This model parallels the original elastoplastic model developed by Nayak and Zienkiewics (1972) and has been implemented in the program NISA by Stegmüller et al. (1983).

An hypolelastic constitutive relation has been adopted for the modeling of concrete. This model was originally formulated by Elwi and Murray (1979). Currently, a modified version, due to Napoleao and Elwi (1990), has been implemented in the program NISA and applied to the modeling of the behavior of large scale reinforced concrete structures.

A standard linearly elastic constitutive relation is used solely in one example designed to study the effect of geometric proportions on the domination of eigenvectors of a plane structure.

The material models used herein have been formulated to deal with plane stress, plane strain and axisymmetric problems, with the exception of the elastoplastic model assigned to the reinforcement element, which describes uniaxial behavior.

A more detailed description of the material constitutive relations employed throughout this study forms the contents of Appendix A.

4.3 Analytical Parameters

4.3.1 Basic Assumptions and Definitions

The derivation of the analytical parameters, to measure the domination of eigenvectors on the displacement response of materially nonlinear structures, is based on the fact that the eigenvectors constitute a basis for the N dimensional vector space of the global degrees of freedom of the discretized structure. This has been discussed in Section 3.4.

Recalling expression [3.22], the actual displacement increment vector computed for a typical solution step, can be expanded as

$$\{\Delta r\} = \Delta\alpha_1 \{\phi\}_1 + \dots + \Delta\alpha_i \{\phi\}_i + \dots + \Delta\alpha_N \{\phi\}_N, \qquad [4.1]$$

where $\Delta\alpha_i$ and $\{\phi\}_i$, $i = 1,\dots,N$, are respectively the generalized displacement increments and the normalized eigenvectors.

Crandall (1983) refers to [4.1] as the mathematical statement of the expansion theorem defined for linear problems. Figure.4.1 illustrates the physical meaning of the expansion theorem in the N-dimensional vector space. The vector $\{\Delta r\}$ embodies an approximation due to the linearization of the incremental nonlinear equilibrium equations as previously discussed in Section 3.4. In addition, the eigenvectors in [4.1] are extracted from the tangent stiffness matrix assembled at the beginning of the considered solution step and are kept the same throughout the step.

The vector $\Delta\alpha_i\{\phi\}_i$ represents an eigenvector component of the actual displacement increment vector $\{\Delta r\}$. This component has an Euclidean norm $\|\Delta\alpha_i\{\phi\}_i\|$ and an angular position θ_i relative to $\{\Delta r\}$ as illustrated in Fig. 4.1. If the actual displacement increment vector is available, then the generalized displacement increment can be calculated by premultiplying [4.1] by $<\phi>_i$ which yields

$$<\phi>_i \{\Delta r\} = \Delta\alpha_1<\phi>_i\{\phi\}_1 + ... + \Delta\alpha_i<\phi>_i\{\phi\}_i + ... + \Delta\alpha_N<\phi>_i\{\phi\}_N. \qquad [4.2]$$

Recognizing the orthonormality property of the eigenvectors stated in [3.20], all terms on the right hand side of [4.2] vanish except the ith term. Thus,

$$\Delta\alpha_i = <\phi>_i \{\Delta r\}. \qquad [4.3]$$

Expression [4.3] represents the scalar product between the normalized eigenvector and the actual displacement increment vector and is of substantial importance regarding the evaluation of the analytical parameters to be formulated in the following sections.

In practice, it would be important to determine the level of participation of a typical eigenvector component $\Delta\alpha_i\{\phi\}_i$ in the formation of $\{\Delta r\}$ in [4.1]. The most effective procedure to carry out this task is to formulate analytical parameters through which a typical eigenvector component can be compared with the actual displacement increment vector. Since the comparison involves vector entities, the size and angular position are naturally selected to comprise the analytical parameters. The mathematical derivation of these parameters is based on simple concepts from vector algebra which is covered by Hawkins (1963).

4.3.2 The Relative Size Parameter

The relative size parameter provides a measure of the size of an eigenvector component relative to the size of the actual displacement increment vector. It is defined in terms of the Euclidean norm for both vectors:

$$\beta_i = \frac{\| \Delta\alpha_i\{\phi\}_i \|}{\| \{\Delta r\} \|} .$$

[4.4]

Applying the concept of vector norm to the numerator of [4.4] yields

$$\beta_i = \frac{\sqrt{\Delta\alpha_i^2 \langle\phi\rangle_i \{\phi\}_i}}{\| \{\Delta r\} \|} .$$

[4.5]

Furthermore, the orthonormality property of the eigenvectors can be applied to the numerator of [4.5]. Thus, the final form of the relative size parameter is:

$$\beta_i = \frac{|\Delta\alpha_i|}{\|\{\Delta r\}\|} .$$

[4.6]

Figure 4.1 illustrates the quantities in the numerator and denominator of [4.4] for a typical eigenvector component. It is further noted that the relative size parameter is a non-negative entity. The domain interval of the size parameter is [0 , 1].

4.3.3 The Angle Parameter

The angle parameter measures the angular position of the eigenvector component relative to the actual displacement increment vector as shown in Fig. 4.1. The derivation of this parameter employs the definition of the included angle between two 3-D vectors, which has been extended by Shilov (1977) to vectors in the N-dimensional vector space. The angle parameter is indirectly defined in terms of its cosine as

$$\cos\theta_i = \frac{\Delta\alpha_i\langle\phi\rangle_i\{\Delta r\}}{\|\Delta\alpha_i\{\phi\}_i\| \, \|\{\Delta r\}\|} .$$

[4.7]

Substituting [4.3] into [4.7] and accounting for the orthonormality property of the eigenvectors, the above expression is reduced to

$$\cos\theta_i = \frac{\Delta\alpha_i^2}{\sqrt{\Delta\alpha_i^2} \, \| \{\Delta r\} \|} \, .$$

[4.8]

and further to

$$c^{\prime} \cdot \frac{|\Delta\alpha_i|}{\| \{\Delta r\} \|} \, .$$

[4.9]

Comparing [4.9] with [4.6], it is directly concluded that

$$\cos\theta_i = \beta_i,$$

[4.10]

which means that the cosine of the angle parameter is equal to the size parameter. Moreover, [4.10] indicates that the concepts of size and angular position of a typical eigenvector component in [4.1] are directly dependent. From [4.10], the angle parameter is computed as

$$\theta_i = \cos^{-1}\beta_i.$$

[4.11]

The angle given above varies in the interval $[0°, 90°]$. Thus, the eigenvector $\{\phi\}_i$ is parallel to the actual displacement increment vector $\{\Delta r\}$ for $\theta_i = 0°$ and orthogonal for $\theta_i = 90°$ as schematically illustrated in Fig. 4.2. According to [4.3], a typical generalized displacement increment vanishes in the case of orthogonality between the normalized eigenvector and the actual displacement increment vector. Therefore, there is no contribution of the corresponding eigenvector component to the addition performed in [4.1].

4.3.4 The Participation Parameter

It is of practical importance to quantify, in percentage, the participation of each eigenvector component in the expansion [4.1]. For this purpose, the actual displacement increment vector is normalized with respect to its Euclidean norm, which gives the corresponding nondimensional unit vector $\{\Delta r\}_u$ as

$$\{\Delta r\}_u = \frac{\{\Delta r\}}{\|\{\Delta r\}\|}.$$ [4.12]

Dividing both sides of [4.1] by $\|\{\Delta r\}\|$ and applying the definition given in [4.12] yields

$$\{\Delta r\}_u = \sum_{i=1}^{N} \frac{\Delta \alpha_i}{\|\{\Delta r\}\|} \{\phi\}_i.$$ [4.13]

Since $\{\Delta r\}_u$ is a unit vector, the Euclidean norm of the vector on the right hand side of [4.13] must be unitary:

$$\left(\sum_{i=1}^{N} \left(\frac{\Delta \alpha_i}{\|\{\Delta r\}\|} \right)^2 \langle\phi\rangle_i \{\phi\}_i \right)^{\frac{1}{2}} = 1$$ [4.14]

Introducing the non-negative term

$$p_i = \left(\frac{\Delta \alpha_i}{\|\{\Delta r\}\|} \right)^2 \qquad i = 1,...N$$ [4.15]

in [4.14] and considering the orthonormality property of the eigenvectors and further the squaring of both sides, [4.14] is reduced to

$$\sum_{i=1}^{N} p_i = 1 .$$ [4.16]

The term p_i is defined in the domain interval [0,1], since it is a non-negative number according to [4.15] and is further constrained to furnish a unitary summation in [4.16]. It can conveniently be expressed in the form of percentage as

$$P_i = 100 \ (p_i) \ \% .$$ [4.17]

The term P_i is hereafter called the participation parameter. This parameter indicates, in percentage, the level of participation of a typical eigenvector component in the actual displacement increment vector defined in [4.1].

Recalling the definition of the cosine of the angle parameter stated in [4.9], expression [4.13] can be rewritten as

$$\left\{ \Delta r \right\}_u = \sum_{i=1}^{N} \cos\theta_i \left\{ \phi \right\}_i$$ [4.18]

where θ_i varies in the interval [0°,90°]. Resorting to the definition of the direction cosines of a line in the N-dimensional vector space, the cosine in [4.   can be interpreted as the direction cosine of the angle

between the directions defined by $\{\phi\}_i$ and $\{\Delta r\}_u$. This is illustrated in Fig. 4.3 for the N eigenvectors.

From [4.9] and [4.15], it is concluded that

$$p_i = \cos^2\theta_i, \qquad\qquad [4.19]$$

which indicates that the participation parameter and the angle parameter are interrelated. Futhermore, from [4.10],

$$p_i = \beta_i^2, \qquad\qquad [4.20]$$

which shows the dependence between the participation and the size parameters. The interdependency present in the derived analytical parameters, given in [4.10], [4.19] and [4.20], stems from the constraint imposed in [4.1]. For example, if the size of an eigenvector component in [4.1] is changed, while preserving $\{\Delta r\}$ constant, the corresponding angular position showed in figure 4.1 must as well change. Nevertheless, this interdependency does not diminish the role of each of the analytical parameters while studying the domination of eigenvectors of materially nonlinear structures. For example, a linearly elastic problem with nonproportional loading which engages different eigenvectors may be best studied through angular variation of the modes. On the other hand, a materially nonlinear problem may require the application of all the analytical parameters throughout the load-deflection history of the structure.

4.4 The Approximate Displacement Increment Vector

It has been indicated in Section 4.3.3 that the orthogonality condition, between a typical eigenvector $\{\phi\}_i$ and the actual displacement increment vector $\{\Delta r\}$, gives rise to a null eigenvector component $\Delta\alpha_i\{\phi\}_i$ in the addition [4.1]. In fact, the relative size and participation parameters vanish if applied to an orthonormal eigenvector component.

Quasi-orthonormal eigenvectors are often present in the expansion [4.1]. The definition of a quasi-orthonormal eigenvector component is based on the values of the corresponding analytical parameters and the assigned domain intervals. The intervals that identify a quasi-eigenvector component are given in Table 4.1.

If the purely orthogonal and the quasi-orthogonal eigenvector components are removed from the expansion [4.1], an approximate displacement increment vector can be defined as

$$\{\Delta r\}_a = \sum_{i=1}^{M} \Delta\alpha_i\{\phi\}_i \, . \qquad M<N \, . \qquad [4.21]$$

where the M eigenvectors in [4.21] are called the participant eigenvectors that effectively contribute to the addition performed in [4.1]. The adopted intervals of variation of the analytical parameters for the participant eigenvector components are listed in Table 4.1.

The vector space whose base vectors are the participant eigenvectors in [4.21] is in fact a subspace of the original N-dimensional vector space of the global degrees of freedom of the structure. A vector in this subspace represents an approximation

$\{\Delta r\}_a$ of the actual displacement increment vector $\{\Delta r\}$ that belongs to the N-dimensional vector space.

The analytical parameters defined in the previous sections can be applied to the approximate displacement increment vector. According to [4.3], an approximate generalized displacement increment can be computed as

$$\Delta \alpha_a = <\Delta r>_a \{\Delta r\},$$
 [4.22]

Analogous to expressions [4.6], [4.11] and [4.19], the analytical parameters for the approximate displacement increment vector can be defined as

$$\beta_a = \frac{\left|\Delta \alpha_a\right|}{\|\{\Delta r\}\|},$$
 [4.23]

$$\theta_a = \cos^{-1} \beta_a$$
 [4.24]

and

$$P_a = 100 \, \beta_a^2 \, \%,$$
 [4.25]

where β_a, θ_a and P_a are respectively the relative size, angle and participation parameters of the approximate displacement increment vector.

It may be practical to work with the approximate displacement increment vector as a unique vector component in [4.1] instead of the individual participant eigenvector components. This approach might

be effective when a considerable number of eigenvector components participate in [4.21]. In fact, the approach based on $\{\Delta r\}_a$ has been applied to the analysis of a deep reinforced concrete beam that forms a case study to be presented in the next Section.

4.5 Case Studies

In this section, five problems have been chosen as case studies. The primary objective in addressing these problems is to apply the analytical parameters formulated in Sections 4.3 and 4.4. to structures with different geometries and material behavior. Some important conclusions about domination of eigenvectors on the displacement response of structures emerge naturally from the analysis of the problems that constitute the content of this Section.

4.5.1 A Plane Structure with Varying Geometric Proportions

In the introduction of the present Chapter, it has been mentioned that the geometric proportions of a structure form a contributing factor of the structural stiffness. Thus, the structural stiffness can be altered through variation of the geometric proportions. In turn, this implies a change in the structural behavior. For example, a shallow beam that deforms fundamentally through bending, accompanied by negligible shear distortion of its cross sections, changes the deformational behavior when the depth of the cross section is substantially increased. In this case, shear distortion is predominantly present in the deformation of the beam.

The objective of this subsection is to investigate the influence of the variation of the geometrical proportions upon the

participation, in terms of level and number, of the eigenvector components of [4.1] in the actual displacement vector of the structure.

To fulfill this objective, a parametric study is carried out by varying the aspect ratio H/L of a plane structure and applying the analytical parameters to measure the contribution of the eigenvector components associated with the lowest eigenvalues extracted from the stiffness matrix of the structure.

Figure 4.4 shows the discretization, type and intensity of the applied loads and the dimensions of the structure selected to form this parametric study. The varying dimensions give rise to values of the aspect ratio H/L of 1/4, 1/2, 1/1, 2/1 and 4/1. The material is linearly elastic with properties $E = 400$ MPa and $v = 0.0$. A null Poisson ratio has been adopted so that the eigenvectors can depict more distinguishable deformational patterns, without transverse effects such as contraction or expansion. The load intensity q_y has been kept constant, whereas q_z varies according to the value of the aspect ratio as showed in Fig. 4.4. This results in a constant shear force at the fixed cross section. The loads in Fig. 4.4 have been chosen so that a general deformation mode, with components such as extension, bending and shear distortion, could be present in the actual displacement vector of the structure. The level of contribution of these components depends on the value of the aspect ratio.

A varying number of the lowest eigenvalues and corresponding eigenvectors were extracted for each case of aspect ratio. This number has been achieved tentatively so that the orthogonal, quasi-orthogonal and participant eigenvector components are exemplified

and the required accuracy in the approximate deflections is obtained. Figures 4.5 to 4.9 show the actual displacement vector, the normalized eigenvectors, the eigenvector components and the approximate displacement vector for the values of the aspect ratio varying from 1/4 to 4/1. The approximate displacement vector is based on the participant eigenvectors as defined in Table 4.1. A constant plot scale has been used throughout the plotting of the aforementioned figures. For each value of the aspect ratio, the analytical parameters are computed for each eigenvector component. The values of the relative size, angle and participation parameters are plotted in the Figs. 4.10, 4.11 and 4.12 respectively. In the following paragraphs, the eigenvector components shown in the Figs. 4.5 to 4.9 are classified according to the criteria outlined in Table 4.1. For this purpose, the values of the analytical parameters should be consulted in the Figs. 4.10 to 4.12. For comparison of deflections in Table 4.2, the resultant deflection of node 21 is selected. For this linear problem, the ratio between the actual (finite element analysis) and the approximate (approximate displacement vector) deflections is the same for all the free nodes of the discretized structure in Fig. 4.4.

For H/L=1/4 (Fig. 4.5), only the first eigenvector component is participant. The second and the third are quasi-orthogonal, whereas the fourth is completely orthogonal. In addition, the normalized eigenvectors depict pure deformational patterns, such as simple bending for the first eigenvector, extension for the second and double curvature bending for the fourth. The third eigenvector, however, shows a combination of shear and bending. The

approximate displacement vector is solely based on the first eigenvector component and reproduces the actual displacement vector accurately, as deduced from the comparison between the approximate and the actual deflections at node 21 for which a ratio of 0.998 is shown in Table 4.2.

For H/L=1/2 (Fig. 4.6), the first and second eigenvector components are participant, whereas the third and the fourth are respectively quasi-orthogonal and orthogonal. Except for the first eigenvector, which appears to represent a simple bending mode, the others are affected by transverse deformation and shear distortion. Nevertheless, the approximate displacement vector provides a ratio of 0.997 between the approximate and actual deflections at node 21 as illustrated in Table 4.2.

For H/L=1/1 (Fig. 4.7), all eigenvector components are participant and the first component contributes with almost 78% to the actual displacement vector. Transverse deformation and shear distortion appear more accentuated than for the previous aspect ratio. A ratio of 0.968 between the approximate and the actual deflections at node 21 is reported in Table 4.2.

For H/L=2/1 (Fig. 4.8), only the fifth eigenvector component is quasi-orthogonal. The remaining components are participant. Shear distortion is apparent in the first component and virtually all components reflect a mixing of different deformational patterns. With five participant components, a ratio of 0.975 between the approximate and the actual deflections is achieved (Table 4.2).

For H/L=4/1 (Fig. 4.9), the fourth and fifth eigenvector components are quasi-orthogonal. All components have lost the

purity of deformation depicted for the case of H/L=1/4. Yet, the five remaining participant components form an approximate displacement vector which provides a ratio of 0.936 between the actual and the approximate deflections of node 21 (Table 4.2).

Figure 4.13 illustrates the variation of the participation parameter, computed for the first and second eigenvector components, with the value of the aspect ratio. For low aspect ratios, the first eigenvector component shows a predominant participation, whereas the first and second components share comparable participation levels in the range of high aspect ratios.

This parametric study demonstrates that a large number of eigenvector components is required while approximating the actual displacement vector of structures with high aspect ratios, such as deep beams and corbels. Therefore, this serves as a guideline to the analyst which wants to estimate the necessary number of eigenvector components to approximate the displacement response of a plane structural problem. In addition, the participant eigenvector components, regardless of the aspect ratio, are based on a reduced number of eigenvectors that are necessary to provide an accurate appoximate displacement vector according to the criteria given in Table 4.1 These eigenvectors are designated the dominant eigenvectors.

4.5.2 An Elastic Perfectly Plastic Cantilever Beam

Generally, a structural member whose material is idealized as elastic perfectly plastic exhibits three identifiable phases in its load-deflection curve. A linearly elastic phase is followed by an

elastoplastic phase in which the plastic zones gradually extend to cover a greater portion of the structure. The third and last phase, designated plastic, coincides with the onset of localized plastic hinges within the material. This, in turn, causes the formation of a failure mechanism which develops under approximately constant load. Further information on the behavior of elastic perfectly plastic structures is provided by Horne and Morris (1981).

An investigation of the domination of some eigenvector components, associated with the lower eigenvalues, upon the incremental displacement response of an elastic perfectly plastic structure constitutes the objective of this Subsection. The study covers all phases of behavior discussed above, from elastic to the establishment of the failure mechanism.

Figure 4.14 shows the discretization, dimensions and loading for the shallow cantilever steel beam selected for the present case study. The beam material is modeled as elastic perfectly plastic with the following properties: E = 200,000 MPa, v = 0.30 and F_y = 300 MPa. Timoshenko and Gere (1972) derived an expression to estimate the free end deflection of the beam which serves as a comparison for the finite element solution in the elastoplastic range. The expression is given in a dimensionless form as

$$\frac{r}{r_y} = \left(\frac{R_y}{R}\right)^2 \left[5 - \left(3 + \frac{R}{R_y}\right)\sqrt{3 - \frac{2R}{R_y}}\right], \qquad 1 \leq \frac{R}{R_y} \leq \frac{3}{2} \qquad [4.26]$$

where r_y (30 mm) and R_y (15 KN) are respectively the deflection and the load at first yield which have been calculated using simple

formulae from strength of materials. The ratio r/r_y is called hereafter the deflection ratio.

Two basic assumptions have been made in the derivation of [4.26]. The influence of shear strains on the deflection is neglected and a plastic hinge with an infinitesimal length is assumed at the fixed cross section of the beam.

Figure 4.15 shows the load-deflection curves given by [4.26], hereafter called simple beam theory, and the finite element analysis. The standard Newton-Raphson method has been used to trace the linear and the beginning of the elastoplastic phases, whereas the constant arc-length method was applied to describe the plastic phase. The finite element solution overestimates the first yield load given by the simple beam theory by 12%. This is caused by the stiffening effect of the adopted discretization in terms of mesh refinement and boundary conditions. However, the general agreement between the two solutions is apparent from Fig. 4.15.

The first plot of Fig. 4.16 shows the effect of the discretized boundary conditions on the initiation of yielding at the vicinity of the fixed end. The yield zones in this figure start to appear at a small distance from the fixed end section. The simple beam theory allows for a fully yielded section considerably earlier than the finite element solution. This is so because the finite element solution incorporates the effect of shear on the development of yield zones. The shear effect, although small in the present case, postpones the yielding in the central regions of the beam as shown at the middle plot of Fig. 4.16. In addition, the length of the formed plastic hinge is not infinitesimal as demonstrated in the last plot of Fig. 4.16. The

length of the plastic hinge in this figure is approximately equal

beam depth.

Table 4.3 presents a comparison between the values of load and tip deflection ratios at the first yield and fully yielded stages given by the finite element analysis and the simple beam theory.

Considering the solution given by the finite element analysis, a series of eigenanalyses has been carried out throughout the load-deflection history of Fig. 4.15. Only the first and second eigenvalues are of interest for this study, since domination is expected to be restricted to a small number of eigenvector components as demonstrated in Section 4.5.1. The corresponding eigenvectors are plotted in Fig. 4.17. Figure 4.18 shows the variation of the first and second eigenvalues, normalized with respect to their initial values, with the deflection ratio. The initial values for the first and second eigenvalues, computed in the linearly elastic regime, are respectively 20.281 N/mm and 555.003 N/mm. The normalized eigenvalues remain constant in the linearly elastic phase and decrease gradually in the elastoplastic phase. Along the plastic phase, both normalized eigenvalues attain approximately constant values. It is noted that the first normalized eigenvalue decreases in the elastoplastic phase through a higher gradient than the second normalized eigenvalue. Moreover, it reaches a very small non-negative value during the plastic phase. Since the eigenvalue is the stiffness associated with the corresponding eigenvector, the first eigenvector component may give rise to the failure mechanism of the beam. However, this comment can only be a conclusive statement after the application of the analytical parameters to the first and second eigenvector

components, shown in Fig. 4.17, throughout the load-deflection history.

Figure 4.19 illustrates the variation of the relative size parameter with the deflection ratio. The size of the first eigenvector component approximates accurately the size of the actual displacement increment vector in the linearly elastic, elastoplastic and plastic phases. The relative size of the second eigenvector component is very small for the linearly elastic and elastoplastic phases and drops to zero in the plastic phase.

With respect to the angle parameter (Fig. 4.20), the first eigenvector component is nearly colinear to the actual displacement increment vector in the elastic and elastoplastic phases and is perfectly colinear in the plastic phase. The second eigenvector component is quasi-orthogonal in the elastic and elastoplastic phases and is completely orthogonal in the plastic phase.

The variation of the participation parameter is shown in Fig. 4.21. It is concluded that the participation of the first eigenvector component is overwhelmingly prevalent for the entire load-deflection history. Thus, this example demonstrates that the first eigenvector component dominates the incremental displacement response of this cantilever beam, from the beginning of the elastic phase to the onset of the failure mechanism. The domination acquires optimum level of efficiency along the plastic behavior of the beam.

Figure 4.17 shows that the approximate displacement increment vector $\{\Delta r\}_a$, based on the first eigenvector component, incorporates all the distinguishable characteristics of the known failure mechanism. In this figure, the high gradient of bending

curvature is very localized within the region adjacent to the fixed end where the plastic hinge, shown in Fig. 4.16, develops. The remaining part of $\{\Delta r\}_a$ does not show any evidence of incremental curvature as expected in the   known mechanism.

4.5.3 An Elastic Softening Beam-Rod

In the field of plasticity, Drucker (1959) defined strain softening as a type of material behavior in which the incremental work performed by the increment of stress upon the increment of strain is negative. The material behavior is unstable within the strain softening range. Studies on the softening behavior of engineering materials have substantially evolved during the present decade mainly due to successful experiments in which the entire stress-strain curve of the specimen has been traced. A review of the present status of the research related to the behavior of engineering softening materials is given by Read and Hegemier (1984).

The objective of this Subsection is to apply the analytical parameters to the eigenvector components extracted from the current stiffness matrix of a structure made of a strain softening material. The beam-rod shown in Fig. 4.22 represents the structural member selected for this investigation. The material is treated as elastic softening with the following properties :   E=200,000 MPa, H'=-5,000 MPa, v=0.30 and F_y = 300 MPa. Pietruszczak and Mroz (1981) demonstrated that the slope of the descending branch of the load-deflection curve of a strain softening material structure is mesh dependent. In addition, a finer mesh tends to allow for a more gradual progress of softening zones. Nevertheless, a coarse mesh has

been adopted in the discretization of the beam-rod since the problem of uniqueness of the descending branch is out of scope of the present study. The type and intensity of the applied reference loads have been designed to induce the appearance of the flexural and extensional deformation modes.

Figure 4.23 shows the relation between the load and the resultant deflection of node 11 of the beam-rod. This particular node experiences the largest resultant deflection among the free nodes and for this reason it has been chosen as target. The eigenvector-based solution strategy, to be introduced in the next Chapter, was applied to trace respectively the ascending and softening descending branches of the load-deflection curve including the limit point. A total of thirty solution steps comprised the presented solution.

The development of softening regions is illustrated in Fig. 4.24 for the equilibrium states A, B ,C , D and E that appear on the load-deflection curve. After the equilibrium state E indicated in the load-deflection curve, the spreading of softening stabilizes according to the pattern depicted in the last plot of Fig. 4.24.

The load combination of uniformly distributed tension and pure bending induces the development of uneven softening through the depth and span of the structural member. This condition influences the level of domination and the deformational patterns of the eigenvector components illustrated in Figs. 4.25 and 4.26.

The value of the aspect ratio of the beam-rod is the same as for the case discussed in Subsection 4.5.1 and Fig. 4.5. Since the fourth eigenvector component in that figure is completely orthogonal to the actual displacement vector, only the first three eigenvectors and

eigenvalues are of interest herein. Specifically, the bending and extensional modes are important while forming th approximate displacement increment vector, since these modes are expected to be activated by the uniformly distributed load and bending moment applied to the structure. In addition, the nomenclature adopted to identify the eigenvector components is set in the linearly elastic regime where the purity of deformation is clearly present. In Fig. 4.25a, the subscripts f, sf and e stand for flexural, shear-flexure and extensional respectively. Such a nomenclature is preserved for other stages of behavior, although the purity of deformation is no longer apparent as illustrated in Figs. 4.25b, 4.26a and 4.26b.

Figure 4.27 shows the variation of the normalized eigenvalues with the free end resultant deflection of node 11 of the beam-rod. The eigenvalues of the linearly elastic stiffness matrix normalize the current eigenvalues and have the values 1746 N/mm, 51911 N/mm and 908.1 N/mm, which are respectively associated with the flexural, shear-flexure and extensional modes. Within the linearly elastic behavior, the normalized eigenvalues are equal to the unity. Upon initiation of uneven softening at the equilibrium state A (Figs. 4.23 and 4.24), their values decrease gradually until the limit point is reached. Immediately after the limit point, the normalized eigenvalues that correspond to the flexural and extensional modes drop suddenly and attain thereafter a short range of stable values. The level of uneven softening throughout this stable range is represented by the pattern associated with the state C in Fig. 4.24. It is noted that the flexural eigenvector is the only mode with a negative stiffness. Therefore, it incorporates the effects of the

unstable material behavior which characterizes the descending branch of the load-deflection curve. At the establishment of even softening, typically exemplified by the state D in Fig. 4.24, the normalized eigenvalues associated with the flexural and extensional modes decrease further to a final series of approximately constant values. The relative eigenvalue related to the shear-flexure mode remains almost unchangeable throughout the range of displacements that corresponds to the descending branch.

Figures 4.28, 4.29 and 4.30 illustrate the variation of the analytical parameters with respect to the free end resultant deflection of the 11. The domination of the eigenvector components is herein investigated for each stage of behavior, from linearly elastic to extensive softening damage. During linearly elastic behavior, the flexural and extensional eigenvector components compose the actual displacement increment vector representing 12% and 88% of participation respectively. The greater participation of the extensional mode is intentional and has been achieved by specifying a reference value of 100 N/mm for the uniformly distributed load (Fig. 2). Fig. 4.25a shows the prevalent participation of the extensional eigenvector component within the linearly elastic regime. The shear-flexure eigenvector component is quasi-orthogonal throughout this range of behavior. Upon initiation of uneven softening, the domination of the flexural eigenvector component starts to increase. At the limit point, all modes participate as shown in Fig. 4.25b and Figs. 4.28, 4.29 and 4.30. After the limit point, when the uneven softening stabilizes at state C (Fig. 4.24), the flexural eigenvector component dominates completely. This condition prevails

within the horizontal segment in Figs. 4.28, 4.29 and 4.30 immediately after the limit point. In this range of behavior, the extensional eigenvector component is quasi-orthogonal to the actual displacement increment of the beam while the shear-flexure eigenvector component is nearly orthogonal. At the onset of even softening, represented by the state D in Fig. 4.24, the flexural and extensional eigenvector components contribute respectively with 84% and 16% of participation. This condition corresponds to the second horizontal segment that takes place after the limit point in Figs. 4.28, 4.29 and 4.30. In this range, the shear-flexure eigenvector component is completely orthogonal to the actual displacement increment vector.

The present case study demonstrates that the domination of some eigenvector components varies along the load-deflection history. In addition, the level of domination within a particular range of behavior depends on the state of development of softening zones which characterizes at range. Furthermore, the pure bending and extensional deformation patterns of the modes extracted in the linearly elastic range disappear in the nonlinear range. Instead, a combination of bending and axial deformation forms the modes in the nonlinear range (Figs. 4.25b, 4.26a and 4.26b).

4.5.4 A Reinforced Concrete Deep Beam

Generally, reinforced concrete deep beams experience different types of material damage when tested to failur Flexural and diagonal cracks, crushing and shearing develop in the concrete, whereas yielding takes place in the reinforcement. These multiple

nonlinear effects render a structural stiffness that changes abruptly throughout the load-deflection history. This may imply that the domination of eigenvector components would not be as evident as for the case of elastic perfectly plastic material behavior where yielding progresses gradually as shown in Subsection 4.5.2.

The objective of this Subsection is to investigate the domination of some eigenvector components which are based on the eigenvectors extracted from the tangent stiffness matrix of a reinforced concrete deep beam. Rogowsky et al. (1983) tested a series of reinforced concrete deep beams from which the simply supported beam, designated as B1/1.5T1, has been chosen for the present case study.

Figure 4.31 shows the discretization, dimensions, loads and boundary conditions for the south shear span of the beam. Contrary to the north span which was designed with tne minimum shear reinforcement ratio, the south span did not incorporate any stirrups. In this way, the failure of the beam could be precipitated in the south shear span. The modeling of the boundary conditions and applied loads has been kept as close as possible to the conditions ified for the test. A roller under the left column support and a ad distributing plate over the center loading column were used during the experiment. The discretized structure is formed by 69 two-dimensional concrete elements and 33 truss elements that model the three layers of reinforcement shown in Fig. 4.31.

The hypoelastic and the multilinear elastoplastic constitutive relationships are applied to model the behavior of the concrete and the reinforcement, respectively. The basic properties of the concrete and the reinforcement are provided in Appendix A.

Figure 4.32 shows the load-deflection curves obtained from the finite element analysis and the experiment. The standard Newton-Raphson and the constant arc-length methods have been used to trace the ascending and descending branches respectively. A total of 21 solution steps comprise the finite element solution.

The behavior of the beam along the ascending branch can be divided to three segments. The first segment ranges from the undeformed state to the appearance of flexural cracks. The load-deflection curve is approximately linear in this range and the beam does not present cracks induced by applied loads. Shrinkage cracks, however, were detected prior to the experiment according to Rogowsky (1982). This may explain the difference in the initial stiffness given by the experiment and the analysis. The value of the initial modulus of elasticity of concrete E_c, adopted in the analysis, is based on the data related to the uniaxial compressive cylinder tests performed and reported by Rogowsky et al. (1983). This value of E_c does not include any adjustment for the effect of shrinkage cracks in the beam. The second segment begins with the occurrence of flexural cracks and ends with the onset of diagonal cracks. Two kinks in each load-deflection curve are associated with the appearance of these nonlinear effects. Within this segment, thin flexural cracks develop through the depth at the mid-span region and towards the left column support. The third segment of behavior ranges from the onset of diagonal cracks to the extensive crushing of the top zone of the compression strut. Flexural and diagonal cracks progress and widen throughout this segment along with the first yielding of the longitudinal reinforcement. At maximum load, crushing and incipient

smashing of concrete localize in the region close to the left face of the center loading column which coincides with the top zone of the compression strut. This condition is illustrated in Figs. 4.33a and 4.33b for the experiment and analysis, respectively..

The point of maximum load capacity coincides with the limit point in each of the load deflection curves. In this stage, the beam attains its ultimate limit state of structural failure. After the structural failure, the beam undergoes a phase associated with the descending branch of its load-deflection curve. In this phase, the beam is still able to sustain decreasing loads. Six solution steps constitute the descending branch traced by the finite element method. The behavior of the beam along the descending branch is affected by progressive material damage in the form of shearing within the developed cracks, crushing and subsequent smashing of concrete and ongoing yielding of the reinforcement. This situation of highly extensive material damage characterizes a condition of postfailure. The postfailure of the beam corresponds to the last point of the load-deflection curve where the tangent stiffness is approximately horizontal. At postfailure, the distribution of material damage in the beam is shown in Fig. 4.34. Since there is an evident predominance of damage caused by shear and compression, it seems appropriate to call this stage of behavior as a shear-compression failure. The experimental descending branch shows only two points. However, it appears that the rate of displacement specified during the test to trace the descending branch was not sufficient to capture some intermediate points of the curve.

Table 4.4 presents some values of applied loads and midspan deflections at node 232 (Fig. 4.31) given by the experiment and the analysis for particular stages of the behavior of the beam.

The domination by some eigenvector components upon the actual displacement increment vector of the reinforced concrete deep beam is investigated throughout the load-deflection history. The beam considered herein can be classified as very short since its shear span ratio of 0.60 is less than 1.0 (MacGregor 1988). Considering this fact, the abrupt changes in the load-deflection curve and the findings of section 4.5.1, the eigenvectors that correspond to the three lowest eigenvalues are selected while studying domination.

Figure 4.35 illustrates the variation of the relative eigenvalues with the midspan deflection evaluated at node 232 of the discretized structure shown in Fig. 4.31. Once more, the eigenvalues extracted from the stir. matrix assembled at the first solution step are used to normalize the current eigenvalues. These initial eigenvalues are 1,443.81 N/mm, 27,218.06 N/mm and 28,729.23 N/mm. The normalized eigenvalues are constant and equal to unity within the segment of behavior that corresponds to the uncracked beam. At the formation of flexural cracks, the normalized eigenvalues experience sudden variations. More variations occur at the onset of diagonal cracks although these are less dramatic than at the onset of flexural cracks. A moderate drop is visible at first yielding of the longitudinal reinforcement. Immediately before the limit point, the normalized eigenvalues attain the lowest values, which correspond to the crushing of the concrete at the top zone of the compression strut. Right after the limit point, there is an increase in the normalized

eigenvalues. This is caused by the approach adopted in the formulation of the material behavior which prescribes tangent and secant constitutive matrices before and after the peak points of the stress-strain relations respectively. However, this disturbance occurs only in the vicinity of the limit point, after which the normalized eigenvalue associated with the first eigenvector drops to approximately 5% of its initial value. This value relates to the condition of the beam at the beginning of the last solution step that ends with the shear-compression failure.

Figure 4.36 shows the normalized eigenvectors $\{\phi\}_1$, $\{\phi\}_2$ and $\{\phi\}_3$ and the eigenvector components $\Delta\alpha_1\{\phi\}_1$, $\Delta\alpha_2\{\phi\}_2$ and $\Delta\alpha_3\{\phi\}_3$, while Fig. 4.37 shows the actual and the approximate displacement increment vectors, respectively $\{\Delta r\}$ and $\{\Delta r\}_a$. The eigenvectors have been computed from the tangent stiffness matrix assembled at the beginning of the last load step of the load-deflection history, which is related to the condition of the beam immediately prior to shear-compression failure. Throughout the load-deflection history, the first eigenvector $\{\phi\}_1$ provides the single curvature pattern of the beam. In addition, this eigenvector incorporates localized deformations which increase from the limit point to the point of shear-compression failure. For the last solution step, the localized deformations are consistent with the distribution of material damage caused by shearing and smashing of the concrete as illustrated in Fig. 4.34. These nonlinearities induce shear distortion and downward punching along the cross sections of the beam close to the left face of the center loading column in Fig. 4.36.

The eigenvectors $\{\phi\}_2$ and $\{\phi\}_3$ represent multiple curvature modes which are as well affected by localized deformations. The second eigenvector $\{\phi\}_2$ shows a pattern of localized deformations similar to that of $\{\phi\}_1$. On the other hand, the localized deformations in $\{\phi\}_3$ concentrate along the row that coincides with the compression strut. For the considered solution step, the approximate displacement increment vector $\{\Delta r\}_a$ is formed by the three eigenvector components, where the first contributes with approximately 93% in terms of participation.

In order to investigate the degree of domination of each eigenvector component upon the actual displacement increment vector, the analytical parameters have been computed for the complete load-deflection history. Figures 4.38, 4.39 and 4.40 show the variation of the relative size, angle and participation parameters with the midspan deflection. In the segments of these figures that correspond to the ascending branch of the load-deflection curve, the first eigenvector component dominates completely. The second and the third eigenvector components alternate as quasi-orthogonal and orthogonal according to the criteria outlined in Table 4.1. Therefore, these eigenvector components do not participate in the approximate displacement increment within the ascending branch. After a small disturbance at the limit point, the level of domination of each eigenvector component oscilates dramatically throughout the segment that is associated with the descending branch of the load-deflection curve. For the majority of the solution steps of this range of behavior, the first eigenvector component provides the greatest level of participation. However, the remaining eigenvector

components still participate in the formation of the approximate displacement increment vector.

The failure mode of the beam is approximately described by the first eigenvector component which provides the lowest eigenvalue or stiffness at shear-compression failure.

The level of domination of the approximate displacement increment vector, as a single vector, upon the actual displacement increment vector, is studied throughout the load-deflection history of the reinforced concrete deep beam. For the ascending branch, it has been demonstrated that the approximate displacement increment vector is formed solely by the first eigenvector component, since this component contributes almost with 100% of participation. For the descending branch and including the limit point, it is necessary to add the eigenvector components $\Delta\alpha_1\{\phi\}_1$, $\Delta\alpha_2\{\phi\}_2$ and $\Delta\alpha_3\{\phi\}_3$ in order to obtain $\{\Delta r\}_a$.

The analytical parameters computed for the approximate displacement increment vector along the ascending and descending branches are illustrated in Figs. 4.41, 4.42 and 4.43. Contrary to the dramatic variation of the analytical parameters along the descending branch, shown in Figs. 4.38, 4.39 and 4.40, the variation of the analytical parameters with the midspan deflection in Figs. 4.41, 4.42 and 4.43 is reasonably smooth. In addition, these figures demonstrate that the approximate displacement increment vector approximates the actual displacement increment vector accurately along the ascending and descending branches of the load-deflection history.

This case study has demonstrated that a small number of eigenvector components dominates the displacement history, and is sufficient to approximate the real incremental response of a structure that embodies a complex material behavior, such as a reinforced concrete deep beam.

4.5.5 A Reinforced Concrete Shallow Beam

Generally, reinforced concrete shallow beams exhibit a behavior in which extensive flexural cracks take place prior to failure. In the case of under-reinforced beams, the longitudinal reinforcement yields before the outer concrete fiber crushes. These conditions characterize a ductile structural behavior. Ductility is enhanced by specifying a reinforcement ratio lower than the balanced ratio. Burns and Siess (1966) have demonstrated through experiments that the failure mode for beams meeting the above conditions is purely flexural. Moreover, the failure mode is triggered by the formation of a plastic hinge at the region of maximum bending moment. This plastic hinge results from extensive crushing of concrete in the compression zone and yielding of the longitudinal reinforcement in the tension zone.

The objective of this Subsection is to study the behavior of the eigenvector components based on the eigenvectors extracted from the tangent stiffness matrix of a ductile reinforced concrete shallow beam.

McCollister (1954) has tested a series of simply supported reinforced concrete beams from which the beam S8 is selected for this study. This specific beam is under-reinforced (reinforcement

ratio is 21% of the balanced ratio) and does not incorporate any stirrups. In addition, its concrete has a considerably low compressive strength (18 MPa).

Figure 4.44 illustrates the model, the applied loads and the boundary conditions adopted for half of the actual beam. The discretization uses 50 two-dimensional elements and 12 truss elements that model, respectively, the concrete and the single layer of longitudinal reinforcement. The hypoelastic and the multilinear elastoplastic constitutive models have been applied to describe the behavior of the concrete and the reinforcement, respectively. The basic properties of both materials are listed in Appendix A.

Figure 4.45 shows the analytical and the experimental load-deflection curves. The deflection has been measured at midspan which corresponds to the node 175 in Fig. 4.44. The standard Newton-Raphson and the constant arc-length methods have been adopted to trace respectively the ascending branch and the nearly flat plateau of the load-deflection curve. Within this flat plateau, the iterative process uses a constant stiffness matrix that has been updated after the first yielding of the longitudinal reinforcement.

The behavior of the beam along the ascending branch of the load-deflection curve can be divided into two segments. The first segment ranges from the undeformed state to the appearance of the first flexural cracks at the midspan region. This causes a moderate kink in the numerical load-deflection curve. The second segment begins with the formation of the first flexural cracks and continues until the onset of yielding in the longitudinal reinforcement. Within

this segment, flexural cracks progress through the beam depth and towards the left support.

The relatively flat plateau of the load-deflection curve presents two phases. The first phase extends from the onset of the first yielding of the reinforcement to the point of maximum load. In this phase, yielding of the reinforcement advances and reaches the hardening range of behavior. This contributes to the slight increase in load which is seen in the load-deflection curve (Fig. 4.45). Also, the first visible crushing in the concrete is detected in the top fiber, after which crushing continues to spread towards the neutral surface of the beam. The condition of complete crushing of the concrete is attained when the crushed zone meets the upper flexural cracks. This situation is visible in Figure 4.46 which shows the distribution of nonlinearities in the concrete at maximum load. In addition, extensive shearing within the flexural cracks appears in this figure. The second phase within the flat plateau is associated with the smooth descending branch present in Fig. 4.45. The observed decrease in load is due to the gradual drop in the internal compressive force in the concrete because of softening. In terms of the material integrity, the drop in load is motivated by ongoing smashing of the concrete at the compression zone. This phase terminates with the fexural failure of the beam.

Table 4.5 lists values of loads and deflections associated with specific stages of the behavior of the beam. The comparison between loads seems reasonably accurate, whereas the correlation between deflections shows some discrepancy for the stage of maximum load. This may be due to the lack of experimental data related to the

descending branch of the compressive stress-strain behavior of the concrete. Without these data, the interpolation of stresses and strains, in the formulation of the compressive constitutive relation, becomes innaccurate.

Considering the various nonlinearities mentioned above, the variation of the lower normalized eigenvalues is now investigated. The first and second eigenvalues and the corresponding eigenvectors are selected for this study in view of the conclusions outlined in Subsection 4.5.1 (case of H/L=1/4). The eigenvalues of the elastic stiffness matrix have the values 83,910 N/mm and 6,667.250 N/mm, respectively for the first and second eigenvalues. In subsequent eigenanalyses, the eigenvalues are normalized with respect to these values. The first and second eigenvalues represent the flexural stiffness coefficients associated respectively with the single curvature mode $\{\phi\}_1$ and the double curvature mode $\{\phi\}_2$ illustrated in Fig. 4.47. Figure 4.49 shows the variation of the first and second normalized eigenvalues with the midspan deflection of the beam. According to this figure, the normalized eigenvalues drop significantly from the initial values at the onset of the first flexural cracks to a value nearly 30% of their initial values just prior to the first yielding of the reinforcement. Following this stage, the normalized eigenvalues decrease steeply. The first normalized eigenvalue attains only 2% of its initial value, whereas the second stabilizes at 25% of its initial value. The drastic reduction in the flexural stiffness (first eigenvalue in the present analysis) that corresponds to the single curvature mode of the beam has been observed during experiments as reported by Burns and Siess (1966).

The participation of the eigenvector components $\Delta\alpha_1\{o\}_1$ and $\Delta\alpha_2\{o\}_2$, shown in Fig. 4.47, in the actual displacement increment vector $\{\Delta r\}$ can be studied through the application of the analytical parameters formulated in Section 4.3. Thus, Figs. 4.50, 4.51 and 4.52 illustrate the variation respectively of the size, angle and participation parameter with the midspan deflection of the beam. Based on these figures, it is demonstrated that the first eigenvector component, which reproduces the single curvature mode of the beam, is fully participant from the beginning to the end of the load-deflection history. On the other hand, the second eigenvector component, which represents the double curvature mode, is orthogonal to the actual displacement increment vector prior to the first crushing of the concrete and becomes quasi-orthogonal thereafter. Therefore, the second eigenvector component can be discarded from the composition of the approximate displacement increment vector $\{\Delta r\}_a$ shown in Fig. 4.48.

The results of this investigation demonstrate that the first eigenvector component $\Delta\alpha_1\{\phi\}_1$, which represents the single curvature mode, dominates the incremental displacement response of the reinforced concrete shallow beam. In addition, a single generalized displacement increment $\Delta\alpha_1$ is sufficient to describe the displacement response.

4.6 Discussion

Recalling the results of the case studies carried out in this Chapter, a comparison between the number N of the global degrees of freedom $\{\Delta r\}$ with the number M of the generalized degrees of

fredom $\{\Delta\alpha\}$, can be summarized. Table 4.6 provides such a summary.

The most important conclusion is that the number of the degrees of freedom of a materially nonlinear structure can be drastically reduced. The beneficial aspects of this conclusion will serve as background for the formulation of an eigenvector-based solution strategy which constitutes the object of the next Chapter.

Type of Eigenvector Component	Orthogonal	Quasi Orthogonal	Participant
Relative Size Parameter	0	(0 . 0.10]	(0.10 . 1.0]
Angle Parameter (degrees)	90	[84 . 90)	[0 . 84)
Participation Parameter (%)	0	(0 . 1]	(1 . 100]

Table 4.1: Intervals of variation of the analytical parameters for the orthogonal, quasi-orthogonal and participant eigenvector components.
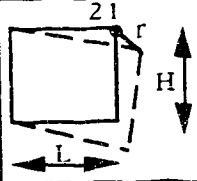
	Resultant Deflection at node 21		Ratio: Approximate
	Actual (mm)	Approximate (mm)	Actual
H/L = 1/4	67.313	67.199	0.998
H/L = 1/2	10.636	10.610	0.997
H/L = 1/1	2.613	2.529	0.968
H/L = 2/1	1.299	1.266	0.975
H/L = 4/1	1.028	0.963	0.936

Table 4.2: Values of the actual and the approximate deflections at node 21 of the plane structure.

Stages / Type of Solution	FirstYield		Fully Yielded	
	$\dfrac{r}{r_y}$	$\dfrac{R}{R_y}$	$\dfrac{r}{r_y}$	$\dfrac{R}{R_y}$
Simple Beam Theory	1.000	1.000	2.220	1.500
Finite Element Analysis	1.120	1.120	4.120	1.556

Table 4.3: Values of the tip deflection and load ratios for the limit stages of behavior of the elastic perfectly plastic cantilever beam.

Particular Stages of the Behavior of the R/C Deep Beam	Applied Load (KN)			Midspan Deflection (mm)		
	TEST[*]	ANAL.	$\dfrac{TEST}{ANAL.}$	TEST[*]	ANAL.	$\dfrac{TEST}{ANAL.}$
Flexural Cracks	125	156	0.80	0.71	0.35	2.03
Diagonal Cracks	240	240	1.00	1.89	0.90	2.10
Yielding of Reinforcement	500	549.60	0.91	4.39	4.00	1.09
Crushing of top of Compression Strut	606	609	0.99	5.18	5.28	0.98

[*] Rogowsky et al (1983)

Table 4.4: Loads and midspan deflections from the analysis and the experiment of the reinforced concrete deep beam.

Particular Stages of the Behavior of the R/C Shallow Beam	Applied Load (KN)			Midspan Deflection (mm)		
	TEST*	ANAL.	TEST/ANAL.	TEST*	ANAL.	TEST/ANAL.
First Flexural Cracks	5.00	7.15	0.700	0.26	0.38	0.699
Yielding of Reinforcement	33.80	36.00	0.938	5.33	5.84	0.913
First Crushing of Concrete	36.92	39.26	0.940	25.40	19.20	1.317
Maximum Load	40.03	40.93	0.978	73.66	52.77	1.396

* Adapted from McCollister (1954)

Table 4.5: Loads and midspan deflections from the analysis and the experiment of the reinforced concrete shallow beam.

Case Study	Linearly Elastic Structure aspect ratio H/L:					Elastic Perfectly Plastic Beam	Elastic Softening Beam-Rod	Reinforced Concrete Deep Beam		Reinforced Concrete Shallow Beam
	1/4	1/2	1/1	2/1	4/1			ascending branch	descending branch	
N	32					286	18	460		346
M	1	2	4	5	5	1	2	1	3	1

Table 4.6: Number of the global and the dominant generalized degrees of freedom for the case studies.
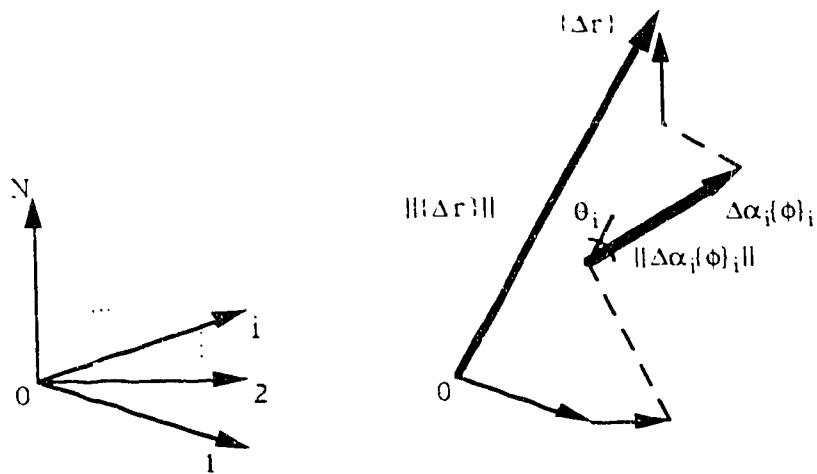
Figure 4.1: An illustration of the expansion theorem in the N-dimensional vector space.
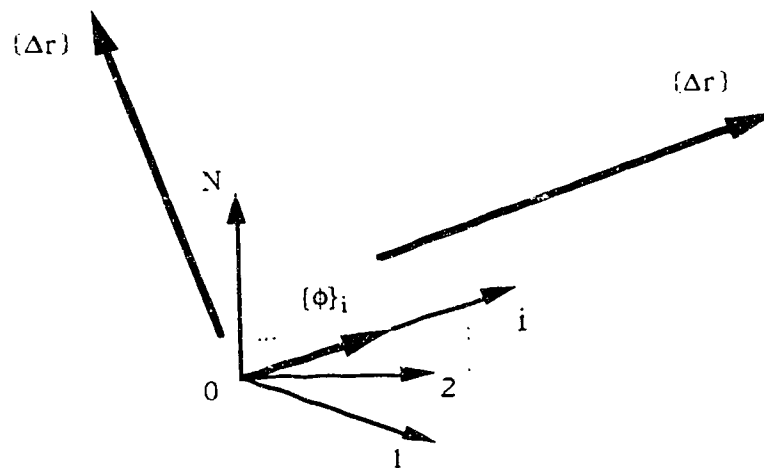
Figure 4.2: An illustration of the conditions of parallelism and orthogonality between the eigenvector and the displacement increment vector.
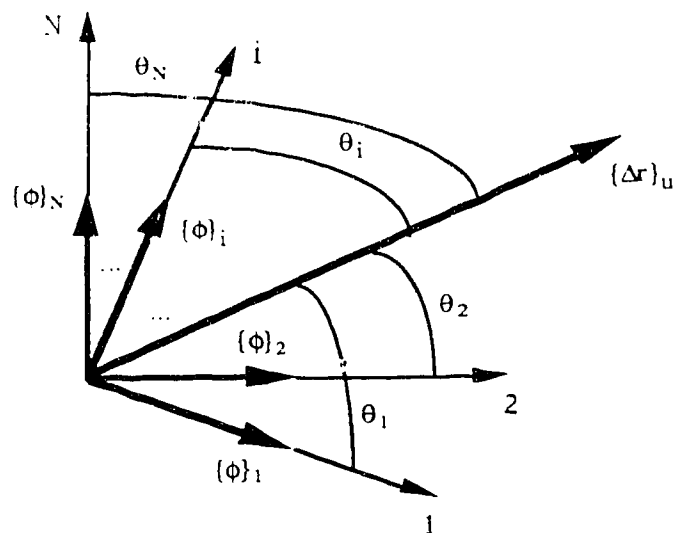
Figure 4.3: The direction angles between the eigenvectors and the unit displacement increment vector.

$$q_z=6.67\left(\frac{H}{L}\right) N/mm$$

$$q_y=10\,N/mm$$

H=400 mm

L = 4H, 2H, H. H/2, H/4

10 mm
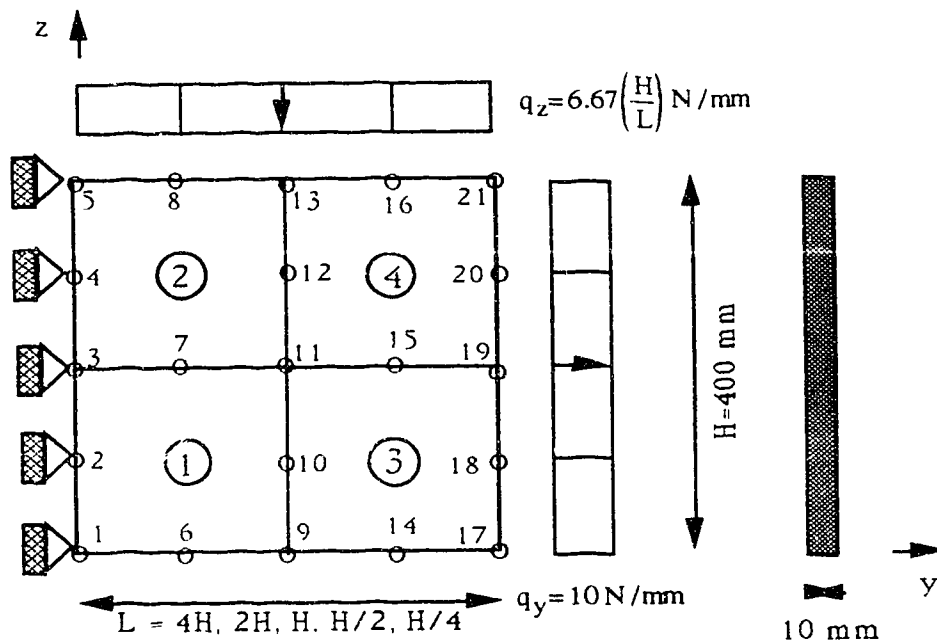
Figure 4.4: Discretization, loads and dimensions of the plane structure with varying geometrical proportions.
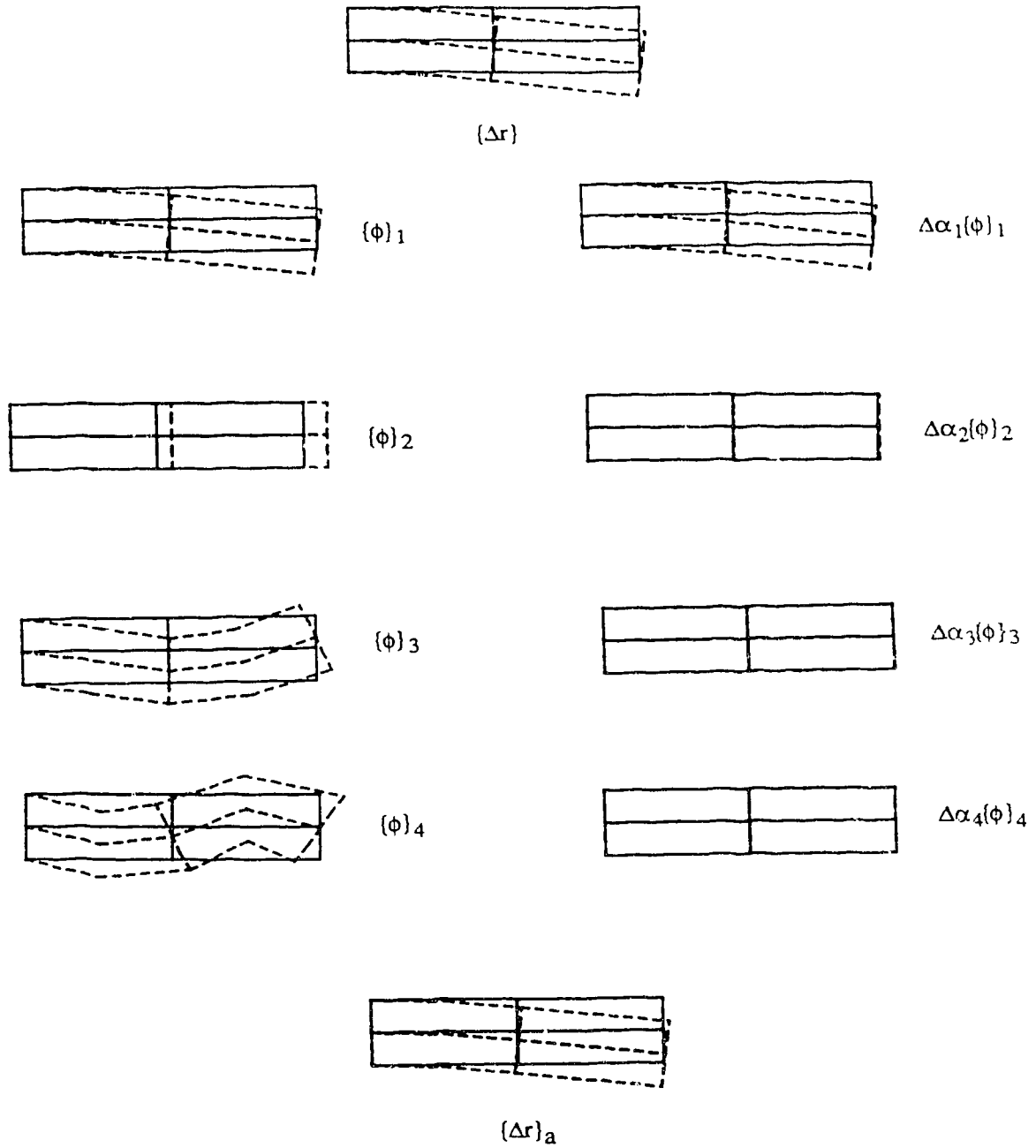
Figure 4.5: Actual displacement vector, eigenvectors, eigenvector components and approximate displacement vector (H/L=1/4)
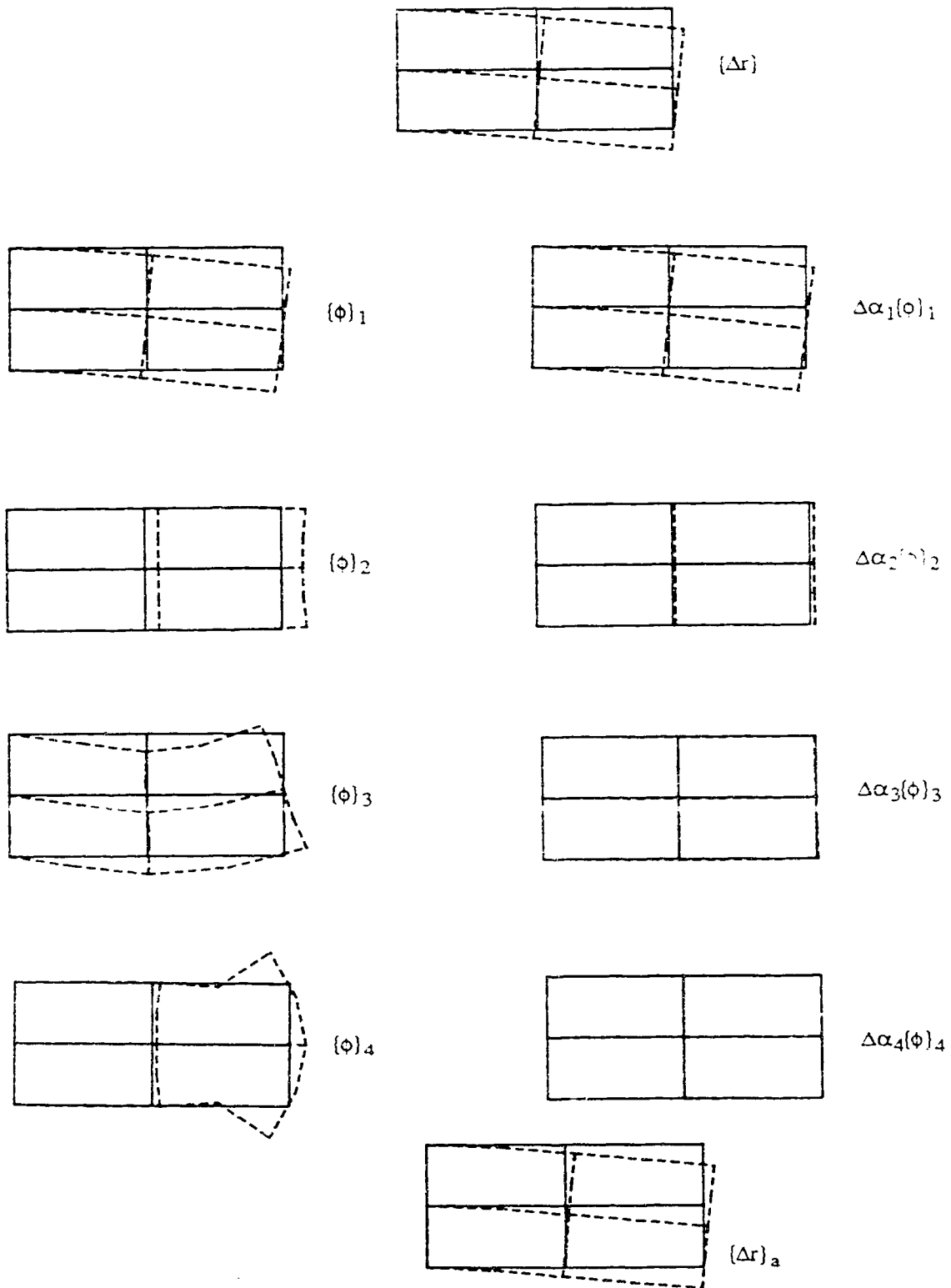
Figure 4.6: Actual displacement vector, eigenvectors, eigenvector components and approximate displacement vector (H/L=1/2).
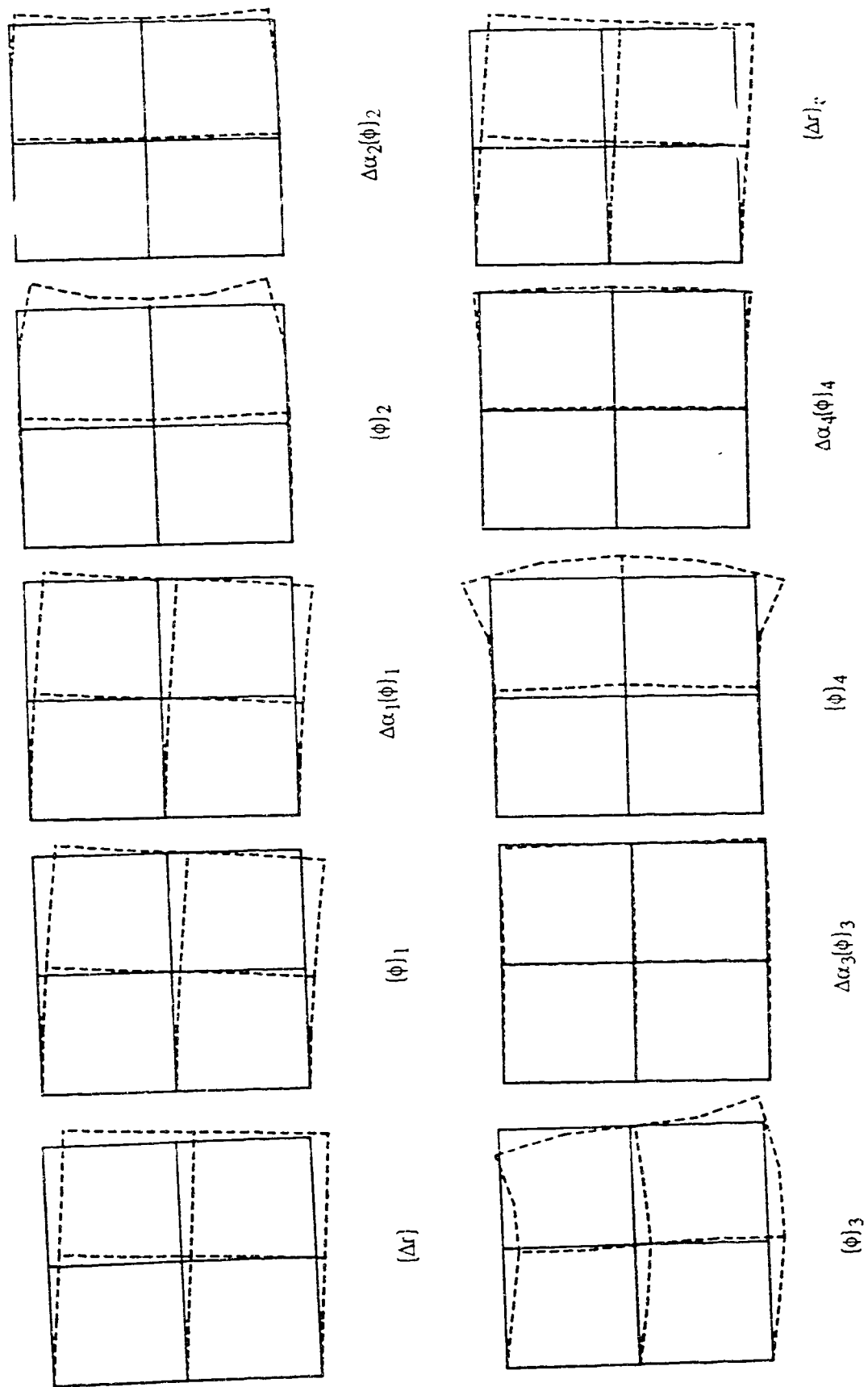
Figure 4.7: Actual displacement vector, eigenvectors, eigenvector components and approximate displacement vector ($ll/L=1/1$).
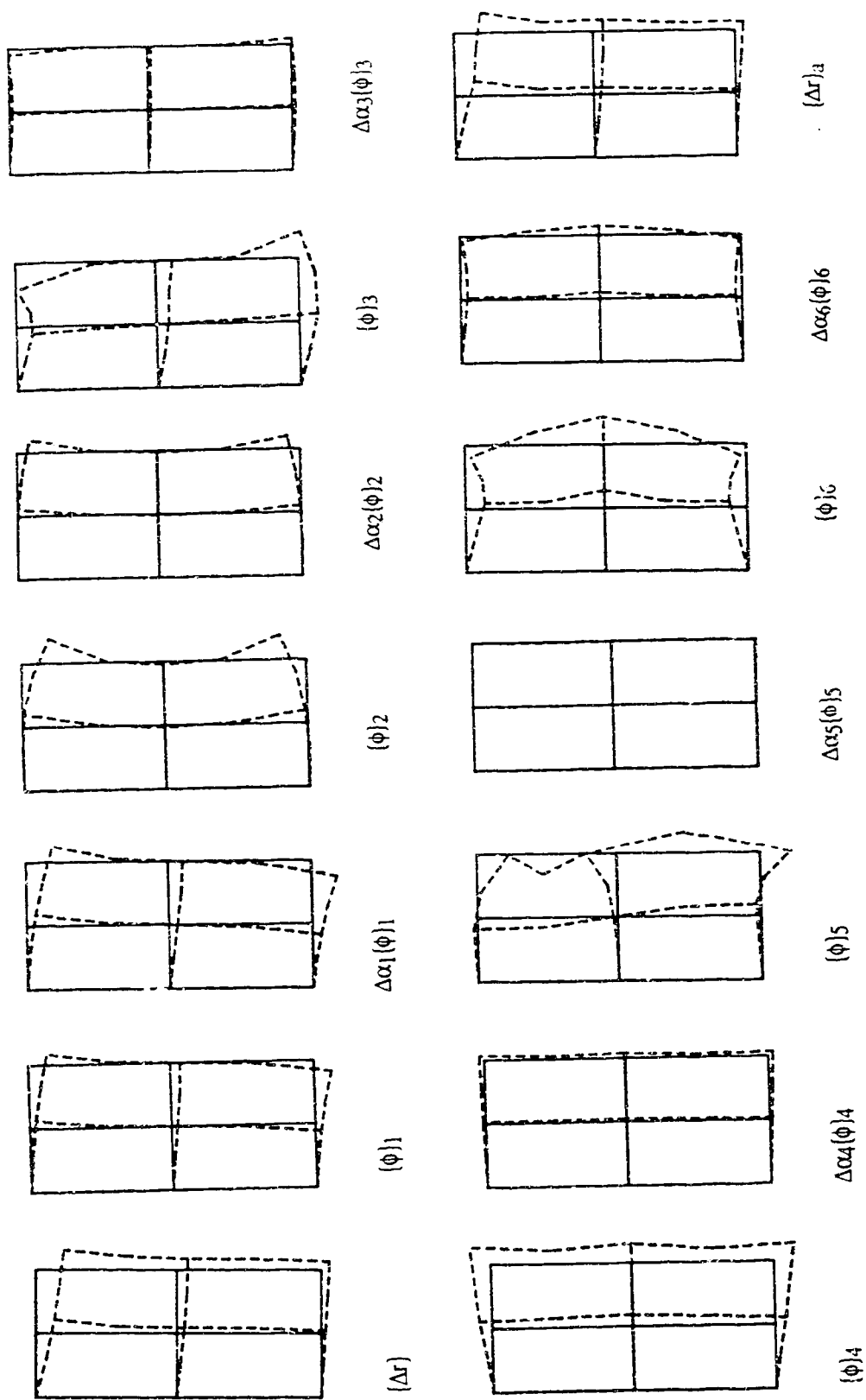
Figure 4.8: Actual displacement vector, eigenvectors, eigenvector components and approximate displacement vector (H/L=2/1).
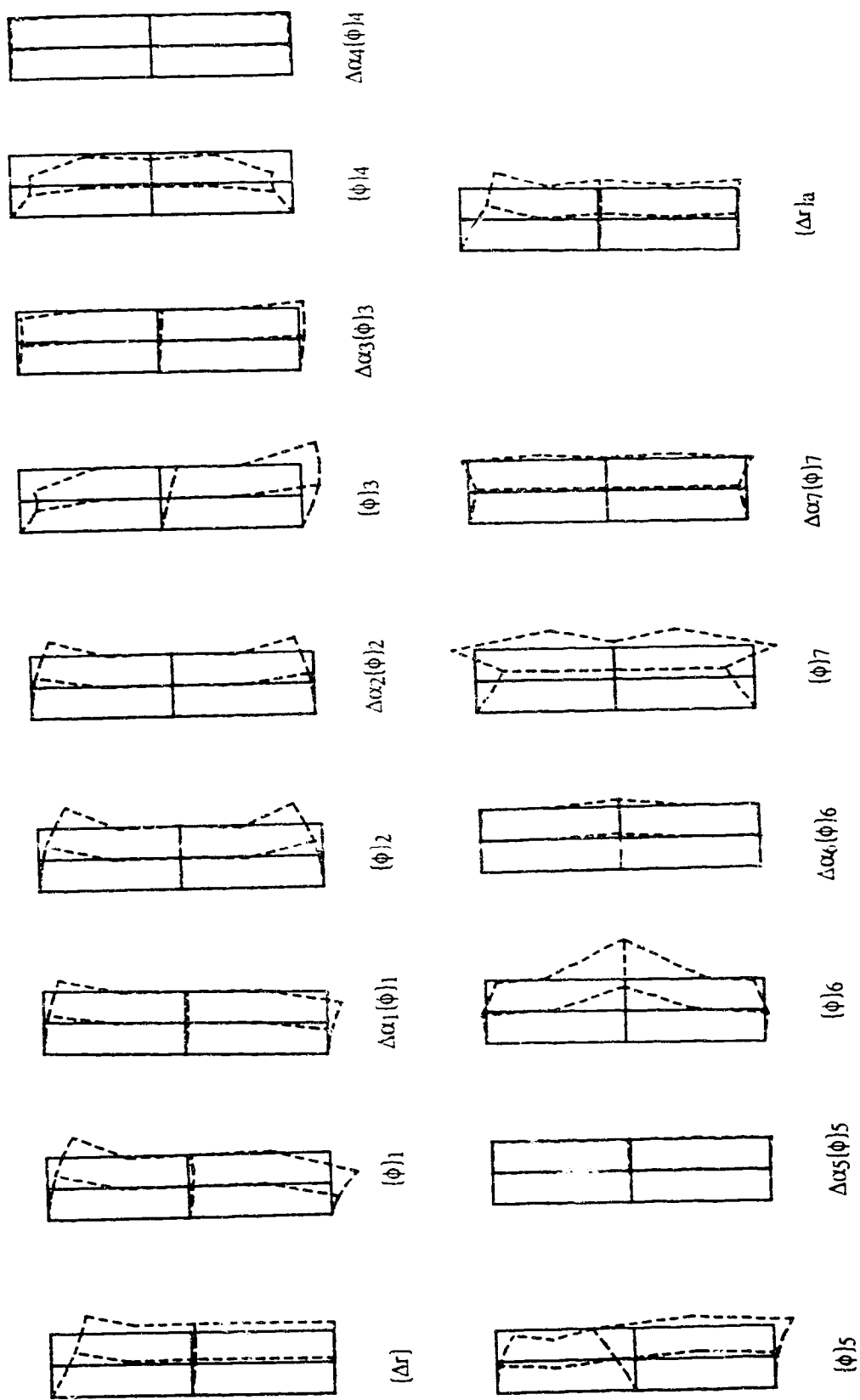
Figure 4.9: Actual displacement vector, eigenvectors, eigenvector components and approximate displacement vector (ll/L=4/1).
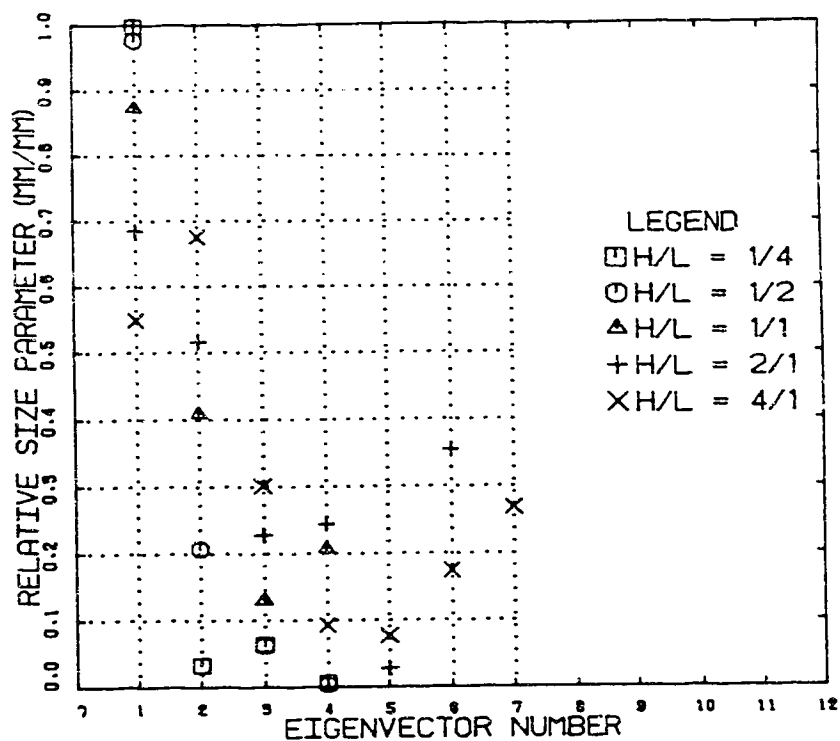
Figure 4.10: Variation of the relative size parameter of the eigenvector components per value of the aspect ratio.
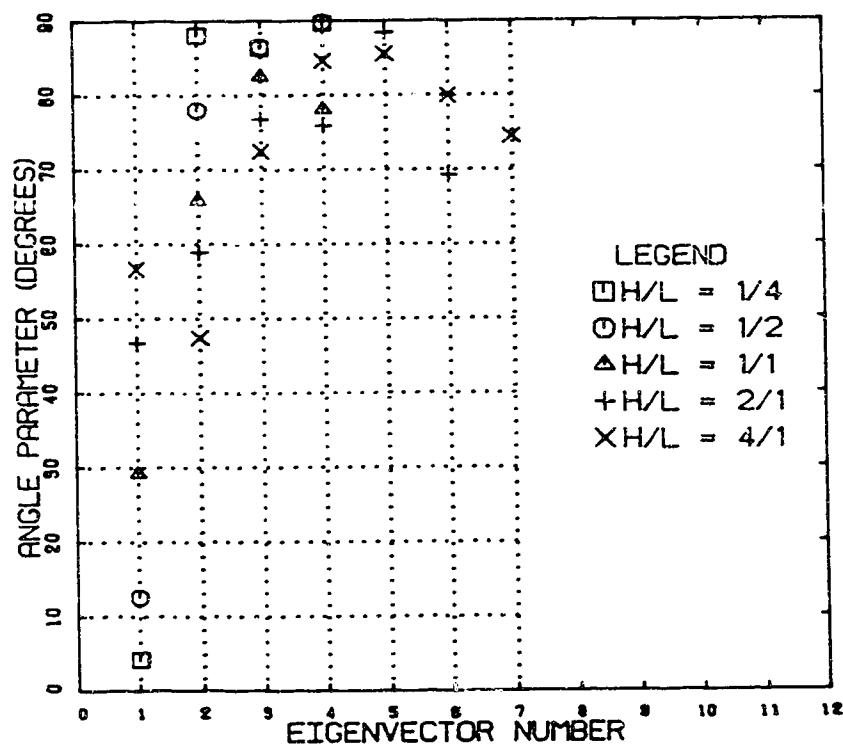
Figure 4.11: Variation of the angle parameter of the eigenvector components per value of the aspect ratio.
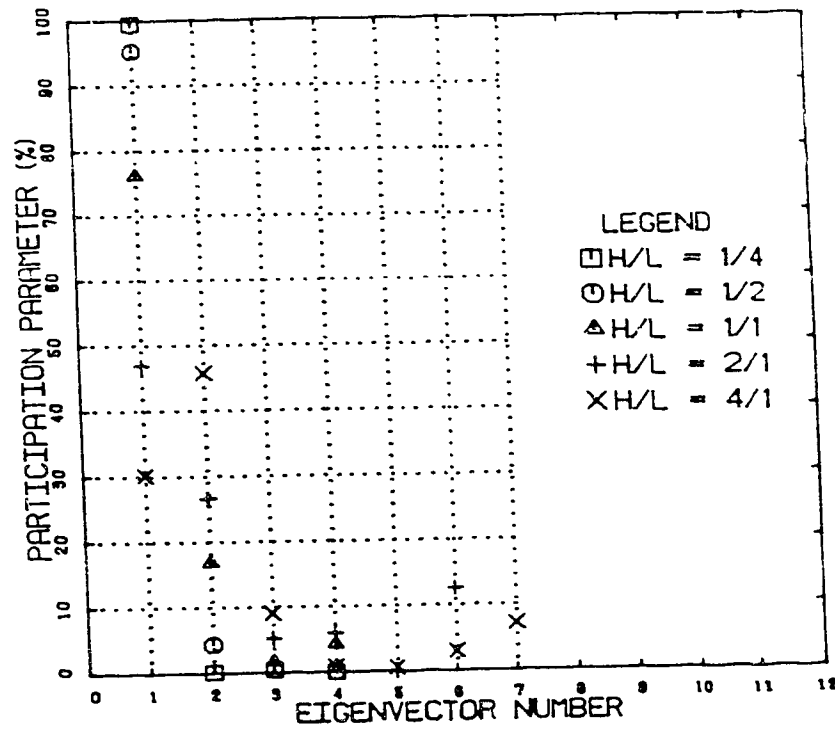
Figure 4.12: Variation of the participation parameter of
the eigenvectors components per value of the aspect ratio.
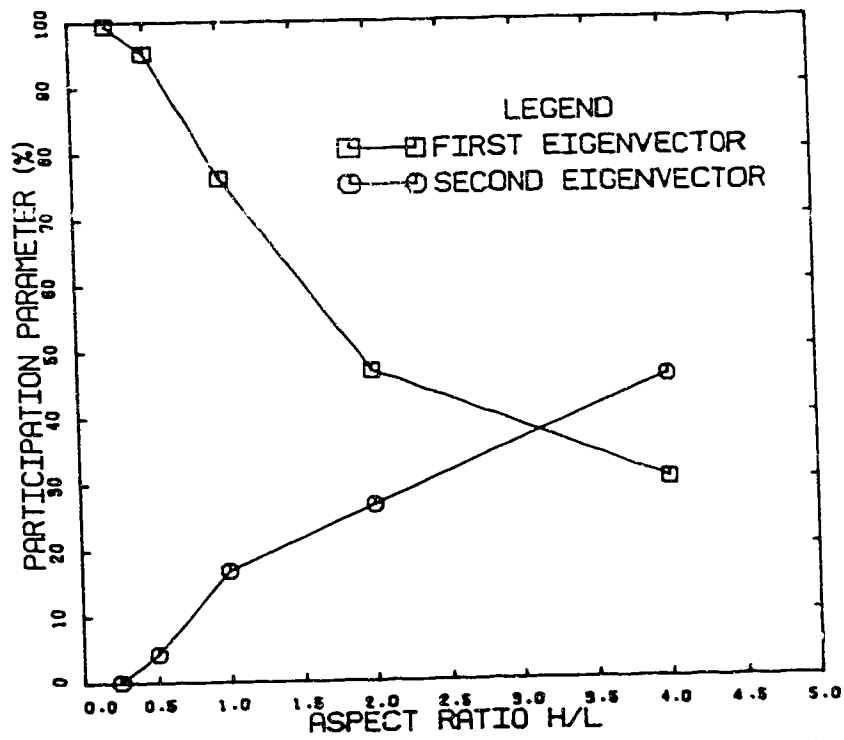
Figure 4.13: Variation of the participation parameter of the first
and second eigenvector components with the aspect ratio.
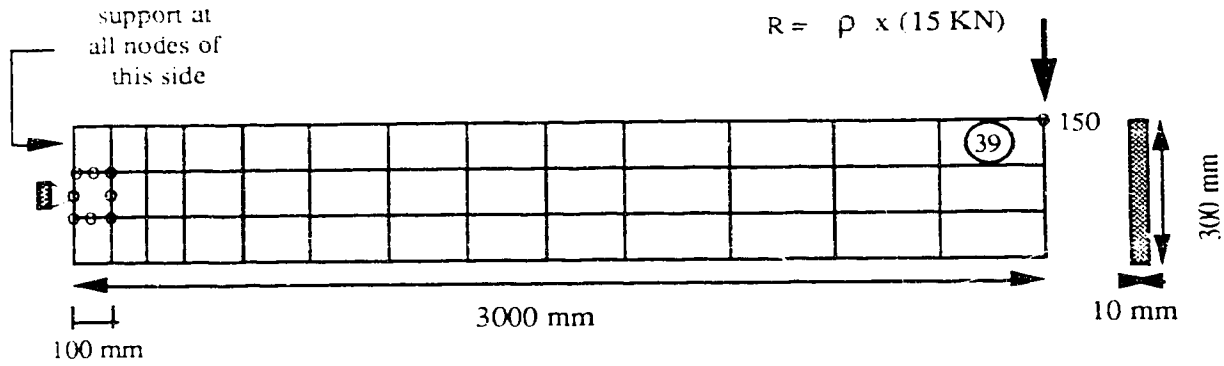
Figure 4.14: Discretization. dimensions and load for the elastic perfectly plastic beam.
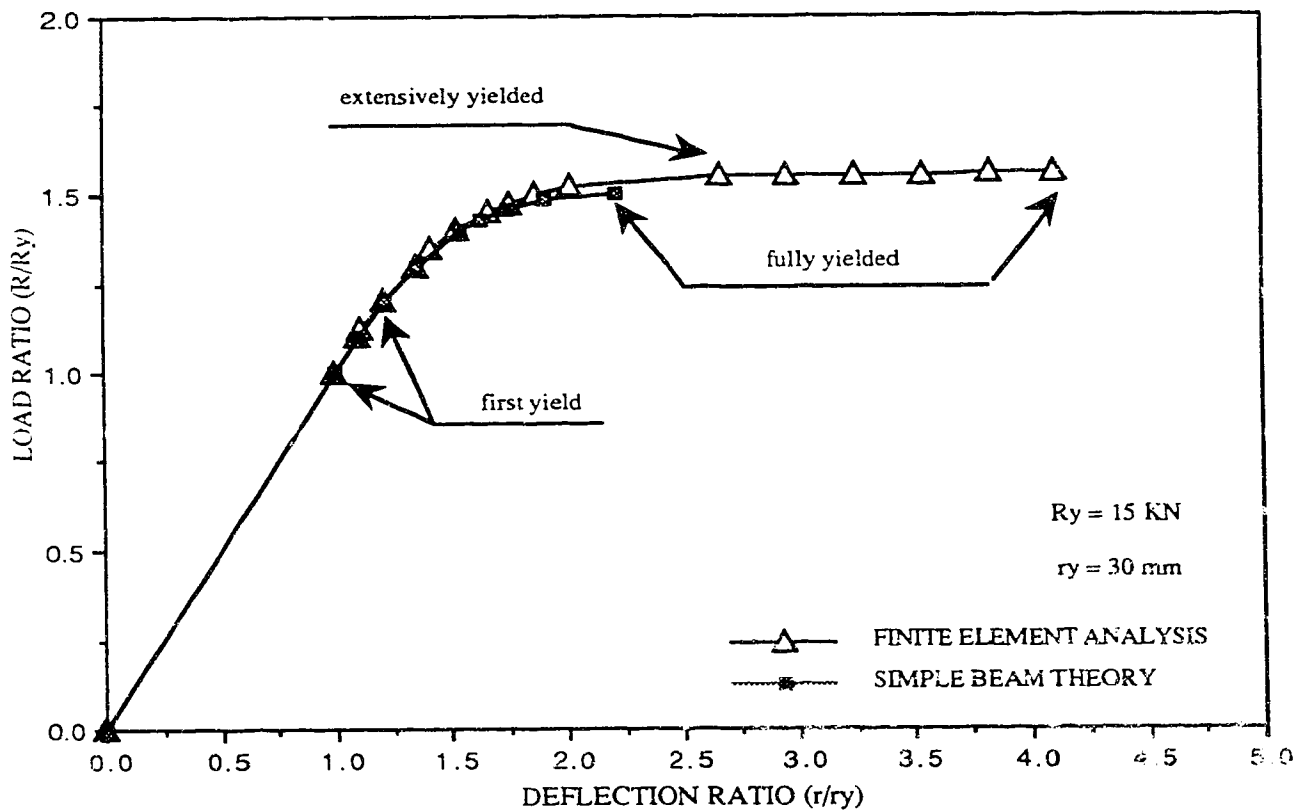
Figure 4.15: Load-deflection curves given by the finite element analysis and simple beam theory for the elastic perfectly plastic cantilever beam.
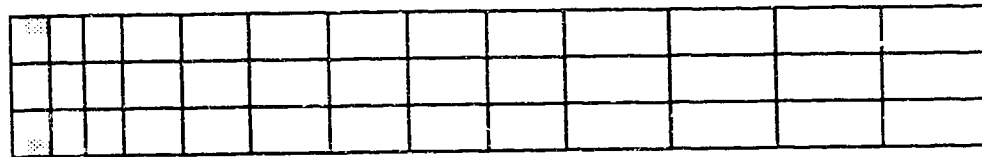
at first yield   (r/ry =1.12)
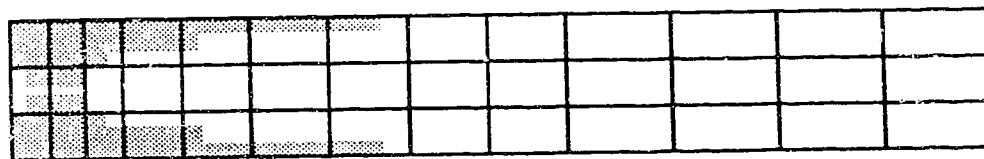
extensively yielded   (r/ry = 2.67)
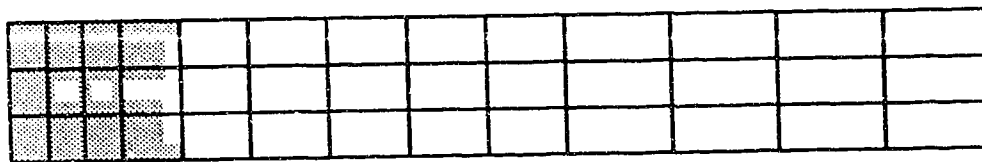
fully yielded   (r/ry = 4.12)

Figure 4.16: Development of yielding zones for the elastic perfectly plastic cantilever beam given by the finite element analysis.
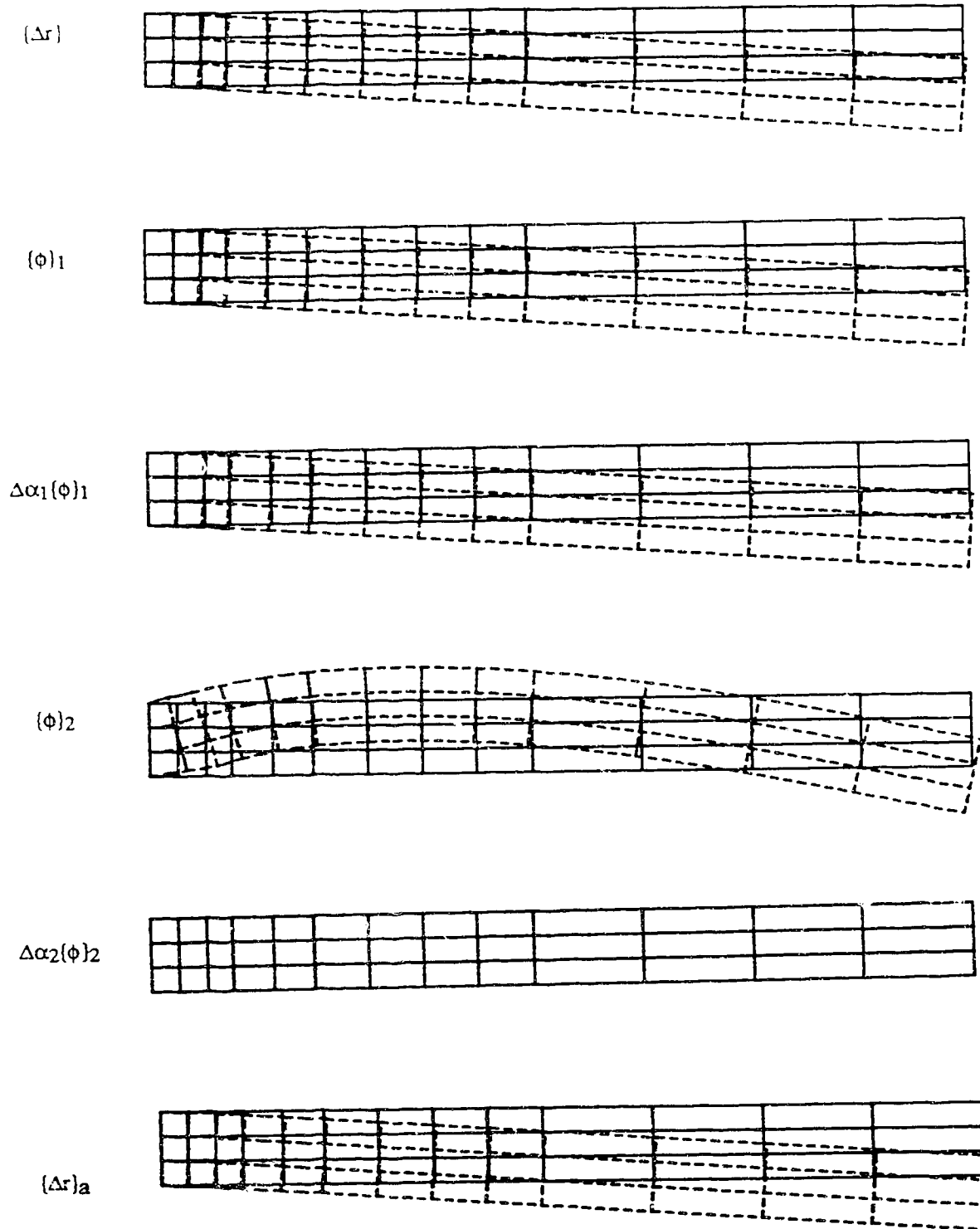
Figure 4.17: From top to bottom: The actual displacement increment vector, the first eigenvector, the first eigenvector component, the second eigenvector, the second eigenvector component and the approximate increment vector at mechanism formation.
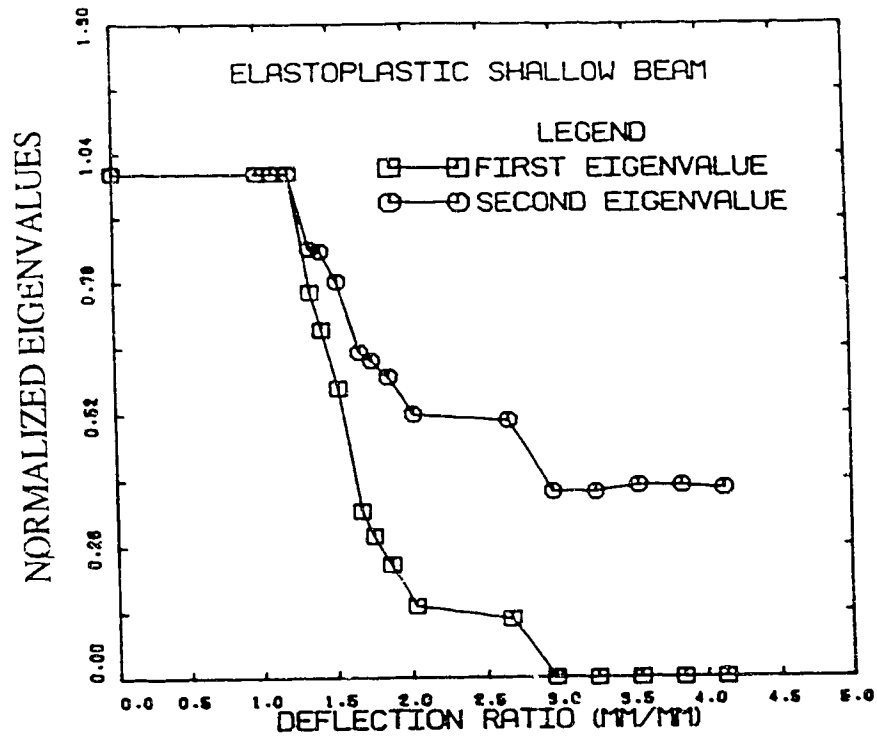
Figure 4.18: Variation of the normalized eigenvalues with deflection ratio for the elastic perfectly plastic beam.
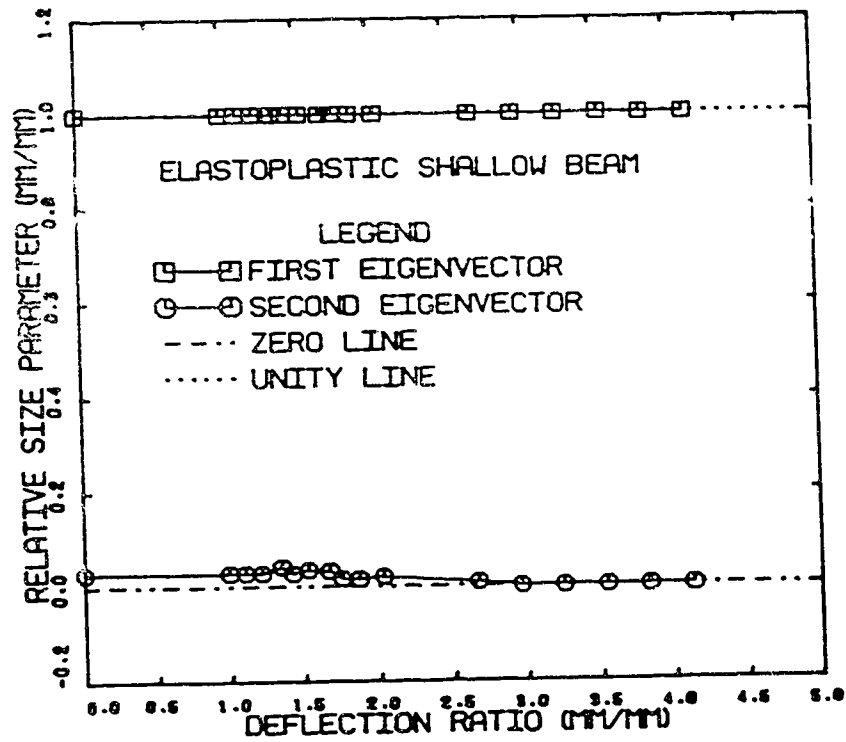
Figure 4.19: Variation of the relative size parameter with the deflection ratio for the elastic perfectly plastic beam.
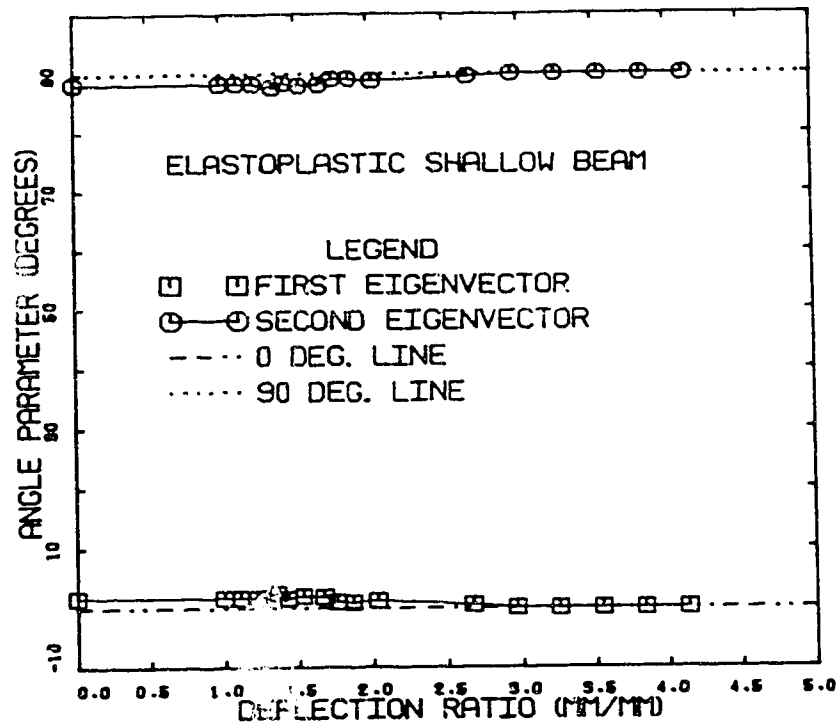
Figure 4.20: Variation of the angle parameter with the deflection ratio for the elastic perfectly plastic beam.
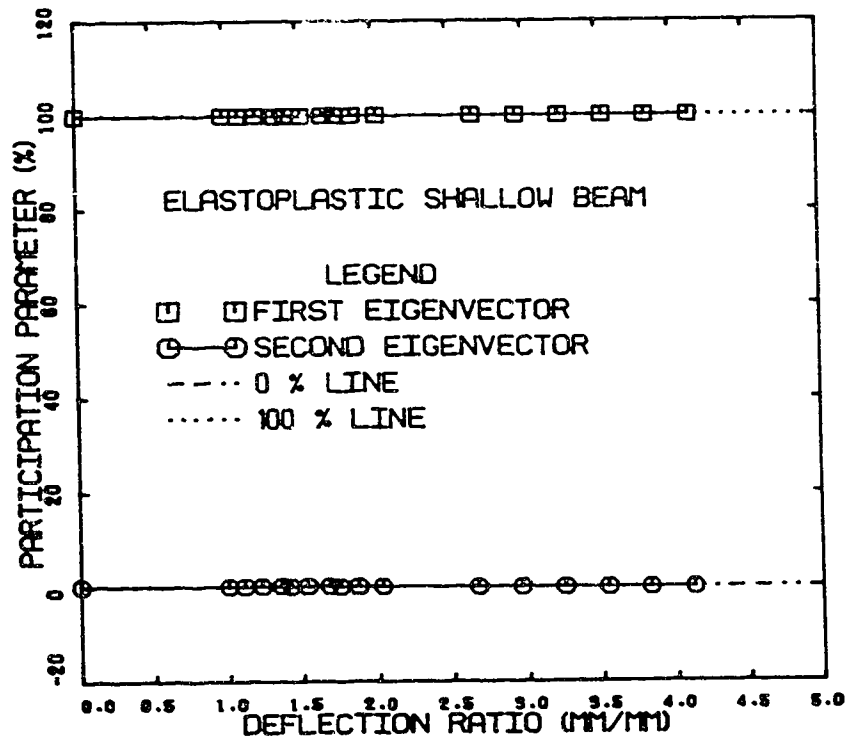
Figure 4.21: Variation of the participation parameter with the deflection ratio for the elastic perfectly plastic beam.
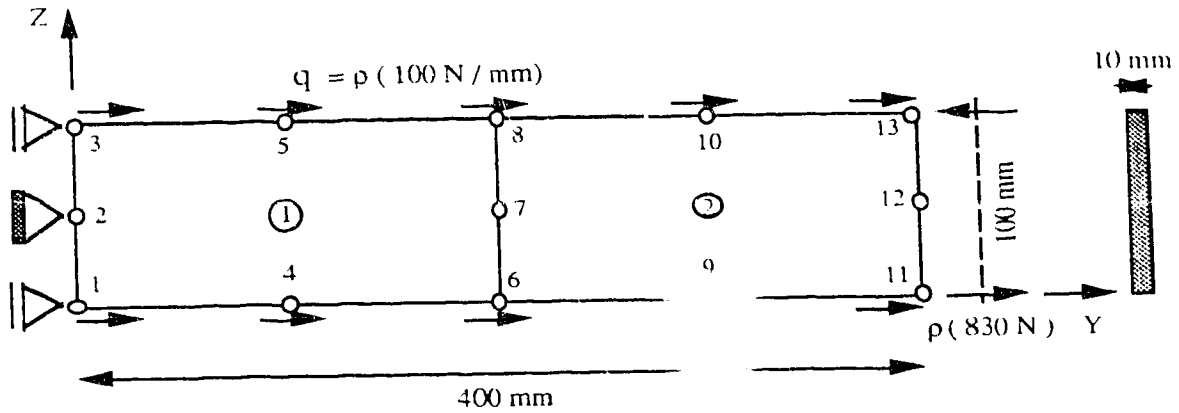
Figure 4.22: Discretization, dimensions and loads for the elastic softening beam-rod.
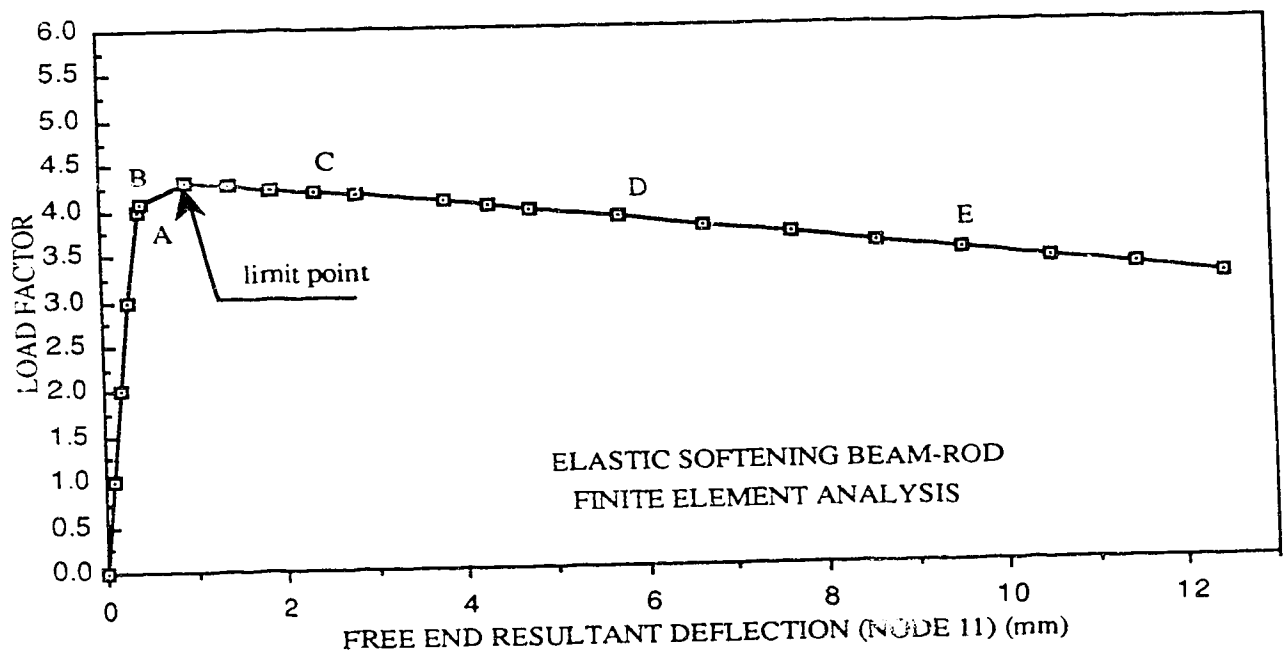
Figure 4.23: Load-deflection curve for the elastic softening beam-rod.

at state A

at state B

at limit point and state C

at state D

at state E
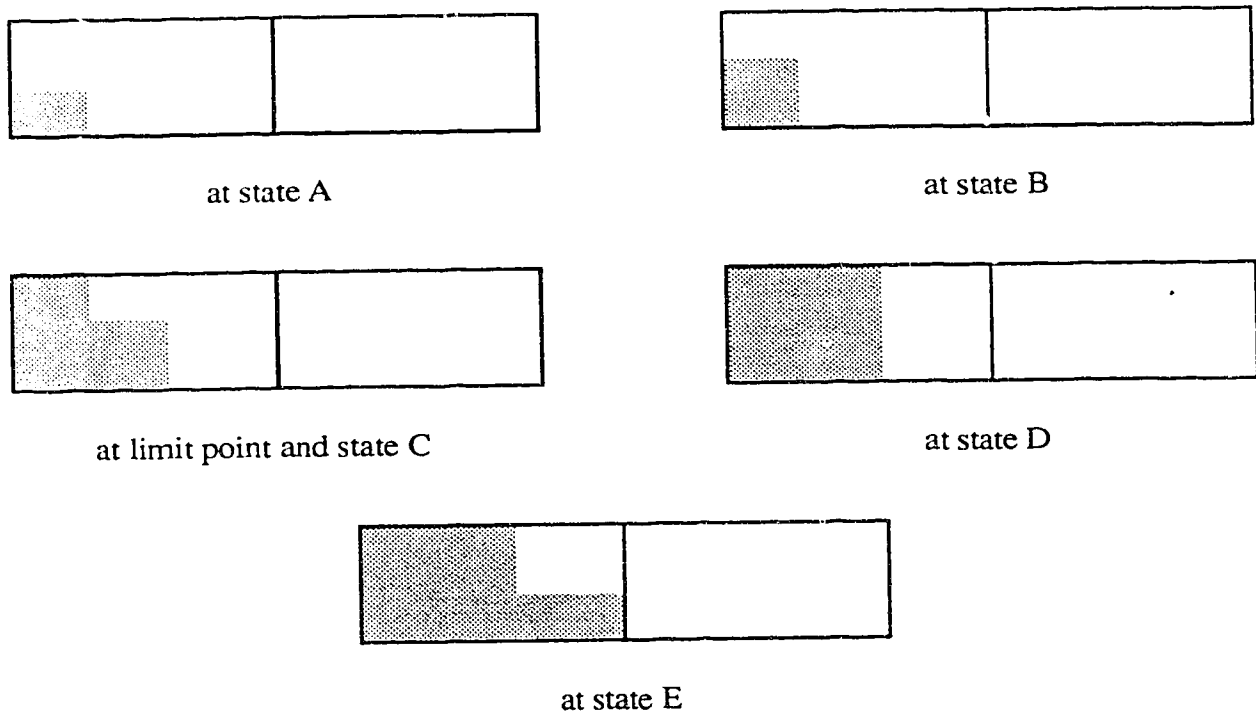
Figure 4.24: Development of softening zones at the equilibrium states A,B,C,D and E for the elastic softening beam-rod.

$\{\Delta r\}$

$\{\phi\}_f$

$\Delta\alpha_f\{\phi\}_f$

$\{\phi\}_{sf}$

$\Delta\alpha_{sf}\{\phi\}_{sf}$

$\{\phi\}_c$

$\Delta\alpha_c\{\phi\}_c$

$\{\Delta r\}_a$
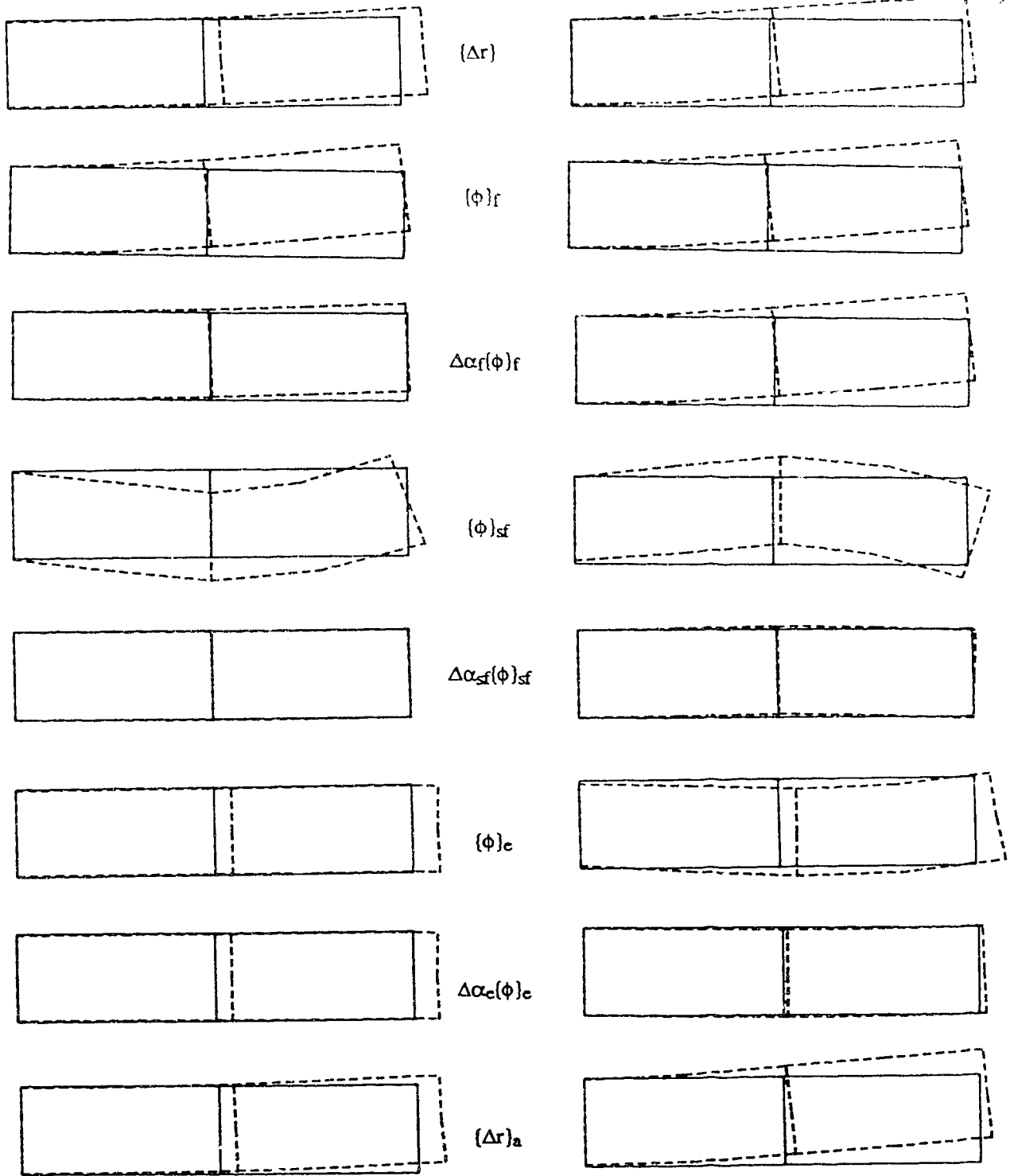
(a): at linearly elastic regime

(b): at limit point

Figure 4.25: Actual displacement increment vector, eigenvectors, eigenvector components and approximate increment vector for the elastic softening beam-rod at linear regime and limit point.

$\{\Delta r\}$

$\{\phi\}_f$

$\Delta \alpha_f \{\phi\}_f$

$\{\phi\}_e$

$\Delta \alpha_e \{\phi\}_e$

$\{\phi\}_{sf}$

$\Delta \alpha_{sf} \{\phi\}_{sf}$

$\{\Delta r\}_a$

(a): at state C   (b): at state D
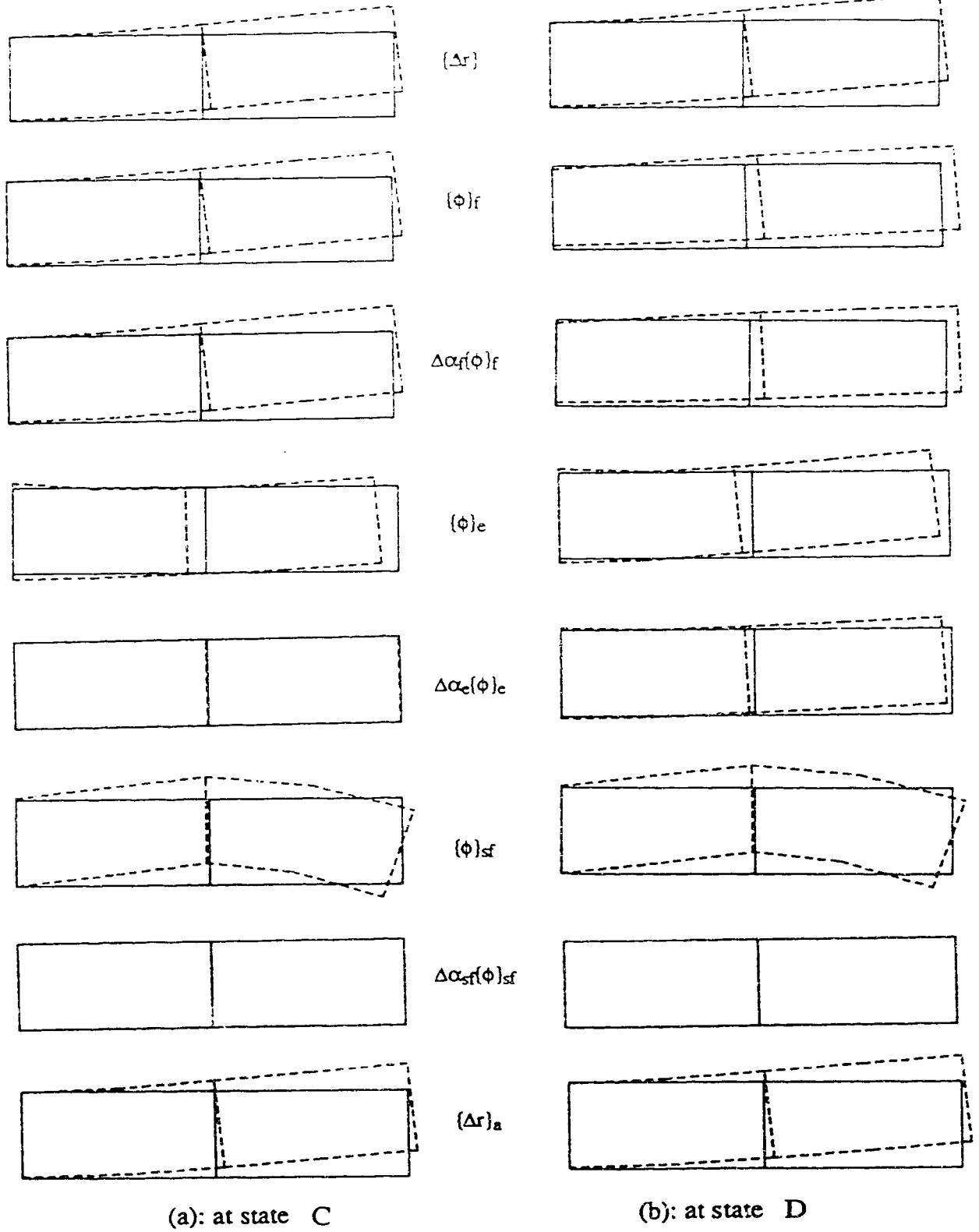
Figure 4.26: Actual displacement increment vector, eigenvectors, eigenvector components and approximate increment vector for the elastic softening beam-rod at states C and D
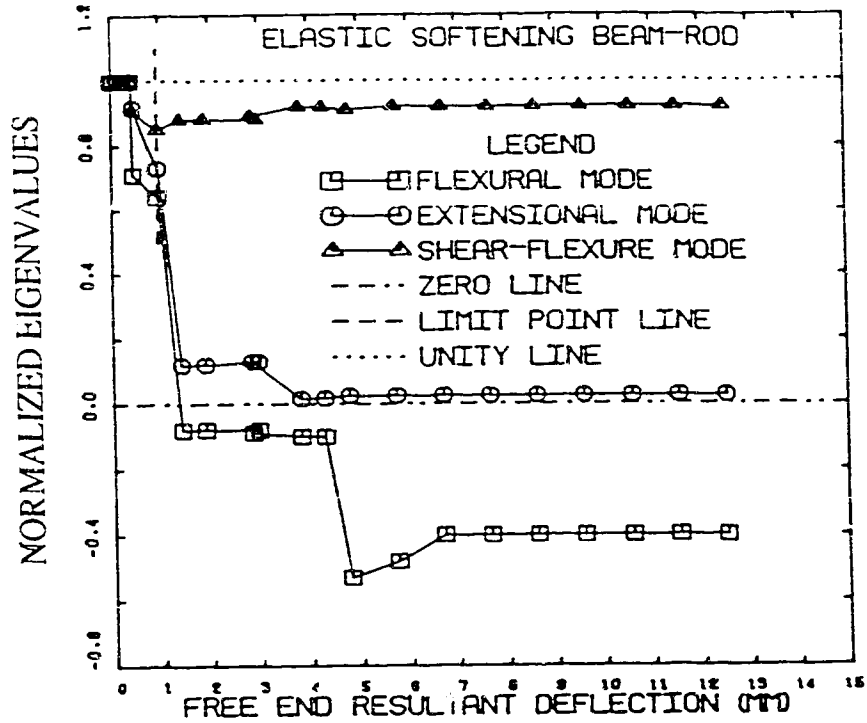
Figure 4.27: Variation of the normalized eigenvalues with the resultant deflection at node 11 for the elastic softening beam-rod.
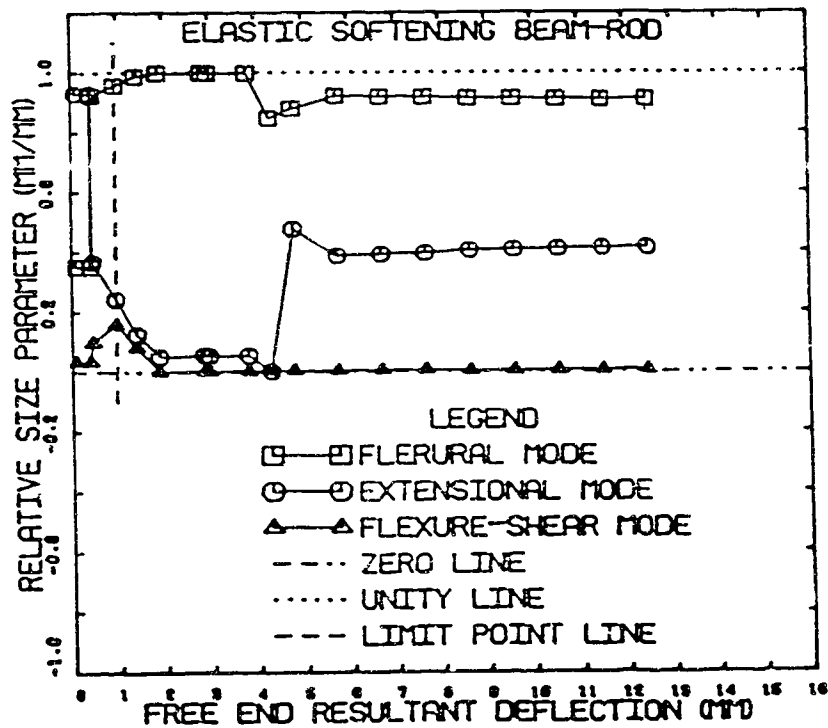
Figure 4.28: Variation of the relative size parameter with the resultant deflection at node 11 for the elastic softening beam-rod.
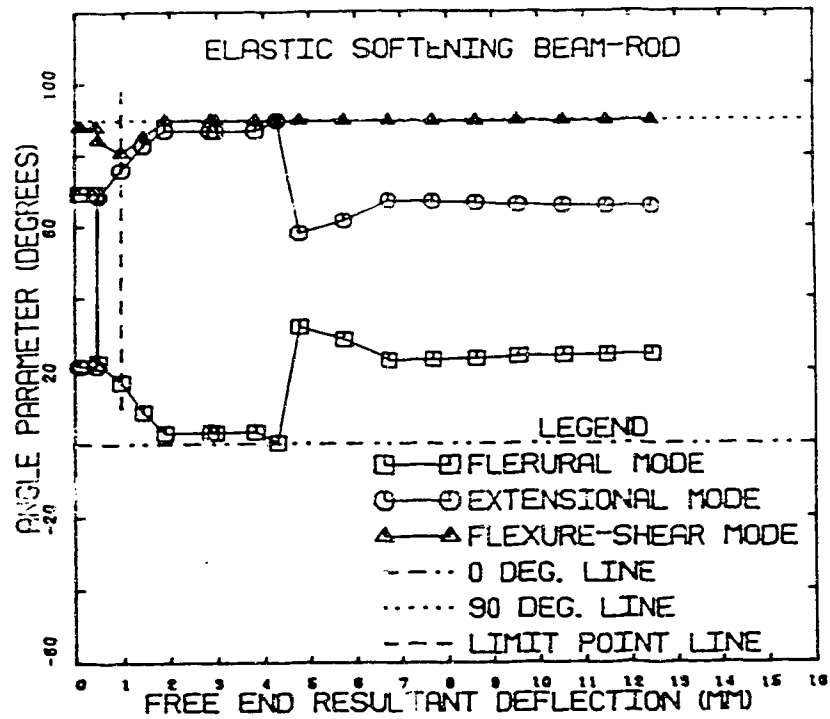
Figure 4.29: Variation of the angle parameter with the resultant deflection at node 11 for the elastic softening beam-rod.
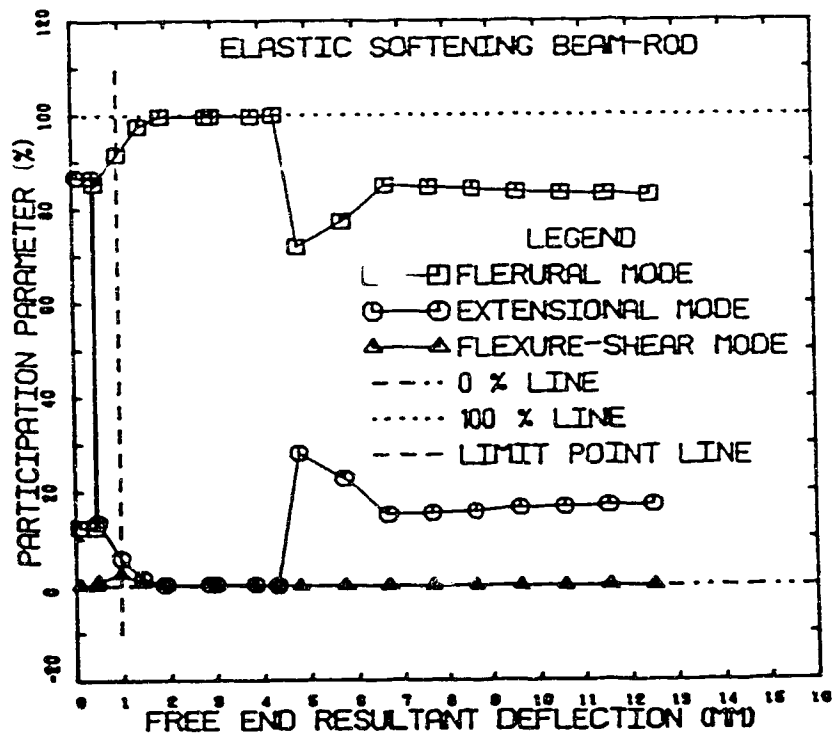
Figure 4.30: Variation of the participation parameter with the resultant deflection at node 11 for the elastic softening beam-rod.
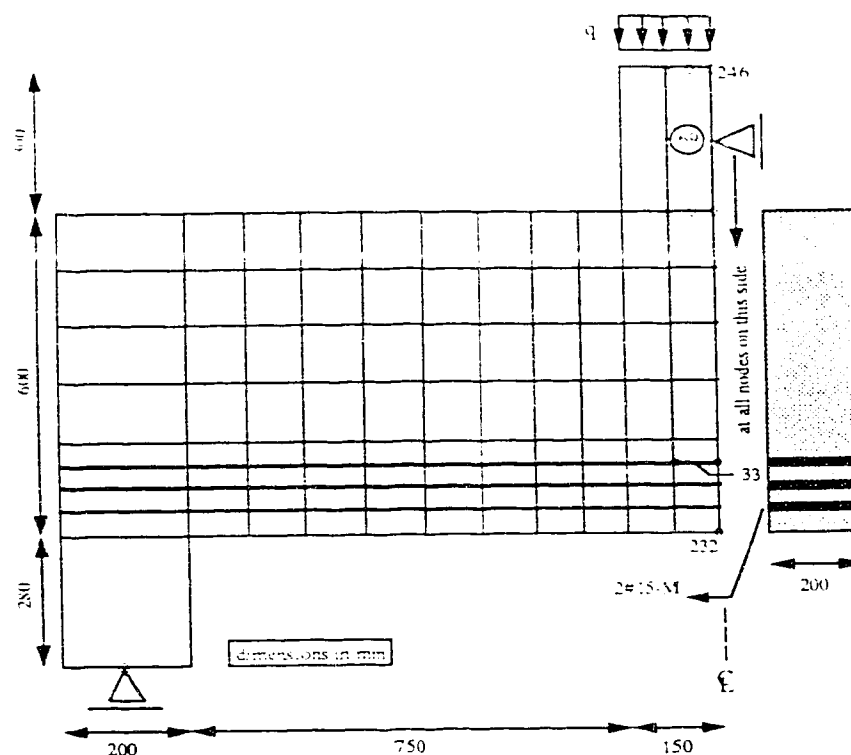
Figure 4.31: Discretization, dimensions, loads and boundary conditions for the south span of the reinforced concrete deep beam.
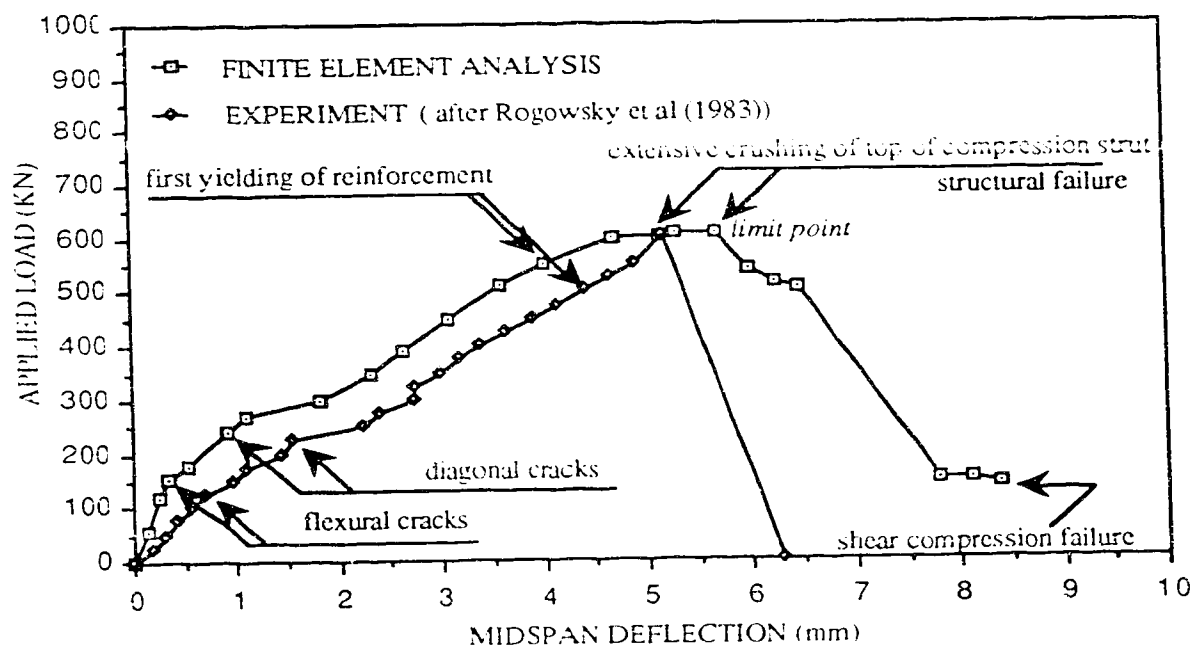
Figure 4.32: Load-deflection curves from the finite element analysis and experiment of the reinforced concrete beam.

(a) Experiment*

	:	CRACK	X	:	SHEARING
	:	CRUSHING	◇	:	SMASHING
∫	:	WIDE CRACK	▲	:	NO AGG INT
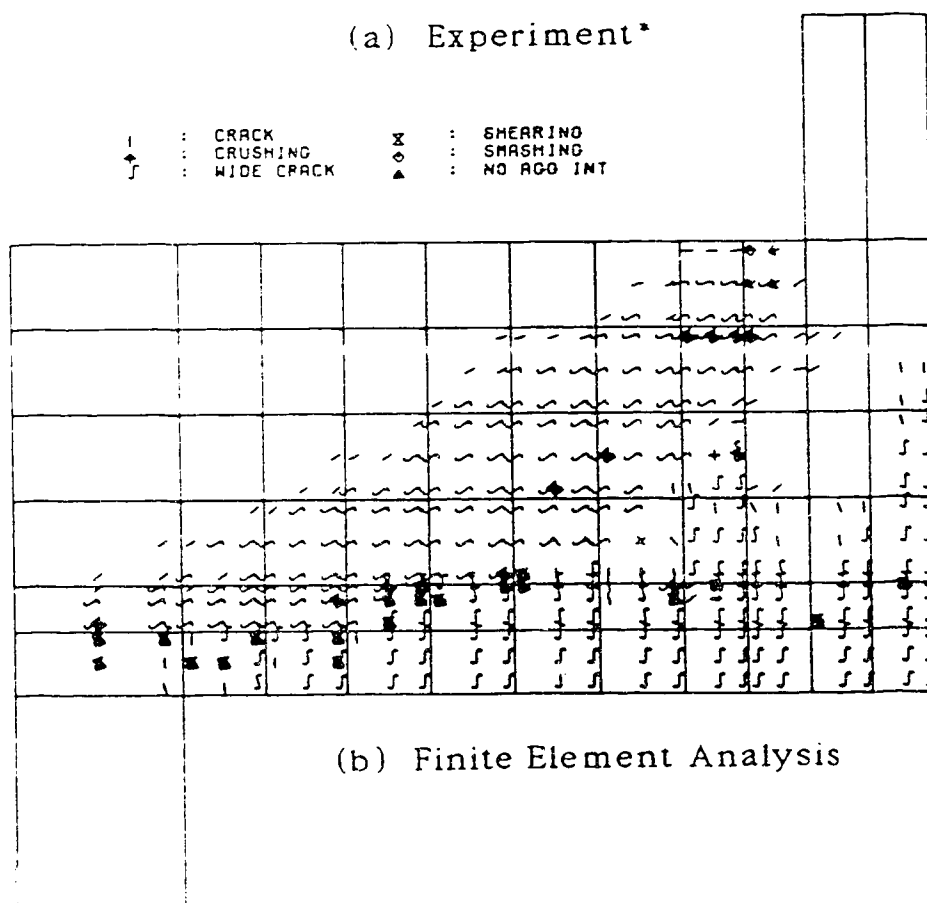
(b) Finite Element Analysis

Figure 4.33: View of the south span of the reinforced concrete deep beam at maximum load.(*reproduced by permission of J.G. MacGregor)
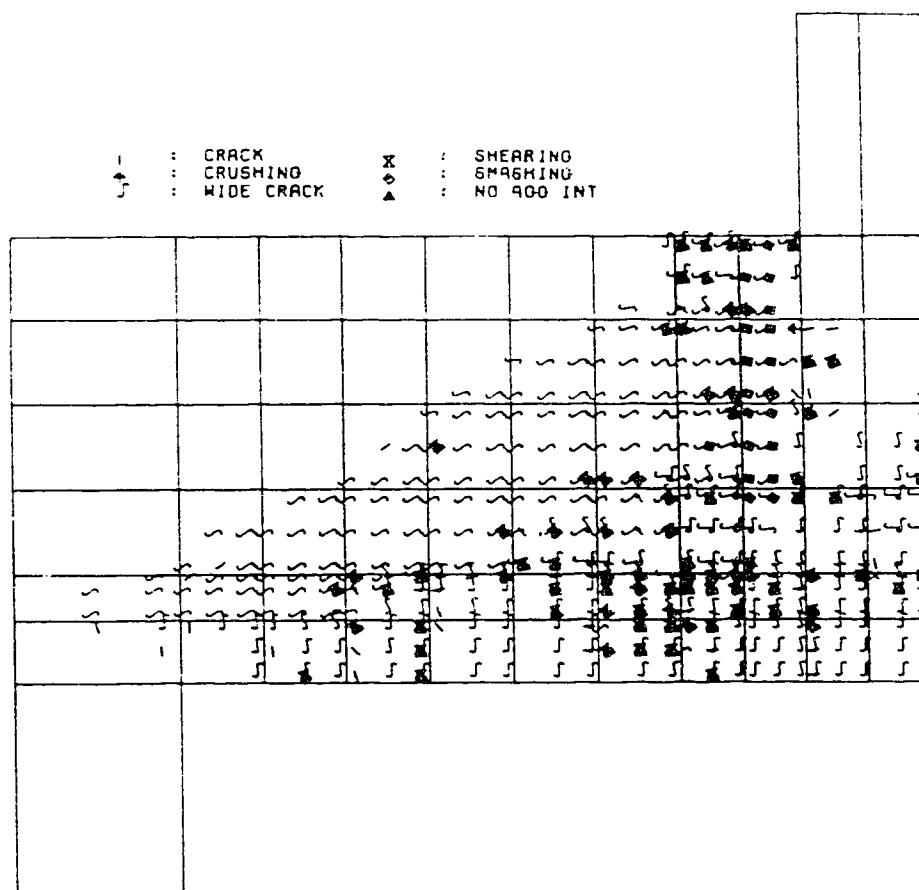
Figure 4.34: Distribution of material damage in the reinforced concrete deep beam at shear compression failure.
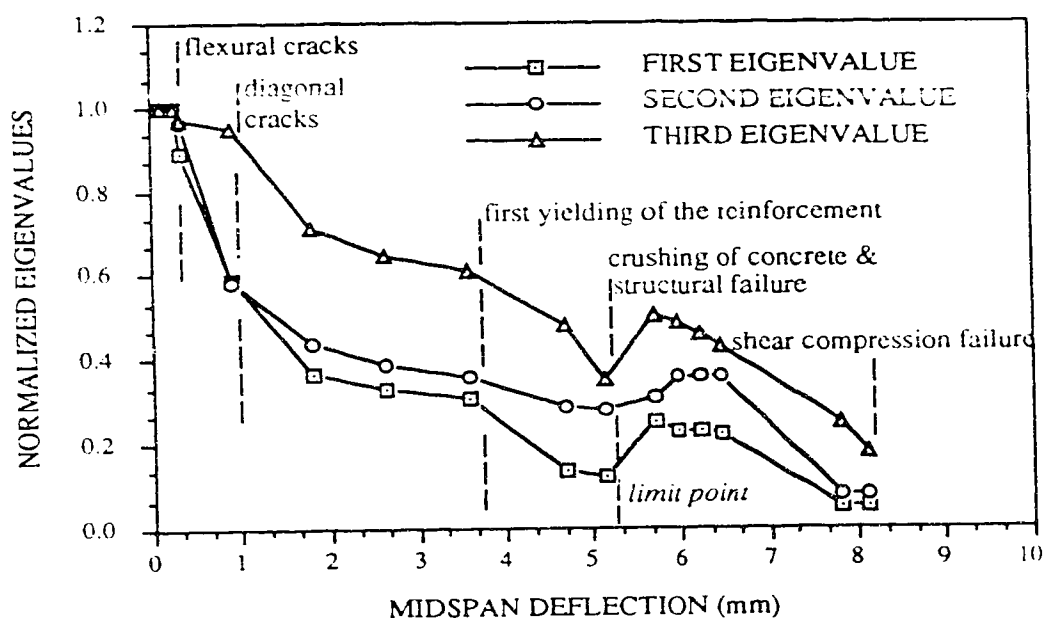
Figure 4.35: Variation of the normalized eigenvalues with the midspan deflection of the reinforced concrete beam.
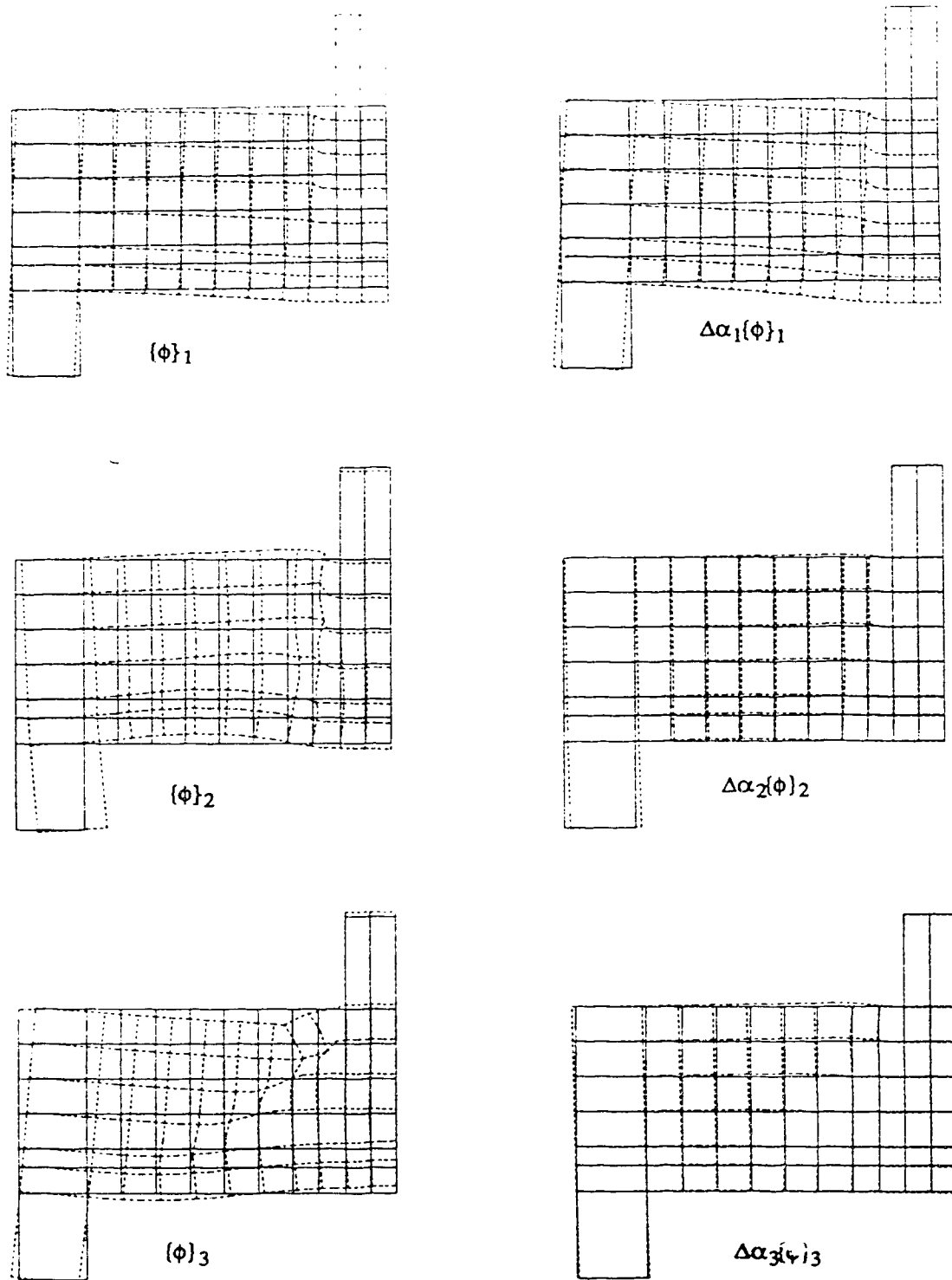
Figure 4.36: The eigenvectors and eigenvector components for the reinforced concrete deep beam at shear compression failure.

{Δr}
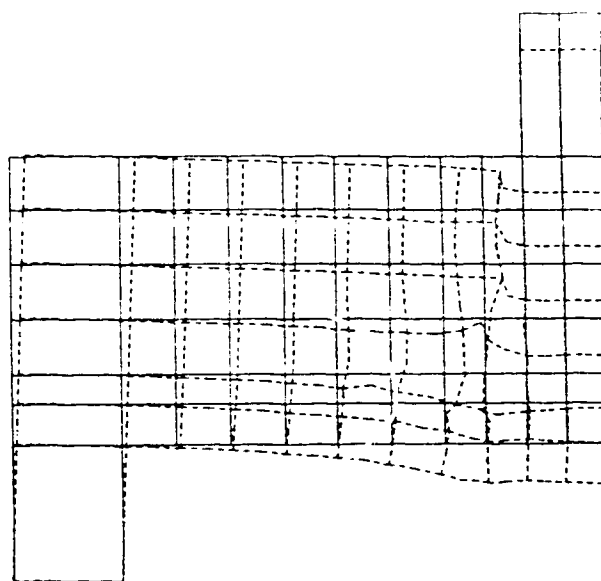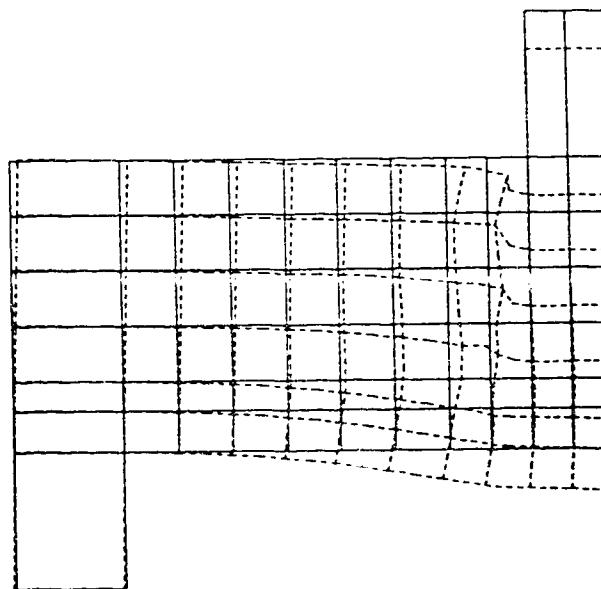
{Δr}$_a$

Figure 4.37: The actual displacement increment vector and the approximate displacement increment vector for the reinforced concrete deep beam at shear compression failure.
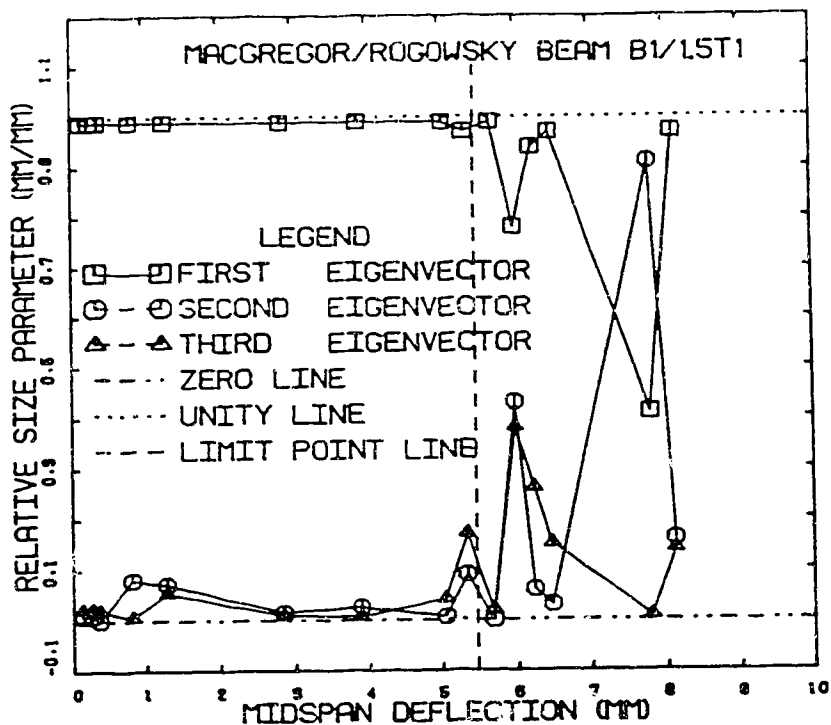
Figure 4.38: Variation of the relative size parameter with the midspan deflection for each eigenvector component of the reinforced concrete deep beam.
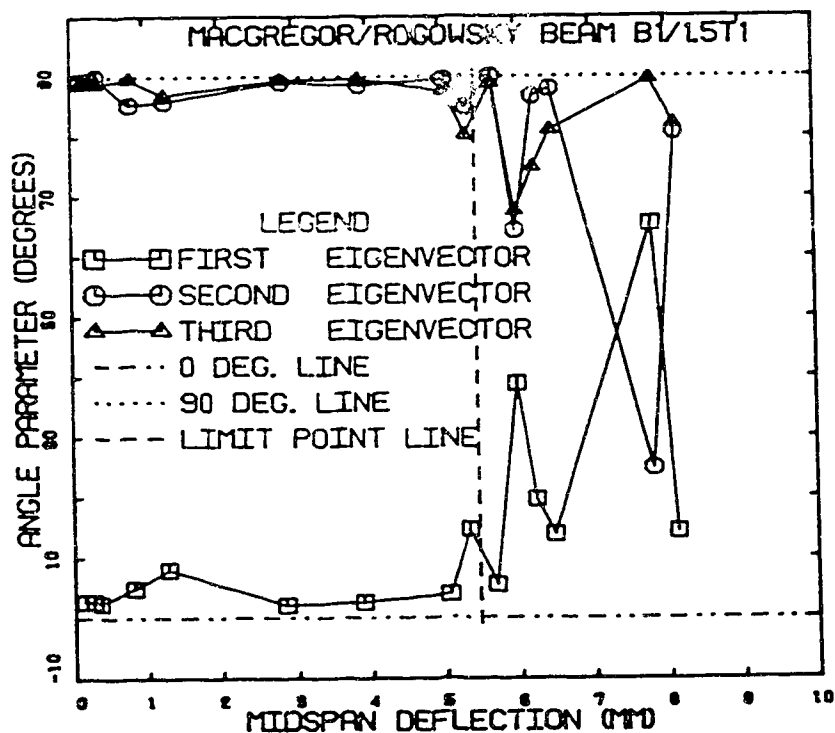
Figure 4.39: Variation of the angle parameter with the midspan deflection for each eigenvector component of the reinforced concrete deep beam.
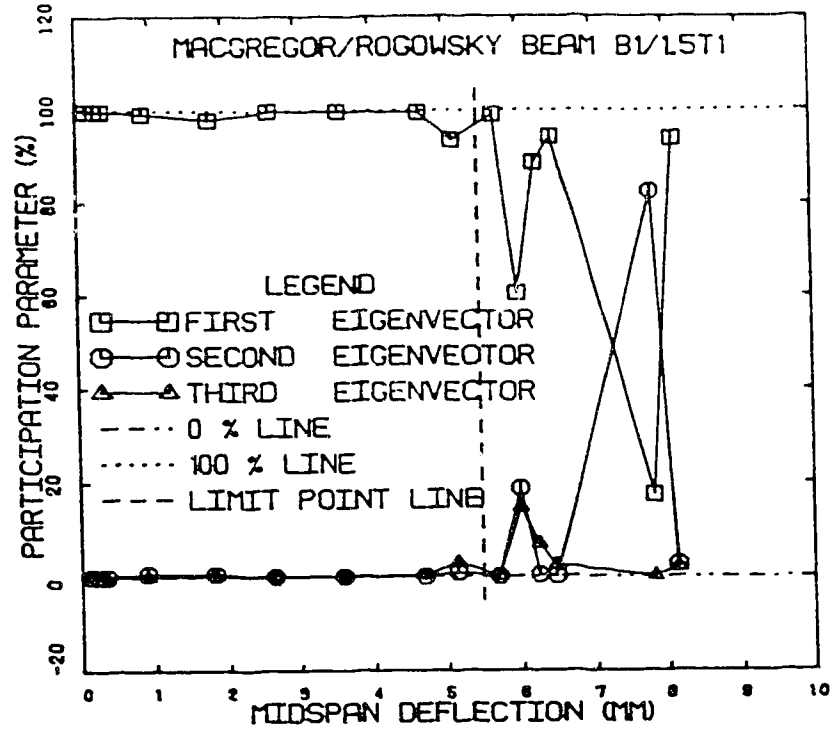
Figure 4.40: Variation of the participation parameter with the midspan deflection for each eigenvector component of the reinforced concrete deep beam.
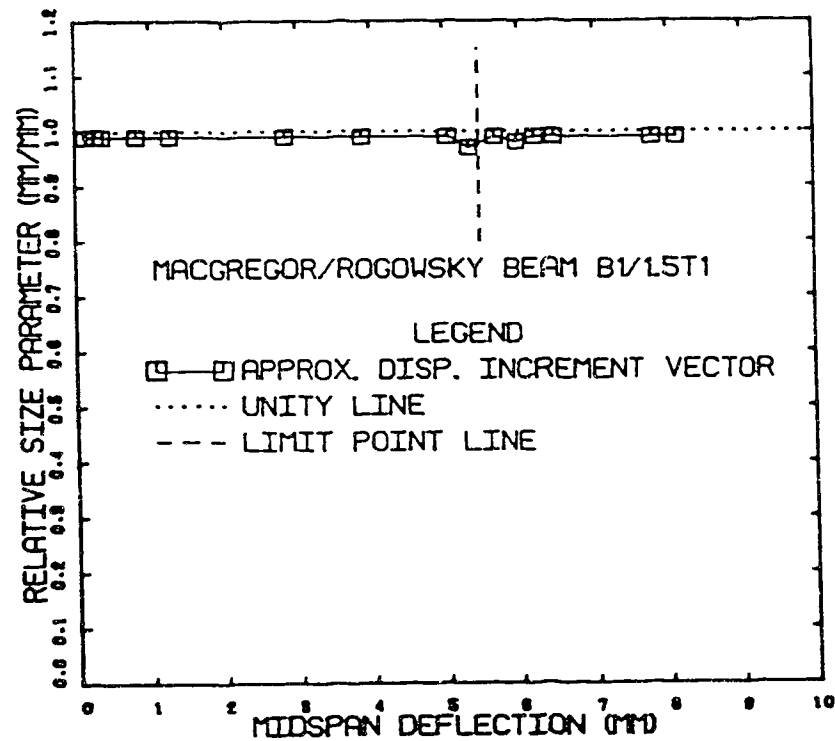
Figure 4.41: Variation of the relative size parameter with the mids an deflection for the approximate displacement increment vector of the reinforced concrete deep beam.
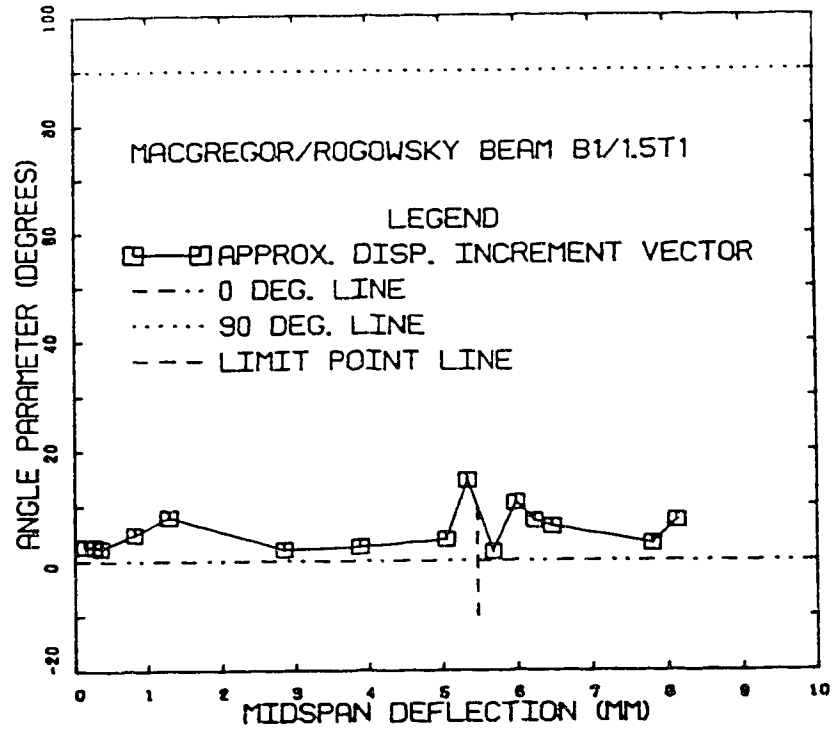
Figure 4.42: Variation of the angle parameter with the midspan deflection for the approximate increment vector of the reinforced concrete deep beam.
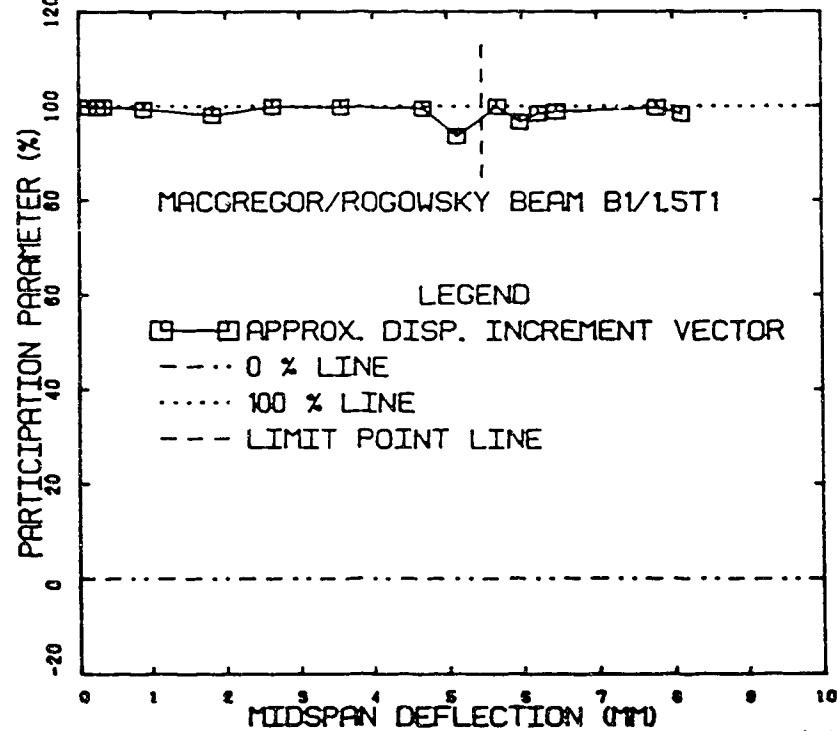
Figure 4.43: Variation of the participation parameter with the midspan deflection for the approximate displacement increment vector of the reinforced concrete deep beam.
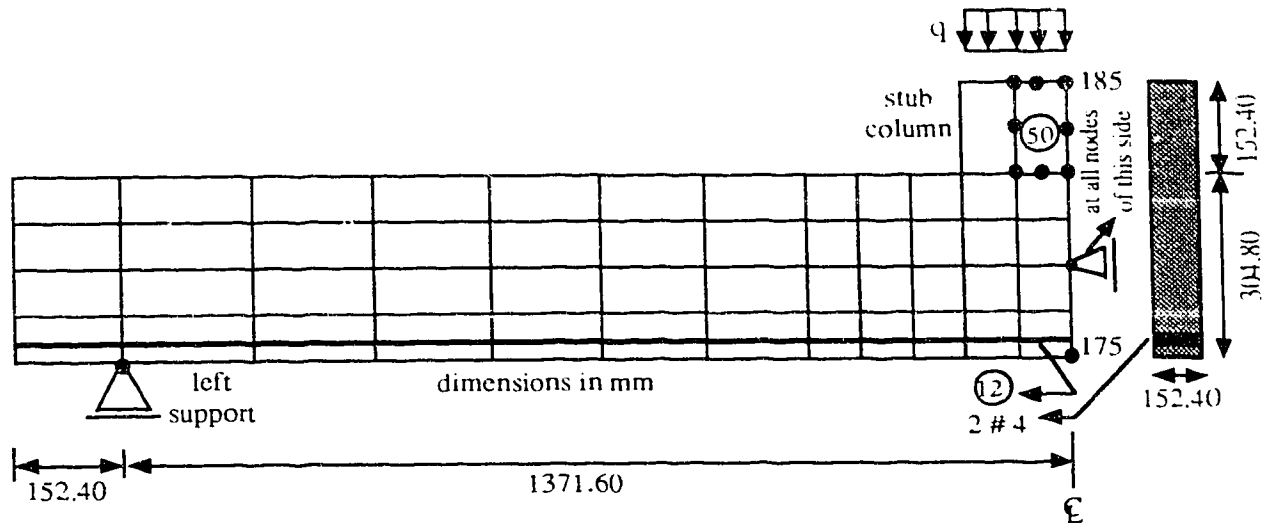
Figure 4.44: Discretization, dimensions, loads and boundary conditions for the reinforced concrete shallow beam.
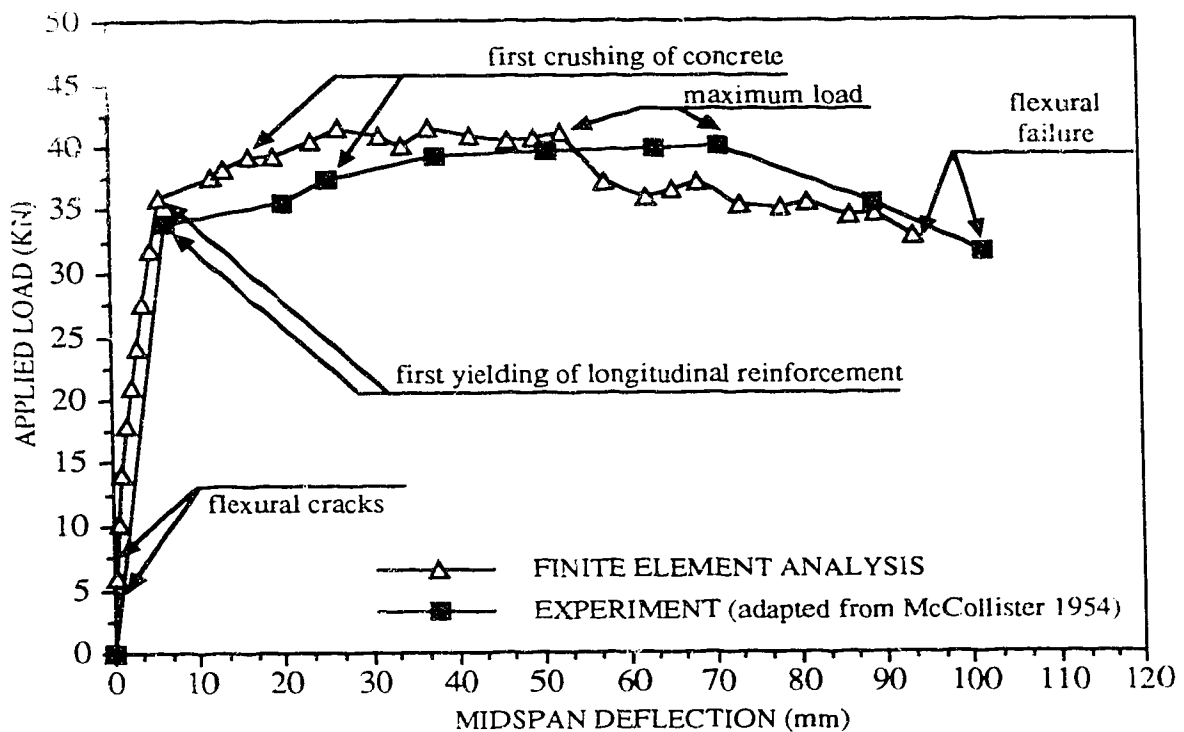
Figure 4.45: Load-deflection curves from the finite element analysis and the experiment for the reinforced concrete shallow beam.
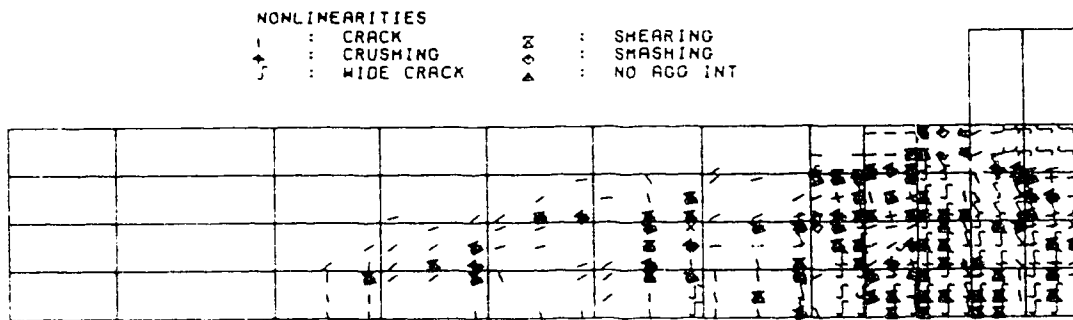
Figure 4.46: View of the reinforced concrete shallow beam at maximum load.

$\{o\}_1$

$\Delta\alpha_1\{\phi\}_1$

$\{o\}_2$

$\Delta\alpha_2\{o\}_2$
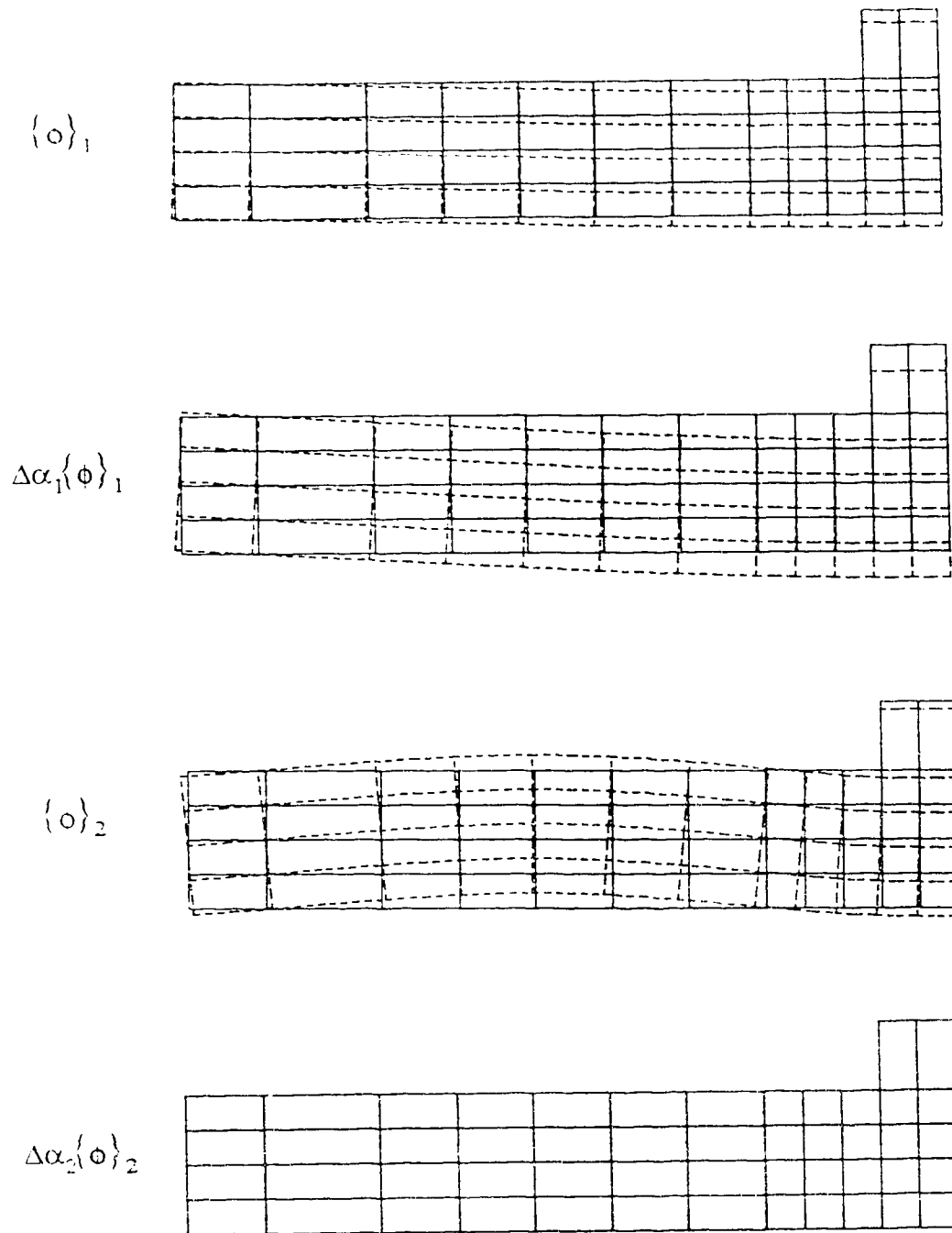
Figure 4.47: The eigenvectors and the eigenvectors components for the reinforced concrete shallow beam.
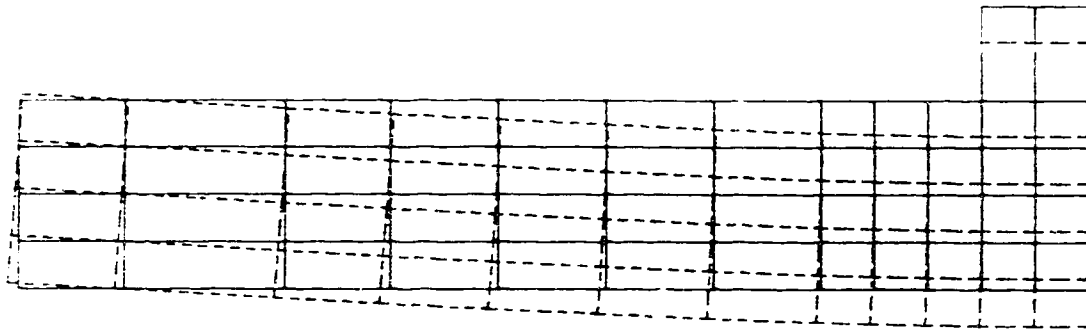
$$\left\{ \Delta r \right\}$$
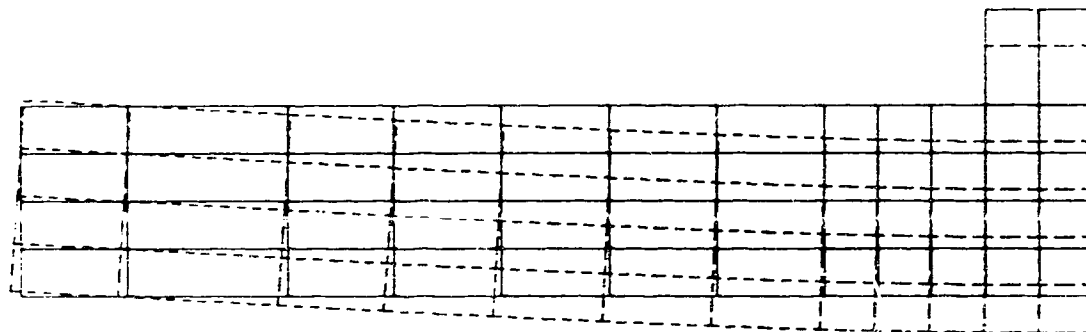
$$\left\{ \Delta r \right\}_a$$

Figure 4.48: The actual displacement increment vector and the approximate displacement increment vector for the reinforced concrete shallow beam.
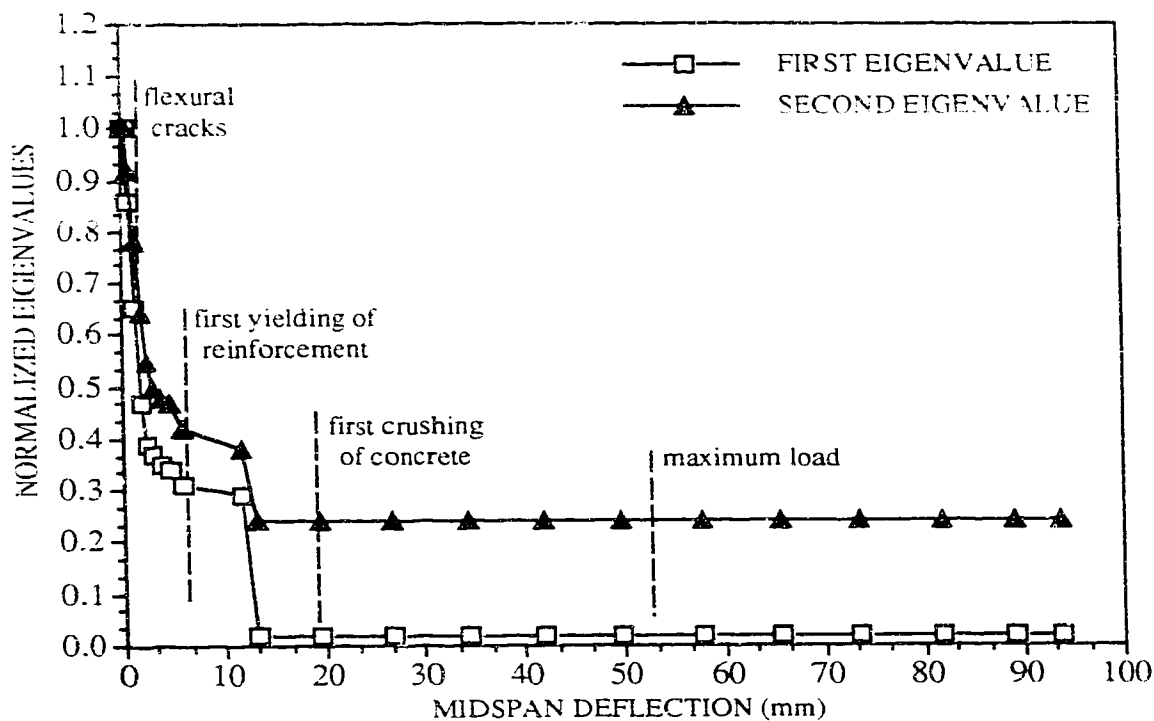
Figure 4.49: Variation of the normalized eigenvalues with the midspan deflection of the reinforced concrete shallow beam.
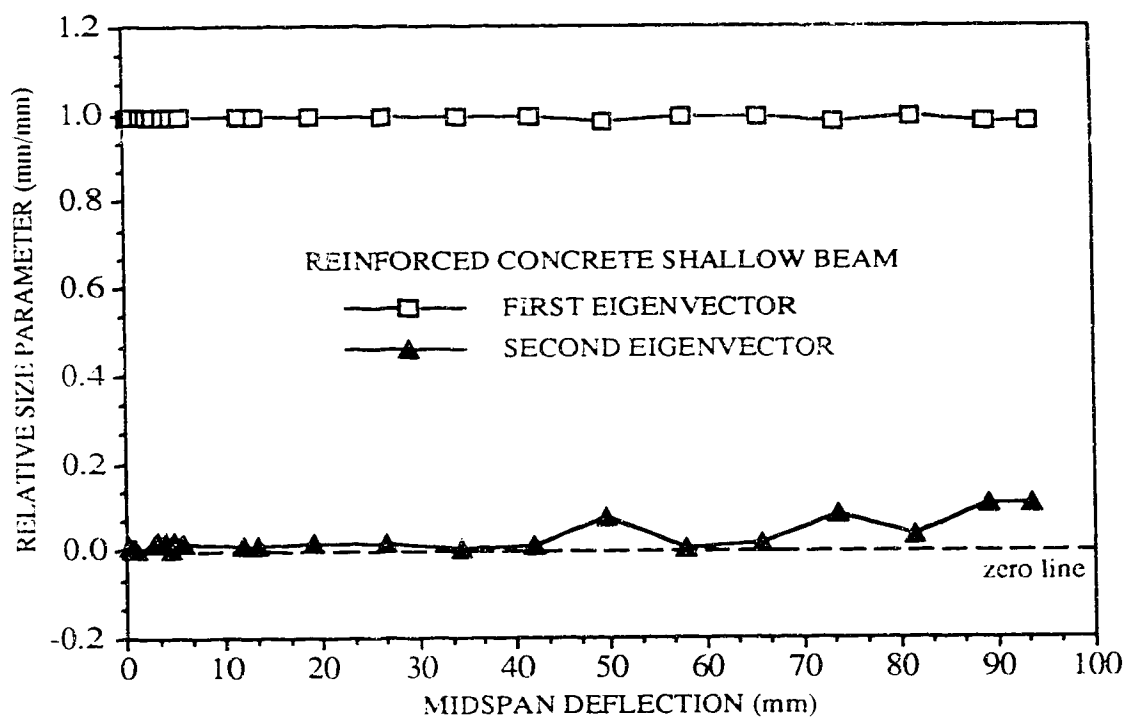
Figure 4.50: Variation of the relative size parameter with the midspan deflection of the reinforced concrete shallow beam.
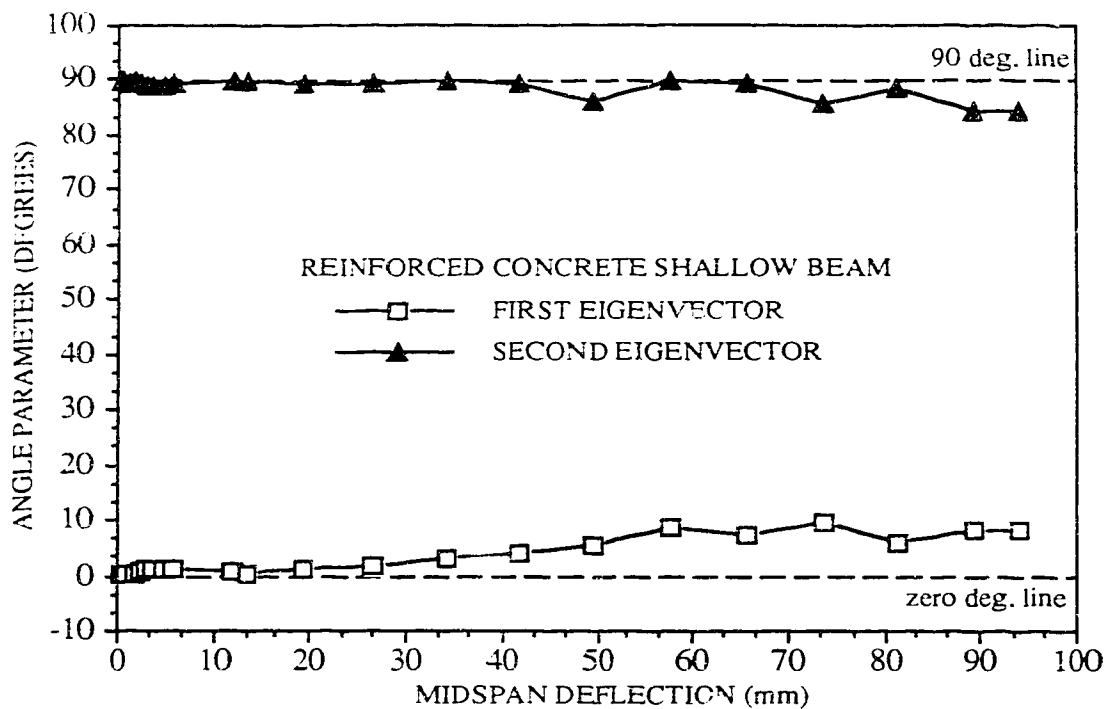
Figure 4.51: Variation of the angle par ieter with the midspan deflection of the reinforced concrete shallow beam.
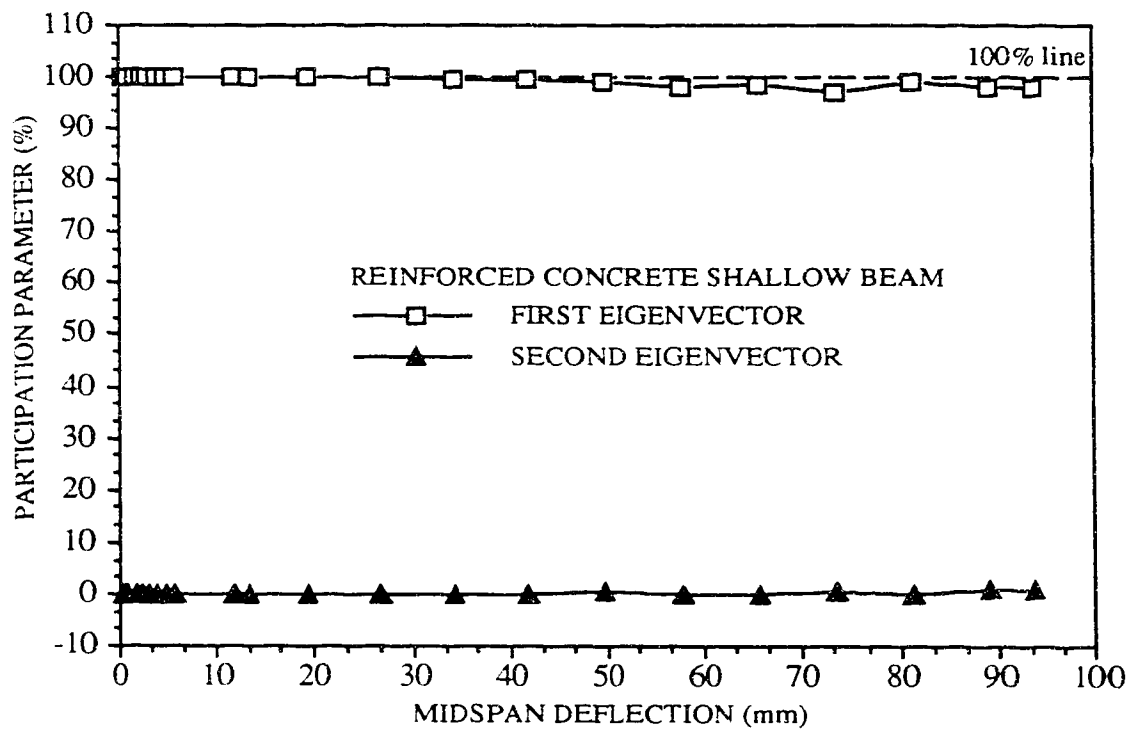
Figure 4.52: Variation of the participation parameter with the midspan deflection of the reinforced concrete shallow beam.

CHAPTER 5

AN EIGENVECTOR-BASED SOLUTION STRATEGY

5.1 Introduction

The solution strategies developed to date for solving materially nonlinear problems have been formulated in the natural basis associated with the N global degrees of freedom of the discretized structure. This is the case of all methods resulting from the Newton-Raphson, displacement control and Riks-Wempner formulations as reviewed in Chapter 2. For these methods, the general form of the iterative and incremental equilibrium equations is given by expression [3.9] which represents a N-dimensional system of banded and coupled equations. Thus, the iterative process involves N-dimensional vectors to store displacement increments and unbalanced loads. In addition, the equation solver usually utilizes out-of-core storage and goes repeatedly through the steps of decomposition of the stiffness matrix, reduction of the load vector and backsubstitution of the degrees of freedom.

Riks (1987) and Felippa (1988), while reviewing the current status of solution strategies for nonlinear problems, have addressed the reduction methods, originally developed by Almroth et al. (1978) and Noor and Peters (1980), as the most promising class of available methods. As outlined in Chapters 2 and 3, Almroth et al. have selected initial displacement vectors and buckling modes, whereas Noor and Peters have chosen path derivatives vectors to comprise the set of base vectors which are applied to reduce the order of the

system of equilibrium equations. Noor and Peters (1981) have improved the existing version of the reduced basis technique by introducing the arc-length as a path parameter. A review of the recent applications of the reduction methods in dynamics and in geometrically nonlinear structural analysis has been covered by Noor (1981). Although effective for geometrically nonlinear problems, the reduction methods have not so far been applied to materially nonlinear problems for which localization of deformation may govern the displacement response. In addition, the reduction methods have utilized nonorthogonal base vectors within the Rayleigh-Ritz technique applied to reduce the number of the global degrees of freedom of the discretized structure. The adoption of nonorthogonal base vectors causes coupling of the equilibrium equations as discussed in Chapter 3, equation [3.16].

It has been demonstrated in Chapter 3 that the selection of the eigenvectors as base vectors results in a system of uncoupled equilibrium equations given by expression [3.28]. Furthermore, it has been concluded in chapter 4 that, among the N eigenvectors extracted from the t. nt stiffness matrix, a much smaller number M of eigenvectors pai.icipate effectively in the actual displacement incremen. vector of the materially nonlinear structure. Recalling the case studies of Chapter 4 and Table 4.6, the maximum values of N and M are respectively 476 for the reinforced concrete deep beam and 5 for the linearly elastic plane structure with aspect ratio 4/1. This implies that the selection of M participant eigenvectors as base vectors in the description of incremental equilibrium expressed in [3.28] results in a reduced system of M uncoupled equilibrium

equations, given in terms of generalized displacements and generalized loads. For the majority of the case studies of Chapter 4, a single generalized displacement increment that multiplies the eigenvector associated with the lowest eigenvalue has described the displacement response of the materially nonlinear structure, including the failure mechanism. This strongly suggests that an accurate and efficient solution can be obtained with a reduced set of incremental equilibrium equations.

The objetive of this chapter is to formulate an eigenvector-based solution strategy that rests on the conclusions of Chapters 3 and 4. For materially nonlinear problems, the specific requirements of the solution strategy correspond to the difficulties that usually hamper the numerical analysis, such as abrupt changes in the stiffness, the condition of near or complete singularity of the updated stiffness matrix at the vicinity of limit points, assessment of limit points, description of the descending branch of the load-deflection curve and the capture of the failure mode of the structure. Other general requirements are cost-effectiveness and a relatively fast rate of convergence.

After this introduction, the chapter follows with the formulation of the eigenvector-based solution strategy for the preiterative and iterative phases. Subsequently, the algorithms for both phases are introduced. Estimates of the rate of convergence and of the computational effort are then presented. A discussion on the potential of the eigenvector-based solution strategy ends the chapter.

5.2 General Characteristics

The conventional arc-length method, due to Wempner (1971) and Riks (1972), describes equilibrium paths in the (N+1)-dimensional load-displacement space. However, if the approximate displacement increment vector, given in [4.21], is inserted in the arc-length equations, the equilibrium paths can be described in the (M+1)-dimensional load-generalized displacement subspace, where M is much less than N. This is the general characteristic that guides the formulation of the solution strategy. Thus, the proposed solution strategy identifies the reduced dominant eigenvector basis and then uses the corresponding generalized displacement increment and the load factor increment as interdependent variables. These variables comprise the finite arc-length, which is the independent variable.

In each load increment, the solution strategy has two phases. In the **preiterative** phase, a trial displacement increment is calculated followed by an assessment of the dominant eigenvector basis, reduction of the system of equilibrium equations into the generalized form and computation of the arc-length and other solution control parameters. The **iterative** phase starts and follows a path which is orthogonal to the arc-length. Within this path, the iterative phase utilizes the modified Newton-Raphson scheme to iterate load factor and generalized displacements. Kao (1974) has compared the performance of different iterative schemes based on Newton-Raphson methodology. The modified Newton-Raphson method has shown an outstanding performance with respect to the degree of accuracy and amount of computational effort for moderate

sizes of solution steps employed in the analysis of nonlinear problems.

This solution strategy is formulated to deal primarily with proportional loads. Nevertheless, the alternative for an additional constant load vector has been taken into account.

5.3 The Preiterative Phase

The preiterative phase starts with the computation of the first displacement increment vector. The set of incremental equilibrium equations is solved in the form of

$$[K]_t^a \{\Delta r\}^c = (\pm 1.0) \{R\}, \qquad\qquad [5.1]$$

where $\{\Delta r\}^c$ is the first displacement increment vector associated with the reference force vector $\{R\}$.

A predetermined number "p" of eigenvectors $\{\phi\}_i$ and corresponding eigenvalues λ_i are then evaluated from the tangent stiffness matrix, as illustrated in Fig. 5.1. The stability of equilibrium is investigated through the sign of the lowest eigenvalue or, alternatively, through the sign of the pivots of the factorized stiffness matrix. The result of this investigation determines the sign of the first load factor increment $\Delta\rho^c$. Based on the vector $\{\Delta r\}^c$ and the extracted eigenvectors, the first generalized displacement increment vector $\{\Delta\alpha\}^c$, shown in Fig. 5.2, is computed. The resulting eigenvector components $\Delta\alpha_i\{\phi\}_i$ are tested for dominance, after which the dominant components are selected. Next, the transformation of the

incremental equilibrium equations, from the conventional (N+1)-dimensional load-displacement vector space to the (M+1)-dimensional load-generalized displacement subspace, takes place. This process gives M uncoupled incremental equilibrium equations. Finally, the stiffness parameter is used to adjust the current arc-length. Generalized displacements and loads are adjusted accordingly.

Figures 5.1 and 5.2 illustrate this phase in both vector spaces and emphasize the referred transformation of basis. In these figures, a right superscript on the variable denotes the order of the iteration within the solution step. The following stages form the preiterative phase.

5.3.1 Eigenanalysis of the Tangent Stiffness Matrix

The eigenanalysis of the tangent stiffness matrix may be required at point "a" in Fig. 5.1, which represents the beginning of a typical solution step. In the case of materially nonlinear problems, the eigenproblem, stated in Chapter 3, can be written in its standard form as

$$[K]_t^a[\Phi] = [I][\Phi][\Lambda],$$

[5.2]

where the eigenvectors in $[\Phi]$ and corresponding eigenvalues in $[\Lambda]$ are extracted from the tangent stiffness matrix $[K]_t^a$ updated and assembled at point "a" in Fig. 5.1. In the current version of the modified program NISA, the updated tangent stiffness matrix $[K]_t^a$ and the identity matrix $[I]$ in [5.2] constitute the input for the

eigenanalysis of materially nonlinear structures through the subspace iteration method (Bathe and Wilson 1976).

In dealing with material nonlinearities and in the vicinity of limit points, singular or nearly singular tangent stiffness matrices may be encountered. This can cause convergence problems in the evaluation of the eigenpairs. For nearly singular tangent stiffness matrices, Moler and Stewart (1973) have proposed the "QZ" algorithm that applies implicit shifts to the matrix to render it nonsingular while iterating for the solution of the correct eigenpairs.

For indefinite stiffness matrices, explicit and positive shifts are utilized to disclose negative eigenvalues which are commonly associated with descending branches of load-deflection curves. Denoting μ as a positive shift, the shifted stiffness matrix is computed as

$$\left[\hat{K}\right]_t^a = [K]_t^a + \mu[\,I\,],$$

[5.3]

where the symbol $\wedge$ denotes "shifted". The standard eigenproblem for the shifted matrix can be stated as

$$\left[\hat{K}\right]_t^a[\Psi] = [\,I\,][\Psi][\Omega],$$

[5.4]

where $[\Psi]$ and $[\Omega]$ contain respectively the eigenvectors and the eigenvalues of the shifted stiffness matrix. Substituting the shifted stiffness matrix given in [5.3] into [5.4], it yields

$$[K]_t^a[\Psi] = [\,I\,][\Psi]\left([\Omega]-[\mu]\right),$$

[5.5]

where the ith eigenvalue is $\omega_i - \mu$. Since the solution of [5.2] and [5.5] is unique, it is concluded that

$$\{\psi\}_i = \{\phi\}_i \qquad\qquad\qquad [5.6a]$$

and

$$\lambda_i = \omega_i - \mu, \qquad\qquad i = 1,..., N. \qquad\qquad [5.6b]$$

Thus, the relations [5.6a] and [5.6b] state that the shifting technique, applied to a nearly singular or indefinite stiffness matrix, does not alter the original eigenvectors. In addition, the eigenvalues of the unshifted matrix can be recovered by subtracting the shift μ from the eigenvalues of the shifted matrix. Implicit and explicit shifts are currently implemented in the program NISA (Stegmüller et al. 1983).

Finally, the subspace iteration method outputs a preselected number of eigenpairs $(\lambda_i, \{\phi\}_i)$, $i = 1,..., p$, where $p<N$. The eigenvalues obey the order

$$\lambda_1 < \lambda_2 < ...\lambda_p \qquad\qquad\qquad\qquad [5.7]$$

from the lowest to the highest. The examples of materially nonlinear structures investigated in Chapter 4 have indicated that the participant eigenvector components are among the first two or three eigenvectors. For this reason, an upperbound for the number of preselected eigenvectors has been set equal to 3 throughout the applications of the present study.

5.3.2 Assessment of the Participation of the Preselected Eigenvector Components

Up to now, the normalized eigenvectors and the first displacement increment vector have been calculated. It is assumed herein that the "p" preselected normalized eigenvectors constitute a basis for a p-dimensional vector subspace in which

$$\{\Delta r\}^c \cong \sum_{i=1}^{p} \Delta \alpha_i^c \{\phi\}_i ,$$

[5.8]

where $\Delta \alpha_i^c$ is the ith generalized displacement increment associated with the first displacement increment vector. The generalized displacement increment in [5.8] is evaluated through expression [4.3], which yields

$$\Delta \alpha_i^c = \langle \phi \rangle_i \{\Delta r\}^c .$$

[5.9]

The computation of [5.9] makes it possible to know all the preselected eigenvector components in [5.8].

The first unit displacement increment vector

$$\{\Delta r\}_u^c = \frac{\{\Delta r\}^c}{\| \{\Delta r\}^c \|} ,$$

[5.10]

determines the current and actual direction of deformation of the structure. The objective now is to assess the participation of each preselected eigenvector component in the first displacement

increment vector given in [5.8]. For this purpose, the participation parameter (Section 4.3.4),

$$P_i = 100 \left(\frac{\Delta \alpha_i^c}{\| \{\Delta r\}^c \|} \right)^2 \% \qquad i = 1, \dots, p \qquad [5.11]$$

is applied to determine the percentage of participation for each of the preselected eigenvector components. It is noted that [5.11] is not sensitive to the size of the first displacement increment vector, since it is normalized with respect the Euclidean norm of this vector. Therefore, variation in participation implies variation in direction between the eigenvector component and the first unit displacement increment vector.

Among all the preselected eigenvector components for which the participation parameter has been computed above, the ones that participate effectively in the actual first displacement increment vector are selected. The selection criterion is based on the domain intervals of the participation parameter provided in Table 4.1. In this table, the orthogonal and quasi-orthogonal eigenvector components, called herein nonparticipants, show participation parameters $P_i \leq 1$. Thus, if all the nonparticipant eigenvector components are excluded from [5.8], the first displacement increment vector can be computed approximately as

$$\{\Delta r\}^c \cong \sum_{i=1}^{M} \Delta \alpha_i^c \{\phi\}_i, \qquad [5.12]$$

where M is the number of participant eigenvector components. Expression [5.12] defines the approximate displacement increment vector treated in Section 4.4.

In practice, the degree of accuracy incorporated in [5.12] is considered satisfactory if

$$\sum_{i=1}^{M} P_i \geq 95\% , \qquad\qquad [5.13]$$

where P_i is the participation parameter for the ith participant eigenvector component.

5.3.3 Transformation and Reduction of the Conventional Incremental Equilibrium Equations

The results of Section 4.4 have demonstrated that the participant eigenvectors form a basis of a M-dimensional vector subspace. In this subspace, the first displacement increment vector and the reference force vector can be expressed respectively as:

$$\{\Delta r\}^c = [\Phi]\{\Delta \alpha\}^c \qquad\qquad [5.14]$$

and

$$\{R\} = [\Phi]\{\gamma\}^c , \qquad\qquad [5.15]$$

where the columns of $[\Phi]$ are the selected participant eigenvectors and $\{\gamma\}^c$ is the generalized reference force vector which can be computed as

$$\{\gamma\}^c = [\Phi]^T \{R\}.$$

[5.16]

Expressions [5.14] and [5.15] relate entities given in the conventional N-dimensional vector space to corresponding entities defined in the M-dimensional vector subspace of the participant eigenvectors. The matrix [Φ] serves as a transformation matrix. Since the M participant eigenvectors are linearly independent, the transformation matrix is nonsingular and defines a unique transformation between both vector spaces. The relation between both vector spaces is illustrated in Figs. 5.1 and 5.2 for displacement and load factor. Figures 5.3 and 5.4, on the other hand, show the transformation relations for force vectors given in both vector spaces.

Substituting expressions [5.14] and [5.15] into the incremental equilibrium equations [5.1] yields

$$[K]_t^a [\Phi] \{\Delta\alpha\}^c = (\pm 1.0)[\Phi]\{\gamma\}^c.$$

[5.17]

Premultiplying [5.17] by [Φ]^T and accounting for the orthonormality property of the eigenvectors, the expression above may be written as

$$[\Phi]^T [K]_t^a [\Phi] \{\Delta\alpha\}^c = (\pm 1.0)\{\gamma\}^c,$$

[5.18]

or yet,

$$[\Lambda]_t^a \{\Delta\alpha\}^c = (\pm 1.0)\{\gamma\}^c.$$

[5.19]

Expression [5.19] represents the set of M incremental equilibrium equations in the basis of the selected participant eigenvectors. In addition, the resulting equations are completely uncoupled.

5.3.4 The Stiffness Parameter

A measure of the degree of nonlinearity of a structure that experiences progressive material damage can be used to control the size of the current solution step. Among other measures, Bergan (1979) has proposed the current stiffness parameter to assess the level of overall nonlinearity of the structure at the beginning of a solution step.

The current stiffness parameter utilizes the concept of stiffness of a discretized structure. Thus, the overall stiffness at the beginning of a solution step can be defined as

$$k^c = \frac{\Delta\rho^c}{\|\{\Delta r\}^c\|},$$

[5.20]

where the numerator and the denominator are respectively the first load factor increment and the Euclidean norm of the first displacement increment vector associated with point "c" in Fig. 5.1. The units of [5.20] are N/mm.

Resorting to relation [5.14] and recalling the definition of Euclidean vector norm, the stiffness measure [5.20] can be expressed in the basis of the selected participant eigenvectors as

$$S_p = \dfrac{\dfrac{\Delta\rho^c}{\|\{\Delta\alpha\}^c\|}}{\dfrac{\Delta\rho_1^c}{\|\{\Delta\alpha\}_1^c\|}}.$$

[5.24]

Noting that $\Delta\rho_1^c = (+1.0)$ and $\Delta\rho^c = (\pm 1.0)$, the last expression is simplified to give

$$S_p = \pm \dfrac{\|\{\Delta\alpha\}_1^c\|}{\|\{\Delta\alpha\}^c\|},$$

[5.25]

where the negative and positive signs account respectively for stable and unstable behavior.

The presented definition of the current stiffness parameter is useful as long as the stiffness matrix is updated at the beginning of the current solution step. This definition conforms with the modified Newton-Raphson scheme adopted herein. However, if the initia' stiffness scheme is selected for the sake of economy, an ade' definition of the stiffness parameter is

$$S_p = - \dfrac{\Delta\rho^b}{\|\sum\limits_{i=1}^{\#ite}\{\Delta\alpha\}^i\|} \Bigg/ - \dfrac{\Delta\rho_1^b}{\|\sum\limits_{i=1}^{\#ite}\{\Delta\alpha\}_1^i\|},$$

[5.26]

where $\Delta\rho^b$ and $\Delta\rho_1^b$ are the load factor increments respectively at the end of the current and first solution steps. The denominators of the

first and second terms of the fraction [5.26] represent respectively the Euclidean norms of the accumulated generalized displacement increment vectors for the current and first solution steps. It is remarked that the definition [5.26] incorporates the concept of an average stiffness related to the current solution step. Therefore, it seems appropriate to call this parameter the average stiffness parameter. Figure 5.6 illustrates this concept and the terms in [5.26].

Figure 5.7 presents different types of structural behavior given in terms of load versus norm of the generalized displacement vector. Behavior type 1 is typical of structures whose load-deflection response incorporates an ascending branch, a limit point and a descending branch. Behavior type 2 is representative of ductile structures for which ascending and flat branches are present. Finally, behavior type 3 is characterized by a hardening branch after the ascending branch. Furthermore, it is remarked that the stability of equilibium varies from stable, neutral and unstable for curve type 1, whereas it changes from stable to ne al for curve type 2 and remains stable throughout curve type 3.

Figure 5.8 shows typical variations of the stiffness parameter [5.25] with respect to the Euclidean norm of the generalized displacement vector and for the types of behavior considered in Fig. 5.7. For all types of behavior, the stiffness parameter remains constant (=1.0) within the linear range of the corresponding load-deflection curve. After this range, the stiffness parameter decreases gradually with increasing level of nonlinearity to attain negative values for behavior type 1, and positive values for behavior types 2 and 3.

5.3.5 Determination of the Arc-Length Size

For a materially nonlinear structure, the level of nonlinearity increases as the load-deformation history progresses.

In the context of material behavior, plastic strain increments are irreversible for the models based on the theory of plasticity. On the other hand, for models based on hypoelasticity, total strain increments are reversible as long as the stress increments remain sufficiently small (Chen and Saleeb 1982). The prescription of a considerably large load step can violate the restrictions related to the formulation of the constitutive relations referred above. Problems, such as iterative returning to the material strength surface from an outside stress point and deviation from the actual stress-strain path, are commonly originated due to a large incremental load step.

Regarding the adopted solution strategy, a large solution step gives rise to a large number of iterations which, in turn, is conducive to a high cost of the solution. Therefore, it seems necessary to control the size of the solution step so that a fair representation of the material behavior is preserved and a cost-effective solution is achieved.

The total size of a solution step is approximately formed by the dimension of the finite arc-length (Fig. 2.4), associated with the preiterative phase, and the length of the iteration path defined within the iterative phase (Figs. 5.1 and 5.2). In practice, however, the size of the finite arc-length is more significant relative to the size of the iteration path. Thus, the control of the size of a typical solution step can be carried out through a rational determination of the total size of the current finite arc-length. This is seen as innovative since

the well known contributions by Ramm (1981) and Noor (1981) deal only with constant arc-lengths. An improved approach has been proposed by Bellini and Chulya (1987) whereby the control of the arc-length is carried out with respect to the load factor.

At the beginning of a typical solution step, the finite arc-length, associated with point "c" in Fig. 5.1, is defined as

$$\Delta L^c = \sqrt{\langle \Delta r \rangle^c \{\Delta r\}^c + (\pm 1.0)^2} \ .$$

[5.27]

Using the relation given in [5.14], the finite arc-length can be written in the basis of the M selected participant eigenvectors as

$$\Delta L^c = \sqrt{\langle \Delta \alpha \rangle^c [\Phi]^T [\Phi] \{\Delta \alpha\}^c + (\pm 1.0)^2} \ .$$

[5.28]

Taking into account the orthonormality property of the participant eigenvectors [3.21], expression [5.28] can be simplified to give

$$\Delta L^c = \sqrt{\langle \Delta \alpha \rangle^c \{\Delta \alpha\}^c + (\pm 1.0)^2} \ ,$$

[5.29]

which represents the current generalized finite arc-length seen in Fig. 5.2. Similarly, the generalized finite arc-length computed at the beginning of the first solution step is designated as

$$\Delta L_1^c = \sqrt{\langle \Delta \alpha \rangle_1^c \{\Delta \alpha\}_1^c + (\pm 1.0)^2} \ ,$$

[5.30]

where the subscript $_1$ denotes the first solution step.

Herein, the current generalized finite arc-length [5.27] is proportioned to be equal to

$$\Delta L^{i} = f \times \Delta L_{1}^{c},$$ [5.31]

where ΔL^{1} is the generalized finite arc-length that corresponds to point 1 in Fig. 5.2 and from which the orthogonal iteration path initiates.

The factor f in [5.31] has been chosen as a positive function of the current or average stiffness parameter and reflects the level of nonlinearity of the structure. Since the variation of the stiffness parameter (Fig. 5.8) depends on the type of structural behavior given in Fig. 5.7, two functions for the factor f are considered.

The first function is recommend in conjunction with behavior type 1 and is defined in a stepwise manner as

$1.00 \geq S_{p} \geq 0.10$,	$f = S_{p}$	[5.32]
$0.10 < S_{p} \geq -0.10$,	$f = 0.10$	[5.33]
$-0.10 < S_{p} \geq -1.0$,	$f = -S_{p}$	[5.34]
$S_{p} < -1.0$,	$f = 1.0$	[5.35]

This function is illustrated in Fig. 5.9. For the behavior type 1, a limit point takes place. Therefore, small solution steps in the vicinity of the limit point are automatically prescribed so that the response can be traced with accuracy in that region. Larger solution steps are allowed in the ranges before and after the limit point vicinity.

The second function, shown also in Fig. 5.9, is suggested for use with behavior types 2 and 3 (Fig. 5.7) and is defined as

$$1.0 \geq S_p \geq 0.20 \ , \qquad f = 1.125 \times S_p - 0.125 \qquad\qquad [5.36]$$

$$0.20 > S_p \geq 0.0 \ , \qquad f = -4.50 \times S_p + 1.0 \qquad\qquad [5.37]$$

In this case, approximately flat plateaus and stable hardening ascending branches are expected after the ascending branch of the corresponding load-deflection curve. Thus, small solution steps are prescribed within the transition branch after the linear branch, whereas larger solution steps can be tolerated throughout the linear and hardening or flat branches of the load-deflection curve.

Following the proportion of the generalized finite arc-length, the first generalized displacement increment vector and the first load factor increment that correspond to point "c" in Fig. 5.2 are scaled to conform with the proportioned arc-length computed in [5.31]. Thus, the scaled first generalized displacement increment vector is calculated as

$$\{\Delta\alpha\}^1 = \left(\frac{f \times \Delta L_1^c}{\Delta L^c}\right) \{\Delta\alpha\}^c , \qquad\qquad [5.38]$$

where $\{\Delta\alpha\}^1$ is shown in Fig. 5.2. Similarly, the scaled first load factor increment is computed as

$$\Delta\rho^1 = \left(\frac{f \times \Delta L_1^c}{\Delta L^c}\right) \Delta\rho^c , \qquad\qquad [5.39]$$

which is as well shown in Fig. 5.2.

of [5.45] results in a positive quantity, although the structure may be unstable.

Ramm (1981) has recommended the monitoring of negative pivots in the matrix of pivots [D]. Thus, if a negative pivot is detected at the beginning of a solution step, the sign of the first load factor increment is altered from positive to negative. This approach has been proposed in a rather numerical way. Some physical insight is needed.

The presence of negative and positive pivots in [D] implies an indefinite tangent stiffness matrix, which is commonly associated with the descending branch of the load-deflection curve. Recalling the application of the concept of quadratic form to assess the definiteness of a matrix (Langhaar 1962), there are displacement increment vectors $\{\Delta r\}$ for which the quadratic form

$$\langle \Delta r \rangle [K]_t^a \{\Delta r\} < 0 .$$ [5.46]

The above expression can be formulated explicitly if the displacement increment vector is written in the basis of the eigenvectors. For this purpose, relation [3.24] is recalled and substituted into [5.46], which yields

$$\langle \Delta\alpha \rangle [\Phi]^T [K]_t^a [\Phi] \{\Delta\alpha\} < 0 ,$$ [5.47]

or yet

$$\langle \Delta\alpha \rangle [\Lambda]_t^a \{\Delta\alpha\} < 0 ,$$ [5.48]

which represents the quadratic form [5.46] in the basis of the eigenvectors. Since the generalized displacements in [5.48] are uncoupled, the quadratic form can be developed as

$$\sum_{i=1}^{N} \lambda_i (\Delta \alpha_i)^2 < 0,$$ [5.49]

or explicitly as

$$\lambda_1 (\Delta \alpha_1)^2 + \ldots + \lambda_i (\Delta \alpha_i)^2 + \ldots + \lambda_N (\Delta \alpha_N)^2 < 0,$$ [5.50]

where the resulting negative sign emerges from the dominance of the eigenvectors associated with negative eigenvalues.

Considering a virtual generalized displacement increment vector for which $\Delta \alpha_i \neq 0$ and $\Delta \alpha_k = 0$ for $k \neq i$, the ith term of [5.50], denoted as

$$\Delta W_i = (\lambda_i \Delta \alpha_i) \Delta \alpha_i,$$ [5.51]

can be interpreted as the incremental virtual work performed by the generalized force increment $(\lambda_i \Delta \alpha_i)$ upon the virtual generalized displacement increment $\Delta \alpha_i$. If the incremental virtual work is negative at the vicinity of the equilibrium point "a" shown in Figs. 5.1 and 5.2, it implies that the structure is unstable with respect to the considered set of generalized displacement increments. Therefore, [5.51] serves as a stability test for the current equilibrium state of the materially nonlinear structure. In practice, negative increments

of the load factor have to be specified in order to describe the unstable behavior of the descending branch under the condition that [5.51] is negative.

In a solution step for which an eigenanalysis is not required, the stability test [5.51] can not be carried out. Instead, one must rely on the correlation between the eigenvalues and the pivots of the factorized tangent stiffness matrix. Fortunately, Strang (1988) has demonstrated that the signs of the pivots match the signs of the eigenvalues. This result implies that the stability test [5.51], applied to the lowest negative eigenvalue, suggests unstable behavior in the case of a negative pivot is detected in [D]. This is the approach adopted in the present solution strategy.

5.4 Comments on the Preiterative Phase

The steps that comprise the preiterative phase of the present solution strategy have the role of preparing the solution strategy to tackle the iterative phase. Figure 5.10 illustrates the preiterative phase for different equilibrium paths and for the common case of a single participant eigenvector component which gives rise to load-deflection curves described in a 2-dimensional vector space. The algorithm for the preiterative phase is provided in Fig. 5.11.

5.5 The Iterative Phase

The iterative phase deals with the computation of the generalized displacement vector $\{\Delta\alpha\}^i$ and the load factor increment $\Delta\rho^i$. These variables are illustrated in Fig. 5.12 for a typical iteration, from point "i-1" to point "i". In the following, the derivation of the

constraint equation that sets the condition of orthogonality between the arc-length and the iteration path is presented. Next, a two-step technique is utilized to compute the generalized displacement components of $\{\Delta\alpha\}^i$. Following this stage, the load factor increment $\Delta\rho^i$ is evaluated through the application of the constraint equation. After the update of the generalized displacements and load level, the convergence criteria for loads and displacements are verified. The procedure follows closely the well known modified constant arc-length method (Ramm 1981).

5.5.1 The Constraint Equation

The vector associated with the finite generalized arc-length [5.31] can be defined as

$$\{T\}_a = [\Phi]\{\Delta\alpha\}^1 + \Delta\rho^1\{\rho\}_u . \tag{5.52}$$

where the columns of $[\Phi]$ are the M participant normalized eigenvectors and $\{\rho\}_u$ is the unit vector corresponding to the load factor. These unit vectors, shown in Fig. 5.12, provide the directin of the deformation and loading. It is remarked that the arc-length vector in [5.52] is tangent to the load-generalized displacement curve at point "a" (Fig. 5.12) only in the case of the modified Newton-Raphson scheme.

Similarly, a vector contained in the iteration path can be described as

$$\{\Delta w\}^i = [\Phi]\{\Delta\alpha\}^i + \Delta\rho^i\{\rho\}_u . \tag{5.53}$$

where the scalar components in [5.53] are the generalized displacement increments $\{\Delta\alpha\}^i$ and the load factor increment $\Delta\rho^i$. The sequence of vectors $\{\Delta w\}^i$ (i=2, ... ,b) describe geometrically the iteration path shown in Fig. 5.12.

The condition of orthogonality between the vectors defined in [5.52] and [5.53] is formulated by means of the scalar product

$$\langle T \rangle_a \{\Delta w\}^i = 0 . \tag{5.54}$$

Substituting the transpose of [5.52] and the vector in [5.53] into [5.54], it yields

$$\langle \Delta\alpha \rangle^1 [\Phi]^T [\Phi]\{\Delta\alpha\}^i + \Delta\rho^1 \Delta\rho^i \langle\rho\rangle_u\{\rho\}_u = 0 . \tag{5.55}$$

Recalling the orthonormality of the participant eigenvectors, equation [5.55] is reduced to

$$\langle \Delta\alpha \rangle^1 \{\Delta\alpha\}^i + \Delta\rho^1 \Delta\rho^i = 0 . \tag{5.56}$$

The equation above represents a constraint for the M+1 interdependent variables that form $\{\Delta\alpha\}^i$ and $\Delta\rho^i$. For this reason, it is frequently called 'the constraint equation'.

5.5.2 The Iterative Equilibrium Equations

The incremental form of the equilibrium equations has been presented in Chapter 3, expression [3.28], in the basis of the N normalized eigenvectors. Herein, the same form is adopted, except that now only M participant eigenvectors are present. Thus, the set of equilibrium equations can be described as

$$
\left[\Lambda\right]_t^a \{\Delta\alpha\} = {}_t\Phi]^T\left[\left(\rho^{i-1} + \Delta\rho^i\right)\{R\} - \{F\}^{i-1}\right],
\qquad [5.57]
$$

where the rows of $[\Phi]^T$ are the M participant eigenvectors. The left member of [5.57] represents a set of incremental forces associated with the trial generalized displacement increments. On the other hand, the right member means a set of generalized unbalanced forces that arises from the difference between the generalized external forces $[\Phi]^T(\rho^{i-1} + \Delta\rho^i)\{R\}$ and the generalized internal forces $[\Phi]^T\{F\}^{i-1}$.

Introducing the transformations given in [3.30] and [5.16], equation [5.57] is reduced to

$$
\left[\Lambda\right]_t^a \{\Delta\alpha\}^i = \Delta\rho^i \{\gamma\}^c + \{\Delta\gamma\}^{i-1}.
\qquad [5.58]
$$

where the generalized unbalanced forces at "i-1" (Fig. 5.12) are

$$
\{\Delta\gamma\}^{i-1} = [\Phi]^T\left[\rho^{i-1}\{R\} - \{F\}^{i-1}\right].
\qquad [5.59]
$$

The terms that comprise the right member of [5.58] are shown in Fig. 5.4. It is noted that the system of equations in [5.58] has M+1 unknowns, which are represented by the load factor increment $\Delta\rho^i$

and by the generalized displacement increments $\{\Delta\alpha\}^i$. In addition, these equations are totally uncoupled and are further reduced to the number M of participant eigenvectors. In this study, $M \leq 3$.

5.5.3 The Combined System of Equations

One possible approach to solve for the unknown variables $\{\Delta\alpha\}^i$ and $\Delta\rho^i$ is based on the combination of the constraint equation [5.56] and the iterative equilibrium equations [5.58]. In matrix form, this gives

$$
\begin{bmatrix} [\Lambda]_t^a & -\{\gamma\}^c \\ \langle\Delta\alpha\rangle^1 & \Delta\rho^1 \end{bmatrix} \begin{Bmatrix} \{\Delta\alpha\}^i \\ \Delta\rho^i \end{Bmatrix} = \begin{Bmatrix} \{\Delta\gamma\}^{i-1} \\ 0 \end{Bmatrix} ,
$$

[5.60]

where all the entries have been defined in the previous subsections.

The approach outlined in [5.60] has been adopted in conjunction with the original form of the arc-length method (Riks 1979). In the original arc-length method, the combined system of equations suffered from lack of symmetry and bandness of the system matrix. Although this problem exists in [5.60], it is not as restrictive as with the full set of equations since the number of unknowns has been reduced drastically.

5.5.4 The Two-Step Technique

Instead of solving the combined system of equations [5.60], Wessels (1977) has proposed a two-step technique to be applied to the conventional arc-length method. Batoz and Dhatt (1979) have

proposed a similar technique in the realm of the displacement control method. Herein, this technique is adapted to deal with the uncoupled and reduced system of equations.

The two-step technique is based on the description of the iteration path vector, given in [5.53], in the alternative form (Fig. 5.13)

$$\{\Delta w\}^i = [\Phi]\{\Delta\alpha\}^i_I + \Delta\rho^i[\Phi]\{\Delta\alpha\}^i_{II} + \Delta\rho^i\{\rho\}_u. \qquad [5.61]$$

where the normalized participant eigenvectors in $[\Phi]$ provide the direction of deformation, whereas the unit vector $\{\rho\}_u$ gives the direction of loading. Also, the generalized displacement increments in [5.61] can be computed through

$$[\Lambda]^a_t\{\Delta\alpha\}^i_I = \{\Delta\gamma\}^{i-1} \qquad [5.62]$$

and

$$[\Lambda]^a_t\{\Delta\alpha\}^i_{II} = \{\gamma\}^c, \qquad [5.63]$$

where $\{\Delta\alpha\}^i_I$ contains the generalized displacement increments associated with the generalized unbalanced forces $\{\Delta\gamma\}^{i-1}$, whereas $\{\Delta\alpha\}^i_{II}$ groups the generalized displacement increments associated with the generalized reference forces $\{\gamma\}^c$ defined in [5.16].

The main diagonal matrix of the eigenvalues $[\Lambda]^a_t$ is kept constant throughout the iterative phase. Therefore, the vector $\{\Delta\alpha\}^i_{II}$ is the same as $\{\Delta\alpha\}^c$ defined within the preiterative phase,

expression [5.19]. This vector is always available in core. It is further noted that the two-step technique mantains the properties of bandness and symmetry of the systems of equations [5.62] and [5.63]. In addition, the equations are completely uncoupled and reduced to the number M of participant eigenvectors. Due to this fact, the steps of factorization of the stiffness matrix, reduction of the load vector and backsubstitution of the degrees of freedom, which are common in the conventional solution strategies, are not required while solving the systems [5.62] and [5.63].

5.5.5 The Load Factor Increment

The second and third vector components of $\{\Delta w\}^i$ in [5.61] depend on the load factor increment $\Delta\rho^i$, which has to be computed. The computation of the load factor increment is carried out through the condition of orthogonality stated in [5.54]. Thus, applying this condition to the vectors defined in [5.52] and [5.61] gives

$$[\Phi]^T[\Phi]\left[\langle\Delta\alpha\rangle^1\{\Delta\alpha\}_I^i + \Delta\rho^i\langle\Delta\alpha\rangle^1\{\Delta\alpha\}_{II}^i\right] + \langle\rho\rangle_u\{\rho\}_u\Delta\rho^1\Delta\rho^i = 0 . \qquad [5.64]$$

Accounting for the orthonormality property of the participant eigenvectors and isolating the load factor increment in [5.64] yields

$$\Delta\rho^i = -\frac{\langle\Delta\alpha\rangle^1\{\Delta\alpha\}_I^i}{\langle\Delta\alpha\rangle^1\{\Delta\alpha\}_{II}^i + \Delta\rho^1} . \qquad [5.65]$$

The load factor increment, defined above, takes into account the generalized displacement increments evaluated within the

preiterative and iterative phases. In addition, the load factor increment associated with the preiterative phase is also included. Therefore, $\Delta\rho^i$ reflects the size of the solution step. In fact, the present solution strategy tends to load control for large values of $\Delta\rho^i$ in [5.65]. On the other hand, it tends to displacement control for small values of $\Delta\rho^1$. Geometrically, expression [5.65] gives the intersection point "i" between the iteration path and the arc-length vector $\{T\}_a$ translated to point "a_{i-1}" in Fig. 5.13.

After the calculation of the load factor increment, the load level can be updated as

$$\rho^i = \rho^{i-1} + \Delta\rho^i .$$

[5.66]

5.5.6 The Generalized Displacement Increment

The generalized displacement increments form the scalar displacement component of the iteration path vector defined in expressions [5.53] and [5.61]. Thus, equating the scalar displacement components of $\{\Delta w\}^i$ in these expressions yields

$$\{\Delta\alpha\}^i = \{\Delta\alpha\}^i_I + \Delta\rho^i \{\Delta\alpha\}^i_{II} .$$

[5.67]

Substituting [5.67] into the incremental equilibrium equations [5.58], gives

$$[\Lambda]^a_t \{\Delta\alpha\}^i_I + \Delta\rho^i [\Lambda]^a_t \{\Delta\alpha\}^i_{II} = \{\Delta\gamma\}^{i-1} + \Delta\rho^i \{\gamma\}^c .$$

[5.68]

This result substantiates the decomposition carried out in [5.62] and [5.63], which has been based on geometric considerations (Fig. 5.13).

For a typical iteration, only the variables in $\{\Delta\alpha\}_i^i$ are computed. The remaining variables in the basic relations [5.65] and [5.67] have been calculated within the preiterative phase and are available in the iterative phase. Furthermore, out-of-core storage is not required since the displacement vectors and the stiffness matrix have small dimensions due to the reduction of the number of degrees of freedom. In this study, the maximum dimension used for vectors and matrices has been set equal to 3.

After the computation of the generalized displacement increment in [5.67], the level of total generalized displacements can be updated. This gives

$$\{\alpha\}^i = \{\alpha\}^{i-1} + \{\Delta\alpha\}^i .$$

[5.69]

Usually, the total displacement vector, given in the N-dimensional vector space of the global degrees of freedom, is required to provide the deformed configuration of the structure. Knowing from chapter 4 that

$$\{\Delta r\}^i = [\Phi]\{\Delta\alpha\}^i ,$$

[5.70]

the total displacements can be updated as

$$\{r\}^i = \{r\}^{i-1} + [\Phi]\{\Delta\alpha\}^i .$$

[5.71]

5.5.7 Convergence Criteria

The generalized displacement increment vector $\{\Delta\alpha\}^i$ and the load factor increment $\Delta\rho^i$ are trial quantities to which the convergence criteria should be applied.

The convergence criterion for generalized displacements is stated as

$$\frac{\|\{\Delta\alpha\}^i\|}{\|\sum_{j=1}^{i}\{\Delta\alpha\}^j\|} \leq TOL .$$

[5.72]

where the numerator is the Euclidean norm of the generalized displacement increments corresponding to the ith iteration, whereas the denominator is the Euclidean norm of the accumulated generalized displacement increments, from the 1st to the ith iteration.

On the other hand, the convergence criterion for the generalized unbalanced forces is defined as

$$\frac{\|\{\Delta\gamma\}^i\|}{\|\left(\rho^i - \rho^a\right)\{\gamma\}^c\|} \leq TOL .$$

[5.73]

where the numerator is the Euclidean norm of the generalized unbalanced forces at the ith iteration, and the denominator is the Euclidean norm of the generalized incremental forces at the ith iteration. The tolerance number TOL above has usually been set equal to 0.01. The terms in [5.72] and [5.73] are illustrated in Figs. 5.12 and 5.4 respectively.

5.6 Conditions and Rate of Convergence

The present solution strategy adopts the modified Newton-Raphson scheme to iterate the generalized displacements and load factor within the iterative phase. This scheme is based on the recurrence relations given in [5.62] and [5.69]. In order to apply successfully these relations, while iterating towards an equilibrium point, some conditions should be observed. These issues, as well as the rate of convergence, are herein examined in a practical way. For rigorous mathematical formulation and proofs, Riks (1979) and Ortega and Rheinboldt (1970) can be consulted.

The first condition to attain convergence can be expressed as

$$\det\left[\Lambda\right]_t^a \neq 0, \tag{5.74}$$

where $\left[\Lambda\right]_t^a$ is the main diagonal stiffness matrix containing the participant eigenvalues extracted at the beginning of the preiterative phase. The condition above assures that the trial generalized displacement increment $\left\{\Delta\alpha\right\}_I^a$ is uniquely determined. In practice, the condition of a nonzero determinant is usually satisfied, since a perfect limit point is unlikely to occur in the numerical modeling of materially nonlinear structures. In addition, the stiffness matrix $\left[\Lambda\right]_t^a$ is updated only at the beginning of a solution step. This aspect diminishes the chances of updating the stiffness matrix at a pure limit point.

If the first condition is satisfied, a second condition states that a finite domain, defined as

$$\|\{\Delta\tau\}\|^2 = \delta^2 , \qquad\qquad [5.75]$$

exists around the equilibrium point "b" in Fig. 5.15. The radius δ is a function of the position vector $\{\tau\}^b$. Assuming that the condition in [5.75] holds, the iterative process will converge if

$$\left(\|\{\Delta\tau\}^i\|\right)^2 < \delta^2 , \qquad\qquad [5.76]$$

where $\{\Delta\tau\}^i$ is an increment of the position vector $\{\tau\}^b$ and corresponds to the ith iteration within the iteration path shown in Fig. 5.15. Ortega and Rheinboldt (1970) have demonstrated that two successive approximations that satisfy [5.76] are related as

$$\|\{\Delta\tau\}^i\| = L \times \|\{\Delta\tau\}^{i-1}\| , \qquad\qquad [5.77]$$

where L depends on the position vector $\{\tau\}^b$ and varies in the interval (0,1) for a convergent iterative process. Relation [5.77] implies a linear rate of convergence. The conditions in [5.75], [5.76] and [5.77] fail when a large finite arc-length is specified. In this case, the iteration path is diverted indefinitely from the equilibrium path, as it is illustrated in Fig. 5.15. In the present solution strategy, however, the automatic adjustment of the size of the arc-length, treated in Section 5.3.5, allows the iteration path to intersect the equilibrium path.

5.7 Computational Work

The computational work of a numerical procedure is defined as the total number of arithmetical operations (typically multiplication and addition) involved in the performance of the procedure. This concept does not account for the type of computer in use. However, the differences between conventional and parallel processors should not affect the performance comparisons, since most of the time cosuming operations take place on N dimensional vectors and matrices in the same manner.

The computational work required for the present solution strategy is herein evaluated and outlined in Tables 5.1 and 5.2. In this table, N is the number of degrees of freedom, h is the halfbandwidth of the stiffness matrix, p is the number of preselected eigenvectors, M is the number of dominant eigenvector components and (#ITE) is the number of iterations in the iterative phase.

Assuming a hypothetical example for which N=300, h=30, p=3, M=1 and (#iter)=15, the results in Tables 5.1 and 5.2 give 1,783,800 operations for the eigenanalysis, 156,014 operations for the preiterative phase without eigenanalysis and 22,710 operations for the iterative phase. These figures demonstrate that the eigenanalysis process requires a very large number of operations. However, it is not necessary to perform eigenanalysis for every solution step. In the example given above, only 9% of the total number of operations is required for a solution step without eigenanalysis.

5.8 Discussion

The potential of the eigenvector-based solution strategy presented in this chapter can be assessed through the numerical analysis of large scale problems. For these problems, a large number of global degrees of freedom is required in the discretization of the structure. It is expected that the savings resulting from the numerical treatment of the reduced and uncoupled equilibrium equations can compensate for the large computational work required for the eigenanalysis in some specific solution steps.

Phase	Description of the step	Equation number	Computational work	Note
PREITERATIVE	Eigenanalysis	[5.2]	Nh²+Nh(3+5p)+2Np +40Np(h+2p+3/2)	(1)
	Solution of incremental equilibrium equations	[5.1]	$1/2 Nh^2 + 2Nh$	(2)
	Computation of first generalized displacement increments	[5.9]	p(2N-1)	
	Computation of participation factors	[5.11]	(2N-1) + 3p	(3)
	Selection of dominant eigenvectors components	[5.13]	(M-1)	(4)
	Transformation and reduction of incremental equilibrium equations	[5.19]	M(2N-1)	(5)
	Computation of stiffness parameter	[5.25]	(2M-1) + 1	(6)
	Determination of arc-length size	[5.29] [5.31]	(2M+1)	
	Adjustment of first generalized displacement increments and load factor	[5.38] [5.39]	(M+2)	
	Update of total generalized displacements and load factor	[5.40] [5.41]	(M+1)	
	SUBTOTAL OF THIS PHASE		$3/2 Nh^2 +5Nh(1+p)+2Np[20(h+2p+3/2)+1]$ $+(2N-1)(p+M+1)+3p+(7M-2)+5$	

Notes:

(1) This figure has been calculated assuming 10 iterations in the subspace iteration method and neglecting zero elements within the bandwidth of the stiffness matrix. The halfbandwidth h of the identity matrix is zero.

(2) The first member of the computational work in this step accounts for the factorization of the stiffness matrix, whereas the second member refers to the reduction of the load vector and backsubstitution of the degrees of freedom.

(3) (2N-1) accounts for the computation of the Euclidean norm of the first generalized displacement increment vector.

(4) In this study $M \leq 3$.

(5) This involves only the reduction of the reference force vector. The reduction of displacements has been carried out in [5.9].

(6) This stiffness parameter is the one associated with the modified Newton-Raphson escheme.

Table 5.1: Computational work of the preiterative phase.

Phase	Description of the step	Equation number	Computational work	Note
ITERATIVE	Computation of current external forces	[5.57]	N	(1)
	Computation of current generalized unbalanced forces	[5.59]	M(2N-1)	(2)
	Computation of generalized displacement increments $\{\Delta\alpha\}_1^i$	[5.62]	M	
	Test of convergence for the generalized unbalanced forces	[5.73]	(2M-1)+3	(3)
	Computation of load factor increment	[5.65]	(2M-1)+1	(4)
	Computation of generalized displacement increments	[5.67]	2M	
	Computation of conventional displacement increments	[5.70]	NM+(M-1)	
	Update of total displacements and load factor	[5.69] [5.71] [5.66]	M+N+1	
	Test of convergence for generalized displacement increments	[5.72]	M+2(2M-1)+1	
	SUBTOTAL OF THIS PHASE		2N+NM+M(2N-1)+(14M-5)+6	
	TOTAL COMPUTATIONAL WORK		3/2 Nh²+5Nh(1+p)+2Np[20(h+2p+3/2)+1] +(2N-1)(p+M+1)+3p+(7M-2)+5 +(#ite)[2N+NM+M(2N-1)+(14M-5)+6]	

Notes:
(1) This refers to $\rho^{i-1}\{R\}$
(2) The process of computation of the conventional unbalanced forces $\{\Delta Q\}^{i-1}$ is standard and is not addressed herein.
(3) The Euclidean norm of $\{\cdot\}^c$ has been computed within the iterative phase and is not accounted for in this step.
(4) The denominator of this expression is kept constant throughout the iterative phase and is not included in the calculation of the computational work for this step.

Table 5.2: Computational work of the iterative phase.

Figure 5.2: Preiterative phase in the (M+1)-dimensional vector subspace of the participant eigenvectors

Figure 5.1: Preiterative phase in the conventional (N+1)-dimensional vector space
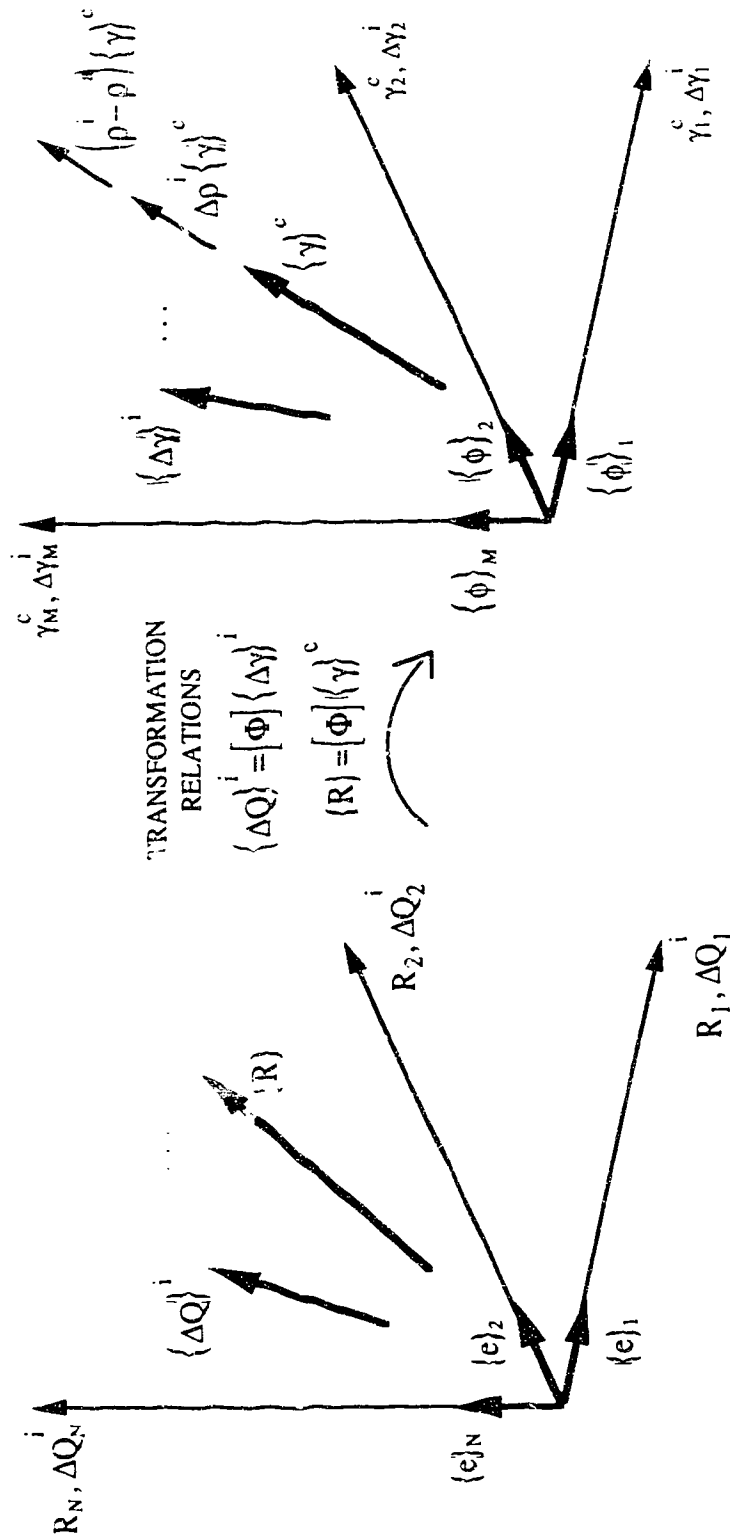
Figure 5.3: The reference force vector and the unbalanced load vector in the conventional N-dimensional vector space.
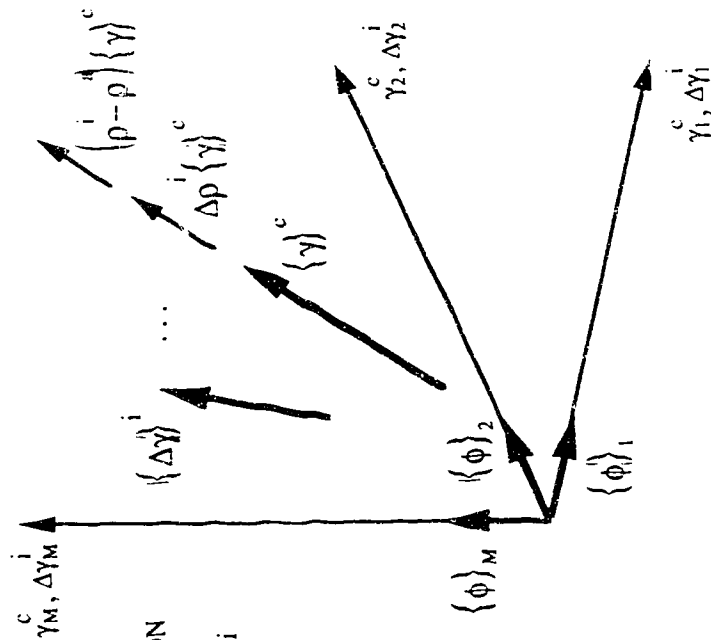
Figure 5.4: The generalized reference force vectors and the generalized unbalanced load vector the in M-dimensional vector subspace of the participant eigenvectors.
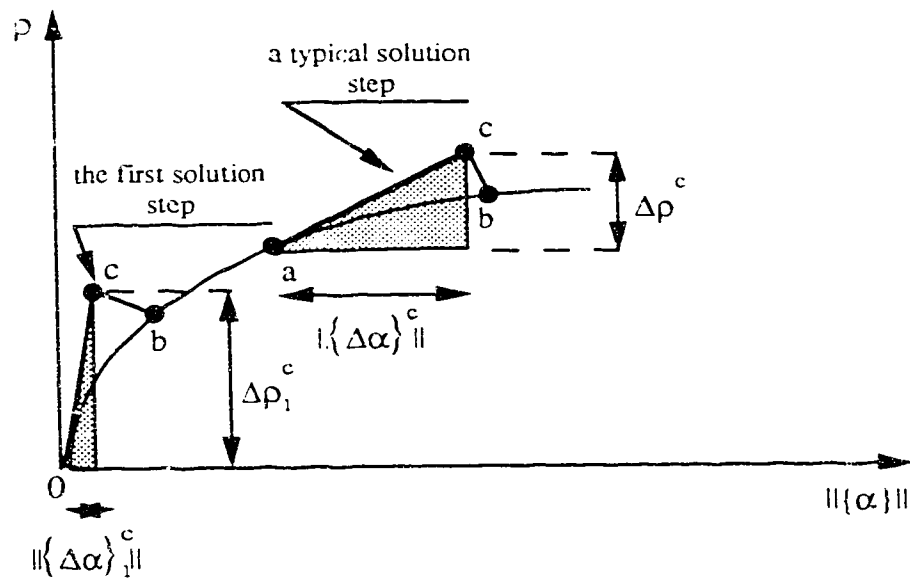
Figure 5.5: Illustration of the terms of the current stiffness parameter.
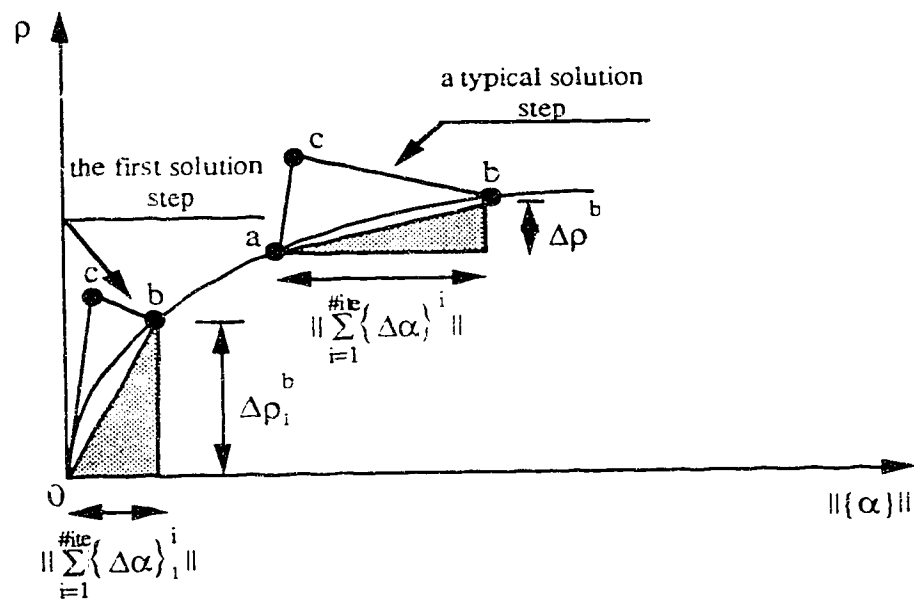
Figure 5.6: Illustration of the terms of the average stiffness parameter
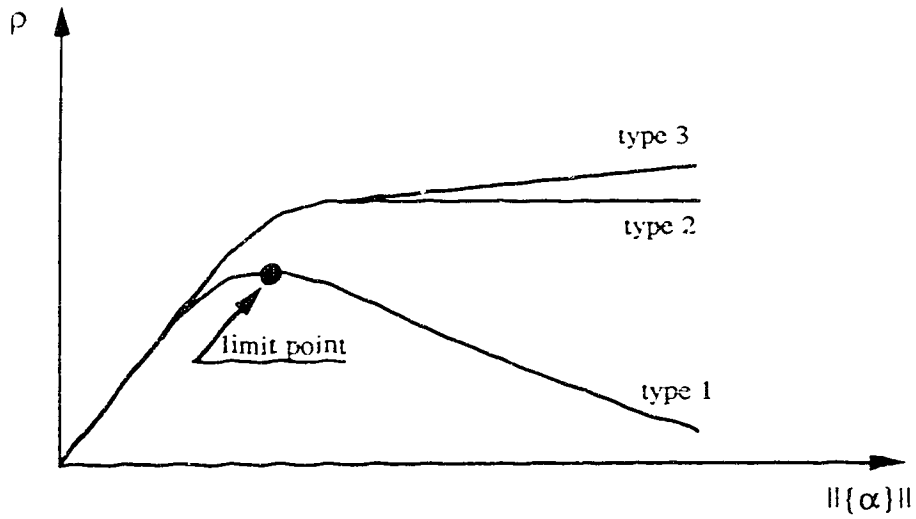
Figure 5.7: Typical load-deflection curves for different types of behavior.
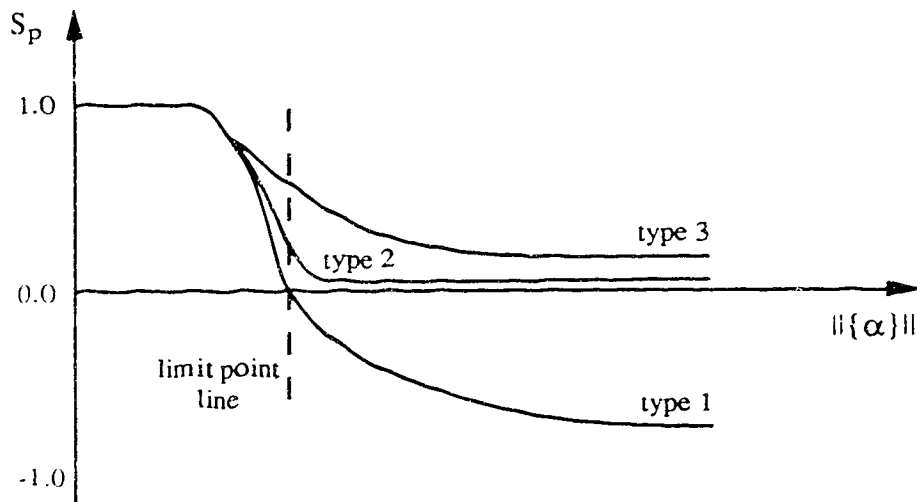
Figure 5.8: Typical variation of the stiffness parameter for different types of behavior.

Figure 5.ᶜ Variation of thᵥ arc-length factor with the stiffness parameter.

Figure 5.10: Illustration of the preiterative phase for different types of load-single generalized displacement equilibrium paths.

Start Preiterative Phase

Update $[K]_t^a$

Select Shift μ

If pivot $d_{ii} \leq 0$
$\mu = 10^{-4}$

If pivot $d_{ii} > 0$
$\mu = 0$

Shift $[K]_t^a$

$$[\hat{K}]_t^a = [K]_t^a + \mu[I]$$

Compute eigenpairs $(\lambda_i, \{\phi\}_i)$
$i = 1, \ldots, p$

$$[\hat{K}]_t^a [\Psi] = [I][\Psi][\Omega]$$

$\{\phi\}_i = \{\psi\}_i$ and $\lambda_i = \omega_i - \mu$

Check stablity of equilibrium and set sign of
first load factor increment

If $\lambda_1 \geq 0$, $\Delta\rho^c = +1.0$ Stable or Neutral

If $\lambda_1 < 0$, $\Delta\rho^c = -1.0$ Unstable

Solve the Incremental
Equilibrium Equations

$$[K]_t^a \{\Delta r\}^c = \Delta\rho^c \{R\}$$

Compute first generalized
displacement increments

$$\Delta\alpha_i^c = \langle\phi\rangle_i \{\Delta r\}^c \qquad i = 1, \ldots, p$$

Investigate participation of eigenvectors

$$P_i = 100 \times \left(\frac{\Delta\alpha_i^c}{\langle\{\Delta r\}^c\rangle} \right)^2 \% \qquad i = 1, \ldots, p$$

Select dominant eigenvector components

$\{\Delta\alpha_1\{\phi\}_1, \ldots, \Delta\alpha_M\{\phi\}_M\}$ such that $\sum_{i=1}^{M} P_i \geq 95\%$?

STOP   no   yes

Transform and reduce the incremental
equilibrium equations

from: $[K]_t^a \{\Delta r\}^c = \Delta\rho^c \{R\}$

to: $[\Lambda]_t^a \{\Delta\alpha\}^c = \Delta\rho^c \{\gamma\}^c$

Compute stiffness parameter

Modified
Newton-Raphson

$$S_p = \pm \frac{\|\{\Delta\alpha\}_i^c\|}{\|\{\Delta\alpha\}^c\|}$$

Initial Stiffness
escheme

$$S_p = \frac{\Delta\rho^b}{\|\sum_{i=1}^{i=n}\{\Delta\alpha\}_i\|} \Bigg/ \frac{\Delta\rho_i^b}{\|\sum_{i=1}^{i=n}\{\Delta\alpha\}_i\|}$$

Compute Arc-length
factor

$$f : f(S_p)$$

Adjust arc-length size

$$\Delta L^1 = f \times \Delta L_1^c$$

Compute current arc-length

$$\Delta L^c = \sqrt{\langle\Delta\alpha\rangle^c \{\Delta\alpha\}^c + (\Delta\rho^c)^2}$$

Adjust generalized displacement
increments and load factor increment

$$\{\Delta\alpha\}^1 = \left(\frac{\Delta L^1}{\Delta L^c}\right)\{\Delta\alpha\}^c \quad \text{and} \quad \Delta\rho^1 = \left(\frac{\Delta L^1}{\Delta L^c}\right)\Delta\rho^c$$

Update total generalized
displacements and load factor

$$\{\alpha\}^1 = \{\alpha\}^a + \{\Delta\alpha\}^1 \quad \text{and} \quad \rho^1 = \rho^a + \Delta\rho^1$$

End of preiterative
phase

Fig. 5.11: Flowchart of the preiterative phase

Iterative
Phase

iteration path

$[\Phi]\{\Delta\alpha\}^1$

ρ^i

ρ^{i-1}

ρ^i

$\{\Delta w\}^i$

$\Delta\rho^i$

$\{T\}_a$

$\Delta\rho^i\{\rho\}_u$

$[\Phi]\{\Delta\alpha\}^i$

$\Delta\rho^1\{\rho\}_u$

a_{i-1} a_i b

$\|\{\Delta\alpha\}^i\|$

$(\rho^{i-1}+\Delta\rho^i)$

ρ^a

a

$\displaystyle\|\sum_{j=1}^{i}\{\Delta\alpha\}^i\|$

α_M

$\{\rho\}_u$

$\{\phi\}_M$

0

$\{\phi\}_1$

α_1
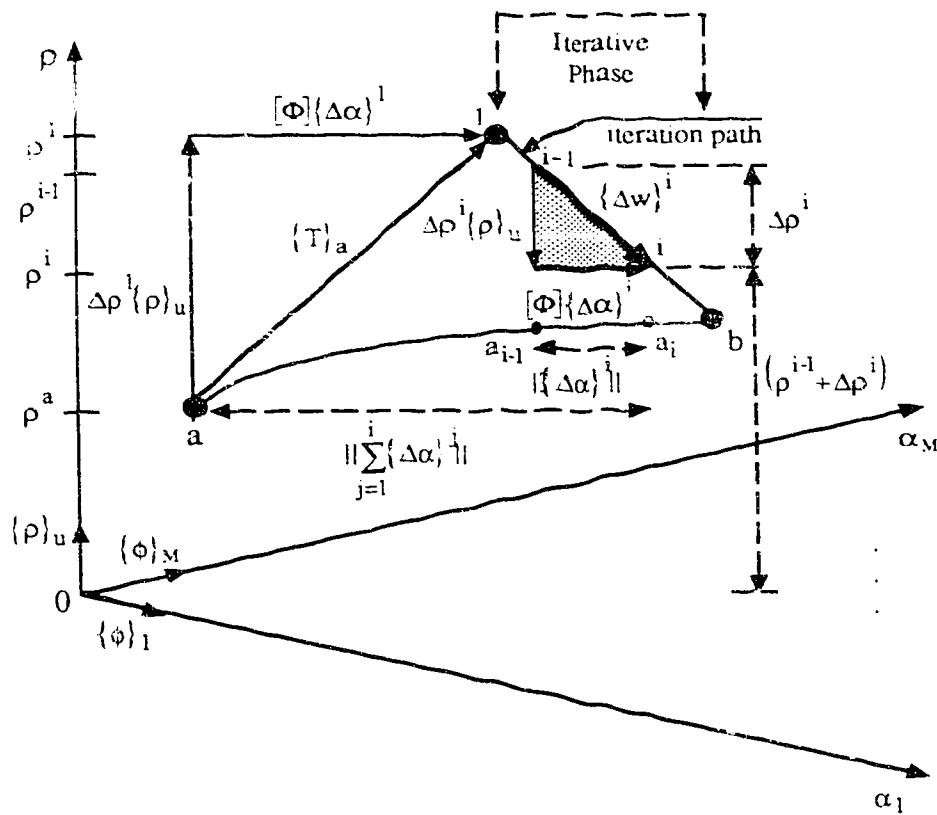
Fig. 5.12: Illustration of the iterative phase in the (M+1)-dimensional load-generalized displacement vector subspace.

iteration path

$[\Phi]\{\Delta\alpha\}^i_I$

$i-1$

$\{T\}_a$

$\{\Delta w\}^i$

$\Delta\rho^i\{\rho\}_u$

$1.0\{\rho\}_u$

$\Delta\rho^i[\Phi]\{\Delta\alpha\}^i_{II}$

b

a_i

ρ

$\{\rho\}_u$ $\{\phi\}_M$

α_M

0

$\{\phi\}_1$

α_1

a_{i-1}

$[\Phi]\{\Delta\alpha\}^i_{II}$

segment of the equilibrium path
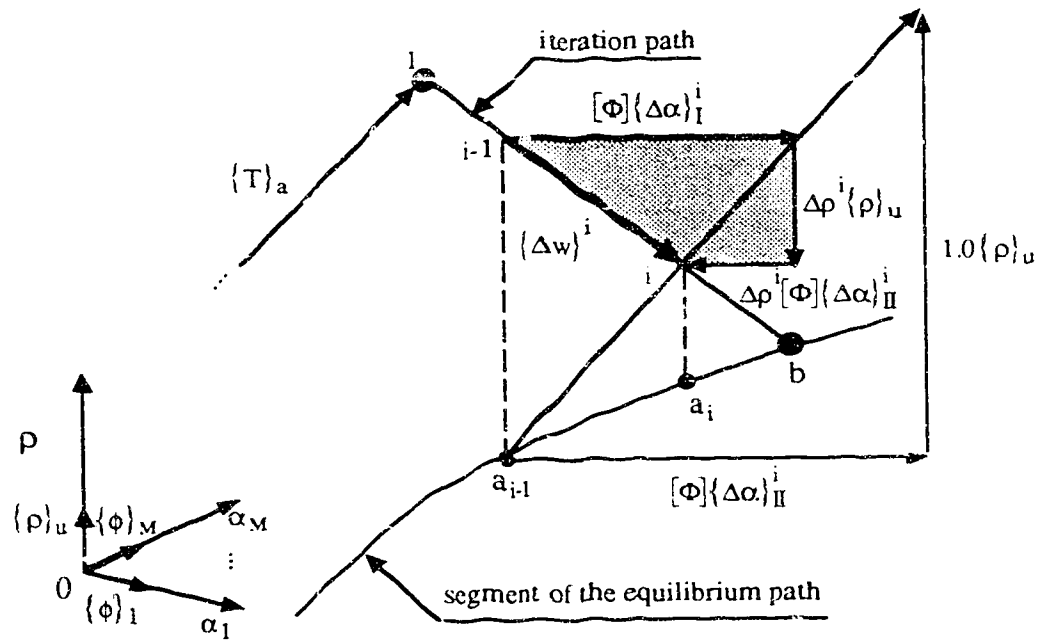
Fig. 5.13: Illustration of the two-step technique in the (M+1) dimensional load-generalized displacement vector subspace.

Start i^{th} iteration

Compute current external forces

$$\{S\}^{i-1}=\rho^{i-1}\{R\}$$

Compute current internal forces

$$\{F\}^{i-1}=\sum_{k=1}^{\#elem.}\int_{V_k}[B]^T\{\sigma\}^{i-1}dV_k$$

Compute unbalanced forces

$$\{\Delta Q\}^{i-1}=\{S\}^{i-1}-\{F\}^{i-1}$$

Compute generalized unbalanced forces

$$\{\Delta\gamma\}^{i-1}=[\Phi]^T\{\Delta Q\}^{i-1}$$

Compute generalized displacement increments associated with generalized unbalanced forces

$$[\Lambda]_i^*\{\Delta\alpha\}_i^i=\{\Delta\gamma\}^{i-1} \text{ where } \left(\Delta\alpha\right)_j^i=\frac{\Delta\gamma_j^{i-1}}{\lambda_j}$$

$$j=1,....,M$$

Test convergence of generalized unbalanced forces

$$\frac{\|\{\Delta\gamma\}^{i-1}\|}{\|(\rho^{i-1}-\rho^a)\{\gamma\}^c\|}\leq TOL ?$$

no   yes

$\#\ ITE \quad ITE]_{MAX} ?$ ————yes

STOP

Compute load factor increment

$$\Delta\rho^i=-\frac{\langle\Delta\alpha\rangle^i\{\Delta\alpha\}_1^i}{\langle\Delta\alpha\rangle^i\{\Delta\alpha\}^c+\Delta\rho^i}$$

Compute generalized displacement increments

$$\{\Delta\alpha\}^i=\{\Delta\alpha\}_1^i+\Delta\rho^i\{\Delta\alpha\}^c$$

Compute conventional displacement increments

$$\{\Delta r\}^i=[\Phi]\{\Delta\alpha\}^i$$

Update total displacements

$$\{\alpha\}^i=\{\alpha\}^{i-1}+\{\Delta\alpha\}^i$$

$$\{r\}^i=\{r\}^{i-1}+\{\Delta r\}^i$$

Update load factor

$$\rho^i=\rho^{i-1}+\Delta\rho^i$$

Test convergence of generalized displacement increments

yes $\frac{\|\{\Delta\alpha\}^i\|}{\|\sum_{j=1}^{i}\{\Delta\alpha\}^j\|}\leq TOL ?$ no

$\#\ ITE\leq(\#\ ITE)_{MAX} ?$

Output results for this solution step

Increment iteration ← yes

no

STOP

Fig. 5.14: Flowchart of the iterative phase

Fig. 5.15: Illustration of the conditions of convergence of the solution strategy.

CHAPTER 6

APPLICATIONS

6.1 Introduction

The structures addressed in Chapter 4 have exhibited different types of load-deflection histories that reflect complex material nonlinearities, such as yielding, softening and cracking. The load-deflection histories have been shown in terms of load-deflection curves which relate the load factor and a preselected global degree of freedom. Different types of branches form the resulting load-deflection curves. For example, an ascending branch shows the concurrent increase of the load factor and the preselected displacement. On the other hand, the load factor decreases while the displacement increases in a descending branch. Along a flat segment, the load factor remains approximately constant under increasing displacements.

The objective of this chapter is to apply the eigenvector-based solution strategy, developed in the previous chapter, to the materially nonlinear structures treated in Chapter 4. For each of the applications, two types of load-defle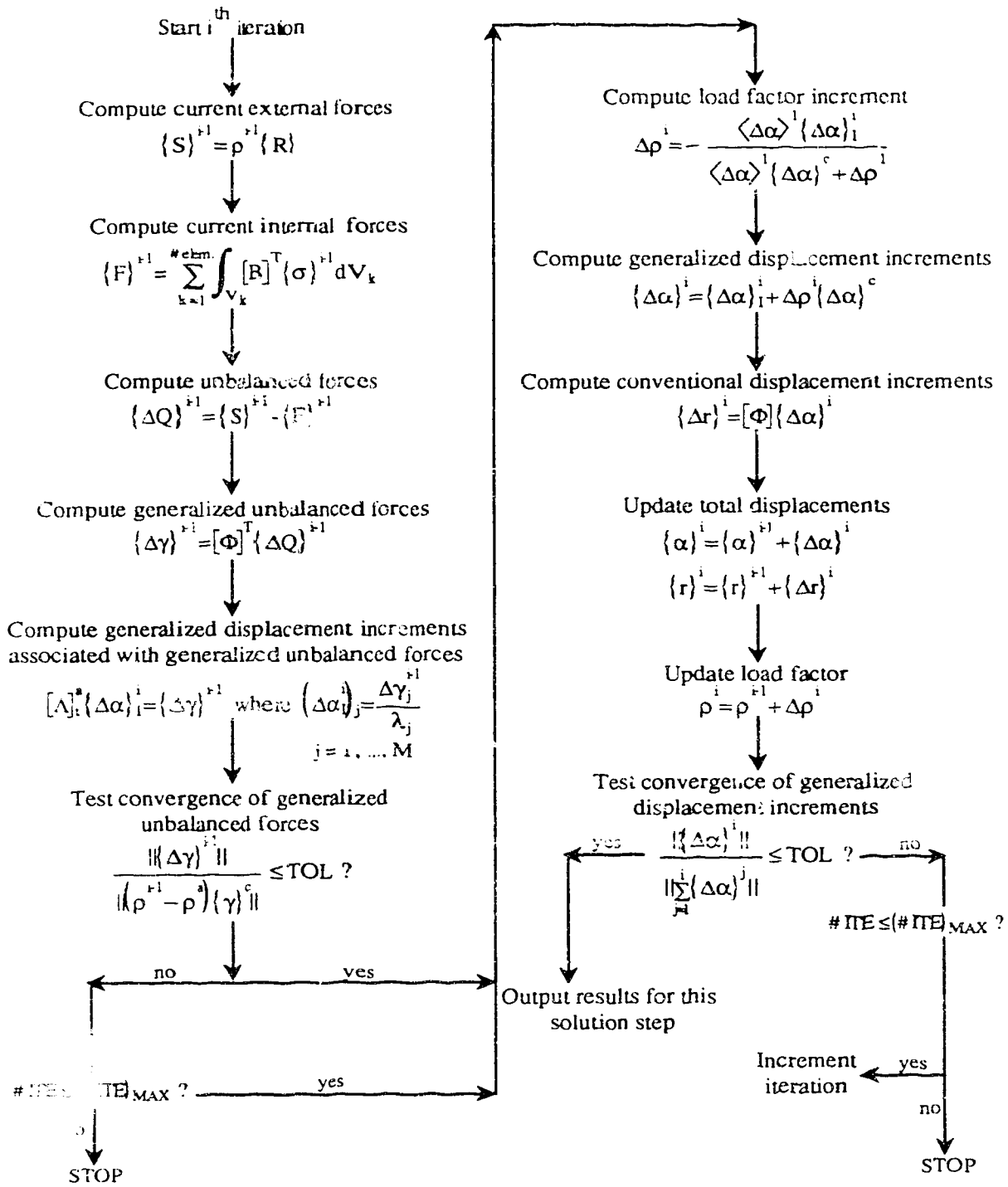ction curves are traced. First, the conventional load-deflection curve, which relates the load factor to a preselected global degree of freedom, is considered. Second, a generalized load-deflection curve, which characterizes a one-to-one relation between the load factor and a dominant generalized displacement, is also presented.

Bergan et al. (1978) argued that conventional load-deflection curves might not represent the true structural response, since the relation between load and deflection may vary according to the preselected degree of freedom. This objection does not apply to the generalized load-deflection curves traced by the eigenvector-based strategy, since the generalized displacements are associated with modes of deformation which dominate the displacement response of the structure.

In addition to the load-deflection curves, the variation of some stiffness parameters with a deflection measure is also provided. Hence, the current and the average stiffness parameters, defined respectively in [5.25] and [5.26], are plotted. A normalized secant stiffness parameter, which is based on the ratio between the current levels of applied load and deflection, is traced and serves as a basis for comparison with the current and the average stiffness parameters. The latter two parameters rely on the tangent stiffness matrix. For some of the examples, the normalized determinant of the updated stiffness is presented in conjunction with the other parameters. The tracing of the variation of these parameters intends to furnish a deeper insight in the interpretation of the behavior of the structure, principally at sharp changes in stiffness and in the vicinity of limit points.

The factor f, treated in Subsection 5.3.5, is utilized to adjust the size of the finite arc-length of the load-deflection curves presented in this chapter. The variation of the factor f with the chosen stiffness parameter is given for each example.

With respect to the overall performance, the eigenvector-based solution strategy is compared with the constant arc-length method that incorporates the modified Newton-Raphson method as the iterative process (Ramm 1981). For some applications, a combination of the standard Newton-Raphson method with the constant arc-length method is also used for the sake of comparison. Furthermore, a combination, via a restart procedure, of the standard Newton-Raphson method with the eigenvector-based strategy is applied to the analysis of the last example. This attempts to demonstrate the flexibility of combining the proposed method with other available strategies. The results of the comparative study are presented in table format and include the CPU time and the number of iterations for each solution strategy. The rates of convergence, given in terms of Euclidean norm of displacement increments, are also compared.

For the sake of simplicity, a nomenclature should be created to identify the solution strategies in the following presentation. Thus, SNRM stands for the Standard Newton-Raphson Method, whereas CALM and ESS denote respectively the Constant Arc-Length Method and the Eigenvector-based Solution Strategy.

6.2. Applications

6.2.1 The Elastic Perfectly Plastic Cantilever Beam

This example represents a broad class of members for which the structural behavior is characterized by a high level of ductility. In practice, the tracing of the complete load-deflection curve is

essential to the evaluation of the level of ductility that the structure may exhibit.

According to Subsection 4.5.2, the conventional load-deflection curve of this beam presents three distinct segments. A straight segment identifies the linearly elastic phase, whereas the curve and flat segments describe respectively the elastic-plastic and plastic phases.

The numerical description of this type of load-deflection curve poses three difficulties. First, large sizes solution steps give rise to large strain increments. This, in turn can cause a nonconvergent iterative subincrementation technique while returning the strain state onto the yield locus. Murray al. (1980) referred to such a drawback in the context of elastic-plastic modeling of concrete. Second, the stiffness matrix is nearly singular throughout the flat segment. Third, the prescription of load increments within the flat segment is impractical since the applied load remains approximately constant in that region. These last two limitations explain why the classical Newton-Raphson methods fail in the analysis of such structures, as reported by Zienkiewicz et al. (1969).

Figure 6.1 shows three conventional load-deflection curves labeled as SNRM & CALM, CALM and ESS. In this figure, the applied load and the resulting deflection are normalized with respect to their values at first yield, which are respectively 15 KN and 30 mm.

The curve denoted as SNRM & CALM in Fig. 6.1 has been traced by the SNRM for the elastic and elastic-plastic segments and by the CALM for the flat segment. The SNRM uses the load at first yield as reference load. The load increments are kept reasonably small (about

10% of the reference load) so that convergence of the iterative subincrementation technique is ensured. At the end of the elastic-plastic segment, the SNRM fails due to the onset of a nearly singular tangent stiffness matrix. At this stage, the solution strategy is changed to CALM through a restart procedure. In the subsequent description of the flat segment, CALM works with a constant stiffness matrix which has been updated at restart. Therefore, the iterative process relies mainly on the updated unbalanced forces. In addition, the reference load is decreased to one-fifth of the yield load. Despite the adoption of a constant stiffness matrix, the flat segment, along which the flexural mechanism develops, is accurately described.

The curve designated as CALM in Fig. 6.1 represents the solution given by CALM that uses the modified Newton-Raphson method as the iterative process. This means that the stiffness matrix is updated only at the beginning of each solution step. A reference load of 5.6 KN has been adopted in this solution. Thus, the CALM is capable of tracing all segments of the load-deflection curve, although using a constant arc-length. The adoption of a constant arc-length generates only two solution steps within the elastic-plastic segment as illustrated in Fig. 6.1.

The eigenvector-based solution strategy provides the load-deflection curve denoted ESS in Fig. 6.1. In this solution, the stiffness matrix is updated only at the beginning of each solution step and a total of six eigenanalyses are performed. The iterative phase is carried out with a single generalized displacement which gives rise to a single generalized unbalanced force. The first eigenvector of Fig. 4.17 represents the dominant bending mode associated with this

single degree of freedom. The corresponding eigenvalue serves as the uncoupled stiffness which is preserved constant within the iterative phase. Due to the condition of uncoupling, a one-to-one relation between the generalized displacement and the load factor exists and gives rise to the generalized load-deflection curve shown in Fig. 6.2.

The current, the average and the secant stiffness parameters, along with the normalized determinant of the tangent stiffness matrix, are plotted against the norm of the generalized displacement in Fig. 6.3. The correlation between the current and the average parameters is very good for all phases of behavior indicated in the figure. This is expected since both parameters utilize the concept of tangent stiffness matrix which is also used in the formulation of the piasticity model. The normalized determinant follows a similar variation, but shows a sharper drop within the elasto-plastic range. In the plastic segment, these parameters decay to nearly zero values. This corresponds to the formation and development of the plastic mechanism shown in Fig. 4.17. On the other hand, the secant stiffness parameter experiences a very shallow decrease after the linear range of behavior. This is caused by the adoption of the concept of secant stiffness in the formulation of this parameter.

Considering the current stiffness parameter as the independent variable, the definition of the factor f, given in [5.36] and [5.37] for behavior type 2 (Figs. 5.7 and 5.9), is applied to the control of the size of the arc-length for the present application. Figure 6.4 shows the resulting reductions in the elasto-plastic range and the extensions in the plastic range. It is noted that the relatively large number of reductions of the arc-length size prior to the plastic range

is responsible for the smooth transition from the elasto-plastic phase to the plastic phase, observed in the load-deflection curve (Fig. 6.1) In addition, a low number of solution steps within the plastic segment (Fig. 6.1) is enhanced due to the the extensions of the arc-length in that range of behavior.

Table 6.1 contains the solution parameters for all the applied solution strategies. Although the ESS requires an intermediate total CPU time relative to the other strategies, it shows the best performance with respect to the CPU time per solution step. This is due to the fact that ESS required a single iteration for each solution step. This further suggests a fast rate of convergence. This is indeed verified in Fig. 6.5 where the convergence rates are plotted for a specific solution step. In this figure, the ESS needs a single iteration to attain convergence, while the SNRM & CALM requires four iterations. Heuristically, the observed fast rate of convergence of the ESS can be explained by the fact that only the dominant modes of deformation are accounted for in this strategy. The other modes, that may contribute to stiffen the displacement response of the structure, are excluded.

6.2.2 The Elastic-Softening Beam-Rod

This example offers the oportunity to test the ESS in view of the presence of two dominant modes of deformation in the displacement response of the beam-rod. These modes represent respectively the flexural and the extensional patterns shown in Fig. 4.25. Moreover, the degree of participation of each mode varies along

the displacement response of the beam-rod as demonstrated in Fig. 4.28.

According to Subsection 4.5.3, it has been demonstrated that the conventional load-deflection curve of the beam-rod presents a distinct limit point. The overcoming of a limit point constitutes a challenge for any solution strategy. This is so because the considered solution strategy should deal with a stiffness matrix that changes from positive definite to a condition of singularity and becomes indefinite at the vicinity of the limit point. This drastic change in stiffness may often cause lack of convergence of the iterative process. As an attempt to avoid these problems, Bergan (1979) has suggested to proceed with solution steps without equilibrium iterations near a limit point. However, this approach may cause drifting from the correct equilibrium path. It is also known that the classical Newton-Raphson methods fail completely prior to the limit point (Riks 1979). In addition, the proper description of the unstable descending branch is important to the evaluation of the load capacity and displacement response beyond the ultimate level.

Herein, CALM and ESS are applied to trace the load-deflection curve of the elastic-softening beam-rod. Figure 6.6 shows the corresponding curves for 30 solution steps. Both methods use the same reference load indicated in Fig. 4.22 and the same number of solution steps. The prescription of the same number of steps for both strategies is intentional and attempts to know how far each strategy is able to trace the load-deflection curve of the beam-rod.

The CALM passes the limit point and traces a small portion of the descending branch. As seen in Fig. 6.6, too many solution steps

are required at and after the limit point. This is motivated by the very small size of the adopted constant arc-length, which is based only on the Euclidean norm of the displacement increment vector computed for the first solution step (Ramm 1981).

The ESS also overcomes the limit point as illustrated in Fig. 6.6. This solution includes 10 eigenanalyses and the iterative phase uses only two generalized displacements. The first and second generalized degrees of freedom correspond respectively to the flexural and the extensional modes shown in Fig. 4.25a. The relations between these generalized displacements and the load factor are illustrated in Fig. 6.7 for the complete range of the beam-rod behavior. At the limit point in Fig. 6.7, the extensional generalized displacement remains stationary, whereas the flexural generalized displacement passes smoothly over that point. It is also noted that the flexural generalized displacement is more significant than the extensional generalized displacement along the descending branch.

The variations of the current, the average and the secant stiffness parameters with the Euclidean norm of the generalized displacements is illustrated in Fig. 6.8. The variation of the normalized determinant is also shown. It is noted that the current, the average and the determinant show similar variations throughout the phases of the behavior of the beam-rod. Specifically in the softening range, these parameters attain small negative values that correspond to the negative stiffness of the descending branch of the load-deflection curve (Fig.6.6). The secant stiffness parameter exhibits a more gradual transition from the elastic phase to the softening phase. Although the secant parameter allows for the decay

in stiffness, this decay is not as steep as for other stiffness parameters.

The factor f that adjusts the size of the arc-length is a function of the current stiffness parameter. Its definition for behavior type 1 (Figs. 5.7 and 5.9) is given in [5.32], [5.33], [5.34] and [5.35]. Figure 6.9 shows the variation of this factor with the value of the current stiffness parameter. A single reduction of the arc-length size takes place in the elastic-softening phase. Close to the limit point, the arc-length size is reduced to 10% of its initial size. On the other hand, the arc-length is extended in the softening range to its initial value. As a result of the control of the arc-length size, the ESS has provided a better distribution of solution steps around the limit point and throughout the descending branch of the load-deflection curve (Fig. 6.6).

Due to the limited number of global degrees of freedom (18), a comparative study about CPU time is meaningless for this present example.

6.2.3 The Reinforced Concrete Deep Beam

To date, the numerical description of load-deflection curves of reinforced concrete structures has faced severe obstacles imposed by a diversified and highly nonlinear material behavior. For instance, cracking, shearing and crushing of concrete as well as yielding of the reinforcement may occur at different stages of the load-deflection curve. Accordingly, the chosen solution strategy should be able to deal with sharp changes of stiffness, to overcome limit points and to trace unstable and sometimes steep descending branches. In

addition, the solution strategy has to capture localization of deformation that may happen within small regions of the structure.

In view of these difficulties and in the absence of a suitable solution strategy, most of the published research has been confined to the description of the part of the load-deflection curve that ranges from zero to ultimate load (Schnobrich 1977, Balakrishnan and Murray 1989, Frantzeskakis and Theillout 1989).

Recently, however, De Borst (1987) has succeeded in describing the post-ultimate response of plain and reinforced concrete structures by means of the indirect displacement control method reviewed in Chapter 2. This method requires a preselected set of global degrees of freedom to constitute the arc-length constraint equation. Apart from being problem-dependent, the arbitrary selection of some global degrees of freedom may not enhance the capture of localization of deformation, since the region of the structure in which this phenomenon takes place can not be anticipated in general.

According to the formulation of the ESS, given in Chapter 5, this solution strategy selects automatically the dominant generalized displacements to form the arc-length constraint equation. It is also known that these generalized displacements are associated with the dominant eigenvectors extracted from the tangent stiffness matrix. Hence, localization of deformation, seen as a material instability, is directly represented within the dominant eigenvectors. This is very evident in Fig. 4.36, where the second and the third eigenvectors of the tangent stiffness matrix of the reinforced concrete deep beam incorporate such localizations.

The behavior of the reinforced concrete deep beam, discussed in subsection 4.5.4, shows all the complex features of sharp changes in stiffness, limit point and unstable and steep descending branch. Therefore, this beam represents a challenge to the application of any solution strategy.

Figure 6.10 shows the load-deflection curves that result from the experiment (Rogowsky et al. 1983) and from the analyses performed by the ESS and the SNRM & CALM.

The curve denoted ESS (1DOF) is traced utilizing a single generalized displacement within the iterative phase. This single generalized displacement is associated with the overall bending mode (first eigenvector in Fig. 4.36) and the corresponding stiffness (first eigenvalue). While solving the incremental-iterative equilibrium equations, a reduction from 460 global degrees of freedom to only one generalized degree of freedom is carried out through the utilization of the overall bending mode. Out of the 30 solution steps, 20 eigenanalyses are performed: one eigenanalysis for each of the first five steps and alternate eigenanalyses thereafter. The resulting load-deflection curve correlates well with the other curves in the initial range of the beam behavior, prior to the onset of diagonal cracks. However, it seems slightly stiffer thereafter. This discrepancy may be caused by the somehow low number of eigenanalyses performed within that range of behavior. Prior to the limit point, the solution is terminated due to the insufficient level of participation (about 77%) of the selected mode.

On the other hand, the load-deflection curve designated as ESS (1DOF & 3DOF) in Fig. 6.10 shows a much better agreement with the

alternative solutions. In this case, eigenanalysis is done at every solution step. As before, the first eigenvector is preserved as the single mode throughout the ascending branch. However, the first three eigenvectors are used as displacement components from the limit point to the end of the descending branch. In doing so, a participation greater than 95% is achieved. In addition, this demonstrates that the modes that incorporate localization of deformation are necessary in the accurate description of the descending branch.

The load-deflection curve labeled SNRM & CALM (460DOF) results from the application of the SNRM and the CALM, respectively for the ascending and the descending branches shown in Fig. 6.10. Load incrementation along the ascending branch is prescribed to conform with the obtained load levels that result from the solution given by the ESS. In addition, the the size of the arc-length in the descending branch has been prescribed to agree with the size furnished by the ESS. Despite the large number of iterations (Table 6.2), the SNRM traces the ascending branch accurately, but fails prior to the limit point due to the occurrence of a nearly singular stiffness matrix. At this stage, the solution strategy is changed to CALM by means of a restart procedure. Thus, the description of the descending branch is successfully achieved.

Figure 6.11 shows the generalized load-deflection curves that relate the dominant generalized displacements to the load factor. It is emphasized that such curves represent one-to-one relationships, since the equilibrium equations are uncoupled. In addition, the predominant participation of the first eigenvector (Fig. 4.36), relative

to the second and third modes, is apparent in Fig. 6.11. The latter modes show relevant levels of paticipation only after the limit point.

In terms of midspan deflection, Fig. 6.12 illustrates the participation, separately and combined, of the first three modes. In this figure, the resulting deflections are compared with the actual midspan deflection which is represented by the 45 degrees straight line. The combination of the deflections, that results from the three modes, approximates the actual deflection very accurately.

The variation of the current, the average and the secant stiffness parameters with the midspan deflection is illustrated in Fig. 6.13. The current stiffness parameter experiences sharp drops at the onset of flexural and diagonal cracks. Then, it suffers a smooth decrease at the first yielding of the longitudinal reinforcement. After the first crushing of concrete, the current stiffness parameter decreases drastically and attains negative values, which are associated with the unstable behavior along the descending branch of the load-deflection curve (Fig. 6.10). The behavior of the average stiffness parameter seems very sensitive to the sharp variations in the beam stiffness that take place after the appearance of flexural cracks. In this example, the secant stiffness parameter follows a similar path as for the other parameters. This is somehow expected since the formulation of the material model utilizes a tangent constitutive matrix before peak values of strains and stresses, whereas it changes to a secant matrix thereafter. As a consequence, the overall variation of the stiffness parameters in the present case (Fig. 6.13) is not as smooth as for the cases in which gradual yielding occurs (Figs. 6.3 and 6.8).

Figure 6.14 shows the variation of the factor that adjusts the size of the arc-length with the current stiffness parameter. Once more, the definition of the factor f given in [5.32], [5.33], [5.34] and [5.35] is adopted herein. Considerable reduction of the arc-length size is automatically generated prior to the limit point. These series of reductions avoid the drifting from the actual curve and helps to overcome the limit point. After this point, the size of the arc-length is relatively extended, although it reaches approximately 40% of its initial value. The extended arc-length is then applied to the description of the descending branch.

Figure 6.15 illustrates the convergence performance of the ESS and the SNRM & CALM for the same stage on the respective load-deflection curves (r= 0.600 mm and P=220 KN), where the diagonal cracking initiates. It is noted that the rate of convergence of the ESS is much faster than the one associated with the SNRM & CALM. While five iterations are required for the SNRM & CALM solution, only two are sufficient to satisfy the prescribed tolerance in the case of the ESS. This favourable property is enhanced by the exclusion of stiffer deformation modes from the generalized equilibrium formulation used in the ESS.

Table 6.2 lists the solution parameters that correspond to the ESS and the SNRM & CALM. Considering the same number of solution steps for both methods, the ESS requires a much lower number of iterations than for the SNRM & CALM. This substantiates the fast rate of convergence demonstrated in Fig. 6.15. As a beneficial effect, the ESS uses approximately 54% (including eigenanalysis) of the total CPU time required by the SNRM & CALM.

6.2.4 The Reinforced Concrete Shallow Beam

According to Subsection 4.5.5, the load-deflection history of an underreinforced concrete shallow beam (Fig. 4.45) shows three distinct phases of behavior. First, the phase that ranges from zero load to the appearance of the first flexural cracks is approximately linear. A slight drop in the beam stiffness is observed at the onset of the first flexural cracks. This phenomenon initiates the second phase which ends with the first yielding of the longitudinal reinforcement. It is noted that the bending stiffness does not experience severe changes during these phases. The third and last phase begins with the yielding of the reinforcement and prolongs extensively until the concrete crushes completely within the compression zone. It is at the start of this stage that the bending stiffness decreases drastically, although no remarkable change is verified thereafter. Thus, the premature yielding of the reinforcement and the gradual formation of the compression zone in the concrete impart considerable ductility to the beam. As a result, this type of structure presents a great capacity of energy absorption.

The description of the segment of the load-deflection curve that corresponds to the phase of ductile behavior mentioned above constitutes a difficult application for a solution strategy. This is so because the solution strategy should accomodate the severe drop in stiffness at the first yielding of the reinforcement, apart from describing the complete range of ductile behavior.

In this section, the solution strategies CALM and ESS, in conjunction with the SNRM, are applied to trace the load-deflection curve of the beam S8 tested by McCollister (1954). First, the SNRM is

employed to describe the nearly linear segment associated with the first two phases of the beam behavior. Then, a restart procedure changes the solution strategy from the SNRM to the CALM or the ESS so that the segment of ductile behavior can be described. The presentation to follow is restricted to the description of this part of the load-deflection curve, which is by far the most troublesome.

Figure 6.16 shows three load-deflection curves, respectively given by the experiment (McCollister 1954), the CALM and the ESS. The stiffness matrix for the CALM and the first eigenvalue for the ESS have been updated only at the first yielding of the reinforcement, which coincides with the step of the restart. A unique and constant arc-length has been prescribed for both strategies.

The curve provided by the CALM in Fig. 6.16 utilizes the total number of global degrees of freedom, which is 346 for the present case. It agrees well with the experimental curve, specifically at the range close to ultimate load. Nevertheless, local unloading has occured in a few steps.

The curve denoted as ESS (1DOF) in Fig. 6 16 results from the iterative solution of an equilibrium equation with a single generalized displacement. This generalized displacement is associated with the single curvature mode shown in Fig. 4.47. The corresponding eigenvalue represents the uncoupled bending stiffness which is kept constant throughout the phase of ductile behavior. Thus, the iterative process relies mainly on the variation of the generalized unbalanced force. The resulting solution is reasonably accurate for the first half of the flat plateau, but overestimates the load (in 15% of the experimental ultimate load) for the second half. A

possible reason for this moderate discrepancy rests on the way that the material model influences the unbalanced force at that specific range of behavior. After crushing, the material model adopts a secant constitutive matrix which may be much stiffer than the tangent constitutive matrix used before crushing. This, in turn, causes a relative increase in the generalized unbalanced force.

The variation of the beam stiffness is suitably described by the average stiffness parameter defined in [5.26]. The current stiffness parameter is not adequate in this case, since the stiffness is kept constant throughout the segment of ductile behavior.

Figure 6.17 illustrates the variation of the average and the secant stiffness parameters with the midspan deflection. It is noted the sharp drop of the average stiffness parameter at the first yielding of the longitudinal reinforcement. In addition, the beam stiffness, as indicated by this parameter, decays to a very low and nearly constant level throughout the remaining part of the segment that corresponds to the ductile behavior. The negative values of the average stiffness parameter shown in the figure reflects local unloading in the load-deflection curve (Fig. 6.16). The automatic adjustment of the arc-length size is not carried out in the present case because of the adoption of a constant arc-length for both strategies.

Table 6.3 lists the solution parameters relative to both solution strategies. Considering the same number of solution steps, the ESS needs 65% of the total number of iterations required by the CALM. The saving in CPU time resulting from the ESS solution amounts to 30% of the total CPU time used by the CALM. Once more, the fast rate

of convergence enhanced by the ESS is observed for all solution steps belonging to the flat plateau. The steady number of one iteration per solution step has been recorded for the ESS strategy. Figure 6.18 shows the convergence performance for both strategies considering a solution step after the first crushing of concrete. While three iterations are required by the CALM, a single iteration is sufficient to satisfy the convergence criterion in the case of the ESS. Again, the fast rate of convergence can be credited to the exclusion of spurious and stiffening modes of deformation from the formulation of the ESS.

SOLUTION STRATEGY	ELASTIC PERFECTLY PLASTIC CANTILEVER BEAM SOLUTION PARAMETERS										
	No. of solution steps	No. of iter. **	No. of iter. per step	No.const arc lengths	No. of red. arc lengths	No. of extended arc leng.	No. of DOF	No. of Eigenan	Total CPU time *	CPU per step	CPU time for eigenan
SNRM & CALM	17	31	1.823	5	-	-	286	-	36	2.117	-
CALM	11	15	1.364	11	-	-	286	-	16	1.454	-
ESS	22	22	1.000	3	9	10	1	6	28	1.273	6

* : CPU time in seconds
**: After the initial iteration.

Table 6.1: Comparative results of the solutions for the elastic-plastic cantilever beam.

SOLUTION STRATEGY	REINFORCED CONCRETE DEEP BEAM SOLUTION PARAMETERS										
	No. of solution steps	No. of iter.**	No. of iter. per step	No. const Arc Length	No. of red. arc lengths	No. of extended arc leng.	No. of DOF	No. of Eigenan	Total CPU time *	CPU per step	CPU time for eigenan
SNRM & CALM	22	93	٬227	7	-	-	460	-	380	17.273	-
ESS	22	40	1.818	0	13	9	1:asc. br 3:des. br	22	136	6.182	68

* : CPU time in seconds
**: After the initial iteration.

Table 6.2: Comparative results of the solutions for the reinforced concrete deep beam.

| SOLUTION STRATEGY	REINFORCED CONCRETE SH LLOW BEAM SOLUTION PARAMETERS (flat plateau)										
	No. of solution steps	No. of iter. **	No. of iter. per step	No. cons Arc Length	No. of red. arc lengths	No. of extended arc leng.	No. of DOF	No. of eigenan.	Total CPU time *	CPU per step	CPU time for eigenan.
CALM	27	41	1.518	27	-	-	346	-	134	4.963	-
ESS	27	27	1	27	0	0	1	1	95	3.518	1

* : CPU time in seconds
**: After the initial iteration

Table 6.3: Comparative results of the solutions for the reinforced concrete shallow beam.
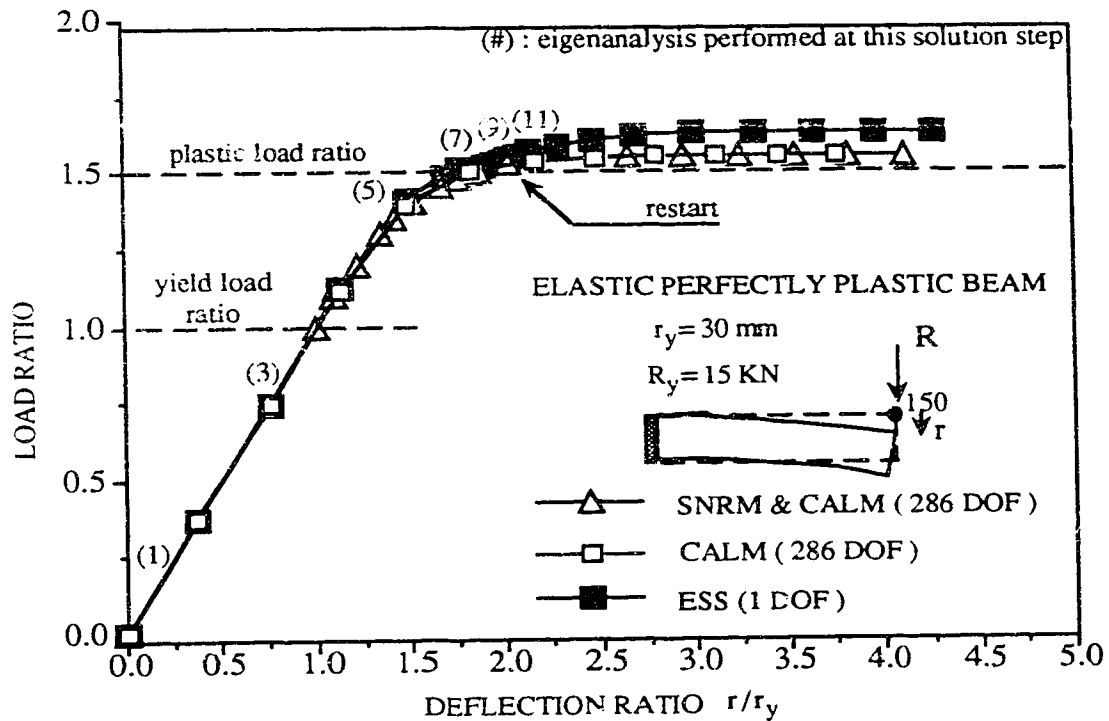
Figure 6.1: Conventional load-deflection curves for the elastic-plastic cantilever beam.
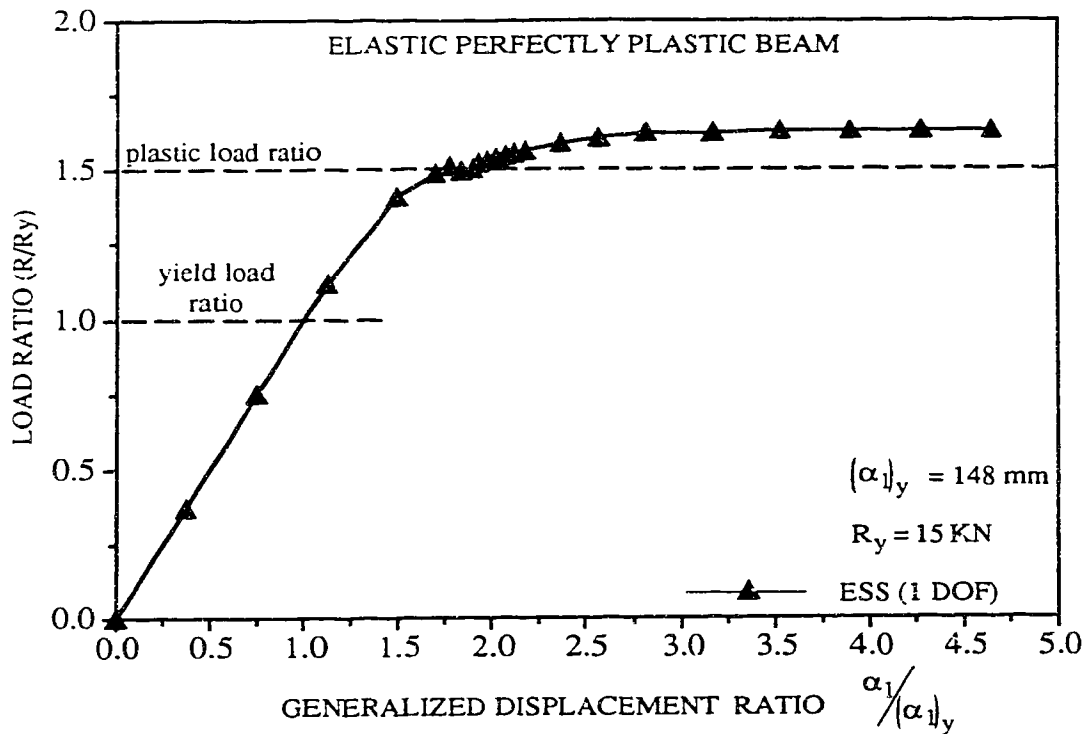
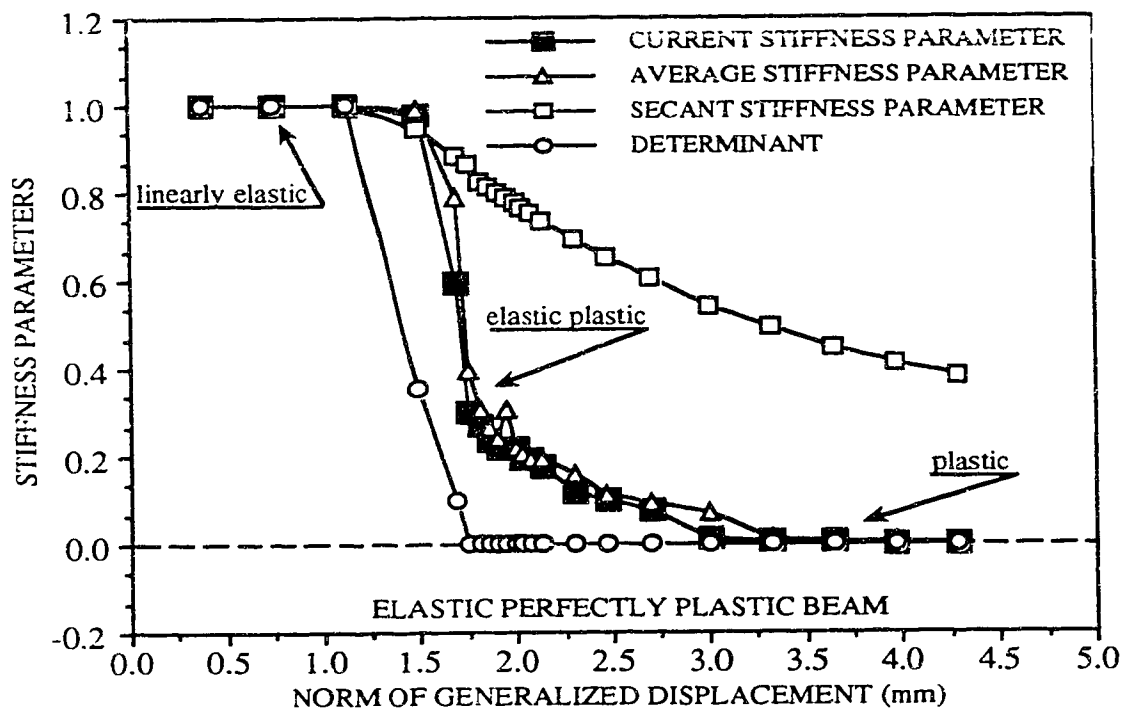Figure 6.2: Generalized load-deflection curve for the elastic-plastic cantilever beam.

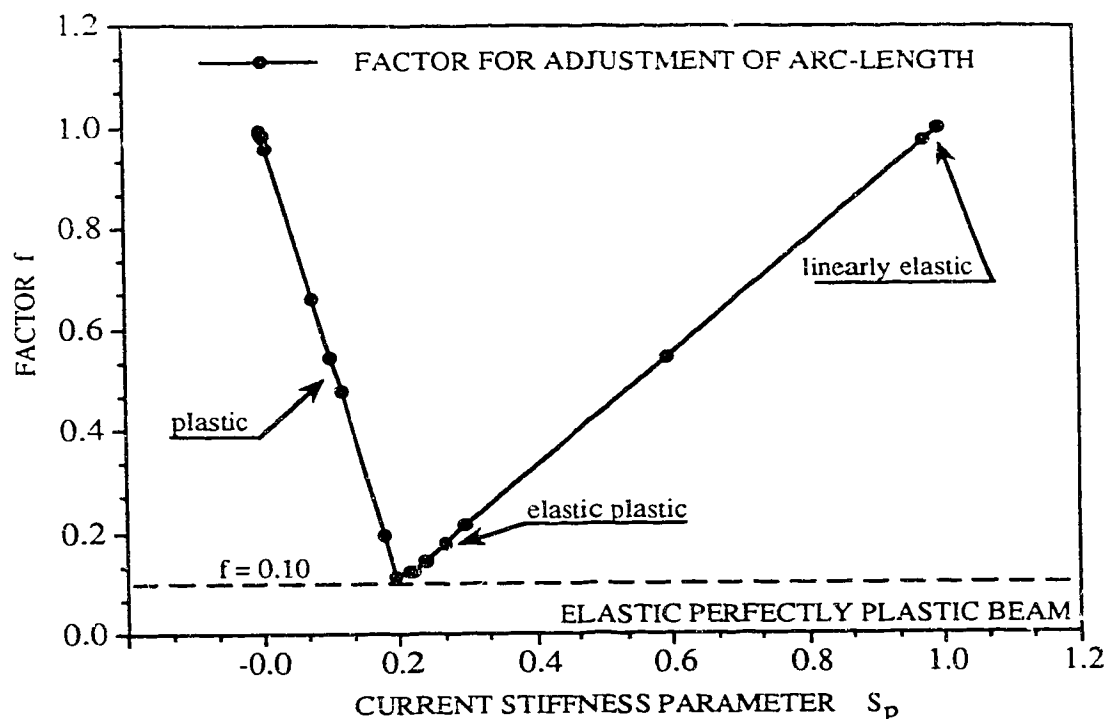Figure 6.3: Stiffness parameters for the elastic-plastic cantilever beam.

Figure 6.4: Variation of the factor f with S_p for the elastic-plastic cantilever beam.
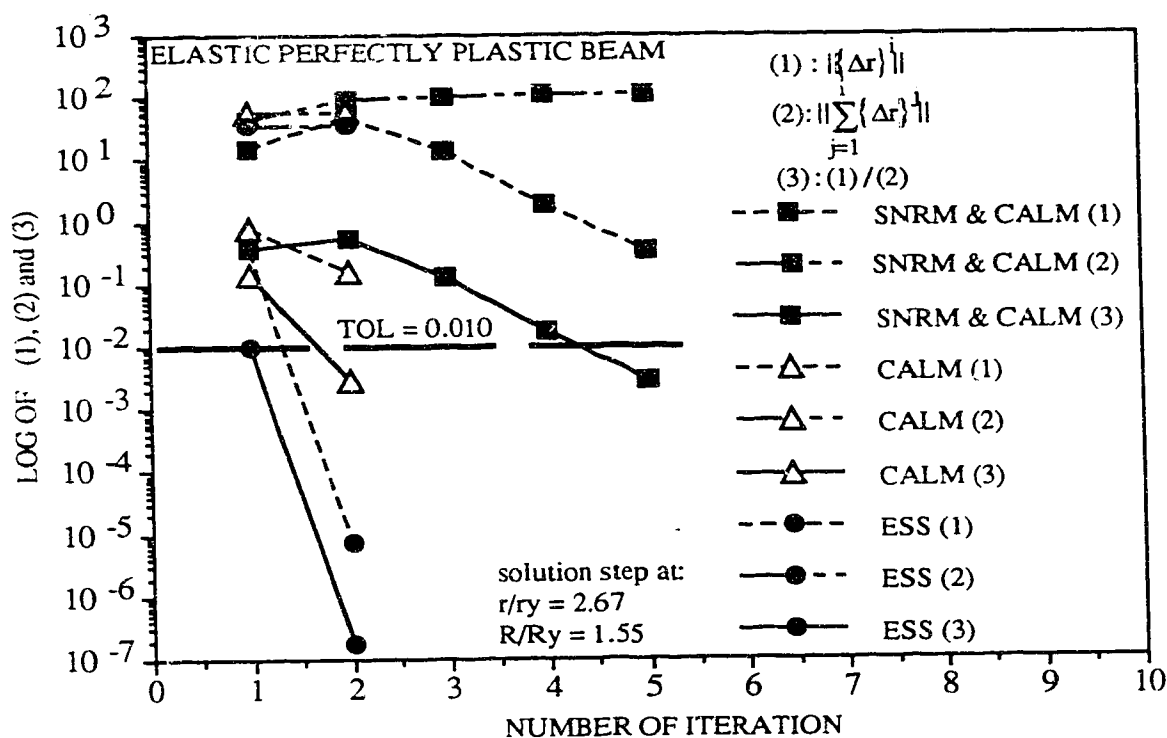

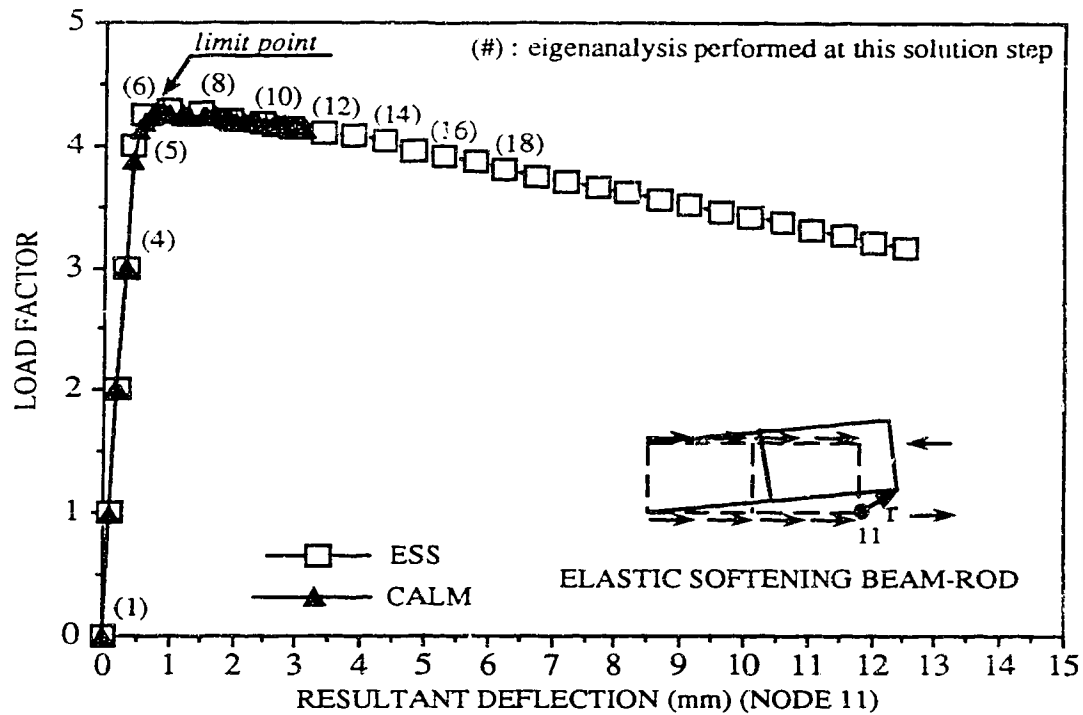
Figure 6.5: Convergence behavior for a solution step.

Figure 6.6: Conventional load-deflection curves for the elastic softening beam-rod.
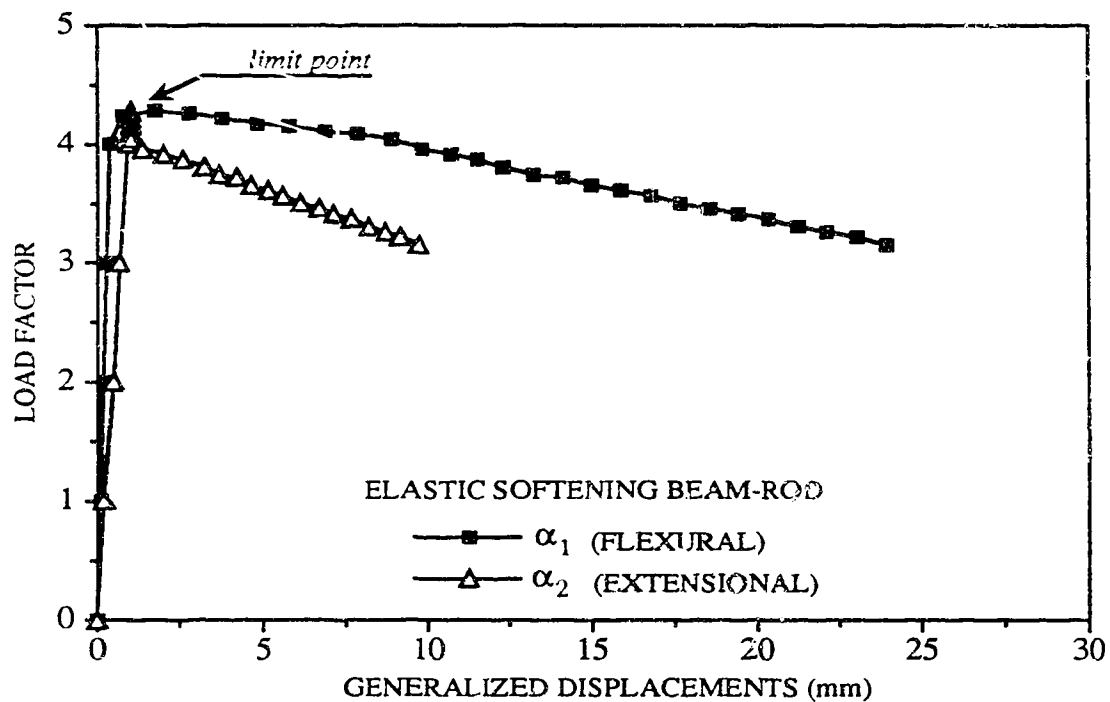

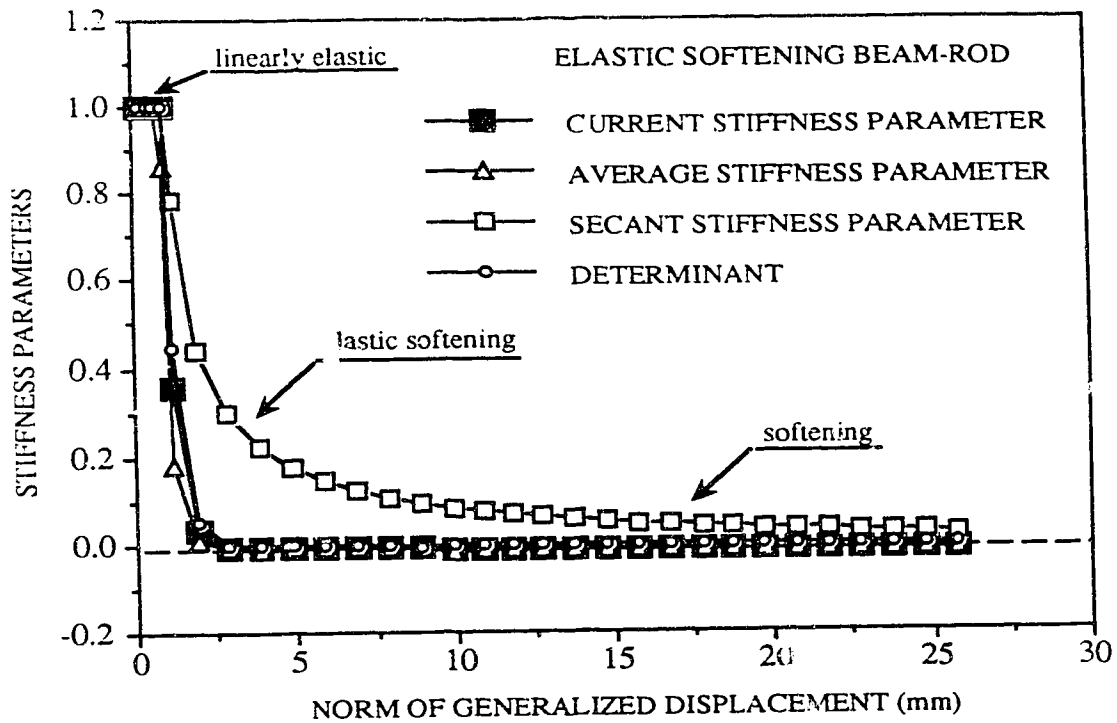Figure 6.7: Generalized load-deflection curves for the elastic softening beam-rod.

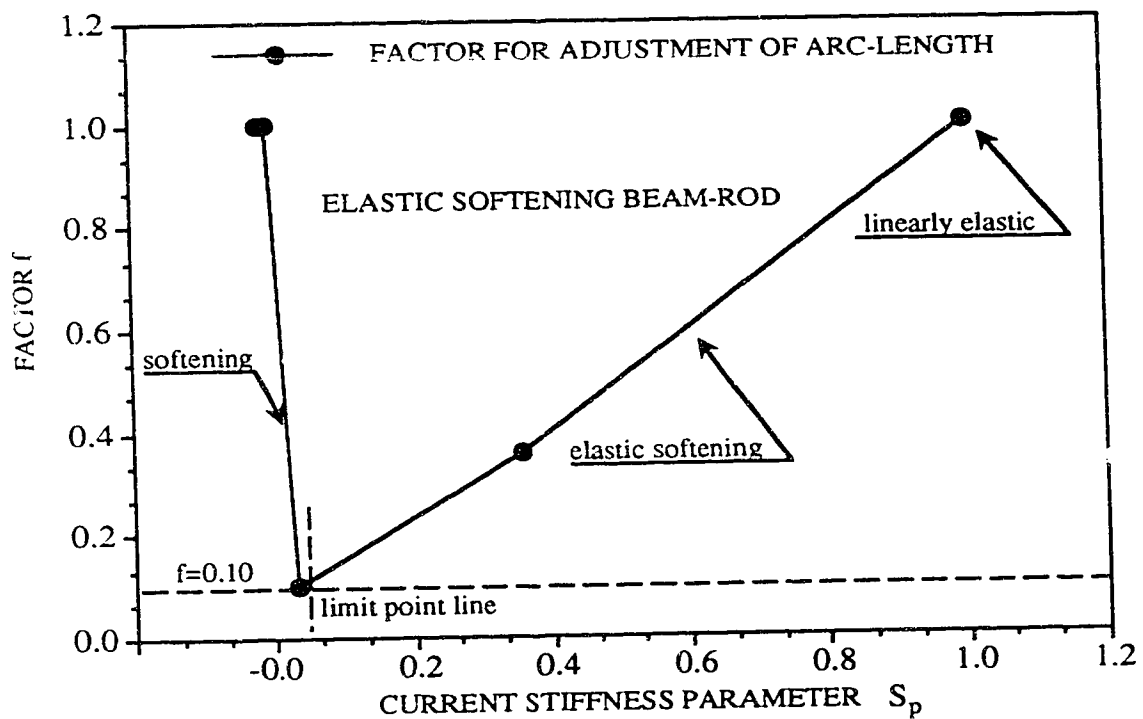Figure 6.8: Stiffness parameters for the elastic softening beam-rod.

Figure 6.9: Variation of the factor f with Sp for the elastic softening beam-rod.
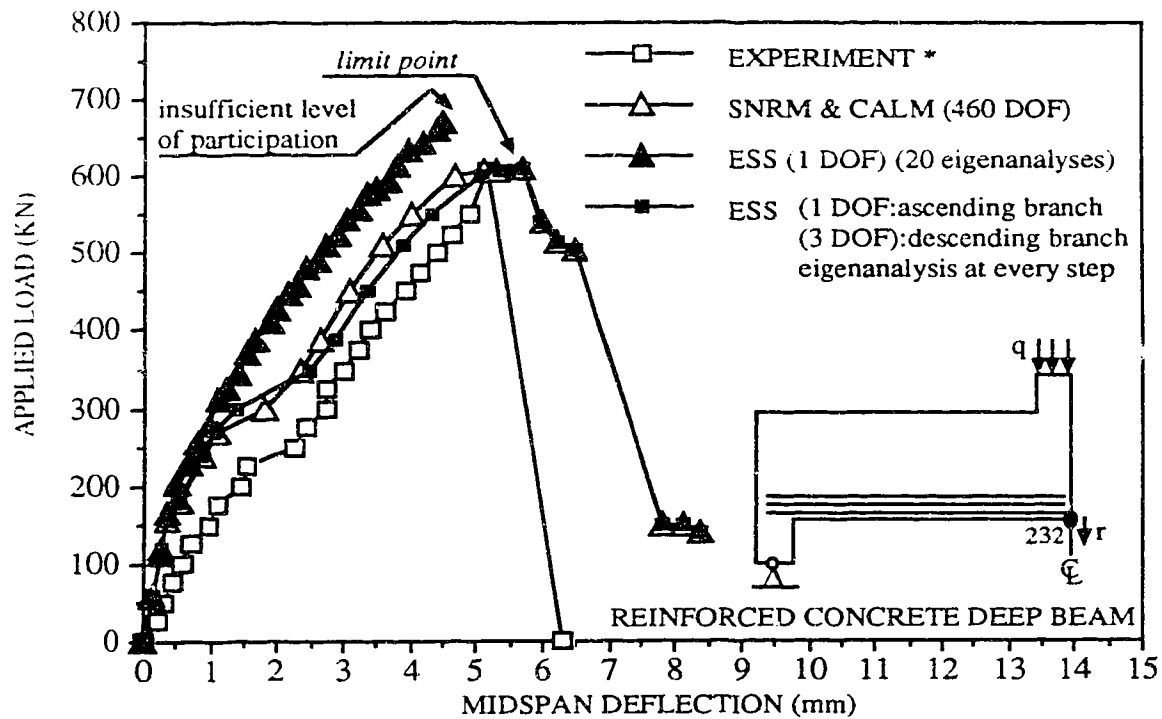
Figure 6.10: Conventional load-deflection curves for the reinforced concrete deep beam (*: adapted from Rogowsky et al. 1983).
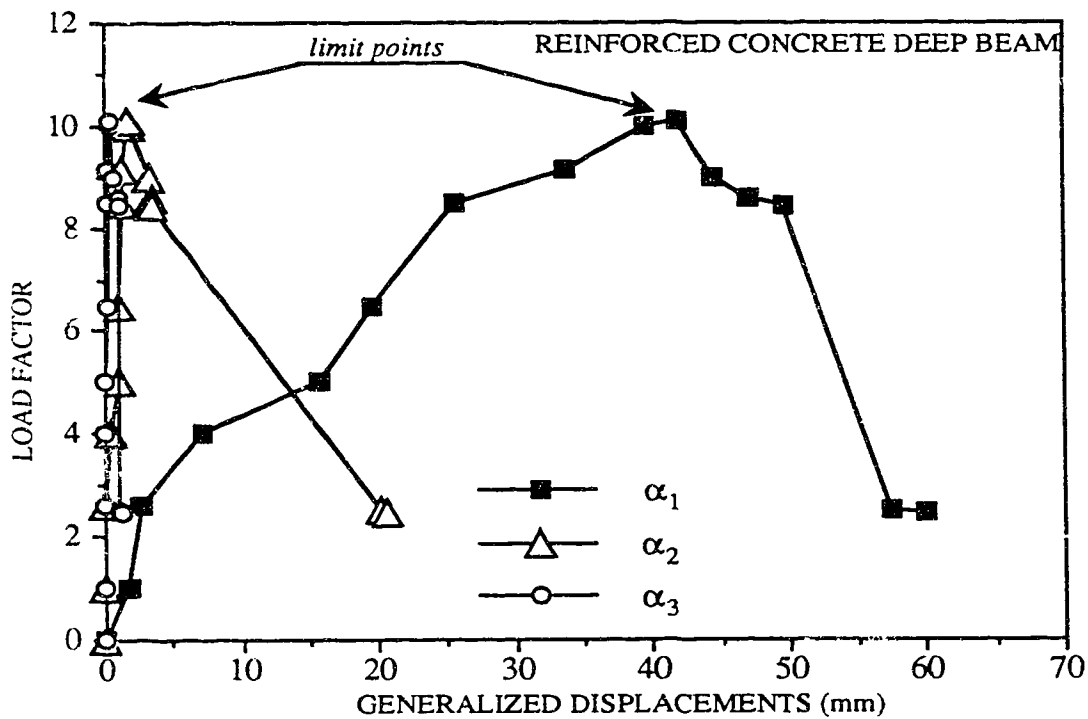

Figure 6.11: Generalized load-deflection curves for the reinforced concrete deep beam.
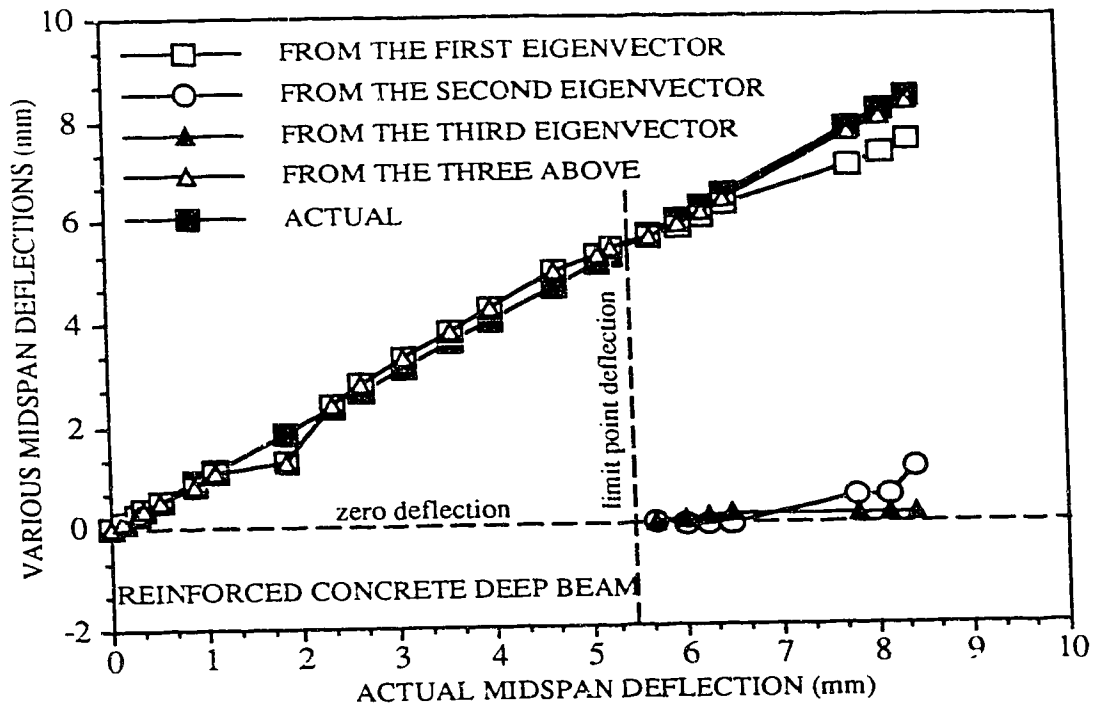
Figure 6.12: Midspan deflections of the reinforced concrete deep beam.
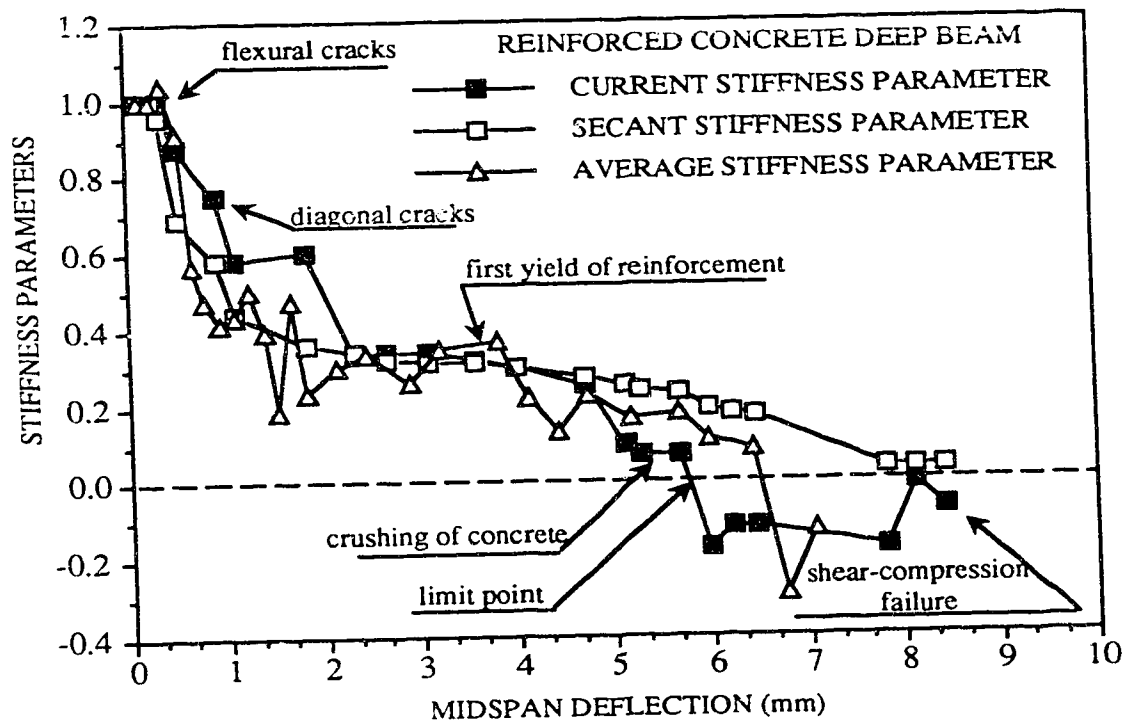
Figure 6.13: Stiffness parameters for the reinforced concrete deep beam.
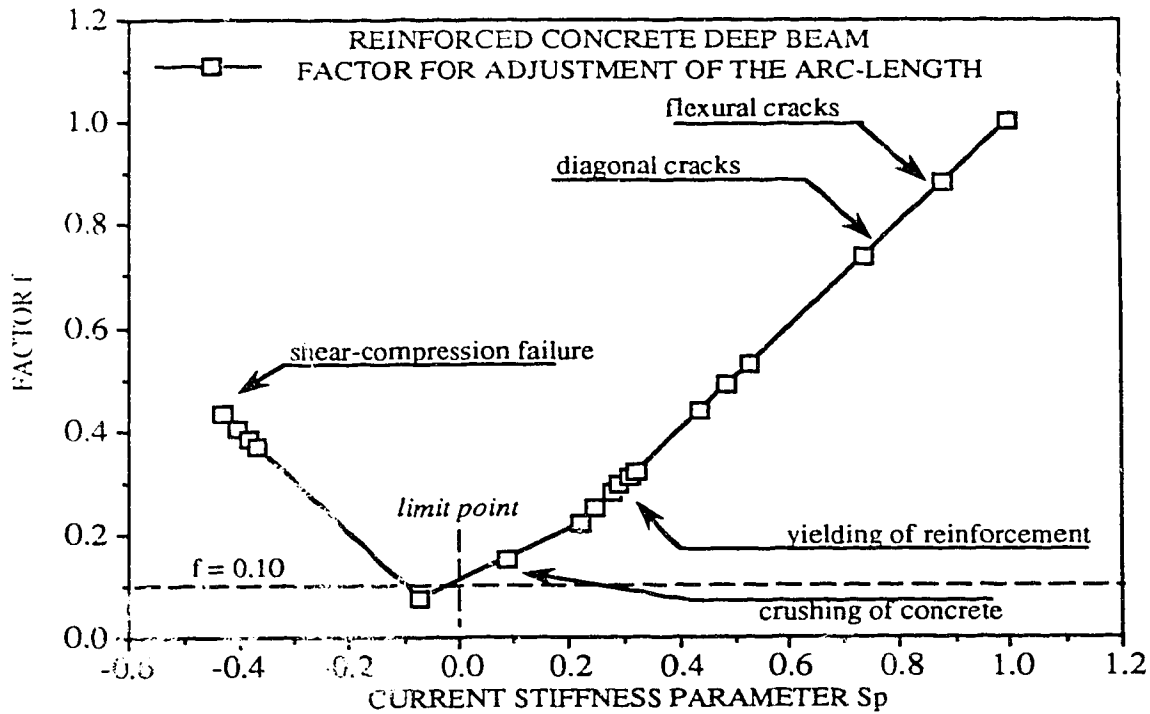
Figure 6.14: Variation of the factor f with Sp for the reinforced concrete deep beam.

Figure 6.15: Convergence behavior for a solution step at cracking.

Figure 6.16: Load-deflection curves for the reinforced concrete shallow beam (* : adapted from McCollister 1954).
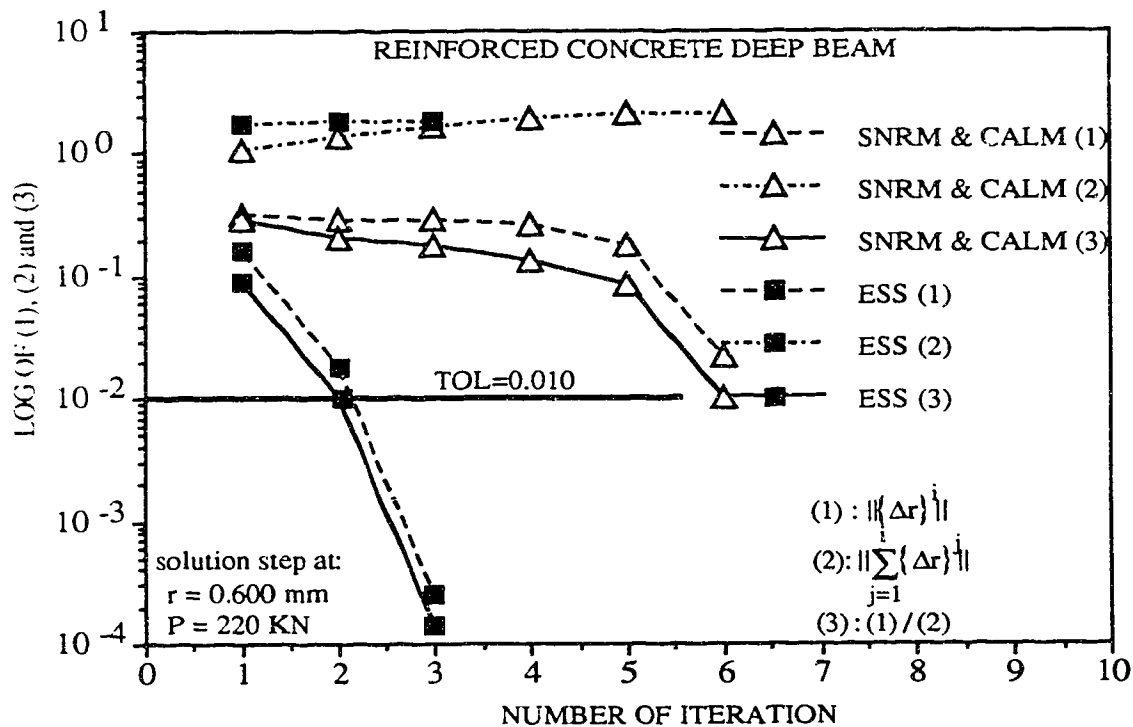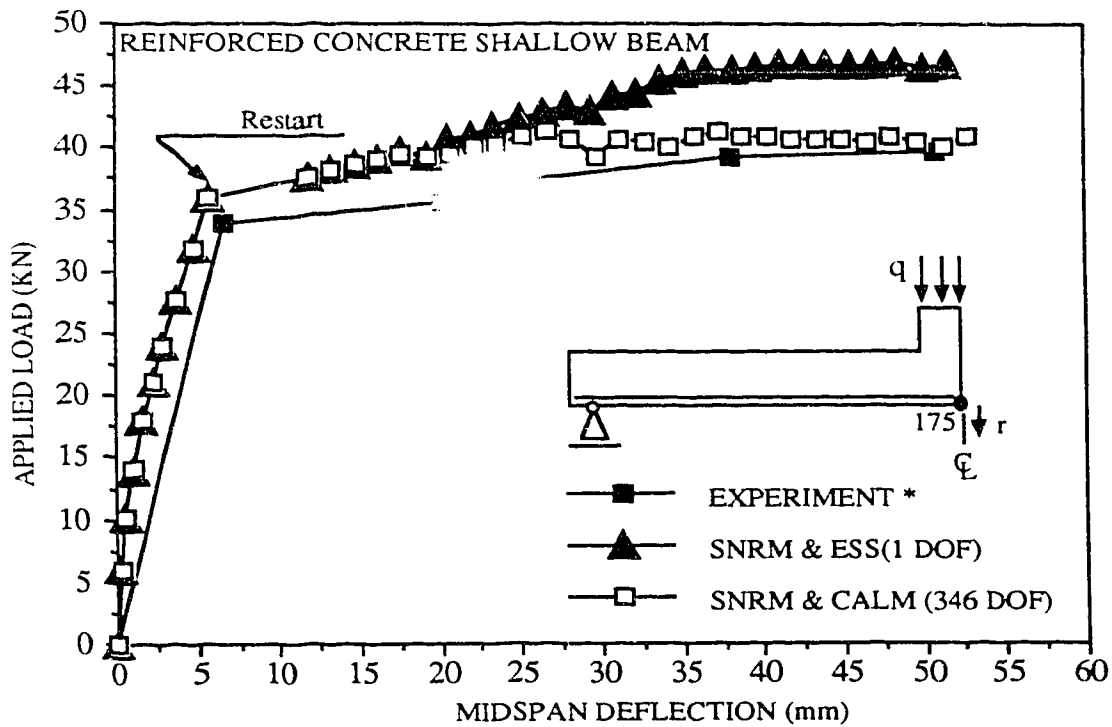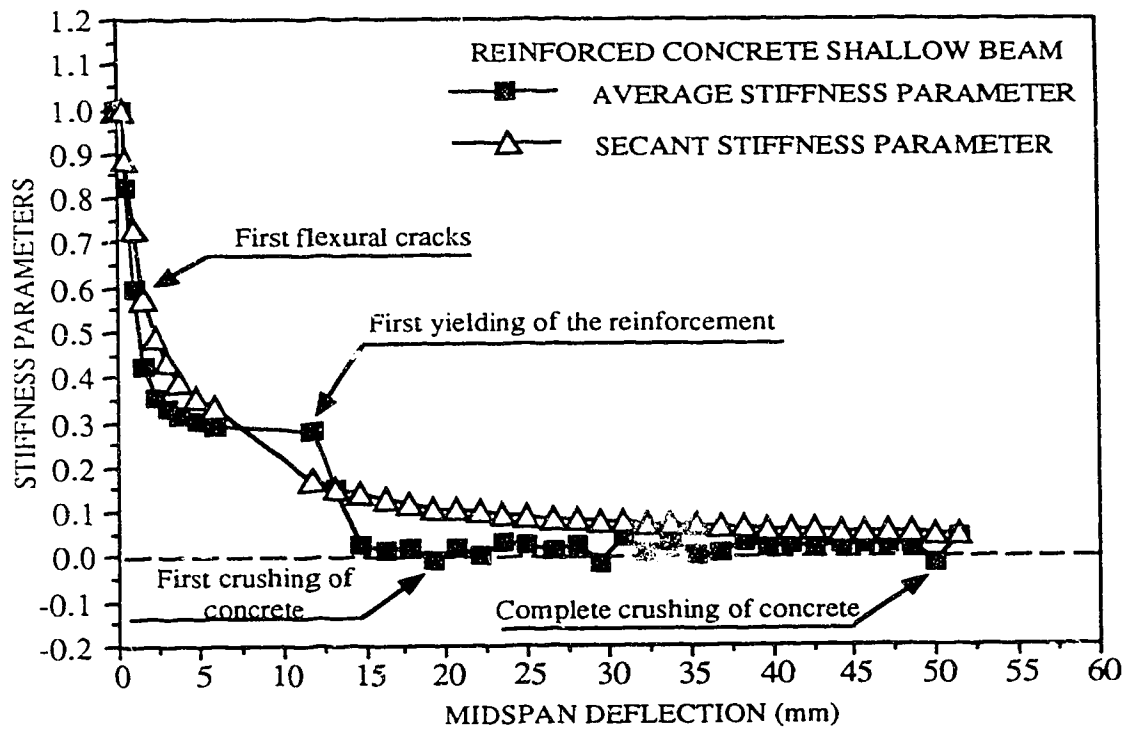

Figure 6.17: Stiffness parameters for the reinforced concrete shallow beam.
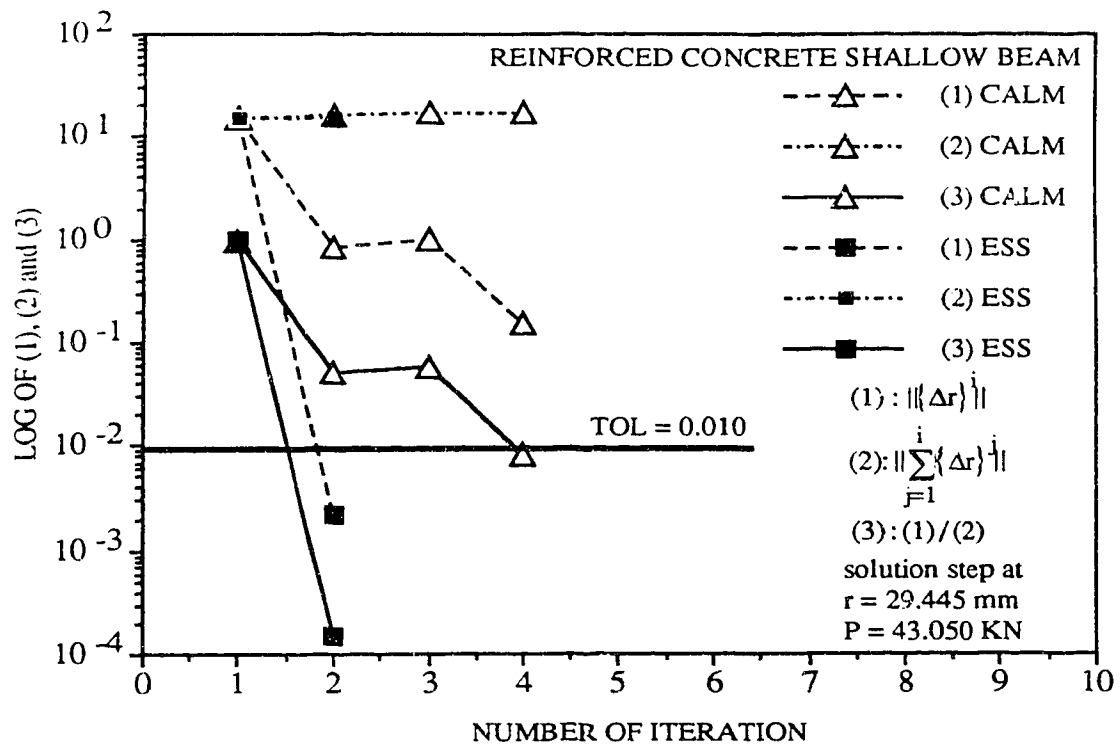
Figure 6.18: Convergence behavior for a solution step after the first crushing of concrete.

CHAPTER 7

SUMMARY, CONCLUSIONS AND RECOMMENDATIONS

7.1 Summary and Conclusions

In this study, an eigenvector-based solution strategy has been developed and applied to the analysis of materially nonlinear structures; in particular, structures subjected to damage reflected in material nonlinearity. The type of damage in a given structure is naturally specific to the type of loading. Such damage would also result in changes in the tangent stiffness matrix of the structure. Thus, it would ultimately result in prefered deformation directions. These directions must be reflected in the eigenvectors of the stiffness matrix itself. A study of the eigenvectors of the stiffness matrix of such structures would not only offer insight into the structural behavior, but also may lead to a reduction in the number of generalized degrees of freedom necessary to adequately describe the structural behavior.

Thus, the eigenvectors of the tangent stiffness matrix have been chosen as the basis vectors while describing the static equilibrium of inelastic structures. A transformation of the equilibrium equations, from the basis of the global degrees of freedom to the basis of the eigenvectors, has been undertaken. A completely uncoupled system of N equilibrium equations has resulted from this transformation. In addition, the condition of equilibrium has been formulated in terms of generalized displacement increments and generalized forces.

A comprehensive study of the dominance of a preselected set of eigenvectors upon the incremental displacement response of materially nonlinear structures has been presented. As tools, analytical parameters have been formulated to investigate dominance. A beam-rod as well as a deep beam and two shallow beams have been used as case studies. Material models, such as elastic perfectly plastic, elastic softening and hypoelastic, have been adopted in the course of this investigation. As a consequence of the study of dominance, a criterion has been set to determine whether or not an eigenvector participates effectively in the incremental displacement response. Following the finding that a drastically small number of eigenvectors participates in the displacement response, the system of equilibrium equations is reduced from N to M, where M is the number of dominant eigenvectors.

The uncoupling and reduction of the degrees of freedom have served as background for the formulation of the eigenvector-based solution strategy. The concept of an arc-length with an orthogonal iteration path has been employed within this formulation. The modified Newton-Raphson method has been chosen as the iterative scheme. This strategy is performed in two phases. First, the pre-iterative phase reduces and uncouples the system of equations. In addition, the control of the arc-length size and the criterion for unloading have been built in this phase. In the iterative phase, the solution of the incremental and iterative equilibrium and constraint equations is carried out in terms of generalized displacement increments and generalized forces.

The proposed strategy was then applied to the solution of four

problems. In these problems, the strategy was able to accomodate sharp changes in stiffness, to pass limit points, to trace prolonged flat segments and to describe steep descending branches. Considerable efficiency resulted from the adoption of an automatically controlled arc-length. For regions of linear behavior, the size of the arc-length was extended, whereas it was reduced for highly nonlinear regions. The expected failure modes of the examined structures have been properly captured. The comparison of performance with other strategies has been done on the basis of some solution parameters, such as the number of iterations, the rate of convergence and the CPU time. A fast rate of convergence has been found of great importance in the demonstrated cost-effectiveness of the proposed strategy. Savings in CPU time, as much as 45%, have been registered.

7.2   Recommendations

Considering the experience gained during the development and application of the eigenvector-based solution strategy, the following points are recommended for future research.

1. An automatic criterion should be developed to determine whether or not an eigenanalysis is required. The change in the value of the stiffness parameter can be used as a possible guideline.

2. The detection of lack of participation of the preselected eigenvectors should be followed by a re-eigenanalysis, incorporating additional eigenvectors. For example, if two eigenvectors are preselected, but three are required to satisfy the participation criterion, a re-eigenanalysis would furnish only the third eigenvector. This interactive eigenanalysis, however, requires

modification of the structure of the subspace iteration method.

3. The solution strategy should be applied to geometrically nonlinear problems, involving possibly global and local buckling. Then, a comparison of performance with the existing reduction methods would be important.

4. Application of the developed solution strategy to structures that exhibit multiple deformation modes, such as membrane and bending modes, would be of great interest.

BIBLIOGRAPHY

ALMROTH, B.O., STERN, P. and BROGAN, F.A. (1978). "Automatic Choice of Global Shape Functions in Structural Analysis". A.I.A.A. Journal, vol. 16, pp. 525-528.

ARGYRIS, J.H. (1965). "Continua and Discontinua", Proceedings of the First Conference on Matrix Methods in Structural Mechanics. Wright-Patterson A.F.B., Ohio, 11-189.

BALAKRISHNAN, S. and MURRAY, D.W. (1988). "Concrete Constitutive Model for NLFE Analysis of Structures", Journal of Structural Engineering, ASCE, vol 114, pp. 1449-1446.

BALAKRISHNAN, S. and MURRAY, D.W. (1989). "Prediction of R/C Panel and Deep Beam Behavior by NLFEA", Journal of Structural Engineering, ASCE, vol. 114, pp. 2323-2342.

BATHE, K-J. (1971). "Solution Methods for Large Generalized Eigenvalue Problems in Structural Engineering", UC SESM 71-20, Department of Civil Engineering, University of California, Berkeley, 138 p.

BATHE, K-J. and WILSON, E.L. (1976). "Numerical Methods in Finite Element Analysis", Prentice-Hall, Inc., Englewood Cliffs, New Jersey, 528 p.

BATOZ, J-L. and DHATT, G. (1979). "Incremental Displacement Algorithms for Nonlinear Problems", International Journal for Numerical Methods in Engineering, vol. 14, pp. 1262-1267.

BELLINI, P.X. and CHULYA, A. (1987). "An Improved Automatic Incremental Algorithm for the Efficient Solution of Nonlinear Finite Element Equations", Computer & Structures, vol. 26, pp. 99-110.

BERGAN, P.G. (1979). "Solution Algorithms for Nonlinear Structural Problems", in Proceedings of the International Conference on Engineering Application of the Finite Element Method, A.S. Computas, Oslo, pp. 13.1-13.38.

196

BERGAN, P.G., HORRIGMOE, G., KRAKELAND, B. and SOREIDE, T.H. (1978). "Solution Techniques for Nonlinear Finite Element Problems", International Journal for Numerical Methods in Engineering, vol. 12, pp. 1677-1696.

BURNS, N.H. and SIESS, C.P. (1966). "Plastic Hinging in Reinforced Concrete", Journal of Structural Division, ASCE, vol. 92, pp. 45-63.

CHEN, W-F and TING, E.C. (1980). "Constitutive Models for Concrete Structures", Journal of the Engineering Mechanics Division, ASCE, vol. 106, pp. 1-17.

CHEN, W-F. and SALEEB, A.F. (1982). "Constitutive Equations for Engineering Materials", John Wiley & Sons, New York, 580 p.

CLOUGH, R.W. and PENZIEN, J. (1975). "Dynamics of Structures", MacGraw-Hill, Inc., New York, 634p.

CRANDALL, S.H. (1983). "Engineering Analysis", Robert E. Krieger Publishing Company, Malabar, 417 p.

CRISFIELD, M.A. (1979). "A Faster Modified Newton-Raphson Iteration", Computer Methods in Applied Mechanics and Engineering, vol. 20, pp. 267-278.

CRISFIELD, M.A. (1981). "A Fast Incremental/Iterative Solution Procedure that Handles Snap-Through", Computers & Structures, vol. 13, pp. 55-62.

CRISFIELD, M.A. (1986). "Snap-Through and Snap-Back Response in Concrete Structures and the Dangers of Under-Integration", International Journal for Numerical Methods in Engineering, vol 22, pp. 751-767.

DARWIN, D. and PECKNOLD, D.A. (1977). "Analysis of Cyclic Loading of Plane R/C Structures", Computer & Structures, vol. 7, pp. 137-147.

De BORST, R. (1986). "Non-Linear Analysis of Frictional Materials", Ph.D. Dissertation, Delft University of Technology, The Netherlands, 140 p.

De BORST, R. (1987). "Computation of Post-Bifurcation and Post Failure Behavior of Strain-Softening Solids", Computer & Structures, vol. 25, pp. 211-224.

De COURSY, J.W. (1987). "The Emergence of Reinforced Concrete 1750-1910", The Structural Engineer, Vol. 65A, pp. 315-322.

DRUCKER, D.C. (1959). "A Definition of Stable Inelastic Material", Journal of Applied Mechanics, March, pp. 101-106.

ELWI, A.A. and MURRAY, D.W. (1979). "A 3D Hypoelastic Concrete Constitutive Relationship", Journal of the Engineering Mechanics Division, ASCE, vol. 105, pp. 623-641.

FELIPPA, C.A. (1988). "Solution of Nonlinear Equations", in Lecture Notes in Engineering, edited by Reddy et al., vol. 37, Springer-Verlag, New York, pp. 274-309.

FRANTZESKAKIS, C. and THEILLOUT, J.N. (1989). "Nonlinear Finite Element Analysis of Reinforced Concrete Structures with Particular Strategy Following the Cracking Process", Computer & Structures, vol. 31, pp. 395-412.

FRIED, I. (1984). "Orthogonal Trajectory Accession to the Nonlinear Equilibrium Curve", Computer Methods in Applied Mechanics and Engineering", vol. 47, pp. 283-297.

GOPALARATNAM, V.S. and SHAH, S.P. (1985). "Softening Response of Plain Concrete in Direct Tension", ACI Journal, May-June, pp. 310-323.

HAWKINS, G.A. (1963). " Multilinear Analysis for Students in Engineering and Sciences", John Wiley and Sons, Inc., New York, 219 p.

HORNE, M.R. and MORRIS, L.J. (1981). "Plastic Design of Low-Rise Frames", Collins, London, 238 p.

HURTY, W.C., COLLINS, J.D. and HART, G.C. (1971). "Dynamic Analysis of Large Structures by Modal Synthesis Technique", Computer & Structures, vol. 1, pp. 553-563.

KAO, R. (1974). "A Comparison of Newton-Raphson Methods and Incremental Procec res for Geometrically Nonlinear Analysis", Computers & Structures, vol. 4, pp. 1091-1097.

KOTSOVOS, M.D. (1983). "Effect of Testing Techniques on the Post-Ultimate Behaviour of Concrete in Compression", Materiaux et Constructions, vol. 16, pp. 3-12.

LANGHAAR, H.L. (1962). "Energy Methods in Applied Mechanics", John Wiley and Sons, Inc., New York, 350 p.

LAY, M.G. (1982). "Structural Steel Fundamentals", Australian Road Research Board, Victoria, 241 p.

MacGREGOR, J.G. (1988). "Reinforced Concrete, Mechanics and Design", Prentice-Hall, Englewood Cliffs, New Jersey, 799 p.

MALVERN, L.E. (1969). "Introduction to the Mechanics of Continuous Medium", Prentice-Hall, Inc., Englewood Cliffs, New Jersey, 713 p.

McCOLLISTER, H.M. (1954). "Load-Deformation Characteristics of Simulated Beam-Column Connections in Reinforced Concrete", M.Sc. Thesis, University of Illinois, 120 p.

MEEK, J.L. and TAN, H.S. (1984). "Geometrically Nonlinear Analysis of Space Frames by an Incremental Iterative Technique", Computer Methods in Applied Mechanics and Engineering, vol. 47, pp. 261-282.

MOLER, C.B. and STEWART, G.W. (1973). "An Algorithm for Generalized Matrix Eigenvalue Problems", SIAM Journal of Numerical Analysis, vol. 10, pp. 241-256.

MURRAY, D.W., CHITNUYANONDH, L. and WONG, C. (1980). "Implementation of an Elastic-Plastic Concrete Relationship", Computer Methods in Applied Mechanics and Engineering, vol. 23, pp. 35-57.

NAGY, D.A. (1977). "Modal Representation of Geometrically Nonlinear Behavior by the Finite Element Method", Transactions of the 4th International Conference on Structural Mechanics in Reactor Technology, San Francisco, August, vol. M, pp. M4/2.

NAPOLEAO, Fo., J. and ELWI, A.A. (1990). "Application of the 3D Hypoelastic Concrete Model to R/C Structures", Structural Engineering Report , Department of Civil Engineering, University of Alberta, Canada, (to be published).

NAYAK, G.C. and ZIENKIEWICZ, O.C. (1972). "Elasto-Plastic Stress Analysis. A Generalization for Various Constitutive Relations Including Strain Softening", International Journal for Numerical Methods in Engineering, vol. 5, pp. 113-135.

NOOR, A.K. (1981). "Recent Advances in Reduction Methods for Nonlinear Problems", Computers & Structures, vol. 13, pp. 31-44.

NOOR, A.K. and PETERS, J.M. (1980). "Reduced Basis Technique for Nonlinear Analysis of Structures", A.I.A.A. Journal, vol. 118, pp. 455-462.

NOOR, A.K. and PETERS, J.M. (1981). "Tracing Post-Limit-Point Paths with Reduced Basis Technique", Computer Methods in Applied Mechanics and Engineering, vol. 28, pp. 217-240.

NOOR, A.K. and PETERS, J.M. (1983). "Recent Advances in Reduction Methods for Instability Analysis of Structures", Computer & Structures, vol. 16, pp. 67-80.

ORTEGA, J.M. and RHEINBOLDT, W.C. (1970). "Iterative Solution of Nonlinear Equations in Several Variables", Academic Press, New York, 572 p.

OWEN, D.R.J. and HINTON, E. (1980). "Finite Element in Plasticity: Theory and Practice", Pineridge Press LTD, Swansea, 594 p.

PARK, K.C. (1982). "A Family of Solution Algorithms for Nonlinear Structural Analysis Based on Relaxation Equations", International Journal for Numerical Methods in Engineering, vol. 18, pp. 1337-1347.

PETTOFREZO, A.J. (1966). "Matrices and Transformations", Dover Publications, Inc, New York, 133p.

PIAN, T.H.H. and TONG, P. (1970). "Variational Formulation of Finite Displacement Analysis", Symposium on High Speed Computing

of Elastic Structures, International Union of Theoretical and Applied Mechanics, Liege, pp. 43-63.

PIETRUSZCZAK, S.T. and MROZ, Z. (1981). "Finite Element Analysis of Deformation of Strain-Softening Materials", International Journal for Numerical Methods in Engineering, vol. 17, pp. 327-334.

RAMM, E. (1981). "Strategies for Tracing the Nonlinear Responses Near Limit Points", in Nonlinear Finite Element Analysis in Structural Mechanics, Proceedings of the U.S. Workshop, edited by Wunderlich, W. et al., Springer-Verlag, pp. 63-89.

READ, H.E. and HEGEMIER, G.A. (1984). "Strain Softening of Rock, Soil and Concrete - A Review Article", Mechanics of Materials, vol. 3, pp. 271-294.

RIKS, E. (1972). "The Application of Newton's Method to the Problem of Elastic Stability", Journal of Applied Mechanics, december, pp. 1060-1065.

RIKS, E. (1979). "An Incremental Approach to the Solution of Snapping and Buckling Problems", International Journal of Solids and Structures, Vol. 15, pp. 529-551.

RIKS, E. (1984). "Some Computation Aspects of the Stability Analysis of Nonlinear Structures", Computer Methods in Applied Mechanics and Engineering, vol. 47, pp. 219-259.

RIKS, E. (1987). "Progress in Collapse Analyses", Journal of Pressure Vessel Technology, vol. 109, pp. 33-41.

ROGOWSKY, D.M. (1982). "BM 1/1.5 : Test Data and Results", Archives of the F. Morrison Laboratory, Departament of Civil Engineering, University of Alberta, (manuscript).

ROGOWSKY, D.M., MacGREGOR, J.G. and ONG, S.Y. (1983). "Tests of Reinforced Concrete Deep Beams", Structural Engineering Report No. 109, Department of Civil Engineering, University of Alberta, Edmonton, Alberta, Canada, 167 p.

ROTS, J.G., HORDIJK, D.A. and De BORST, R. (1987). "Numerical Simulation of Concrete Fracture in Direct Tension", in Numerical

Methods in Fracture Mechanics, edited by Luxmoore, A.R. et al., Pineridge Press, Swansea, pp. 457-471.

SAENZ, I.P. (1964). discussion of "Equation for the Stress-Strain Curve of Concrete", by Desayi, P. and Krishnan, S., American Concrete Institute Journal, Proceedings, vol. 61, pp. 1229-1235.

SCHNOBRICH, W.C. (1977). "Behavior of Reinforced Concrete Structures Predicted by the Finite Element Method", Computer & Structures, vol. 7, pp. 365-376.

SHILOV, G.E. (1977). "Linear Algebra", Dover Publications, Inc., New York, 387 p.

STEGMÜLLER, H., HAFNER, L., RAMM, E. and SATTELE, J.M. (1983). "Theoretische Grundlagen zum FE-Programmsystem NISA 80", Institut für Baustatik der Universität Stuttgart, 93p.

STRANG, G. (1988). "Linear Algebra and Its Applications", 3rd edition, Harcourt Brace Jovanich, Publishers, San Diego, 505 p.

THOMPSON, J.M.T. (1963). "Basic Principles in the General Theory of Elastic Stability", Journal of Mechanics and Physics of Solids, vol. 11, pp. 13-20.

TILLERSON, J.R., STRICKLIN, J.A. and HAISLER, W.E. (1973). "Numerical Methods for the Solution of Nonlinear Problems in Structural Analysis", Proceedings of the Winter Annual Meeting of the American Society of Mechanical Engineers, Detroit, Michigan, November 11-15, pp. 67-101.

TIMOSHENKO, S.P. (1983). "History of Strength of Materials", Dover Publications, Inc., New York, 439 p.

TIMOSHENKO, S.P. and GERE, J.M. (1972). "Mechanics of Materials", D. Van Nostrand Company, New York, 552 p.

WEMPNER, G.A. (1971). "Discrete Approximations Related to Nonlinear Theories of Solids", International Journal of Solids and Structures, vol.7, pp. 1581-1599.

WESSELS, M. (1977). "Das Statische und Dynamische Durchschlagsproblem der Imperfekten flachen Kugelschale bei Elastischer Rotationssymmetrischer Verformung", Dissertation, TU Hannover, Mitteil. Nr. 23 des Instituts für Statik.

WILKINSON, J.H. (1965). " The Algebraic Eigenvalue Problem", Claredon Press, 450 p.

WILLAM, K.J. and WARNKE, E.P. (1975). "Constitutive Model for the Triaxial Behavior of Concrete", International Association for Bridge and Structural Engineering, Proceedings, vol. 19, pp. 1-30.

WILSON, E.L. (1989). "Numerical Methods for Solution of Finite Element Systems", in Computer Utilization in Structural Engineering, Structures Congress'89, ASCE, edited by J.K. Nelson Jr., San Francisco, LA, pp. 21-30.

WILSON, E.L. and BAYO, E.P. (1986). "Use of Special Ritz Vectors in Dynamic Substructure Analysis", Journal of Structural Engineering, ASCE, vol. 112, pp. 1944-1954.

WILSON, E.L. and FARHAT, C.H. (1988). "Linear and Nonlinear Finite Element Analysis on Multiprocessor Computer Systems", Communications in Applied Numerical Methods, vol. 4, pp. 425-434.

ZIENKIEWICZ, O.C., VALLIAPPAN, S. and KING, I.P. (1969). "Elasto-Plastic Solutions of Engineering Problems 'Initial Stress', Finite Element Approach", International Journal for Numerical Methods in Engineering, vol. 1, pp. 75-100.

APPENDIX A

MATERIAL MODELS

A.1 Introduction

In this appendix, a brief and informative review of the material models used in the analysis of the structures treated in Chapters 4 and 5 is presented. The classical linearly elastic and elastic-plastic relationships and the hypoleastic constitutive relation for the concrete comprise the set of material models. Following the presentation of the models, the steel and concrete data utilized as input of the analysis of the reinforced concrete deep and shallow beams are listed in tabular format. Some comparisons of the strains in the steel reinforcement, as given by the experiment and the analysis, form the last section of this appendix. In what follows, small strains and plane stress condition are assumed.

A.2 Material Models
A.2.1 The Linearly Elastic Model

In this model, the stress-strain relation that describes the material behavior is nonincremental and assumes the form

$$\{\sigma\} = [C]_e \{\varepsilon\}\ , \tag{A.1}$$

where $\{\sigma\}$ and $\{\varepsilon\}$ are the vectors of total stresses and strains, respectively. The matrix $[C]_e$ is the elastic constitutive matrix given as

$$[C]_e = \frac{E}{1-v^2}\begin{bmatrix} 1 & v & 0 \\ v & 1 & 0 \\ 0 & 0 & \frac{1-v}{2} \end{bmatrix}$$

[A.2]

In [A.2], E and v are respectively the modulus of elasticity and the Poisson's ratio. The prime assumptions governing this model are: isotropy, reversibility of the stress and the strain states and independency with respect to the stress path. In addition, the model has been applied without a strength criterion. Figure A.1 illustrates the stress-strain law for the uniaxial case.

A.2.2 The Elastic-Plastic Model.

The most important ingredients of this model are the postulated existence of a yield criterion, the flow rule and the partition of the increment of total strains into the elastic and plastic strain increments. Considering the von Mises yield criterion and isotropic hardening or softening, the incremental constitutive relation can be derived as

$$\{\Delta\sigma\} = [C]_{ep}\{\Delta\varepsilon\},$$

[A.3]

where the elastic-plastic matrix $[C]_{ep}$ is given as

$$[C]_{ep} = [C]_e - [C]_e\left\{\frac{\partial F}{\partial\{\sigma\}}\right\}\left\{\frac{\partial F}{\partial\{\sigma\}}\right\}^T [C]_e\left[H' + \left\{\frac{\partial F}{\partial\{\sigma\}}\right\}^T [C]_e\left\{\frac{\partial F}{\partial\{\sigma\}}\right\}\right]^{-1},$$

[A.4]

where F is the von Mises yield function, $\{\sigma\}$ is the vector of total

stresses. $[C]_e$ is the elastic constitutive matrix defined in [A.2] and H' is the hardening or softening modulus. The input constants for this model are E, ν, H' and the uniaxial yielding stress F_y. The possibilities of hardening, yielding and softening are shown in the uniaxial stress-strain relation shown in Fig. A.2. Complete derivation of the constitutive relation [A.4] can be found in the reference by Zienkiewicz et al. (1969).

A.2.3 The Multilinear Elastic-Plastic Model.

This model describes the behavior of the reinforcement element within the reinforced concrete member. Its input parameters are the modulus of elasticity E and a number (maximum of 10) of stress-strain pairs $(\varepsilon_i, \sigma_i)$ that trace the experimental stress-strain curve as shown in Fig. A.3.

Two types of behavior of the reinforcement layer can occur. First, linear behavior is accounted for in the case of stress levels below the prescribed stress-strain history (unloading case) (Fig. A.3.). The constitutive relation is then formulated as

$$\sigma = E\left(\varepsilon - \varepsilon_p\right),$$

[A.5]

where σ and ε are respectively the total stress and the total strain and ε_p is the accumulated plastic strain. On the other hand, if the stress-strain point is on or above the prescribed stress-strain curve (loading case) (Fig. A.3), the constitutive relation assumes the form

$$\sigma = \sigma_{i-1} + E_i\left(\varepsilon - \varepsilon_{i-1}\right),$$

[A.6]

where ε_{i-1} and σ_{i-1} define the prescribed stress-strain point and E_i is the secant modulus computed as

$$E_i = \frac{\sigma_i - \sigma_{i-1}}{\varepsilon_i - \varepsilon_{i-1}} \; .$$

[A.7]

The linear piecewise description of the experimental curve allows for a variety of behaviors depending on the type of steel adopted in the structure.

A.2.4 The Hypoelastic Model

This model has been used in the description of the concrete behavior. The basic assumptions underlying this model are the material orthotropy, stress path dependency, incremental reversibility of the stress-strain state and the lack of coupling between normal and shear stresses. In addition, the orthotropy axes follow the axes of principal strains up to the point the material is damaged. The axes are fixed thereafter.

The incremental constitutive relation, when referred to the orthotropic axes can be written as

$$\{\Delta\sigma\} = [C]_{hp}\{\Delta\varepsilon\} \; ,$$

[A.8]

where $[C]_{hp}$ is herein called the hypoelastic constitutive matrix and can be evaluated as

$$[C]_{hp} = \begin{bmatrix} E_1\left(1 - \mu_{23}^2\right) & \sqrt{E_1 E_2}\left(\mu_{13}\mu_{32} + \mu_{12}\right) & 0 \\ & E_2\left(1 - \mu_{13}^2\right) & 0 \\ \text{SYM.} & & G_{12}\phi_G \end{bmatrix}, \qquad [A.9]$$

where

$$\mu_{12}^2 = \nu_{12}\nu_{21}, \qquad\qquad [A.10]$$

$$\mu_{23}^2 = \nu_{23}\nu_{32}, \qquad\qquad [A.11]$$

$$\mu_{13}^2 = \nu_{13}\nu_{31}, \qquad\qquad [A.12]$$

$$\phi_G = 1 - \mu_{12}^2 - \mu_{23}^2 - \mu_{13}^2 - 2\mu_{13}\mu_{23}\mu_{12}. \qquad\qquad [A.13]$$

In expressions [A.10], [A.11] and [A.12], ν_{ij} is the Poisson's ratio evaluated with respect to the orthotropic axes i and j. In addition, E_1, E_2 and G_{12} in [A.9] are respectively the moduli of elasticity and the shear modulus measured with respect to the orthotropic axes 1 and 2.

In the original 3D formulation, due to Elwi and Murray (1979), seven independent variables formed the set of material properties. This model relies further on the concept of equivalent uniaxial strains (Darwin and Pecknold 1977). This concept gives rise to the derivation of material moduli in function of the current level of stress. The curves of stress versus equivalent uniaxial strain, for the cases of tension, compression and shear, are illustrated respectively in Figs. A.4, A.5 and A.6. The ascending branches of these curves follow the parabola proposed by Saenz (1965). On the other hand, the descending branches of the tensile and shear curves obey straight degrading lines defined in terms of fracture properties, such as the fracture energy density and

characteristic length. The adopted strength criterion is based on the surface proposed by Willam and Warnke (1975). Two surfaces, one for stress and the other for strain, are implemented in the model. A complete derivation of this material model is included in the reference by Napoleao and Elwi (1990).

A.3 Steel and Concrete Data

Tables A.1 and A.3 provide respectively the steel and the concrete data used in the analysis of the reinforced concrete deep beam. Similarly, Tables A.2 a . A.4 list the data corresponding to the reinforced concrete shallow beam.

A.4 Analytical and Experimental Reinforcement Strains

Figure A.7 shows the variation of the strains in the longitudinal reinforcement of the reinforced concrete shallow beam at maximum load (Figs. 4.44 and 4.45). Both variations demonstrate that a plastic hinge forms at midspan, since the concrete is already crushed at this load level (Fig. 4.46). However, the extent of yielding in the longitudinal reinforcement is longer for the experimental variation than for the analytical solution. This may be caused by the effect of the discretization of the reinforcement through truss elements.

Similarly, Fig. A.8 illustrates the variation of the strains in the bottom reinforcement of the reinforced concrete deep beam (Fig. 4.31) for the load levels of 350KN and 550KN (Fig. 4.32). Despite some local discrepancies, both solutions show a reasonable correlation.

Material Property	Value
E	205,000 MPa
(ε, σ)	mm/mm MPa 0.000 0.000 0.002 455.000 0.010 455.000 0.040 679.060 0.100 741.310

Table A.1: Steel data for the reinforced concrete deep beam.

Material Property	Value
E	161,458MPa
(ε, σ)	mm/mm MPa 0.000 0.000 0.002 310.000 0.011 310.000 0.108 498.000

Table A.2: Steel data for the reinforced concrete shallow beam.

Material Property	Value
Elasticity and Shear Moduli:	
E_i, $i = 1,2,3$.	21,100.000 MPa
G_{12}	8,792.000 MPa
Poisson's Ratio:	
v_{12}, v_{13} and v_{23}	0.200
Parameters of the Stress Surface:	
f_{cu}	-42.400 MPa
f_{cb}/f_{cu}	1.160
f_u/f_{cu}	0.087
ξ_1	13.500
ζ_1	0.000
ξ_2	4.000
ζ_2	0.000
Parameters of the Strain Surface:	
ε_{cu}	-0.003 mm/mm
$\varepsilon_{cb}/\varepsilon_{cu}$	1.200
$\varepsilon_u/\varepsilon_{cu}$	0.066
ξ_1	50.000
ζ_1	0.000
ξ_2	4.300
ζ_2	0.000
Parameters of the Tensile Behavior:	
G_f	0.044 N/mm
d_{gp}	77.000 mm
α_{DBR}	0.060

Table A.3: Concrete data for the reinforced concrete deep beam.

Material Property	Value
Elasticity and Shear Moduli:	
$E_i, i = 1,2,3$	20,186.000 MPa
G_{12}	8,412.000 MPa
Poisson's Ratio:	
v_{12}, v_{13} and v_{23}	0.200
Parameters of the Stress Surface:	
f_{cu}	-18.200 MPa
f_{cb}/f_{cu}	1.170
f_{tu}/f_{cu}	0.072
ξ_1	13.500
ζ_1	0.000
ξ_2	4.000
ζ_2	0.000
Parameters of the Strain Surface:	
ε_{cu}	-0.002 mm/mm
$\varepsilon_{cb}/\varepsilon_{cu}$	1.170
$\varepsilon_{tu}/\varepsilon_{cu}$	0.072
ξ_1	50.000
ζ_1	0.000
ξ_2	4.300
ζ_2	0.000
Parameters of the Tensile Behavior:	
G_f	0.044 N/mm
d_{gp}	25.400 mm
α_{DBR}	0.060

Table A.4: Concrete data for the reinforced concrete shallow beam.
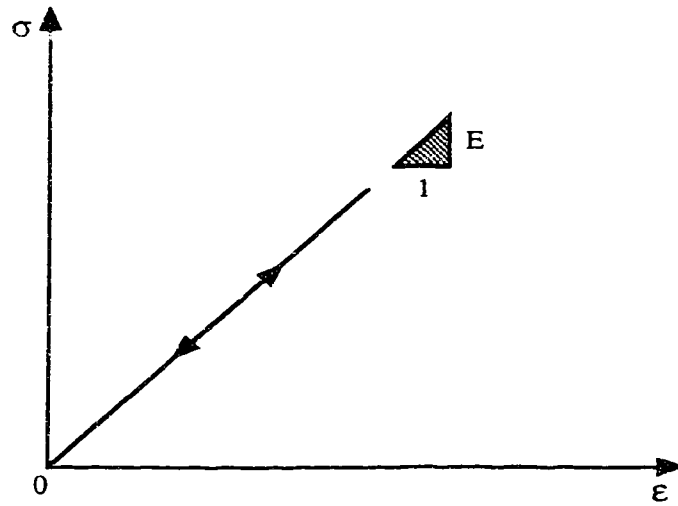
Figure A.1: Linearly elastic behavior (uniaxial case).
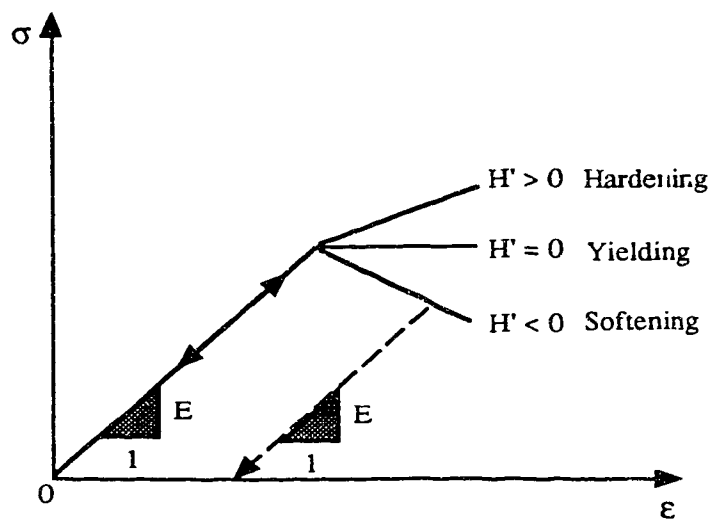
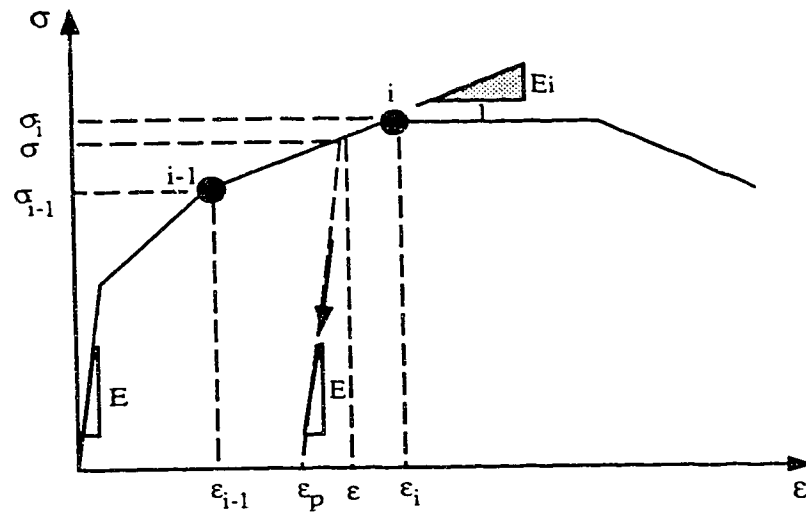Figure A.2: Elastoplastic behavior (uniaxial case).

Figure A.3: Multilinear elastic-plastic behavior of the reinforcement.
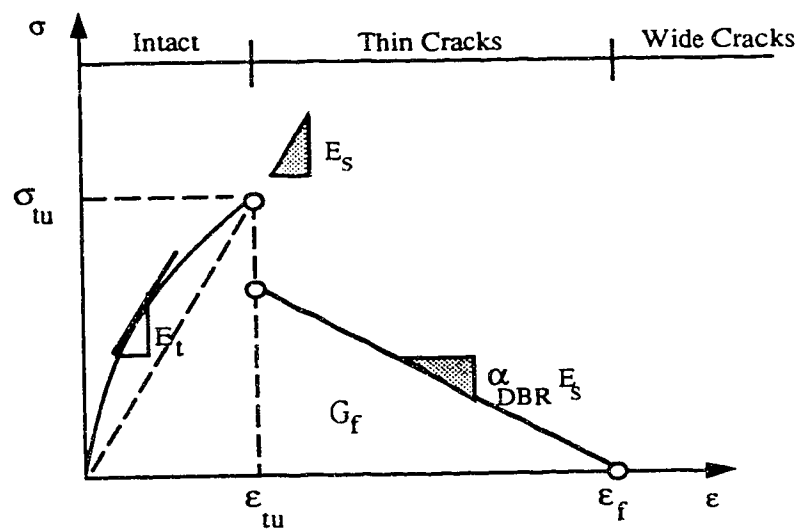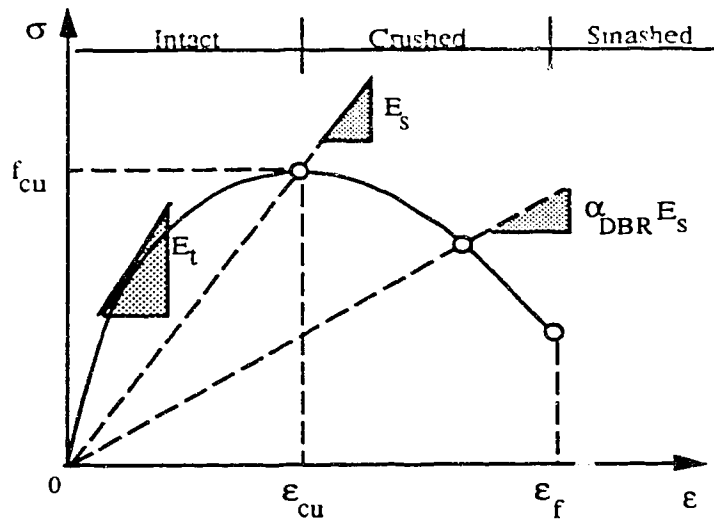

Figure A.4: Tensile behavior of concrete

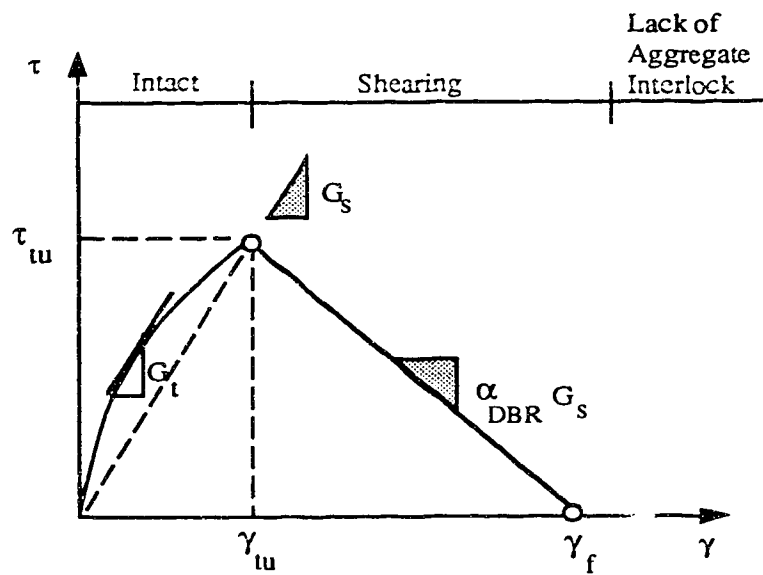Figure A.5: Compressive behavior of concrete.
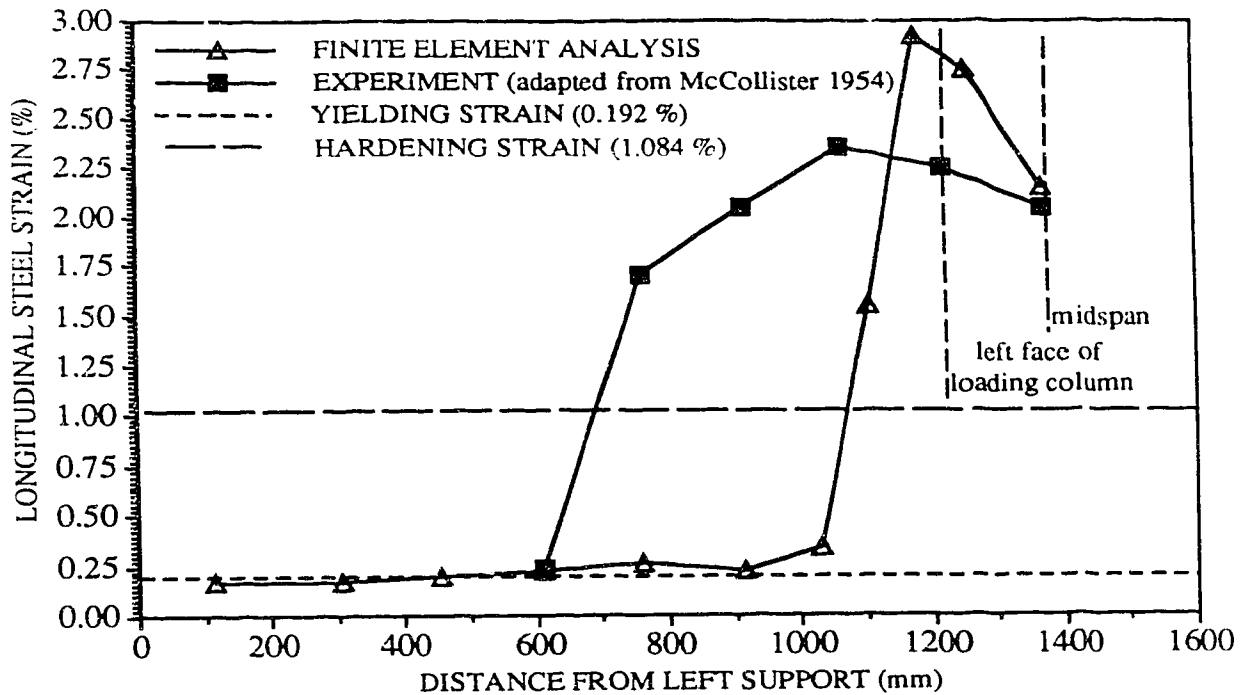

Figure A.6: Shear behavior of concrete.

Figure A.7: Variation of the strains in the reinforcement of the reinforced concrete shallow beam.
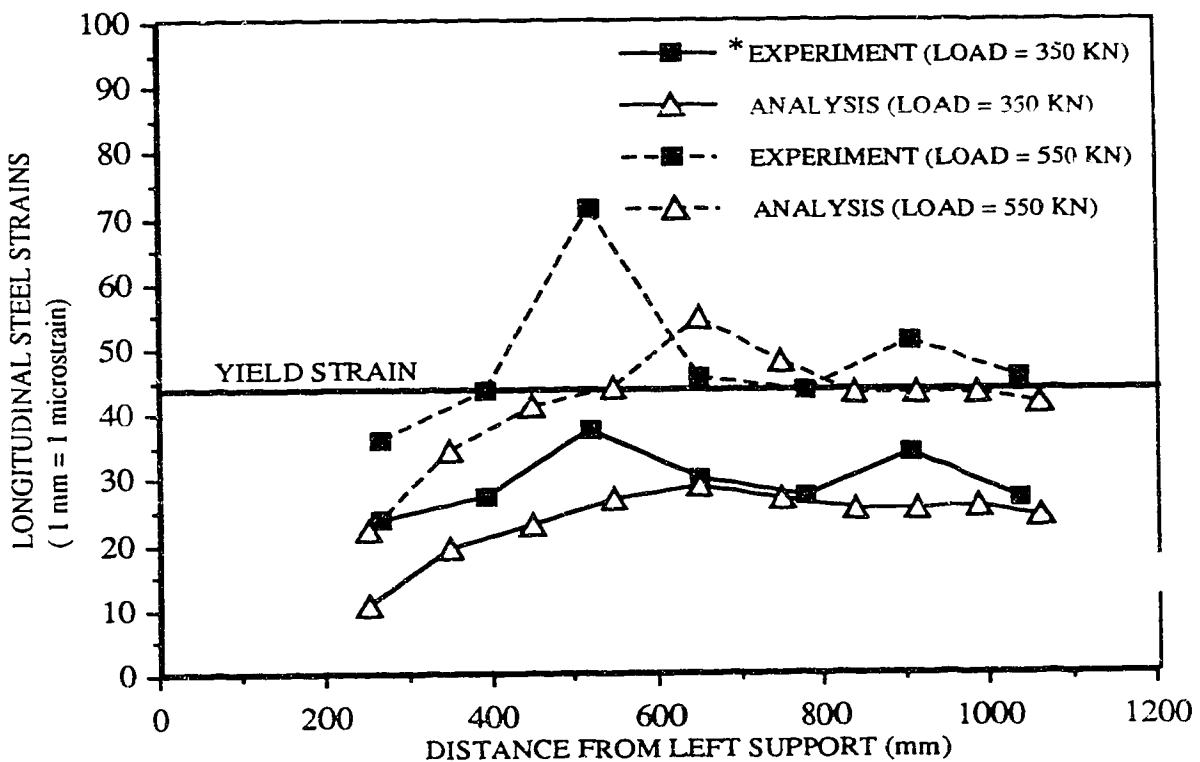

Figure A.8: Variation of the strains in the bottom reinforcement of the reinforced concrete deep beam.
(* Adapted from Rogowsky et al. 1983).